



MONASH University

Self-Assembly of Peptide-Based Materials

A thesis submitted for the degree of Doctor of Philosophy

By

Nathan Habila

B.Sc. (ABU), M.Sc. (ABU)

Department of Biochemistry and Molecular Biology

Monash University

Victoria 3800, Australia

October 2017

Copyright notice

© Habila Nathan (2017).

I certify that I have made all reasonable efforts to secure copyright permissions for third-party content included in this thesis and have not knowingly added copyright content to my work without the owner's permission.

Dedication

This Thesis is dedicated to;

“I Am that I Am (say this to the people of Israel)”, The way, The truth, The Light,

To Him be glory forever.

Declaration

This thesis contains no material which has been accepted for the award of any other degree or diploma at any university or equivalent institution and that, to the best of my knowledge and belief, this thesis contains no material previously published or written by another person, except where due reference is made in the text of the thesis.

Signature:



Print Name: **Nathan Habila**

Date: **11/10/2017**

Acknowledgements

I would like to thank my principal supervisor Professor Marie-Isabel Aguilar for her patient guidance, encouragement and advice throughout my time as her student. From day one, she graciously welcomed me to the group and I am grateful for the opportunity to be able to pursue my passion for research in your group. My gratitude also goes to my second supervisor Dr. Mark P. Del Borgo for his advice, be it science- or career-related. I am extremely lucky to have you as a supervisor who cared so much about my work and who responded to my questions and queries so promptly. Your enthusiasm and encouragement propelled me to take my project to the highest level possible. You have been a tremendous mentor for me. I would like to thank my third supervisor Dr. Tzong-Hsien (John) Lee for his support, guidance and insightful comments which were helpful in fulfilling many of the tasks in the Lab. I would like to thank Dr. Ketav P. Kulkarni for his encouragement and suggestions in the chemistry side of things. I must also express my gratitude to Christian Gow for all the training and support for the atomic force microscopy. I would like to thank Dr. Georg Ramm, Joan Clark and Adam Costin for the training and use of transmission electron microscopy at the Ramaciotti Centre for Structural Cryo-Electron Microscopy.

I would like to thank Kerstin, Enzo, Baydaa, Julie, Shrini, Dr Pravena, Dr Emmanuel Laryea and all my friends for all the wonderful time we shared at Monash University.

I would like to express my profound gratitude to Monash University for the award of Monash Graduate Scholarship and Monash International Postgraduate Graduate Scholarship which enabled me to pursue my research dreams. I would also like to thank the Department of Biochemistry and Molecular Biology for Monash Departmental Scholarship.

My special thanks will go to Denby and Judy Ward for their outstanding support throughout this journey. Your invaluable support will be treasured forever. Special thanks also go to all the members of St Mark's Church Templestowe for your love and constant support. I would also like to thank Mamman M. Immam, Dr. (Sir) Edward Ogabiela, Arigu J. Emmanuel, Yusuf, Fatima Mahmoud, Fred Alale and the Nigerian community in Victoria for all your support over the years.

I would like to thank Ahmadu Bello University Zaria for the support which is highly appreciated.

I would like to thank my family for their continuous prayers and unconditional support. My parents Asabe and Habila Chindo have always provided the driving force throughout my career. Raising me to adulthood was surely a terrible burden, but they never slowed down. Thank you for keeping the faith in me.

Finally, I would like to thank my wife, Mary Nathan-Habila for all your support. You are simply my Diamond. We are extremely blessed to have two amazing girls Bonnie-Eden (The Best) and Aaliyah-Bliss (The Greatest). Postgraduate study is often times compared with running a marathon and indeed, that has been my experience. I can proudly say that without the quintessential friendship, I would not be at the finish line. However, glory be to God in the highest! The Lord is good!

Abstract

Supramolecular self-assembly of *N*-acetyl- β^3 -peptides leads to fibrous architectures of varying sizes (from nano- to macro-scale) and shapes irrespective of amino acid sequence. However, there is a need for fine control of β^3 -peptide self-assembly to exploit the potential of these materials in future applications. In order to achieve this control, β^3 -peptides were functionalised by incorporating a single alkyl chain of either C₁₂, C₁₄ or C₁₆ onto a β^3 -peptide sequence to form β^3 -peptide amphiphiles. A total of 12 β^3 -peptide amphiphiles were designated as R₀, R₁, R₂ and R₃ based on the position of the alkyl chain in the *N*-acetyl β^3 -tripeptide sequence. Atomic force microscopy (AFM) and transmission electron microscopy (TEM) were used to capture the images of the self-assembled nanostructures. The results revealed that R₀ and R₁ β^3 -peptide amphiphiles self-assembled into twisted ribbons that exhibited a fibrous mesh architecture with surface periodicity. The height values were between 5-8 nm for R₀ and R₁ β^3 -peptide amphiphiles. In contrast, R₂ and R₃ β^3 -peptide amphiphiles formed straight and flat nanobelts with higher height values between 14-32 nm. The position of the alkyl chain on the *N*-acetyl β^3 -tripeptide sequence exerted significant control over the morphology and size of the self-assembled nanostructures compared to previously reported non-acylated β^3 -peptides. These β^3 -peptide amphiphiles also formed stable supramolecular hydrogels under physiological conditions which makes them attractive materials for potential application in tissue engineering, drug delivery, and three-dimensional (3D) cell culture.

In order to propose a self-assembly model for β^3 -peptide amphiphiles, AFM nanoindentation on the R₂ series of β^3 -peptide amphiphiles was carried out to probe the internal molecular organisation of the self-assembled nanobelts. The indentation was performed in an aqueous environment where the AFM tip was used to generate holes through the surface of the self-assembled nanobelts. The indentation of the nanobelts revealed the presence of multiple internal bilayers. The topographic images of the holes revealed a sheet-like organisation of the internal architecture with a spacing of ≈ 2.6 nm, ≈ 2.8 nm and ≈ 3.0 nm. These dimensions were used to propose a structural model mediated by the collective balance of hydrogen bonding, hydrophobic interactions and electrostatic attraction. In addition, the stiffness of the three R₂ nanobelt β^3 -peptides were found to be ≈ 7.4 MPa, ≈ 12.4 MPa and ≈ 16.5 MPa respectively suggesting that as the alkyl chain increases, the stiffness also increases. Apart

from the ability to measure the mechanical properties of the nanobelts, AFM nanoindentation was demonstrated to be a versatile imaging technique that offers an additional high-resolution alternative for studying the internal packing order of self-assembled peptide-based nanostructures.

The role of hydrogen bonding during head-to-tail and electrostatic interactions during lateral self-assembly of β^3 -peptide amphiphiles was also investigated. To achieve this, a new series of R_0 , R_1 , R_2 and R_3 β^3 -peptides were synthesised which comprised a β R residue and a C-terminal amide in the *N*-acetyl β^3 -tripeptide sequence and self-assembly was monitored at pH 4, 7 and 13. Both acidic and basic pH disrupted head-to-tail and lateral self-assembly resulting in truncated discrete nanofibres which contrasted with twisted ribbons and nanobelts of β^3 -peptide amphiphiles with C-terminal free acids, while at neutral pH all modified β^3 -peptides amphiphiles formed a nanofibrous mesh. The height data at acidic, neutral and basic pH values revealed a significant decrease in size indicating that lateral assembly had been inhibited by the introduction of electrostatic repulsion. These studies demonstrated that pH can be used to control fibre length and bundling to form different nanostructures.

Overall, the results presented in this Thesis provide a new platform to create novel nanostructures by supramolecular self-assembly of β^3 -peptide amphiphiles via simple changes in the alkyl chain position and manipulation of the forces involved in lateral interactions. This dissertation therefore provides strategies for the design of a new generation of β^3 -peptide-based nanostructures that can be tailored for specific applications.

Abbreviations

Å	Angstrom
Ac	Acetyl
ACN	Acetonitrile
Alloc	Allyloxycarbonyl
N ₃ ⁻	Azide
AFM	Atomic force microscopy
CAC	Critical aggregation concentration
CD	Circular dichroism
CMP	Collagen mimetic peptides
CPA	CMP amphiphiles
DCM	Dichloromethane
DMAP	4-Dimethylaminopyridine
DMEM	Dulbecco's modified Eagle's medium
DIPEA	N,N-Diisopropylethylamine
DMF	N,N-Dimethylformamide
ECM	Extracellular matrix
EDTA	Ethylenediaminetetraacetic acid
eq.	Equivalents
ESI-MS	Electrospray ionisation mass spectrometry
Ether	Diethyl ether
HPLC	High performance liquid chromatography
FF	Homodimer L-diphenylalanine

Fmoc	9-fluorenylmethyloxycarbonyl
GPa	GigaPascal
G	Gel
HBTU	O-benzotriazole-N,N,N',N'-tetramethyl-uronium-hexafluoro-phosphate
kHz	Kilohertz
TIS	Triisopropylsilane
THF	Tetrahydrofuran
<i>H</i>	Hydrophobic residues
<i>P</i>	hydrophilic residues
IKVAV	Isoleucine–lysine–valine–alanine–valine
LIA	β^3 Leu- β^3 Ile- β^3 Ala
LC	Liquid chromatography
MPa	Megapascal
μ M	Micromolar
mq-H ₂ O	MilliQ water
mm	Millimeter
mg mL ⁻¹	Milligram per milliliter
NG	No gel
C ₁₂	Lauric acid
C ₁₄	Myristic acid
C ₁₆	Palmitic acid
PF-QNM	Peak force quantitative nanomechanical mapping
nm	Nanometer
N/m	Newton per meter

OD	Optical density
1D	One-dimensional
PBS	Phosphate buffer saline
pKa	Negative base-10 logarithm of the acid dissociation constant
pH	Potential hydrogen ion
RGD	Arginine–glycine–aspartic acid
RP-HPLC	Reversed phase high performance liquid chromatography
SANS	Small-angle neutron scattering
SAX	small angle X-ray scattering
SD	Standard deviation
SEM	Scanning electron microscopy
SEM*	Standard error of mean
SPPS	Solid phase peptide synthesis
SSA	Supramolecular self-assembly
TEM	Transmission electron microscopy
TFA	Trifluoroacetic acid
ACHC	trans-2-aminocyclohexanecarboxylic acid
ACPC	trans-(S, S)-2-aminocyclopentanecarboxylic acid
2-D	Two-dimensional
3-D	Three-dimensional
H ₂ O	Water
XRD	X-ray diffraction

β^3 -Amino acids

β A	β^3 -homoalanine
β K	β^3 -homolysine
β Az*	β^3 -homoazidoalanine
β R	β^3 -homoarginine

Table of Content

Copyright notice	i
Dedication.....	ii
Declaration	iii
Acknowledgments	iv
Abstract	vi
Abbreviations	viii
β^3 -Amino acids	xi
Chapter One.....	1
1.1 Introduction.....	1
1.2 Peptide-based self-assembly.....	2
1.2.1 α -Helical and coiled-coil assemblies.....	3
1.2.2 Collagen mimic α -peptides	5
1.3 β -Sheet assemblies.....	8
1.3.1 Ionic-complementary α -peptides	9
1.3.2 Dipeptide assemblies.....	11
1.3.3 Fmoc α -peptide assemblies	13
1.3.4 β -Hairpin assemblies	16
1.3.5 Cyclic α -peptide assemblies	17
1.4 Peptide amphiphiles/surfactant-like peptides.....	19
1.4.1 Isomeric α -peptide amphiphile assemblies.....	24
1.4.2 pH-Dependent self-assembly of peptide amphiphiles	26
1.5 β -peptides	29
1.5.1 Secondary structures of β -peptides	29
1.5.2 β -Peptide bundles.....	32

1.5.3 Supramolecular self-assembly of β -peptides	34
1.6 <i>N</i> -acetyl β^3 -peptide assemblies.....	36
1.6.1 Functionalised β^3 -peptide materials	38
1.7 Aims of this project	40
References.....	41
Chapter Two	67
2.1 Introduction.....	68
2.2 Design of β^3 -Peptide Amphiphiles	68
2.3 Materials and methods	72
2.3.1 Materials, Chemicals and Reagents.....	72
2.3.2 Synthesis of β^3 -peptide amphiphiles.....	72
2.3.3 Purification of β^3 -peptide amphiphiles	73
2.3.4 Atomic force microscopy	75
2.3.5 Transmission electron microscopy	75
2.3.6 Hydrogel formation	75
2.4 Results	77
2.4.1 Synthesis and purification of β^3 -peptide amphiphiles	77
2.4.2 Self-assembly of R_0 β^3 -peptide amphiphiles	82
2.4.3 Self-assembly of R_1 β^3 -peptide amphiphiles	86
2.4.4 Self-assembly of R_2 β^3 -peptide amphiphiles	90
2.4.5 Self-assembly of R_3 β^3 -peptide amphiphiles	95
2.4.6 Self-assembly of unacylated β^3 -peptides	98
2.4.7 Hydrogel formation	99
2.5 Discussion	102
2.5.1 Self-assembled morphologies of β^3 -peptide amphiphiles	103
2.5.2 Towards a model for the self-assembly of β^3 -peptide amphiphiles	108

2.6 Conclusion	110
References	111
Chapter Three	120
3.1 Introduction.....	121
3.2 Materials and methods	122
3.2.1 Materials.....	122
3.2.2 AFM Nanoindentation	122
3.2.3 Quantitative nanomechanical mapping of P7 , P8 and P9 nanobelts.....	122
3.3 Results	124
3.3.1 AFM nanoindentation of R ₂ β ³ -peptide amphiphile nanobelts.....	124
3.3.2 Nanoindentation of P7 nanobelts	124
3.3.3 Nanoindentation of P8 nanobelts	126
3.3.4 Nanoindentation of P9 nanobelts	129
3.3.5 PeakForce nanomechanical properties	132
3.4 Discussion.....	134
3.4.1 Structural and mechanical properties of P7 , P8 and P9 nanobelts.....	134
3.4.2 Self-assembly model for P7 , P8 and P9 nanobelts.....	136
3.5 Conclusion	144
References.....	145
Chapter Four	151
4.1 Introduction.....	152
4.2 Design of β ³ -peptide amphiphiles with a C-terminal amide.....	152
4.3 Materials and Methods	156
4.3.1 Materials, Chemicals and Reagents.....	156
4.3.2 Synthesis of β ³ -peptide amphiphiles with C-terminal amides	156
4.3.3 Atomic Force Microscopy in Fluid	157

4.4 Results and Discussion	158
4.4.1 Self-assembly of β^3 -peptide amphiphiles with a C-terminal amide.....	160
4.4.2 Self-assembly of R_0 β^3 -peptides (P15 and P3).....	163
4.4.3 Self-assembly of R_1 peptides (P16 and P6).....	167
4.4.4 Self-assembly of R_2 peptides (P17 and P9).....	170
4.4.5 Self-assembly of R_3 peptides (P18 and P12).....	173
4.4.6 Self-assembly of β K-amide peptide and β R peptide with a free acid (P19 and P20)	176
4.4.7 General Discussion	179
4.6 Conclusion	184
References.....	185
Chapter Five	191
5.1 Conclusions.....	192
5.2 Future Directions in β^3 -Peptide Amphiphile Design	197
References.....	200
Appendix	204

Chapter One

Introduction and Literature Review

1.1 Introduction

Self-assembly is the spontaneous organisation of small components into higher-order structures facilitated by the collective balance of non-covalent interactions [1-3]. Peptide-based self-assembly systems have been used to produce a range of well-defined nanostructures such as nanotubes, nanofibres, nanoribbons, nanospheres, nanotapes, nanorods, and hydrogels [4-6]. The peptides used to generate these nanostructures are classified as ionic self-complimentary [7], collagen mimetic [8, 9], β -hairpin [10, 11], multidomain [12-14], Fmoc-protected [15-17] and α -peptide amphiphiles [18-28].

Through a rational design of the classes of peptides mentioned above, nanostructures have also been functionalised to produce biomaterials that are tailored for applications in tissue engineering, three-dimensional (3D) cell culture, and as drug delivery materials [29-38]. However, the long-term applications of these biomaterials are limited by the degradation of α -peptides by proteolytic enzymes. Therefore, it is necessary to develop alternative materials that possess metabolic stability for long-term applications.

The metabolic stability of β -peptides makes them promising candidates to overcome the proteolytic degradation of α -peptide-based materials [39, 40]. In general, β -peptides consist of β -amino acids which differ from α -amino acids by the insertion of an extra $-\text{CH}_2$ in the backbone between the amino group and $^{\alpha}\text{C}$ atom [41-43]. Structurally, β -peptides can adopt a variety of secondary helical structures with short sequences [43-45] and can self-assemble into well-defined hierarchical structures. My host laboratory was the first to demonstrate the formation of head-to-tail self-assembly motif of *N*-acetyl β^3 -peptides using at least three β^3 -amino acids in a sequence [46]. The self-assembly of these β^3 -peptides resulted in fibrous

materials of varying sizes and shapes, from nano- to macro-scale, irrespective of the sequence. As a consequence of this self-assembly, the side chains are aligned laterally, resulting in a high degree of symmetry along the periphery of the β^3 -peptide nanorods, and this provides an opportunity to functionalise the structure at the side chain position [47]. In order to exploit the potential of these proteolytically stable materials, strategies to control the morphology are required.

Previously, the incorporation of a hydrophobic alkyl chain to the *N*-terminus of α -peptide monomers has been used as an effective strategy to control self-assembly [19, 23, 25, 48]. In this Thesis, this strategy was similarly used to control self-assembled nanostructures of β^3 -peptides. Its use could provide novel peptide-based biomaterials. This chapter comprises a literature review of self-assembled peptide nanostructures, particularly those that have a broad range of applications as biomaterials.

1.2 Peptide-based self-assembly

Peptide-based self-assembly is the spontaneous formation of a stable hierarchical structure via a combination of molecular interactions between the components including hydrogen bonding, hydrophobic interactions, electrostatic interactions, π - π stacking and van der Waals forces (without an external trigger). Peptides comprised of α -amino acids can form secondary structures through the judicious choice of the amino acid sequence [49]. For example, α -helices, β -sheets and coiled-coils have been shown to be involved in peptide-based self-assembly processes and they also display diverse potential applications (Figure 1.1) [35]. The self-assembly of peptides are classified based on the various types of secondary structural conformations and are discussed below.

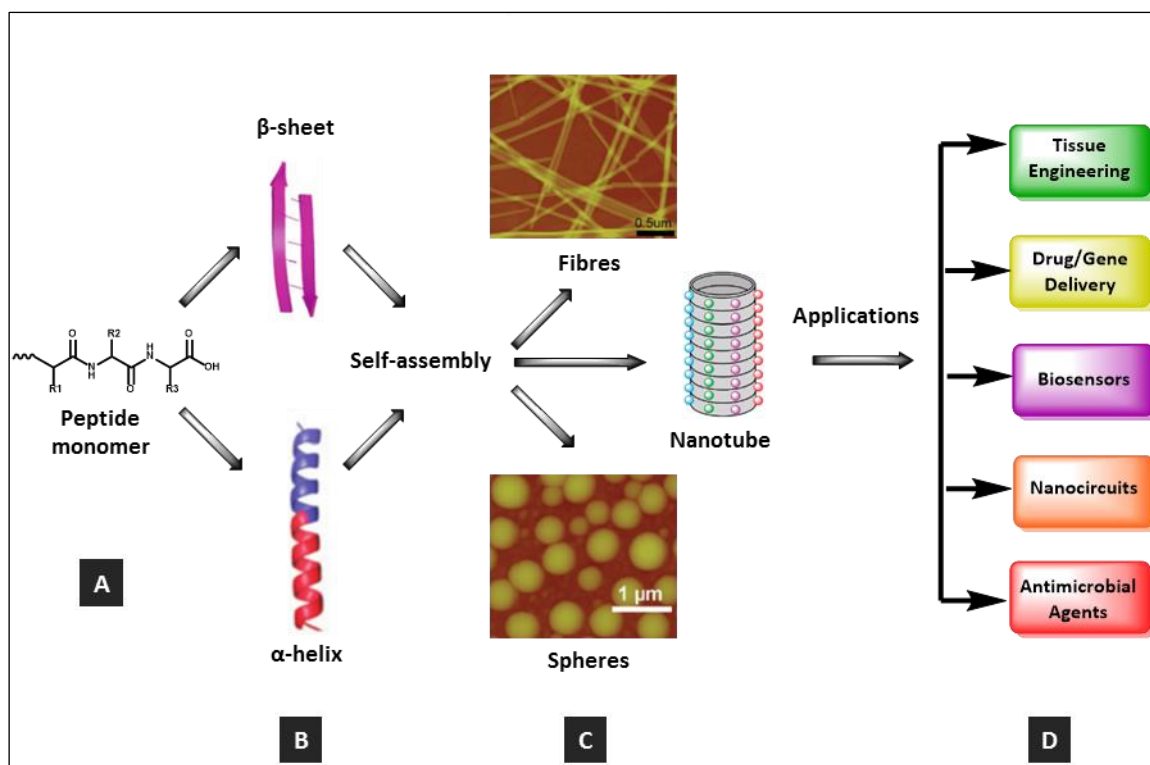


Figure 1.1: Peptide-based self-assembly. (A) Peptide monomer [5], (B) secondary structures [5], (C) different nanostructures including fibres [50], spheres [51] and nanotubes [52] and (D) potential fields of application (adapted from reference [35]).

1.2.1 α -Helical and coiled-coil assemblies

The α -helix is a secondary structural motif with a periodicity of 3.6 amino acids per turn and stabilised by hydrogen bonding between the carbonyl oxygen atoms of residues, i , and the amide hydrogen atoms of the fourth residues along the chain ($i + 4$) [53]. The side chains of the α -amino acids protrude outwards from the helix and are involved in interactions with other α -helices that increase stability facilitated by non-covalent interactions and exploited in the formation of coiled-coil assemblies [53, 49].

The coiled-coil consists of two to five α -helices wrapped around each other to form a supercoil [5, 49, 53-58]. The constituent α -helices are amphipathic; that is, they have a non-polar face which comprises hydrophobic residues (H) and a polar face with hydrophilic residues (P). The design of coiled-coil relies on designing the polypeptide sequences to form amphipathic α -helices that bundle together to form dimers, trimers and pentamers which consist of heptad repeats, $(HPPHPPP)_n$ designated as **abcdefg** [5, 59, 60]. Figure 1.2 shows the helical wheel diagram in which the positions of α -amino acid residues in a heptad repeat, “a” and “d” are

occupied by hydrophobic residues while the other residues are polar. Woolfson’s group used this design to obtain two different structures by changing the ionic interactions between residues **b** and **c** to produce thick fibres (Figure 1.2(A)) while changing residues **b**, **c** and **f** resulted in fibrous hydrogels (Figure 1.2(B)). The two structures were determined by the residues at position “H”, which form the core of the structure [61, 62, 54, 63].

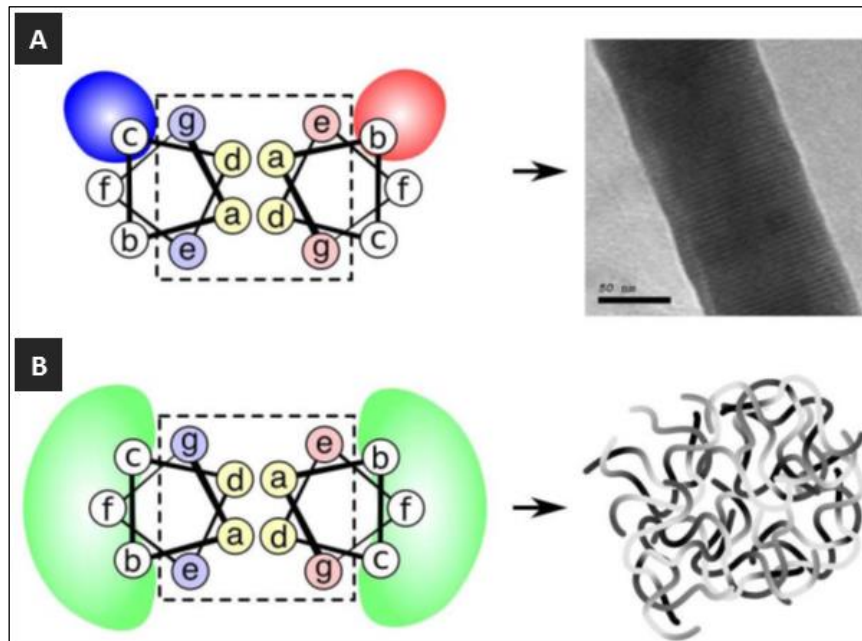


Figure 1.2: Design principles of helical self-assembled fibres. (A) Helical wheel diagram showing modification between position **b** and **c** led to peptide alignment and fibre thickening. (B) Helical wheel diagram showing that the modification of positions **b**, **c** and **f**, resulted into smaller, more flexible, bundles of thinner fibres (adapted from reference [64]).

Woolfson and co-workers have also designed a self-assembling system in which they developed the “sticky-ends” motif by placing complementary charged α -amino acids at positions “**e**” and “**g**” of the heptad repeat. The two complementary polypeptides (with 28-residues) combined to form a parallel, “sticky ended” dimer (Figure 1.3) [65]. Axial organisation of each dimer was facilitated by the presence of a complementary core and electrostatic interaction. The lateral assembly was made possible by complementary features, present in the repeating structures and resulted in thick nanofibres that are 40–50 nm in diameter and several hundred micrometers long. The Woolfson laboratory has also published several other related designs with the same template that formed structures referred to as

fibre branches [66], kinks [67], cages [68], nanotubes, barrels [69-72] and decorated peptide fibres using charged peptides as tags [73], and scaffold for three-dimensional (3D) cell culture [64, 74].

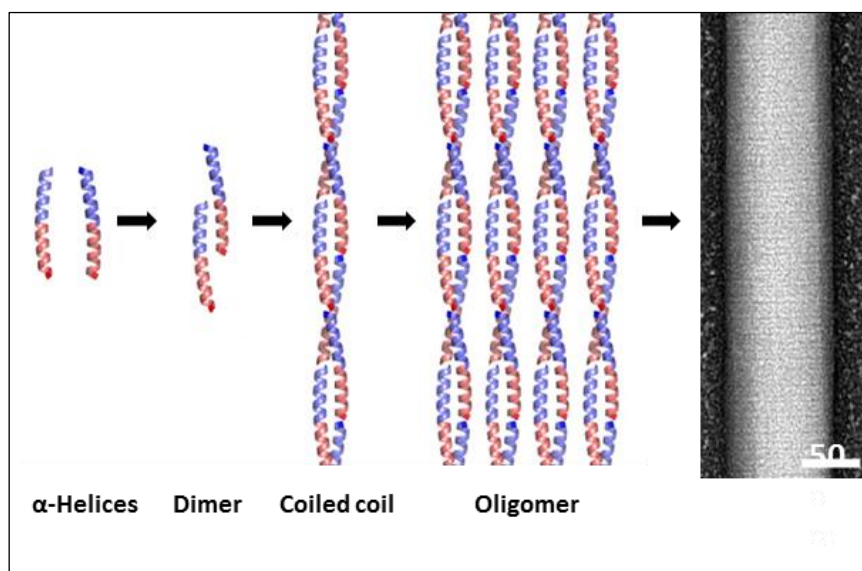


Figure 1.3: Hierarchical self-assembly in which α -helices form a dimer with sticky ends that resulted into fibre (adapted from reference [75]).

Hartgerink and colleagues presented a different strategy by demonstrating that sticky ended dimers are not a prerequisite for the formation of a coiled coil nanofibre. They showed that blunt-ended dimers are able to form nanofibres with a uniform diameter of 4 nm and hundreds of nanometers in length [56]. The key features in the design were the selection of charged amino acids in the peripheral positions “b”, “c”, and “f” which played a major role in controlling the length and the diameter of the nanofibres. Several other peptides with heptad repeat have also been used as building blocks to form supramolecular assemblies by modifying the α -amino acid residues at positions a, d, e and g [60, 76-80].

1.2.2 Collagen mimic α -peptides

The most abundant protein in humans is collagen which accounts for approximately 25% of all vertebrate body proteins [81, 82]. Collagen is comprised of a triple helix with a repetitive

α -amino acid sequence (Glycine-X-Y)_n, where X is usually proline and Y is hydroxyproline [9, 82-86]. Collagen mimetic peptides (CMPs) are oligomers of synthetic collagen peptides that have been used to mimic and elucidate collagen structure, function and factors responsible for its stabilisation [9]. Scientists are now utilizing the CMPs model to generate unique higher assemblies with the potential for biological applications in drug delivery, tissue engineering, and regenerative medicine [87].

The formation of collagen fibres occurs when three peptide chains come together to form a triple helix. The three chains in the collagen helix can either be identical (homotrimer), two identical chains (AAB heterotrimer), or different chains (ABC-heterotrimer) [88]. Therefore, CMPs require multiple subunits to undergo self-assembly into longer fibres that can form inter-strand fibrous networks by varying the leading, middle and lagging chains [89].

Hartgerink and coworkers have reported several designs based on CMPs that self-assembled into homotrimeric and heterotrimeric compositions [90-93]. For example, a binary mixture of peptides A and B (Figure 1.4) could form homotrimers (A₃ and B₃) and heterotrimers (A₂B and AB₂) [88]. Therefore, a total of 27 distinct helices are possible for a ternary mixture. Figure 1.4 shows the triple helices with 6 distinct registers of an ABC heterotrimer which self-assembled into fibres [89]. However, the peptide chain composition in the CMP heterotrimers is critical for developing systems that mimic the native collagen structure [88, 93].

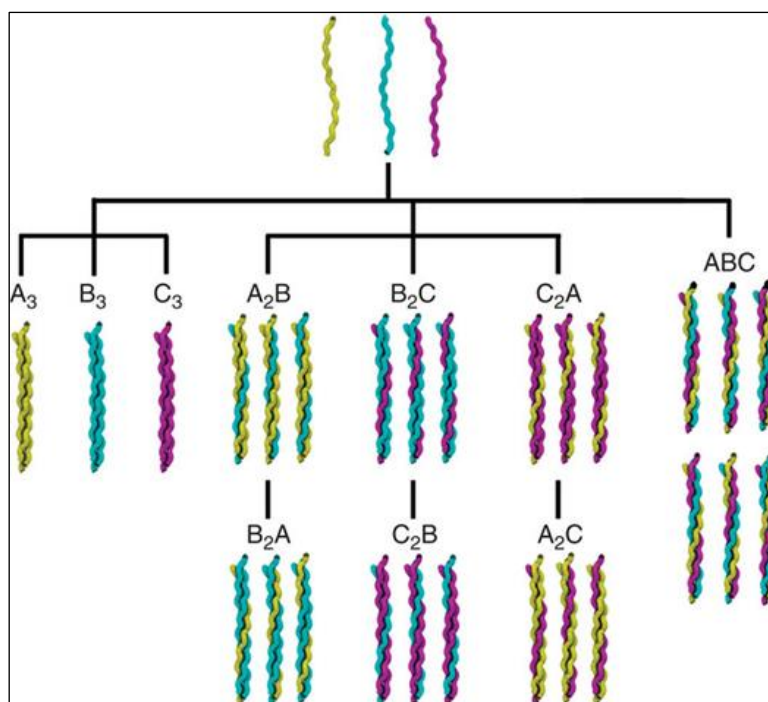


Figure 1.4: Schematic representation of ABC triple helix with 27 unit compositions underpinning the design of CMPs (adapted from reference [89]).

CMPs have also been further functionalised to produce CMP amphiphiles (CPA) which consist of a hydrophilic CMP domain and a hydrophobic tail in the monomer [94]. The CPA was functionalised at the C-terminus to produce the sequence $C_{16}-A_5K_4G[GPO]_3GFOGER[GPO]_3G-NH_2$ in which GFOGER is a cell-binding motif that is found in native collagens. The CPA self-assembled into nanofibrous hydrogels with the characteristic collagen-mimetic triple-helical conformation that promoted cell adhesion and development. Other examples are the formation of hydrogels by a collagen-mimetic dendrimer which was used as a thermosensitive drug carrier [95] and collagen-mimetic dendrimers containing an integrin-binding epitope that exhibited cell adhesive binding activity [96, 97]. Several other CMPs have also been synthesised further demonstrating the potential of these CMP-based compounds as biomaterials for biomedical applications [98-103].

1.3 β -Sheet assemblies

The second important secondary structure is the β -sheet in which the assemblies are composed of two or more α -peptide chains (β -strands) that are connected laterally by hydrogen bonds between the backbone amide and carbonyl groups (Figure 1.5) [104, 105]. The β -strands can form parallel β -sheets in which all the C-termini lie at one end, while in an antiparallel arrangement, the N and C termini run in the opposite directions [104]. In both positions, the β -strands become oriented in such a way that alternate α -amino acid side chains remain at opposite sides of the sheet which has an important influence on the hydrogen bond orientation between sheets and side chain orientations and interactions [33].

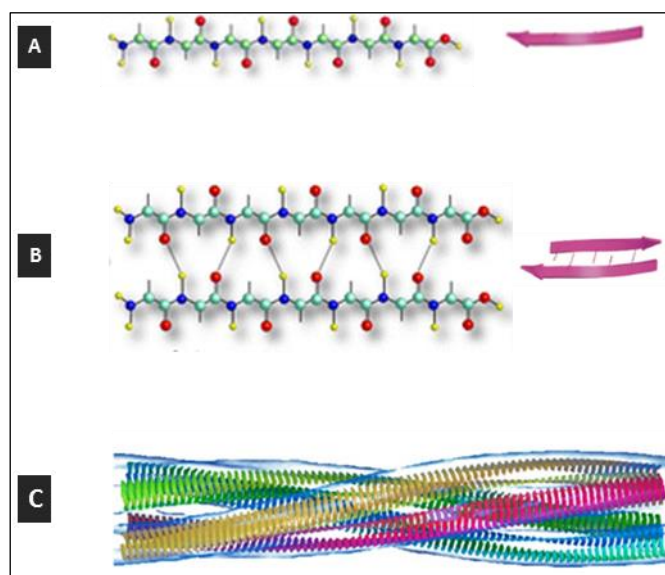


Figure 1.5: Molecular presentation of β -sheet secondary structure (A) β -strand and (B) the β -strands self-associate into β -sheets stabilized by hydrogen bonding [106] and (C) β -sheets then assemble to form cross- β -structured fibrils (adapted from reference [107]).

Several peptides have been designed with the β -sheet motif to form fibrillar nanostructures [108]. For example, the β -amyloid polypeptide sequence has been used to design new peptides that self-assembled into β -sheet structures reminiscent of the amyloid structure [109-118]. This has resulted in an exploration of α -peptides with related sequences using the basic parameters for a β -sheet secondary structure [119].

1.3.1 Ionic-complementary α -peptides

The first example of a β -sheet based self-assembled fibre was serendipitously discovered from a natural protein of the Z-DNA binding protein “Zuotin” with the sequence EAK16-II (AEAEAKAKAEAEAKAK) [120]. These peptides have now become the basis for an entire group of peptides often referred to as the ionic-complementary peptides (or peptide Lego). They consist of building blocks that have alternating hydrophilic and hydrophobic residues similar to the “Lego bricks” that have both pegs and holes positioned in a well-ordered fashion, allowing precise assembly into a predetermined β -sheet structural organisation [120-123]. Since the discovery of EAK16, further studies have been undertaken using peptides derived from this sequence. The new peptides are designed to maintain the basic motif of alternating hydrophilic and hydrophobic amino acids sequences. A series of peptides were studied with this motif in order to identify which properties are critical among the α -amino acid side-chains that influence the self-assembly characteristics of the peptides into β -sheet fibrils. For example, these peptides RADA16-I (RADARADARADARADA) and RADA16-II (RARADADARARADADA) have a similar periodic repeat of ionic hydrophilic and hydrophobic α -amino acids residues [123]. As shown in Figure 1.6, the self-assembly was mediated by hydrophobic interactions between α -alanine residues, while the positively charged α -arginine and negatively charged α -aspartic acid of adjacent peptides self-assemble through intermolecular ionic interactions to form nanofibres bundles with an anti-parallel β -sheet conformation [123]. The non-specific hydrophobic interactions permit the nanofibre to slide by diffusion along the fibre in either direction, which minimizes the exposure of the hydrophobic α -alanines and eventually fills the gaps (Figure 1.6 (A), (B) and (C)) [124].

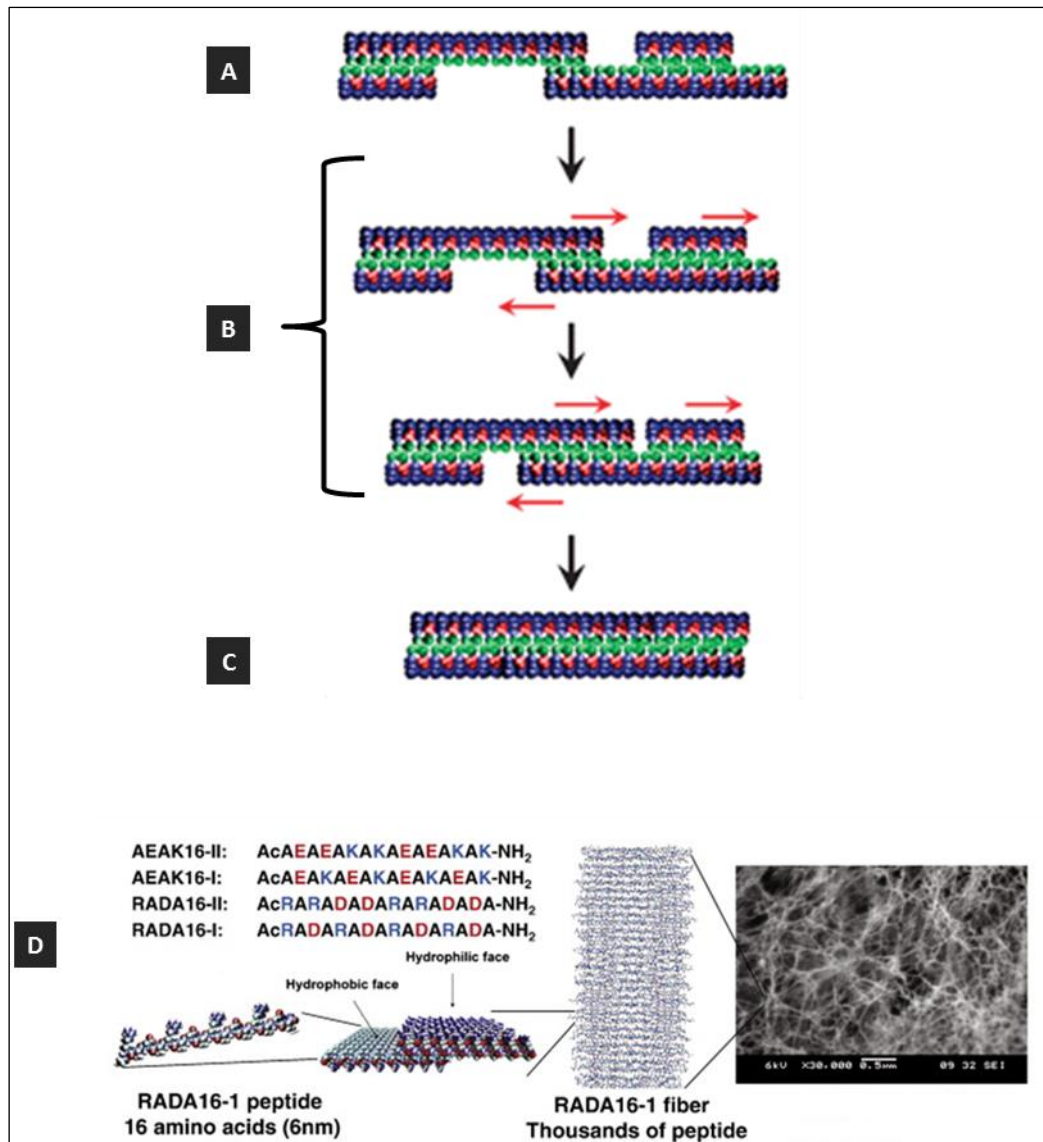


Figure 1.6: A proposed sliding diffusion molecular model for the self-assembly of ionic complementary peptides. (A) Initial state of building blocks, (B) sliding diffusion of β -strands with alternating ionic-complementary properties, (C) final state after filling all gaps [124] and (D) four different ionic complementary α -peptide sequences that self-assembled into nanofibrous scaffolds using the sliding diffusion motif (fibre image of RADA16-I by electron microscopy adapted from reference [123]).

Many of the peptides synthesised with the ionic-complementary motif have been developed as materials with nanofibrous networks with scaffolds for use in regenerative medicine and other biomedical applications [125-127]. Self-assembling peptide hydrogel scaffold with this motif has demonstrated the potential to promote accumulation of a true cartilage-like extracellular matrix within a 3D cell culture for cartilage tissue repair [128], as well as matrix metalloprotease cleavage sites to accelerate biodegradation by self-assembled peptide

hydrogels [129, 123]. RADA16-I in particular was used to generate a 3D scaffold hydrogel for dopaminergic differentiation in which the differentiated neurons expressed specific dopaminergic markers and produced appropriate patterns of action potential firing [130]. In another study, RADA16-I hydrogel also facilitated reconstruction of acute traumatically injured brain, by supporting cells to migrate and survive within the lesion site and reduce the glia reaction and inflammation of the injured brain tissue [131]. It also created a permissive environment for brain repair and axon regeneration with functional return of vision [132].

RADA-16 has now been developed into a commercial product called PuraMatrix® peptide hydrogel as the first self-assembling peptides for clinical application [133]. It has been used to create a biocompatible, biodegradable as well as non-toxic 3D environment for a variety of cells. PuraMatrix® consists of 1% peptides and 99% water which self-assembles and creates a water-soluble β -sheet structure as well as a 3D environment [134]. Clinical trials have also been conducted using 20 patients to determine the safety and sealing properties in postoperative lymphorrhea following pelvic surgery in humans and there was no adverse effect observed during the 2 to 3-month follow-up period [135]. PuraMatrix® has also shown promising results for human fetal Schwann cells (SCs) in spinal cord regeneration [136]. In vitro and in vivo studies revealed that the human fetal SCs survived and proliferated within the PuraMatrix® 3D scaffold.

1.3.2 Dipeptide assemblies

The homodimer L-diphenylalanine (FF) is the most investigated building block for aromatic dipeptide assemblies. Since the emergence of FF in 2003 [137], several studies have been carried out to design the FF-based building blocks into various functional nanostructures [138-140]. The short peptide sequence (Figure 1.7(A)) can form highly stable hollow nanotubes in solution. The self-assembly of FF is promoted by the backbone hydrogen bonds and π - π stacking interactions from the aromatic peptide side-chains of phenylalanine. Tubular structures form when six FF units assemble into a cyclic hexamer (Figure 1.7(B)). The FF hexamers stacked together to form honeycomb-like arrays (Figure 1.7(C)), which give rise to nanotubes. Subsequently, stable nanotubes cluster into larger microtubular channel with a diameter of approximately 10 Å (Figure 1.7(D)) [141].

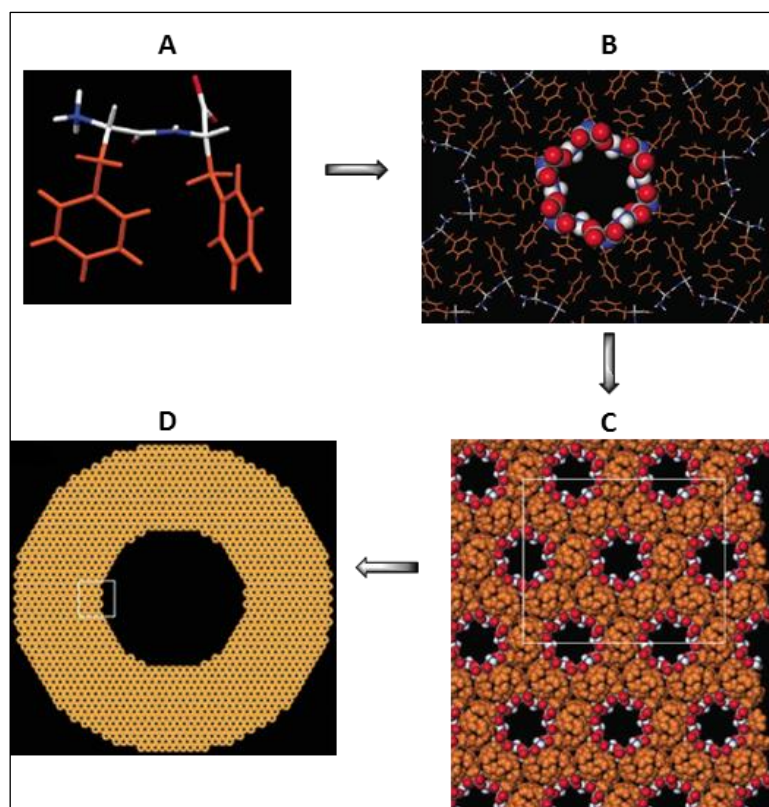


Figure 1.7: A Molecular model of $\text{NH}_2\text{-FF-COOH}$ self-assembly. (A) The molecular structure of FF (side-chain atoms orange colour) (B) FF units form cyclic hexamers, (C) hexamers stack to form honeycomb-like arrays, which give rise to nanotubes and, (D) cluster of nanotubes to a larger microtube (adapted from reference [111]).

The inner core of the tubule is surrounded by the amine and carboxyl groups of the α -amino acids which facilitate anchoring polar molecules onto the peptide matrix. At the upper level, the narrow channels self-associate in a hexagonal packing formation to produce β -sheets conformations [141]. The tubes were found to be rigid, with an averaged point stiffness of 160 N/m and an estimated Young's modulus of ≈ 19 GPa [124]. In order to explore the potential role of electrostatic interaction in the assembly process of $\text{NH}_2\text{-FF-COOH}$, Reches and Gazit studied a modified peptide analog with a zero net charge, in which the N-terminal amine and the C-terminal carboxyl groups were acetylated and amidated to give Ac-FF-NH_2 and $\text{NH}_2\text{-FF-NH}_2$ [142]. Scanning and transmission electron microscopy analyses of both peptides revealed a highly-ordered tubular structure. The ability of the peptide to form ordered supramolecular structures was demonstrated to be driven by π - π stacking of aromatic FF in place of electrostatic interaction.

Several studies have also shown that the β -sheet secondary structure of FF-based building blocks can self-assemble into various other nanostructures such as nanospheres or vesicles [143, 144], nanofibre organogels [145] and nanowires [146]. FF-Based microtubes have been used as molecular carriers and, in particular, as vehicles for the delivery of a hydrophilic compound [141]. Most of these studies have shown that FF can form well-ordered in organic solvents but cannot form supramolecular structures under biological conditions, without the use of an inorganic solvent [147]. Through the introduction of aromatic capping residues such as the Fmoc-group, FF can spontaneously form supramolecular structures. Other aromatic dipeptides assemblies have been studied using different aromatic amino acids (e.g. NH_2 -WW-COOH) and other aromatic molecules as building blocks (e.g. di-para-fluoro-Phe, di-pentafluoro-Phe, di-para-iodo-Phe) [137, 139].

1.3.3 Fmoc α -peptide assemblies

The 9-fluorenyl methoxy carbonyl (Fmoc) moiety is widely used as a protecting group in peptide chemistry for Fmoc solid-phase peptide synthesis in which Fmoc-amino acids are used as the building blocks. Fmoc-based α -peptides consist of a peptide sequence that has an aromatic Fmoc moiety attached to the amino *N*-terminus. In 1991 Burch et al. reported that a number of Fmoc α -amino acids were found to possess a broad spectrum of anti-inflammatory activities [148]. Since then, research has been focused on Fmoc-protected α -peptides which can drive self-assembly of short peptide sequences into nanofibrils through π - π stacking of the Fmoc aromatic moieties [149-151]. Vegners et al. reported the first self-assembled fibre network with Fmoc-protected dipeptides which eventually formed viscoelastic gels in aqueous solution at 2 mg mL⁻¹ [152]. Thereafter Gazit and co-workers reported the self-assembly of Fmoc-FF into a hydrogel with remarkable mechanical rigidity that supports cell viability and proliferation [150]. Subsequently, Ulijn and coworkers identified the self-assembly mechanism whereby aromatic interactions of Fmoc-peptide derivatives formed antiparallel β -sheets between the pendant α -peptide. The resulting α -amino acid side chains were expressed on the surface through what is known as π - β interactions [16]. Several other reports have also demonstrated that the aromatic groups in the Fmoc moiety share electrons to form π - π interactions, interlocking the α -peptide derivatives in which the α -peptide chains are then brought into close proximity allowing them

to interact with each other through anti-parallel β -sheets. Nanofibres are formed from the combination of several of these assemblies [15, 153-156]. Bundles of these nanofibres form highly branched nanofibrous network through supramolecular self-assembly to presents macroscale hydrogel. Thus, the α -amino acid side chains are located on the surface of the nanofibres to provide surface bio-functionality through interactions with cell surface receptors [16, 147]. The molecular model for supramolecular self-assembly of Fmoc-FF is shown in Figure 1.8 in which the individual nanofibrils bundled to form supramolecular structures leading to the formation of a fibrous hydrogel [16, 157, 158].

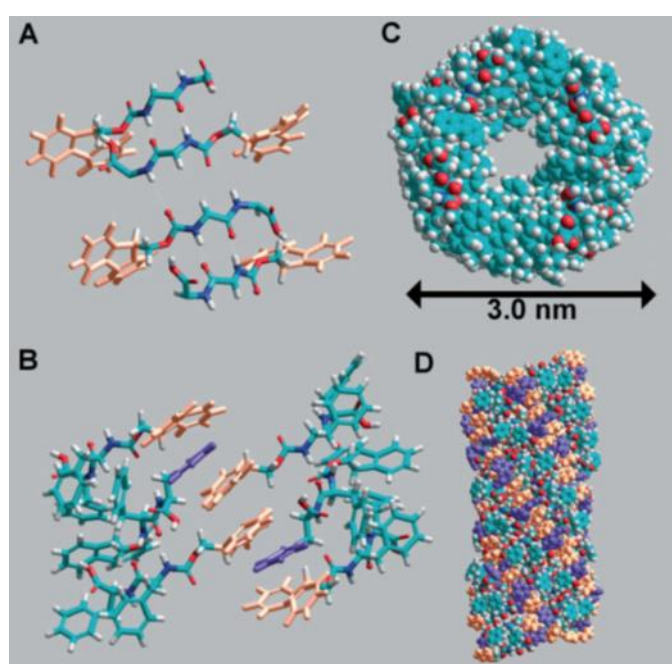


Figure 1.8: A structural model for self-assembled Fmoc-FF peptides using molecular dynamics. (A) Anti-parallel β -sheet pattern, the alignment is interlocked by four twisted antiparallel β -sheets via π - π interactions between fluorenyl groups, (B) interlocked Fmoc groups from alternate β -sheets to create π -stacked pairs with phenyl rings, (C) top view of the cylindrical structure created by fluorenyl groups and (D) side view of (C). Fluorenyl groups are coloured orange and the phenyl groups are coloured purple (in (A) (B) and (D)) (adapted from reference [16]).

The ability to control the assembly of Fmoc-FF structures have been demonstrated by the application of external triggers such as enzymes [149, 159, 160] and biocatalyst [161]. Several other types of Fmoc-modified peptides were synthesised with non-aromatic amino acids as building blocks including, Fmoc-GG, Fmoc-GF, Fmoc-LL, Fmoc-LG, Fmoc-GL, Fmoc-KK [162],

Fmoc-AA, Fmoc-GA and Fmoc-GS [163]. The replacement of FF with non-aromatic amino acids did not affect the propensity of the Fmoc-modified peptides to self-assemble into fibrillary structures, which suggested that the π - π interaction of the fluorenyl group played a key role in driving the self-assembly.

The functionalisation of Fmoc-peptide using the bioactive cell adhesive RGD was demonstrated to give the sequences Fmoc-FRGD, Fmoc-RGDF [164, 165] and Fmoc-FRGDF [166]. These peptides form hydrogels and thus offers new opportunities for developing cell adhesive biomedical hydrogel scaffolds for biomedical applications. Fmoc-FRGDF has been shown to be an efficient hydrogelator via π - β self-assembly mechanism. The mechanical properties and morphology of Fmoc-FRGDF hydrogels were controlled by tuning both the final ionic strength and the rate of pH change [166]. Co-assembly of Fmoc-FF and Fmoc-RGD have also been reported as a biomimetic and highly fibrous network that presented bioactive ligands at the fibre surface [167]. The RGD functionalised hydrogel promoted adhesion of encapsulated human dermal fibroblasts through specific RGD–integrin binding, with subsequent cell proliferation [167], fibroblast support, extracellular matrix (ECM) organisation and reconstruction of a normal dermal tissue [168]. The co-assembled hydrogel using Fmoc-FRGDF and fucoidan was recently reported to support healthy cells, while inducing apoptosis in cancerous epithelial cells [169]. This can potentially be applied in cancer immunotherapy and drug delivery.

Significant efforts have also been made to include IKVAV (a laminin epitope) functional sequence to Fmoc-peptides without disrupting the mechanism of assembly. The control of Fmoc-peptide self-assembly was achieved by a rational modification of the pKa of four different Fmoc peptides consisting of IKVAV, which is an important component of the ECM [17]. The Fmoc-peptide sequences used include Fmoc-IKVAV, Fmoc-DIKVAV, Fmoc-DDIKVAV and Fmoc-DDDIKVAV. The sequence of amino acids strongly determined the pKa of the peptide and therefore the pH at which self-assembly occurred. The modification of the bioactive peptide sequence (IKVAV) with acidic residues was found to have no effect on the non-covalent interactions between individual self-assembling peptides. The individual Fmoc-peptides interacted non-covalently to form hydrogels at physiological pH which supported cell survival both *in vitro* and/or *in vivo* for localised viral vector gene delivery [17, 170].

The co-assembly of Fmoc-FRGDF and Fmoc-DIKVAV was also demonstrated to form stable hybrid nanofibres containing dual epitopes with superior, stable, transparent, shear thinning hydrogels at biological pH. The hydrogel possesses ideal characteristics for tissue engineering applications better than the individual self-assembling peptide [171].

1.3.4 β -Hairpin assemblies

β -Hairpins are secondary structural motifs which comprise two β -strands that are oriented in anti-parallel directions and linked by a kink or short loop of two to five amino acids [51]. They can be rationally designed, synthesised and self-assembled into fibrous hydrogels [123, 172]. Schneider and colleagues described a series of peptides which self-assembled into a fibrous hydrogel network consisting of a β -hairpin motif [10, 173-175]. Pochan and Schneider proposed a β -hairpin design composed of alternating valine (hydrophobic) and lysine (hydrophilic) residues [173, 176]. The amphiphilic peptide, MAX1, has the sequence VKVKVKVKV^DPPTKVKVKVKV-NH₂ with the incorporation of β -turn-forming tetrapeptide (-V^DPPT-) into the sequence (where ^DP is an enantiomer of proline) [51, 176]. Lateral assembly was driven by intermolecular hydrogen bonding, van der Waals forces and hydrophobic interactions [123, 177, 178]. Figure 1.9 shows the self-assembly model for folded MAX1 and MAX8 β -hairpin peptides in which the peptides exist in random coil conformations due to electrostatic repulsions between positively charged lysine side chains. However, the addition of Dulbecco's modified Eagle's medium (DMEM) for cell culture, containing approximately 160 mM salt, screens this charge and allows the peptide to self-assemble into hydrogels [179]. Several other analogs of this design also form hydrogels in response to a variety of other stimuli including pH [176], temperature [180] and salt [174]. Other reports have shown that peptides with the V^DPPT recognition motif can undergo a transition from random coil to β -hairpin structures in response to variations to specific stimuli such as light-activation [181, 179], ionic triggers [182], temperature [173] and pH [183].

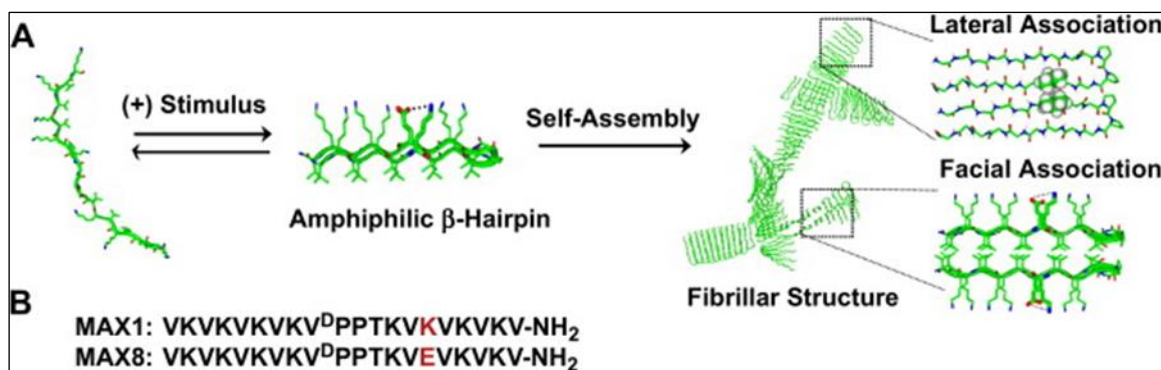


Figure 1.9: Self-assembly model for folded β -hairpin peptides. (A) Unfolded MAX1 or MAX8 was triggered to fold into a β -hairpin via the addition of DMEM and (B) peptide sequences of MAX1 and MAX8 (adapted from reference [179]).

MAX8 (VKVKVKVKV^DPPTKVEVKVKV-NH₂) is a peptide-based β -hairpin hydrogel with unique properties that have been exploited for potential applications in drug delivery and stem cell research [184, 185]. It has an overall positive charge at pH 7, due to charged lysine residues and self-assembled upon dissolution in DMEM cell culture media resulting in hydrogel formation. The hydrogel exhibited shear-thinning which allows homogeneous encapsulation and subsequent delivery of mesenchymal stem cells via syringe with precision to target sites in tissue regeneration [185]. MAX8 has also shown injectable time-released dosage control, improving the efficacy of nerve growth factor and brain-derived neurotrophic factor in experimental treatments of spinal cord injuries [186].

1.3.5 Cyclic α -peptide assemblies

Cyclic α -peptides are polypeptide chains that form a cyclic ring structure by linking one end of the peptide and the other via an amide bond, or other chemical bonds [187]. Tubular nanostructures formed from cyclic peptides are one of the earliest self-assembled nanotubes that were first developed by Ghadiri and co-workers [188, 189]. The concept was based on the rational design of heterochiral cyclic peptides which comprised D- and L-amino acids to generate a planar ring that could self-assemble on top of each other, to form β -sheet tubular structures of the desired diameter. The nanotube was prepared using the sequence, cyclo-[(L-Gln-D-Ala-L-Glu-D-Ala)₂], where the ring-shaped subunits stack through antiparallel β -sheet hydrogen bonding to form ordered hollow tubes with a uniform internal diameter of 7.5 Å

and distances of 4.73 Å between ring-shaped subunits [189]. The peptide rings formed a flat ring conformation through an even number of alternating D- and L-residues, which enabled unidirectional stacking (Figure 1.10). The planar structure of the cyclic peptide backbone projects the peptide side chains to the external periphery leaving a hollow channel [188-191, 52] which can be decorated with specific functional properties by side chain modifications [192].

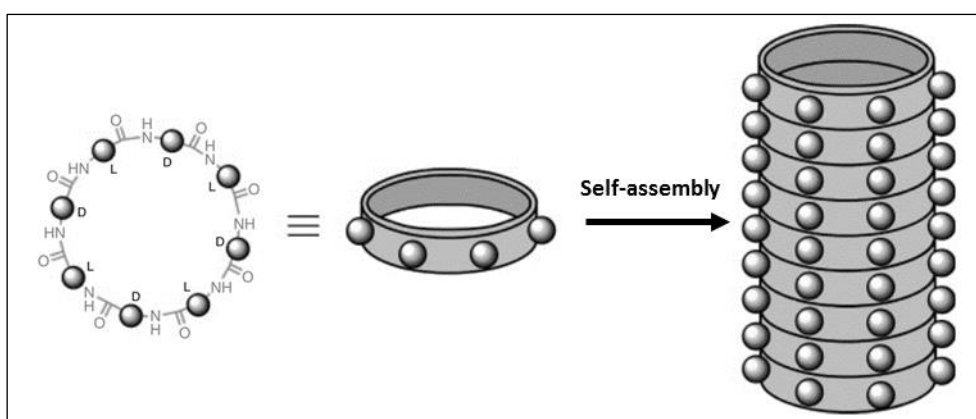


Figure 1.10: Schematic representation of alternating D- and L-amino acid cyclic peptide to form elongated and hollow nanotubes (adapted from reference [191]).

Ghadiri and co-workers also described the design of an artificial transmembrane ion channel from self-assembled nanotubes that can mimic the biological function of natural ion channels [188]. This could have potential application in molecular transport across lipid bilayers and can be used as a delivery tool into living cells in antisense and gene therapy applications [188]. Other applications of cyclic α -peptide nanotubes include ion sensing [193] and as antibacterial agents [194].

Jolliffe and Perrier have also reported a new series of self-assembled cyclic peptide–polymer nanotubes with improved solubility, functionality and control over size [195, 196]. The monomer self-assembled by exploiting the β -sheet configuration of the alternating (D and L) cyclic peptide core [197]. In this design, the cyclic peptides were coupled to the polymeric chains via a copper catalysed azide–alkyne click reaction, to yield well-defined conjugates [198]. The nanotubes were prepared from a range of polymers including poly(butyl acrylate), poly(dimethylamino ethyl acrylate), poly(acrylic acid), poly(styrene) and poly(hydroxyethyl

acrylate) [198]. The polymer was used to shield the peptide core from the solvent and to put a strain on the peptide core through steric repulsions. Figure 1.11 shows cyclic peptide-polymer nanotubes designed with two different polymeric chains which resulted in hybrid nanotubes consisting of a cyclic peptide core surrounded by a polymeric external shell. The external shell of the nanotube assumed two different faces, one where the polymeric chains are 'demixed' (Figure 1.11(A)) and the other mixed (Figure 1.11(B)) [199]. The peptides were able to assemble as artificial pores in lipid bilayers which could be useful for intracellular delivery of small molecules or drugs [200].

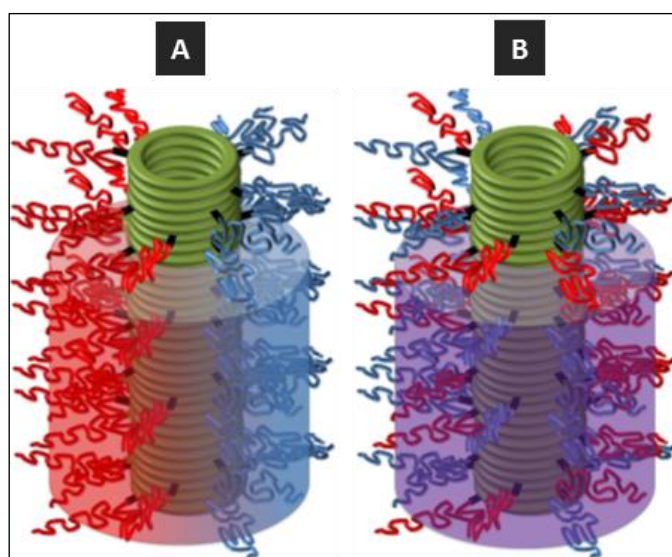


Figure 1.11: Cyclic α -peptide–polymer nanotubes with two different faces. (a) “Demixed” assembly and (b) “mixed” or hybrid assembly (adapted from reference [199]).

1.4 Peptide amphiphiles/surfactant-like peptides

Peptide amphiphile is a term used to describe a molecule that comprises a hydrophobic lipid chain coupled to a hydrophilic oligopeptide sequence [20, 201-206]. Peptide amphiphiles can self-assemble into a range of nanostructures including nanofibres [19, 207, 208], nanotubes [203], twisted and helical ribbons [209], micelles [210] and nanotapes [211]. The most widely studied class of peptide amphiphiles consist of one alkyl tail that is attached to the N-terminus which can self-assemble in water and through the influence of pH [212], light [213],

temperature [214], enzyme [215] and ionic strength [20] with chemical diversity that is well tolerated within the new nanostructure [216].

The first example of a α -peptide amphiphile was reported in 1995 by Tirrell and co-workers, in which a dialkylester tail was appended to an α -peptide sequence from collagen which resulted in the assembly of a monolayer at the air-water interface [217]. Thereafter, the Stupp Laboratory has made significant contributions to understanding the self-assembly properties of α -peptide amphiphiles [25, 203, 206, 218]. Figure 1.12(A) shows the chemical structure of a typical peptide amphiphile molecule, which is generally composed of four key structural regions [201]. The first segment is the hydrophobic domain, which consists of a long, saturated alkyl tail. The second segment is adjacent to the alkyl tail and consists of a short α -peptide sequence that promotes hydrogen bonding by the formation of intermolecular β -sheets. The third segment contains acidic or basic α -amino acids to provide charge and enhance solubility in water and also to trigger structural changes such as gelation through pH changes or addition of salts. Finally, the fourth segment, at the C-terminus, is used to integrate a bioactive signal, which may consist of an epitope that interacts with cell receptors to bind proteins or biomolecules, or a pharmacological agent [201, 203].

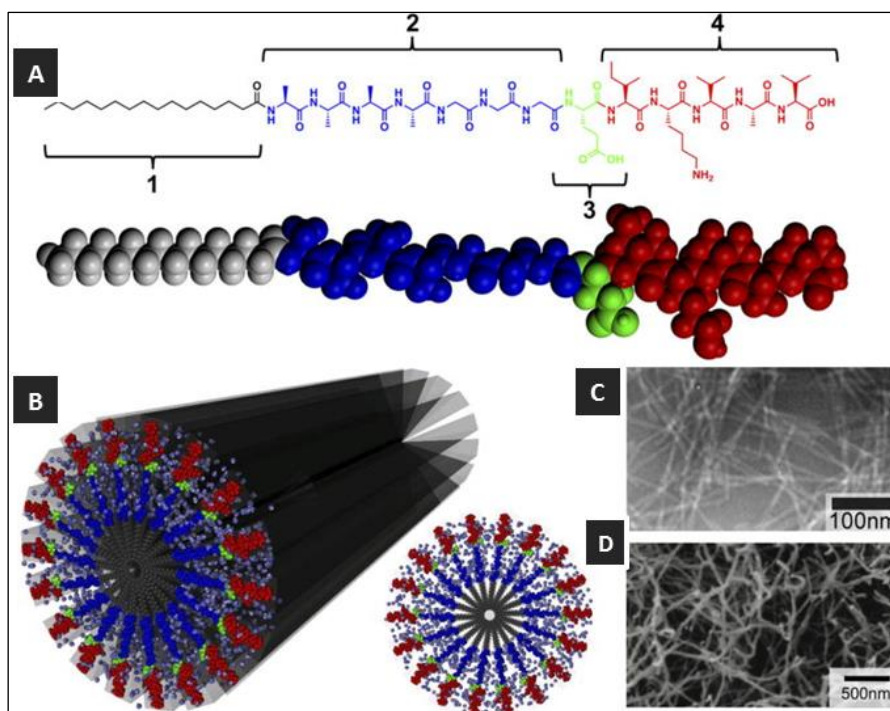


Figure 1.12: Molecular structure and self-assembly of peptide amphiphile. (A) Chemical structure with four regions, (B) molecular graphics of self-assembled nanofibre as well as illustration of the cross-section of this fibre, (C) TEM micrograph and (D) SEM micrograph of C₁₆-AAAAGGGEIKVAV-COOH (adapted from reference [201]).

When dissolved in water, the hydrophobic alkyl tails drive the self-assembly of the peptide amphiphile molecules resulting in hydrophobic collapse and hydrogen bond formation between α -amino acids in the β -sheet domain [49, 219]. Transmission electron microscopy (TEM) and scanning electron microscopy (SEM) (Figure 1.12(C) and (D)) shows self-assembled cylindrical nanofibres with a diameter of 6–10 nm and many micrometers in length in which the molecules are tightly packed with the hydrophobic tail and peptide segment oriented toward the core and aqueous environment respectively. This enabled the precise display of biological signaling epitopes attached to the terminus of the peptide segment at the surface of the fibre.

The molecular mechanism involved in the formation of the cylindrical nanofibres is shown in Figure 1.13 which was described based on simulation studies in aqueous solution [203, 219]. The model takes into account only hydrophobic interactions and intermolecular hydrogen bonding which are predominant in α -peptide amphiphile self-assembly. Micelles are obtained when hydrophobic interactions are employed in the absence of any hydrogen bonding (Figure

1.13(b)). In contrast, when only hydrogen bonding was involved, a broad distribution of 1D β -sheet resulted from stepwise aggregation of monomers (Figure 1.13(f)). When both hydrophobic interactions and hydrogen bonding coexist in a system, the phase properties and self-assembly kinetics differ depending on the strength of each. For example, micelles formed with random β -sheets interspersed in a relatively weak hydrogen bonding system (Figure 1.13(b)), while any increase in the hydrogen bonding energy breaks the spherical symmetry and eventually results in long 1D cylindrical nanofibres (Figure 1.13(d)). This combined effect of intermolecular hydrogen bonding among the peptide segments and the hydrophobic collapse of alkyl tails leads to the formation of cylindrical nanofibres in aqueous solutions [203].

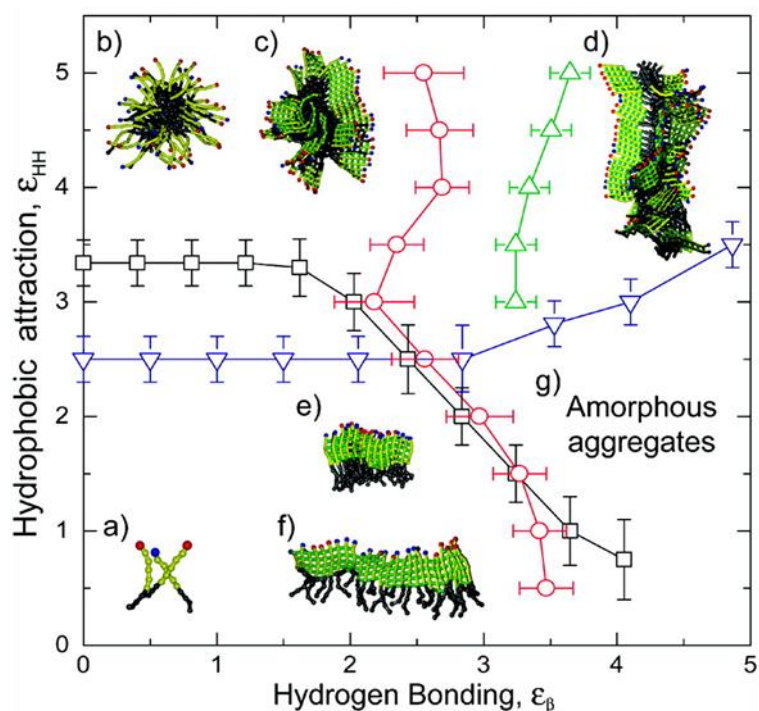


Figure 1.13: Schematic phase diagram of α -peptide amphiphile from molecular simulation studies. (a) Free molecules, (b) spherical micelles, (c) micelles with β -sheets, (d) long cylindrical fibres, (e) stacks of parallel β -sheets, (f) single β -sheets, and (g) the amorphous aggregate phase (adapted from reference [219]).

The Stupp's laboratory has extensively studied a broad range of α -peptide amphiphiles, using various conditions to induce self-assembly into fibrous scaffolds reminiscent of the ECM [50, 220, 221]. Translating the supramolecular assemblies of peptide amphiphiles as candidates

for clinical applications are still being investigated by modifying and tuning the molecular structure for specific therapeutic target. The domain that is most frequently modified in order to incorporate bioactive epitope is the C-terminal region. The bioactive sequences selected are based on their ability to promote regeneration by favouring adhesion or proliferation of a specific cell type, facilitate the binding or delivery of a specific growth factor, signaling protein, and activate endogenous repair mechanisms within a diseased tissue [201]. An example is the self-assembly of a bioactive α -peptide amphiphile with the sequence C₁₆-V₃A₃K₃RGDS which formed nanofibres. The RGDS-presenting nanofibres demonstrated enhanced viability, proliferation and adhesion of associated bone marrow-derived stem and progenitor cells for ischemic diseases [221]. Another α -peptide amphiphile was synthesised with a laminin-derived IKVAV epitope sequence, which provided neural cells with the signal that is known to play a significant role in neurite growth, cell attachment, migration, and differentiation. The scaffold induced very rapid differentiation of cells into neurons for spinal cord injury by promoting axonal regeneration in the damaged spinal cord [204].

Similarly, Hartgerink and colleagues investigated the role of hydrogen bonding and amphiphilic packing in the self-assembly of α -peptide amphiphiles using the sequence C₁₆-G₇ERGDS [216]. They found that the four amino acid residues next to the hydrophobic tail formed β -sheets by hydrogen bonding in the nanofibre. When the hydrogen bonds were disrupted, the ability to form elongated cylindrical nanostructure was eliminated and, spherical micelles were formed instead. The hydrogen bonding from the backbone amides was prevented by removing specific amide hydrogen atoms and substituting them with methyl groups. Other groups have reported the control of α -peptide amphiphile self-assembly using different hydrophobic alkyl chain lengths [26, 222-224].

Other research groups have exploited new design motifs, for example Hamley and colleagues synthesised an α -peptide amphiphile without the β -sheet forming region, C₁₆-KTTKS, derived from collagen. The monomer self-assembled into tape-like structures and spherical micelles. Circular dichroism (CD) spectra at both pH 4 and 7 revealed β -sheet secondary conformation, which was promoted by intermolecular hydrogen bonding between the pentapeptide headgroup [212]. This group also reported a different α -peptide amphiphile with the sequence C₁₆-YEALRVANEVTLN that was derived from the last 13 α -amino acids of the C-terminus of lumican [225]. Twisted and curved nanotapes were observed in which small angle

X-ray scattering (SAX) and fibre X-ray diffraction (XRD) revealed the internal packing order of the nanotapes to contain interdigitated bilayers of the peptide amphiphile molecules. Tirrell and co-workers also reported a different class of α -peptide amphiphile synthesised with diglycine and diethylene oxide spacers and denoted as C₁₆GSH and C₁₆EOSH respectively [18]. A pH-responsive hydrogel was obtained in which histidine residues were used as molecular switches. At pH 7.4, more than 90% of the imidazoles were in the basic form and capable of hydrogen bonding and the α -peptide amphiphiles self-assembled to give nanorods and ribbons.

1.4.1 Isomeric α -peptide amphiphile assemblies

Isomeric peptides are compounds that have an identical chemical composition but different sequence. In 2014, Stupp and colleagues reported the use of isomeric tetrapeptide amphiphiles as a molecular building block to create supramolecular 1D nanostructures [22]. Four α -peptide amphiphile isomers, with identical composition but with different amino acid sequence, self-assembled into different types of 1D nanostructures by only switching the α -amino acid sequence order. Figure 1.14 shows the self-assembled features of the isomeric α -peptide amphiphiles in which alternating hydrophobic and hydrophilic α -amino acid sequences C₁₆-VEVE and C₁₆-EVEV formed nanobelts with an average width of \sim 140 nm and twisted ribbon morphology with an average width of \sim 60 nm respectively. By comparison non-alternating α -amino acids C₁₆-VVEE and C₁₆-EEVV, self-assembled into cylindrical nanofibres with a diameter of \sim 9 nm and \sim 18 nm respectively. CD measurements for all the α -peptide amphiphiles in aqueous solution revealed a β -sheet conformation due to intermolecular hydrogen bonding which favours cylindrical nanofibre formation.

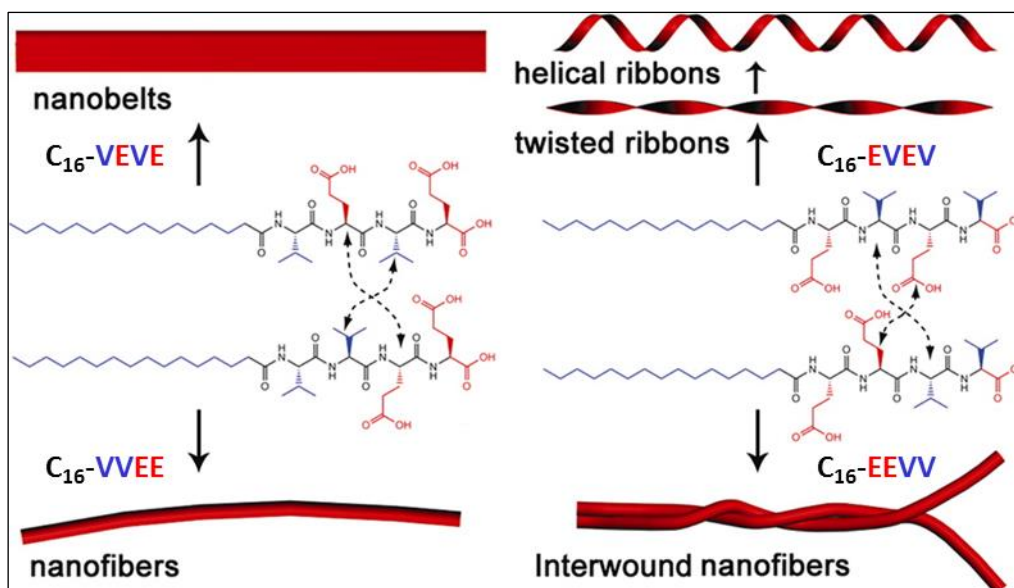


Figure 1.14: Schematic representation of isomeric α -peptide amphiphiles comprising four different α -peptides monomers that self-assembled into 1D nanostructures (adapted from reference [22]).

The observed supramolecular architectures were proposed to be due to two principles of molecular design. Firstly, the monomers with an alternating sequence of hydrophobic and hydrophilic α -amino acids, self-assembled to flat nanostructures which were attributed to the dimerization of two molecules caused by the association of hydrophobic valine surface. The dimerized molecules with two alkyl tails tended to assemble further into a flat morphology that eliminated the interfacial curvature between the peptide segments and the alkyl tails [22]. The disruption of this structural motif leads to the formation of cylindrical nanofibres resulting from the combination of alkyl tail-induced hydrophobic collapse and intermolecular hydrogen bonding among peptide segments. Secondly, the first α -amino acid connected to the alkyl tail played a critical role in determining the final nanostructure. When the glutamic acid was placed next to the alkyl chain, steric effects and electrostatic repulsion among the side chains of glutamic acid had a greater effect on the internal packing of molecules within the self-assembled structure. The increased repulsions were considered to have limited the lateral growth of the assembled structures, leading to the formation of twisted ribbons. Wide-angle X-ray diffraction of C_{16} -VEVE and C_{16} -EVEV assemblies also revealed that the alkyl tails within the nanobelts were packed in an interdigitated pattern due to the innermost reflection that corresponds to a spacing of 39.29 Å. However, the XRD for C_{16} -EVEV assemblies revealed

only one reflection peak at 4.71 Å which corresponds to β -sheet conformation and this implies that the molecules were packed more loosely within the twisted ribbons [22]. These results highlighted the significance of modifying α -peptide amphiphile monomer in order to direct the final self-assembly.

1.4.2 pH-Dependent self-assembly of peptide amphiphiles

Apart from modifying the chemical composition of building blocks, variation in the solution conditions is another important strategy that has been used to switch the self-assembly of α -peptide amphiphiles [18, 212, 226-231]. An example is the lateral self-assembly of 6 α -peptide amphiphiles at pH 4, 11 and 13 that was reported by Chen et al., 2015. The designed sequences were, $C_{16}\text{-A}_4\text{K}_4\text{G(RADA)}_n$ (where $n = 1, 2$ or 3), $C_{16}\text{-A}_4\text{K}_4\text{GRA}_2\text{D}_2\text{A}_2\text{R}$, $C_{16}\text{-A}_4\text{K}_4\text{G(RA)}_2\text{(RA)}_2$ and $C_{16}\text{-A}_4\text{K}_4\text{G(RGDS)}_2$ [229]. The surface charge of the individual α -amino acids was selectively altered as the pH was raised above or below the pKa values of arginine, lysine and aspartic acid. At pH 4, micellular formation occurred (Figure 1.15(b) and (c)). Since the pKa values of lysine and arginine are 10.67 and 12.1 respectively, at pH 11, aspartic acid and lysine residues were deprotonated while the arginine residues remain protonated (Figure 1.15(e)). The sequence $C_{16}\text{-A}_4\text{K}_4\text{G(RADA)}_n$ contained alternating positive and negative charges at pH 7 and this enabled interdigitating and bundling of nanofibres due to electrostatic attraction. At pH 13, only the negatively charged surface was created from the deprotonation of aspartic acid and this prevented lateral assembly due to electrostatic repulsion (Figure 1.15(g)). The lateral assembly of these α -peptides was controlled by designing α -peptide amphiphiles with opposite charges using arginine and aspartic acid.

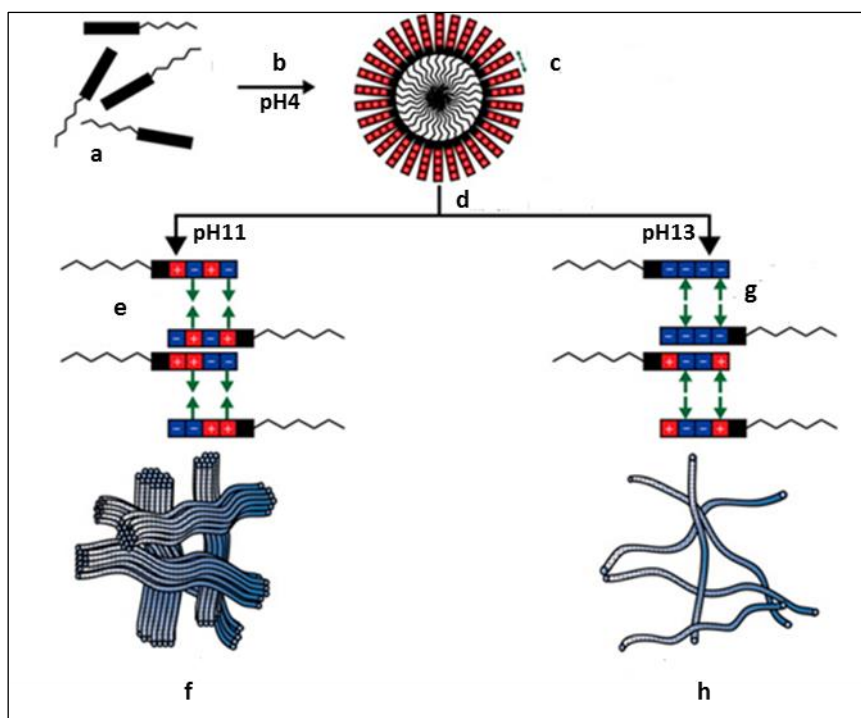


Figure 1.15: Schematic diagram of pH controlled self-assembly. (a) α -Peptide amphiphile monomer, (b) formation of micelles at pH 4, (c) repulsion of positively charged lysine, (d) formation of nanofibres when pH was greater than pKa, (e) attraction of charged Arg or Asp residues, (f) lateral assembly of nanofibres into bundles, (g) repulsion between residues with identical charges and (h) absence of lateral assembly (adapted from reference [229]).

In another report, Ghost et al., 2012 developed a series of peptide amphiphiles that transformed from spherical micelles into nanofibres when the pH was reduced from 7.4 to 6.6 in isotonic salt solution (Figure 1.16) [232]. This was achieved by balancing hydrophobic and hydrogen-bonding forces, and the repulsive electrostatic and steric forces which resulted in rapid and reversible morphological changes. The phase diagram (Figure 1.16(C)) represents the overall influence of concentration and pH on the nature of the self-assembly. This was obtained by critical aggregation concentration (CAC) measurements performed at pH 4.0–10.0, and CD spectra at 10–30 μ M concentrations. The transition points were determined from both techniques and then plotted to generate a concentration versus pH phase diagram.

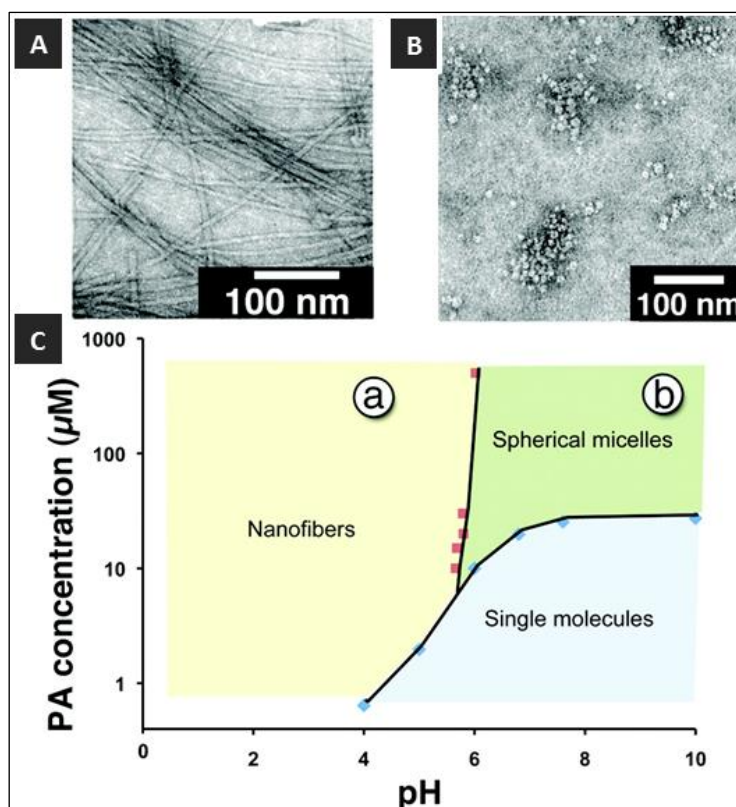


Figure 1.16: TEM images of pH-controlled self-assembly measured at pH (a) 4.0 and (b) 10.0 and (c) phase diagram of concentration against pH (adapted from reference [232]).

Dehsorkhi et al. also reported the transition in nanostructures driven by pH changes that were observed for the α -peptide amphiphile with the sequence C_{16} -KTTKS [212]. At pH 3, the α -peptide amphiphile formed flat tape-like structures, while at pH 4 it self-assembled into twisted right-handed structures. These twisted structures transformed again to flat tape-like structures at pH 7. In contrast, spherical micelles were observed at pH 2. In another study, Deng et al. also reported the morphological transition of a α -peptide amphiphile with the sequence of C_{12} -EVHHQKL [233]. At pH 3 and pH 10, the α -peptide amphiphile self-assembled into nanofibrils and nanoribbons respectively. There are several other strategies that have also been used for tuning the self-assembly of α -peptide amphiphiles in order to obtain new morphologies, some including changes in response to temperature [214], light [213] and enzyme action [215].

1.5 β -peptides

β -Peptides are polyamides composed of β -amino acid which differ from α -amino acids due to the presence of an additional carbon atom in the backbone [234, 235]. The extra CH_2 group (Figure 1.17) is inserted between the amino and α -carboxy termini [235, 236]. The side chains can be positioned at either the α - or β -carbon, resulting in either β^2 or β^3 -amino acids [234, 237].

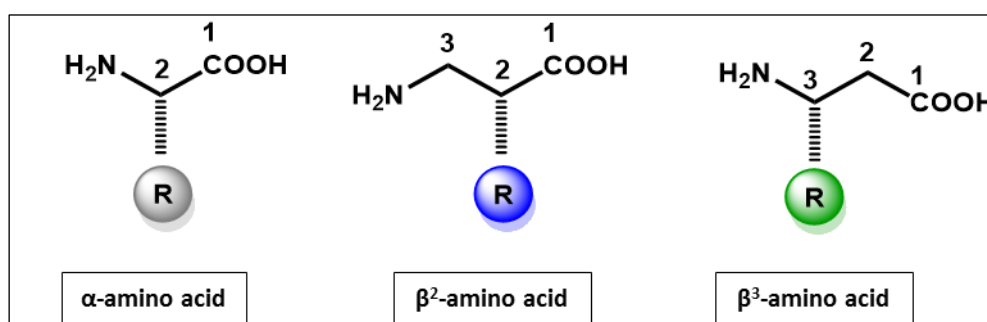


Figure 1.17: Structural features of α -amino acid, β^2 and β^3 -amino acids.

The synthesis of chiral β -amino acids from the corresponding α -amino acids by Arndt Eistert homologation has previously been established by the Seebach and Gellman groups [43, 45, 238, 239]. The incorporation of an additional carbon atom results in the increase in the number of possible compositional and configurational isomers [240] which are R or S isomers at either the α -(C^2) carbon or the β -(C^3) carbon which gives a total of 4 possible isomers for any given side chain [240, 241].

1.5.1 Secondary structures of β -peptides

β -Peptides have been shown to adopt well-defined helical structures stabilised by hydrogen bonding [242, 243]. There are at least five different helices known for β -peptides namely; 8-helix, 10-helix, 12-helix, 10/12-helix and 14-helix (Figure 1.18) [235, 243, 244] and are identified based on the number of atoms in the hydrogen-bonded patterns. The oligomers of β^3 -peptides, in particular, are predominantly defined by a 14- and 12-helical conformation [235, 245]. The 14-helix is stabilised by hydrogen bonding between an amide proton (HN) at

position i and the main chain carbonyl (CO) at position $i+2$, forming a 14-membered pattern [235]. Similarly, the 12-helix is stabilised by hydrogen bonds between the backbone amides (HN) at positions i and $i+3$ (CO) [235]. The structural features of the 12-helix, 10/12-helix and 14-helix are shown in Figure 1.19 and the geometrical parameters for 14-helix, 12-helix, 10-helix and α -helix are shown in Table 1.1. The overall structure of the 14-helix differs from that of the α -helix with a slightly wider radius (14-helix = 2.7 Å and α -helix = 2.2 Å) a lower number of residues per turn (14-helix = 3.0 Å and α -helix = 3.6 Å) and a shorter rise per residue for a given chain length than the α -helix (14-helix = 1.56 Å and α -helix = 1.5 Å). The 12-helix has a radius of 2.3 Å and consists of 2.5 residues per turn with a rise per residue of 2.1 Å [235].

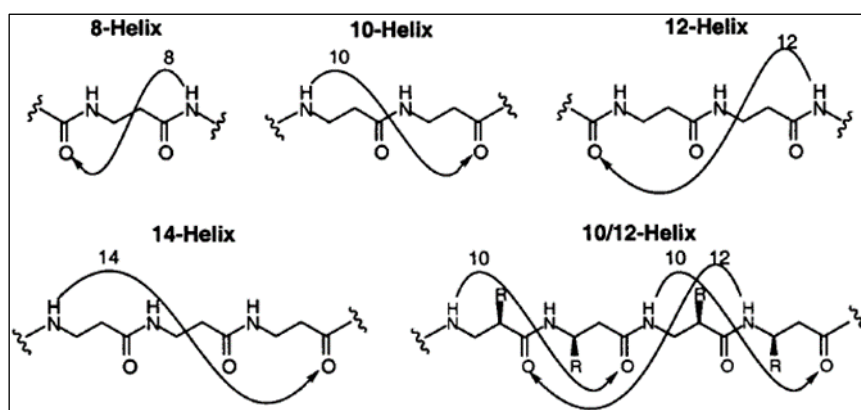


Figure 1.18: Nomenclature for β -peptide helices based on hydrogen-bonding patterns (adapted from reference [235]).

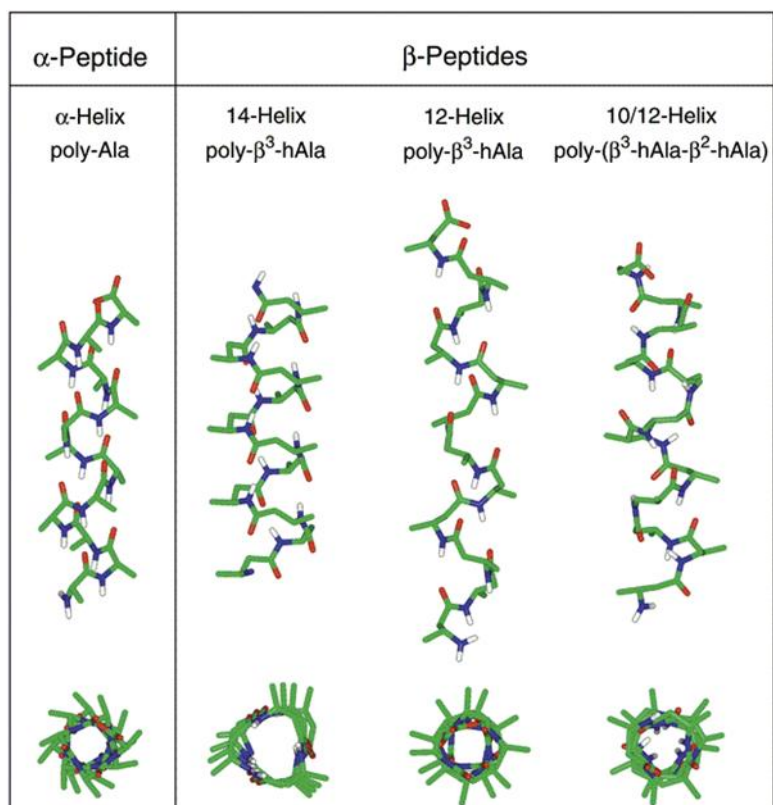


Figure 1.19: Structure of the α -helix, 14-helix, 12-helix, and 10/12-helix. Carbon atoms are shown in green, nitrogen in blue, and oxygen in red. The hydrogens are omitted for clarity, except for the white coloured amide hydrogens (adapted from reference [235]).

The 14-helix is characterised by approximately 3 residues per turn which result in the alignment of the side chains of every third residue directly along one face of the helix (Figure 1.19) [235]. Although less prevalent, other secondary structural motifs that have been observed in β -peptides are parallel sheet [246, 247] and β -hairpin [248] conformations. Following the pioneering work of Seebach and Gellman, several research laboratories are presently exploiting the use of β -peptides beyond just the secondary structure to develop higher ordered structures by appropriate design of β -peptide oligomers.

Table 1.1: Geometrical parameters for β -peptide helices and α -helix (adapted from references [235] and [249]).

Geometrical parameter	14-helix	12-helix	10-helix	α -helix
Residue/turn	3.0	2.5	2.6	3.6
Rise/residue (Å)	1.6	2.1	2.3	1.5
Pitch (Å)	5.0	5.6	6.0	5.5
Helical radius (Å)	2.7	2.3	-	2.2

1.5.2 β -Peptide bundles

A β^3 -peptide bundle arises from the cooperative folding of β^3 -peptides into higher-order quaternary assemblies in solution [250]. The folded structures are notable for their protein-like properties which bury their hydrophobic surfaces to the interior. The Zwit-1F β -peptide bundle is an example which consists of 8 identical β^3 -peptides, each folded into a 14-helix, arranged as a pair of tetra-helix “hands” at a 90° angle relative to each other. The control over the structure (by changing individual components) and assembly of β -peptides could lead to a new generation of biomaterials for specific applications.

The initial steps towards creating a specific helical-bundle with β -amino acid oligomers were reported by Gellman and co-workers using two oligomers of optically active trans-2-aminocyclohexanecarboxylic acid (ACHC) that assembled into a tetramer and a hexamer [251]. Similarly, a 10-residue β -peptide designed to adopt amphiphilic helical conformation was also observed to self-assemble in aqueous solution to form tetrameric and hexameric bundles [252]. This group has also demonstrated the self-assembly of helical quaternary bundles that are arranged in a parallel orientation formed by oligomers containing a mixture of α/β -peptides in different combinations in aqueous solution and in the crystalline state [253-255]. Subsequently, Cheng and Degrado also reported the folded structure of 14-helical β -oligomers that were stabilised via long-range interhelical interactions and stapled together by a disulfide bond [256].

The first stoichiometrically defined β -peptide bundle with several high-resolution octameric structures and with full biophysical characterisation was reported by Schepartz and coworkers [257-260]. The octameric bundles were made up of β^3 -decapeptides with three

distinct faces: a hydrophobic β^3 -Leu face, a salt bridge face of alternating β^3 -Orn and β^3 -Asp residues, and an aromatic face that contains two β^3 -Tyr or β^3 -Phe residues. The β -peptide oligomer assembled as antiparallel helices in which β^3 -Leu side chains formed the core of the bundle. Schepartz et al. also described a series of β^3 -peptides, which assembled into octameric β -peptide bundles of known structure and high stability with the sequences defined as Acid-1Y, Base-1F, Zwit-1F, Acid-1Y, Zwit-EYYO and Zwit-EYYK (Figure 1.20). The observed thermodynamic and kinetic stability of the structure rendered it an ideal prototype for the design and functionalisation of a new series of protein-like β -peptide bundles.

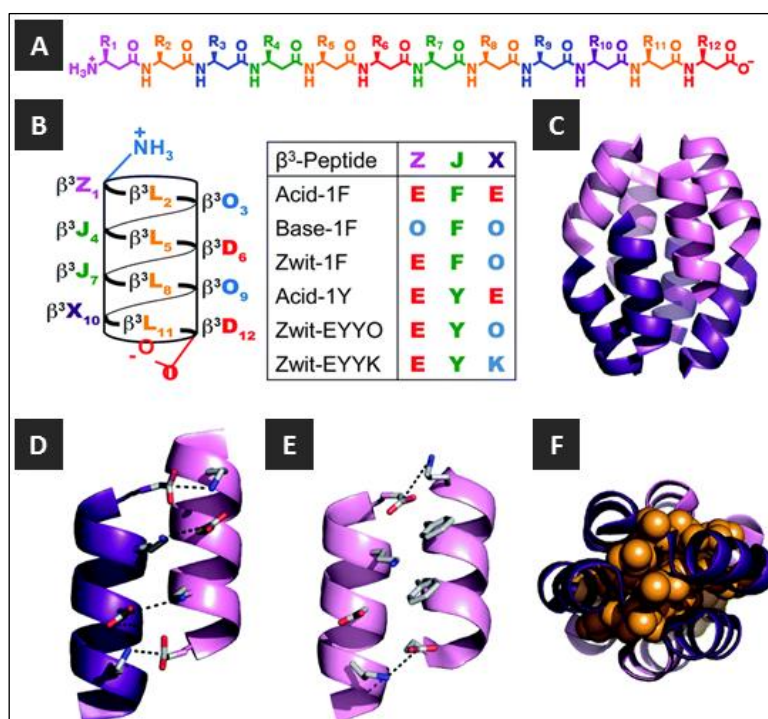


Figure 1.20: (a) Chemical structure of β -dodecapeptide, (b) helical net representation of a β -dodecapeptide folded into a 14-helix with the different β^3 -peptide sequences (c) β -peptide bundle, the homo-octamer of Zwit-1F, (d and e) close-up view of salt-bridging interactions at the (d) anti-parallel and (e) parallel helical interfaces of Zwit-1F, and (f) space-filling model (orange) showing tight packing of β^3 -homoleucine side-chains in the Zwit-1F core (adapted from references [258] and [250]).

As a follow up to this model, the first functional β^3 -peptide helical bundle was recently reported [261]. The β^3 -peptide bundles were capable of both substrate binding and catalysis of 8-acetoxypyrene-1,3,6-trisulfonate which releases the fluorescent product pyranine upon ester hydrolysis. This is useful for optical sensor applications and a fluorescent pH indicator

for the physiological range [261]. A combination of kinetic and high-resolution structural analysis suggested the presence of an esterase-active site composed of three functional groups, positioned at separate strands of the octameric bundle structure [261].

1.5.3 Supramolecular self-assembly of β -peptides

Supramolecular self-assembly of β -peptides is the formation of a well-defined large structure from the organisation of β -peptide monomers. Supramolecular structures are held together by hydrogen bonding, π - π stacking, metal-ligand interactions, electrostatic forces, strong dipole-dipole association, and hydrophobic forces [3]. In the context of materials, supramolecular self-assembly indicates that monomers are programmed by design to create a higher ordered structure with incorporated functional property [262]. Supramolecular self-assembly of β -peptides can occur leading to materials ranging from nano- to macroscopic in dimension.

One of the earliest examples of a supramolecular self-assembling of β -peptide was reported by Gellman et al., with the hierarchical organisation and lyotropic liquid crystalline behavior of self-assembling β -peptides composed of ACHC [263, 264]. The designed peptide contained a minimum of three repeats of the ACHC-ACHC- β^3 -Lys triad (Figure 1.21). This peptide folded into a 14-helical conformation, leading to the segregation of the hydrophobic cyclohexyl ring and hydrophilic β^3 -Lys residue. The cyclohexyl units of neighboring β -peptide interdigitated to form a zipper-like motif referred to as a “cyclohexyl zipper” that was achieved by intermolecular association mediated by the amphiphilic nature of the molecule. Structural analysis revealed the existence of two different types of species, globular aggregates, and nanofibres which are the predominant self-assembled structure that leads to LC phase formation [263].

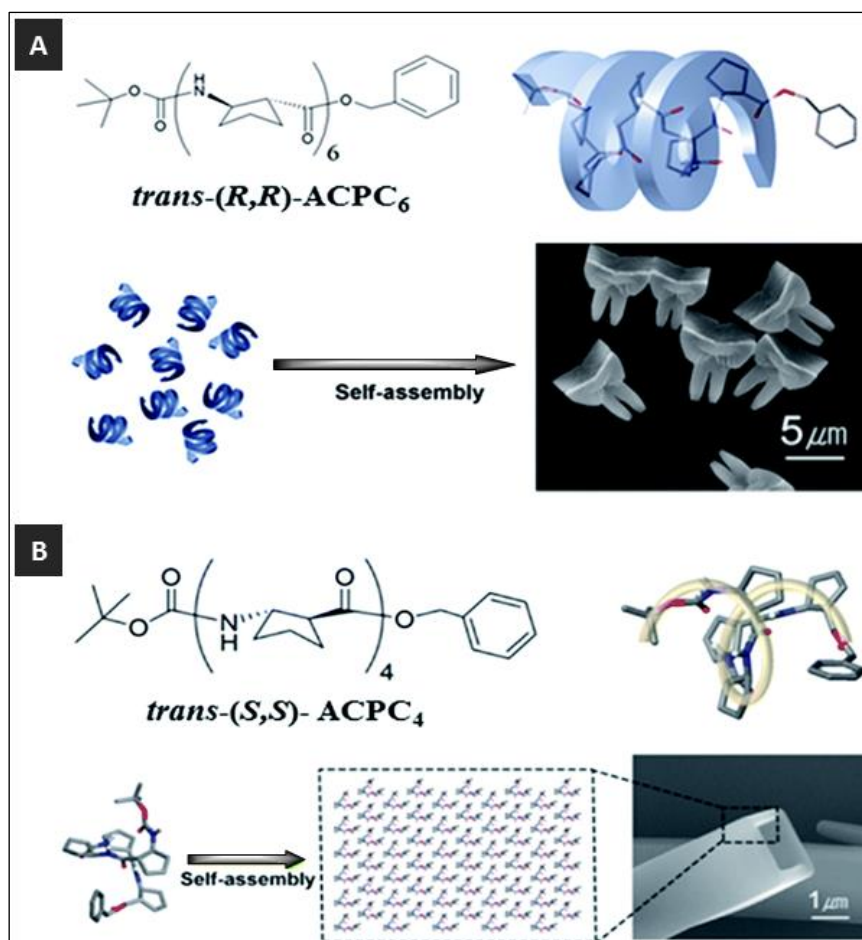


Figure 1.22: (A) Self-assembly of tooth-shaped architectures from *trans*-(R,R)-ACPC₆ and (B) self-assembly of rectangular microtubes from *trans*-(S,S)-ACPC₄ (adapted from references [270], [268] and [265]).

1.6 *N*-acetyl β^3 -peptide assemblies

N-acetyl capped β^3 -peptide assembly is a unique process of supramolecular self-assembly which was first reported in 2013 [46]. Capping the *N*-terminus with an acetyl group provided a 3-point hydrogen bonding stabilisation for the 14-helical conformation that is associated with β^3 -peptides (Figure 1.23) as suggested by X-ray crystallography [46]. The *N*-acetyl group plays a critical role by providing the third donor-acceptor interaction pair and thus promotes axial self-assembly and fibre growth into higher ordered structures. TEM and atomic force microscopy (AFM) revealed that the peptides with a free amine showed no signs of self-assembly, whereas the *N*-acetylated peptides showed self-assembled fibrous morphologies of varying sizes and shapes in several solvents [46, 237]. The structures of two tripeptide monomers could be superimposed with a β -hexapeptide to exhibit a typical left-handed 14-

helical structure with exactly two turns, and internally supported by $i, i+3$ intramolecular hydrogen bonds.

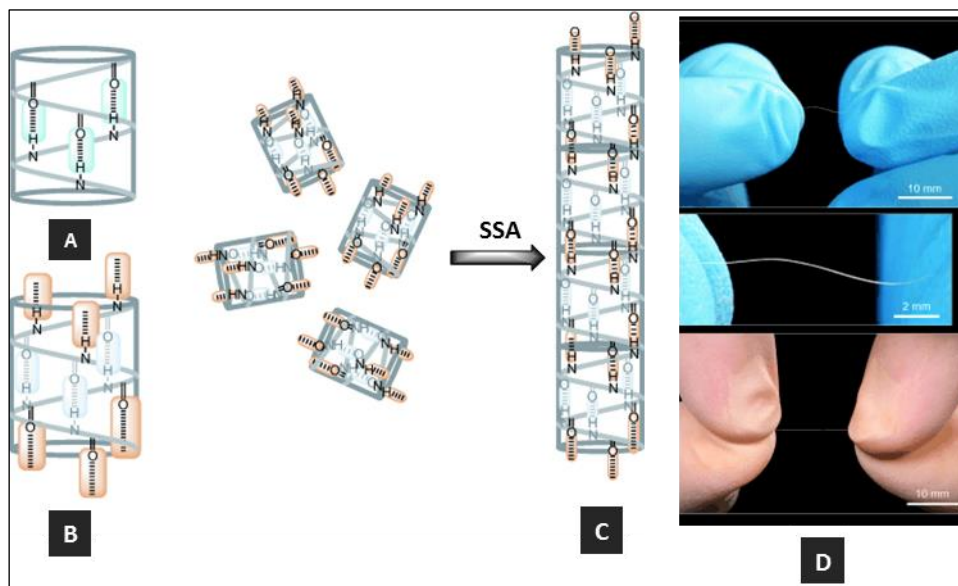


Figure 1.23: Self-assembly of 14-helical β^3 -peptides. (A) Intramolecular hydrogen bonding motif for helix stabilisation, (B) supramolecular self-assembly (SSA) by intermolecular hydrogen-bonding motif (C) fibre formation by head to tail hydrogen bonding, and (D) macroscopic fibres formed by β^3 -hexapeptide A_C -WKVWEV-OH (adapted from reference [46]).

The β^3 -peptides self-assembled in water and methanol resulting into fibre formation from several micrometers up to 3 cm in length and approximately 0.25 mm in diameter within one hour of incubation (Figure 1.23(D)). The large fibrillary structures self-assembled from β^3 -peptides monomers which comprised of β^3 -amino acids in multiples of three residues [46]. The head-to-tail model of β^3 -peptides self-assembly was shown to be persistent under a variety of conditions with fibres growing into large structures. Similarly, a β^3 -tripeptide with the sequence β^3 Leu- β^3 Ile- β^3 Ala (LIA), revealed the same trend of head-to-tail self-assembly in different solvents [271-273].

This “head-to-tail” self-assembly model, in combination with the unique helical structure of the β^3 -peptide monomer, offers the opportunity for the introduction of a wide variety of functions by modifying the side chains of the β^3 -amino acids, without perturbation of the self-assembly motif [234]. The inherent flexibility in this unique design, as well as ease of

synthesis, provide a new strategy for the development of novel bio- and nanomaterials via *N*-acetyl β^3 -peptide supramolecular self-assembly.

1.6.1 Functionalised β^3 -peptide materials

Supramolecular self-assembly of β^3 -peptides provides a strategy for developing new materials for future applications by the incorporation of specific functional components onto building blocks without disrupting the structural motif and fibre stability. Luder et al., 2016 reported the decoration of *N*-acetyl β^3 -tripeptides (without lipidation of the monomer) with either RGD or IKVAV conjugated to the side chain [274]. The β^3 -tripeptides spontaneously self-assembled to give nanofibres with biologically active signals that supported the growth of cardiac fibroblasts and bone-marrow derived macrophage cells. Modulation of these biological signals led to the optimisation of cellular attachment and proliferation. Figure 1.24 shows the proposed self-assembly model for the decorated β^3 -peptide nanofibres with side chain functionalised with α -peptide cell-attachment signals RGD or IKVAV. The integrity of each β^3 -tripeptides was maintained and supramolecular self-assembly of these β^3 -tripeptides was unperturbed even with the inclusion of α -peptides onto the side chain.

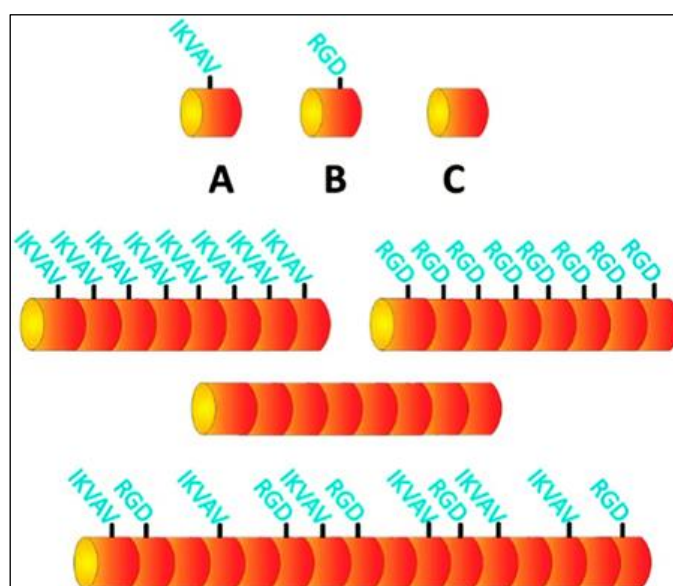


Figure 1.24: Design and self-assembly model of decorated β^3 -tripeptide nanofibres with side chains functionalised with cell-attachment signals IKVAV (peptide A) and RGD (peptide B). A non-decorated β^3 -tripeptide with the sequence LIA (peptide C) was used as control [274].

During the course of this thesis, two papers were published [47, 275]. The first was functionalisation of β^3 -tripeptide with a C_{14} alkyl chain by coupling onto the side chain of β^3 -peptide backbone. Figure 1.25 shows the self-assembled nanofibres of *N*-acetylated- β^3 -tripeptides functionalised with a C_{14} hydrophobic alkyl tail. The peptide formed a hydrogel (Figure 1.25(C)) at a concentration of 10 mg mL^{-1} in phosphate-buffered saline (PBS) pH 7.4 and maintained a stable structure under the physiological condition that sustained neuronal cell growth and differentiation [47, 275].

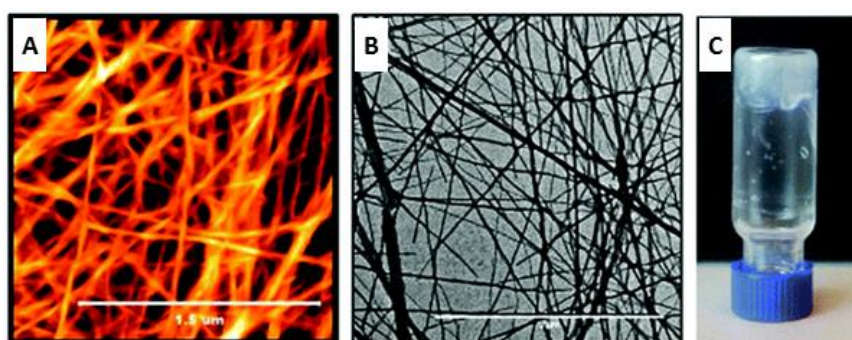


Figure 1.25: Supramolecular self-assembled of *N*-acetyl- β^3 -tripeptide functionalised with a hydrophobic acyl chain, (A) AFM image of nanofibres, (B) TEM image of nanofibres and (C) stable hydrogel (adapted from reference [275]).

The second was the dual functionalisation of β^3 -tripeptide with a C_{14} alkyl chain and a cell signaling epitope, RGD. This was achieved by first synthesising a new β^3 -amino acid with an Allyloxycarbonyl (Alloc) protected aminoethyl amide side chain to allow the orthogonal attachment of two functionalities to the β^3 -tripeptide using solid-phase peptide synthesis [47]. The peptide was dissolved in PBS solution and formed a stable hydrogel at a concentration of 10 mg mL^{-1} . The dual-functionalised β^3 -tripeptide showed enhanced L929 cell (mouse fibroblastic cell line) adhesion by increasing the RGD concentration from 2% to 8% [47].

The design and functionalisation of β^3 -peptides may open a new era of biomaterials that possess proteolytic stability and controlled self-assembly pattern for specific applications.

1.7 Aims of this project

Previous studies involving *N*-acetyl β^3 -peptides exploited the head-to-tail self-assembly motif to form fibrous structures. However, finer control of the overall architecture was required, and the overall aim of this study was to develop a strategy for the control of β^3 -peptide self-assembly.

The specific aims are;

- 1) To synthesise β^3 -peptide amphiphiles using different lengths of alkyl chains, and characterisation of the self-assembled nanostructures
- 2) To investigate the internal molecular packing of self-assembled nanostructures of β^3 -peptide amphiphiles
- 3) To determine the influence of hydrogen bonding and electrostatic interaction during axial and lateral self-assembly of β^3 -peptide amphiphiles.

This thesis comprises three experimental Chapters (2, 3 and 4). Briefly, **Chapter 2** describes the rational design and synthesis of β^3 -peptide amphiphiles using 3 different lengths of hydrophobic alkyl chains (C_{12} , C_{14} , and C_{16}). A series of 12 different peptides were synthesised and the self-assembled morphologies were characterised using AFM and TEM. **Chapter 3** explored the use of nanoindentation by AFM to study the internal molecular packing of self-assembled nanostructures. High-resolution images and dimensions of the internal structural organisation were obtained and compared with calculated values which resulted in a proposed self-assembly model for β^3 -peptide amphiphiles. **Chapter 4** describes the influence of pH changes on axial and lateral self-assembly of β^3 -peptide amphiphiles. Another series of β^3 -peptide amphiphiles were synthesised with a C-terminal amide and the incorporation of β^3 -arginine residues within the sequence. Self-assembly was studied in solution using AFM. **Chapter 5** gives the general conclusions of this project and possible future directions. Overall, this thesis has explored the design, synthesis and structural properties of β^3 -peptide amphiphiles and the results lay the foundation for the future application of these novel materials.

References

1. Whitesides, G.M. and M. Boncheva, *Beyond molecules: Self-assembly of mesoscopic and macroscopic components*. Proceedings of the National Academy of Sciences of the United States of America, 2002. **99**(8): p. 4769-4774.
2. Subramani, K. and W. Ahmed, *Self-Assembly of Proteins and Peptides and Their Applications in Bionanotechnology and Dentistry*. 2012, Elsevier Inc. p. 209-224.
3. Whitesides, G.M. and B. Grzybowski, *Self-assembly at all scales*. Science, 2002. **295**(5564): p. 2418-2421.
4. Liu, L., K. Busutil, S. Zhang, Y. Yang, C. Wang, F. Besenbacher, and M. Dong, *The role of self-assembling polypeptides in building nanomaterials*. Physical Chemistry Chemical Physics, 2011. **13**(39): p. 17435-17444.
5. Woolfson, D.N. and Z.N. Mahmoud, *More than just bare scaffolds: towards multi-component and decorated fibrous biomaterials*. Chemical Society Reviews, 2010. **39**(9): p. 3464-3479.
6. Castillo-León, J., L. Sasso, and W.E. Svendsen, *Self-assembled peptide nanostructures: Advances and applications in nanobiotechnology*. Self-Assembled Peptide Nanostructures. Florida (USA): Taylor & Francis; 2012. p. 65-141.
7. Zhang, S, Self-assembling peptide materials. Amino Acids, Peptides and Proteins, 2012. 37: p. 40-65.
8. O'Leary, L.E.R., J.A. Fallas, E.L. Bakota, M.K. Kang, and J.D. Hartgerink, *Multi-hierarchical self-assembly of a collagen mimetic peptide from triple helix to nanofibre and hydrogel*. Nature Chemistry, 2011. **3**(10): p. 821-828.
9. Yu, S.M., Y. Li, and D. Kim, *Collagen mimetic peptides: Progress towards functional applications*. Soft Matter, 2011. **7**(18): p. 7927-7938.
10. Nagarkar, R.P., R.A. Hule, D.J. Pochan, and J.P. Schneider, *De novo design of strand-swapped β -hairpin hydrogels*. Journal of the American Chemical Society, 2008. **130**(13): p. 4466-4474.
11. Hule, R.A., R.P. Nagarkar, A. Altunbas, H.R. Ramay, M.C. Branco, J.P. Schneider, and D.J. Pochan, *Correlations between structure, material properties and bioproperties in self-assembled β -hairpin peptide hydrogels*. Faraday Discussions, 2008. **139**: p. 251-264.

12. Aulisa, L., H. Dong, and J.D. Hartgerink, *Self-assembly of multidomain peptides: Sequence variation allows control over cross-linking and viscoelasticity*. *Biomacromolecules*, 2009. **10**(9): p. 2694-2698.
13. Kumar, V.A., S. Shi, B.K. Wang, I.C. Li, A.A. Jalan, B. Sarkar, N.C. Wickremasinghe, and J.D. Hartgerink, *Drug-Triggered and Cross-Linked Self-Assembling Nanofibrous Hydrogels*. *Journal of the American Chemical Society*, 2015. **137**(14): p. 4823-4830.
14. Bakota, E.L., O. Sensoy, B. Ozgur, M. Sayar, and J.D. Hartgerink, *Self-assembling multidomain peptide fibers with aromatic cores*. *Biomacromolecules*, 2013. **14**(5): p. 1370-1378.
15. Hughes, M., H. Xu, P.W.J.M. Frederix, A.M. Smith, N.T. Hunt, T. Tuttle, I.A. Kinloch, and R.V. Ulijn, *Biocatalytic self-assembly of 2D peptide-based nanostructures*. *Soft Matter*, 2011. **7**(21): p. 10032-10038.
16. Smith, A.M., R.J. Williams, C. Tang, P. Coppo, R.F. Collins, M.L. Turner, A. Saiani, and R.V. Ulijn, *Fmoc-diphenylalanine self assembles to a hydrogel via a novel architecture based on π - π interlocked β -sheets*. *Advanced Materials*, 2008. **20**(1): p. 37-41.
17. Rodriguez, A.L., C.L. Parish, D.R. Nisbet, and R.J. Williams, *Tuning the amino acid sequence of minimalist peptides to present biological signals via charge neutralised self assembly*. *Soft Matter*, 2013. **9**(15): p. 3915-3919.
18. Lin, B.F., K.A. Megley, N. Viswanathan, D.V. Krogstad, L.B. Drews, M.J. Kade, Y. Qian, and M.V. Tirrell, *pH-responsive branched peptide amphiphile hydrogel designed for applications in regenerative medicine with potential as injectable tissue scaffolds*. *Journal of Materials Chemistry*, 2012. **22**(37): p. 19447-19454.
19. Hartgerink, J.D., E. Beniash, and S.I. Stupp, *Peptide-amphiphile nanofibers: A versatile scaffold for the preparation of self-assembling materials*. *Proceedings of the National Academy of Sciences of the United States of America*, 2002. **99**(8): p. 5133-5138.
20. Dehsorkhi, A., V. Castelletto, and I.W. Hamley, *Self-assembling amphiphilic peptides*. *Journal of Peptide Science*, 2014. **7**: 453-67.
21. Löwik, D.W.P.M. and J.C.M. Van Hest, *Peptide based amphiphiles*. *Chemical Society Reviews*, 2004. **33**(4): p. 234-245.
22. Cui, H., A.G. Cheetham, E.T. Pashuck, and S.I. Stupp, *Amino acid sequence in constitutionally isomeric tetrapeptide amphiphiles dictates architecture of one-*

- dimensional nanostructures*. Journal of the American Chemical Society, 2014. **136**(35): p. 12461-12468.
23. Da Silva, R.M.P., D. Van Der Zwaag, L. Albertazzi, S.S. Lee, E.W. Meijer, and S.I. Stupp, *Super-resolution microscopy reveals structural diversity in molecular exchange among peptide amphiphile nanofibres*. Nature Communications, 2016. **7**. 11561.
 24. Hartgerink, J.D., E. Beniash, and S.I. Stupp, *Self-assembly and mineralization of peptide-amphiphile nanofibers*. Science, 2001. **294**(5547): p. 1684-8.
 25. Korevaar, P.A., C.J. Newcomb, E.W. Meijer, and S.I. Stupp, *Pathway selection in peptide amphiphile assembly*. Journal of the American Chemical Society, 2014. **136**(24): p. 8540-8543.
 26. Gore, T., Y. Dori, Y. Talmon, M. Tirrell, and H. Bianco-Peled, *Self-assembly of model collagen peptide amphiphiles*. Langmuir, 2001. **17**(17): p. 5352-5360.
 27. Versluis, F., H.R. Marsden, and A. Kros, *Power struggles in peptide-amphiphile nanostructures*. Chemical Society Reviews, 2010. **39**(9): p. 3434-3444.
 28. Zhao, X., F. Pan, H. Xu, M. Yaseen, H. Shan, C.A.E. Hauser, S. Zhang, and J.R. Lu, *Molecular self-assembly and applications of designer peptide amphiphiles*. Chemical Society Reviews, 2010. **39**(9): p. 3480-3498.
 29. Tsutsumi, H. and H. Mihara, *Soft materials based on designed self-assembling peptides: From design to application*. Molecular BioSystems, 2013. **9**(4): p. 609-617.
 30. Shah, R.N., N.A. Shah, M.M. Del Rosario Lim, C. Hsieh, G. Nuber, and S.I. Stupp, *Supramolecular design of self-assembling nanofibers for cartilage regeneration*. Proceedings of the National Academy of Sciences, 2010. **107**(8): p. 3293-3298.
 31. Tysseling-Mattiace, V.M., V. Sahni, K.L. Niece, D. Birch, C. Czeisler, M.G. Fehlings, S.I. Stupp, and J.A. Kessler, *Self-assembling nanofibers inhibit glial scar formation and promote axon elongation after spinal cord injury*. Journal of Neuroscience, 2008. **28**(14): p. 3814-3823.
 32. Holmes, T.C., *Novel peptide-based biomaterial scaffolds for tissue engineering*. Trends in Biotechnology, 2002. **20**(1): p. 16-21.
 33. Mandal, D., A. Nasrolahi Shirazi, and K. Parang, *Self-assembly of peptides to nanostructures*. Organic and Biomolecular Chemistry, 2014. **12**(22): p. 3544-3561.

34. Yu, C.Y., W. Huang, Z.P. Li, X.Y. Lei, D.X. He, and L. Sun, *Progress in self-assembling peptide-based nanomaterials for biomedical applications*. Current Topics in Medicinal Chemistry, 2016. **16**(3): p. 281-290.
35. Panda, J.J. and V.S. Chauhan, *Short peptide based self-assembled nanostructures: Implications in drug delivery and tissue engineering*. Polymer Chemistry, 2014. **5**(15): p. 4418-4436.
36. Roy, A., O.L. Franco, and S.M. Mandal, *Biomedical exploitation of self assembled peptide based nanostructures*. Current Protein and Peptide Science, 2013. **14**(7): p. 580-587.
37. Matson, J.B., R.H. Zha, and S.I. Stupp, *Peptide self-assembly for crafting functional biological materials*. Current Opinion in Solid State and Materials Science, 2011. **15**(6): p. 225-235.
38. Wang, H. and Z. Yang, *Short-peptide-based molecular hydrogels: Novel gelation strategies and applications for tissue engineering and drug delivery*. Nanoscale, 2012. **4**(17): p. 5259-5267.
39. Hook, D.F., P. Bindschädler, Y.R. Mahajan, R. Šebesta, P. Kast, and D. Seebach, *The proteolytic stability of 'designed' β -peptides containing α -peptide-bond mimics and of mixed α,β -peptides: Application to the construction of MHC-binding peptides*. Chemistry and Biodiversity, 2005. **2**(5): p. 591-632.
40. Wiegand, H., B. Wirz, A. Schweitzer, G.P. Camenisch, M.I. Rodriguez Perez, G. Gross, R. Woessner, R. Voges, P.I. Arvidsson, J. Frackenpohl, and D. Seebach, *The outstanding metabolic stability of a ^{14}C -labeled β -nonapeptide in rats - In vitro and in vivo pharmacokinetic studies*. Biopharmaceutics and Drug Disposition, 2002. **23**(6): p. 251-262.
41. Seebach, D., S. Abele, T. Sifferlen, M. Hänggi, S. Gruner, and P. Seiler, *Preparation and structure of β -peptides consisting of geminally disubstituted β 2,2- and β 3,3-amino acids: A turn motif for β - peptides*. Helvetica Chimica Acta, 1998. **81**(12): p. 2218-2243.
42. Seebach, D., A.K. Beck, and D.J. Bierbaum, *The world of β - And γ -Peptides comprised of homologated proteinogenic amino acids and other components*. Chemistry and Biodiversity, 2004. **1**(8): p. 1111-1239.
43. Seebach, D., M. Overhand, F.N.M. Kühnle, B. Martinoni, L. Oberer, U. Hommel, and H. Widmer, *80. β -peptides: Synthesis by Arndt-Eistert homologation with concomitant*

- peptide coupling. Structure determination by NMR and CD spectroscopy and by X-Ray crystallography. Helical secondary structure of a β -hexapeptide in solution and its stability towards pepsin.* Helvetica Chimica Acta, 1996. **79**(4): p. 913-941.
44. Lee, M.R., T.L. Raguse, M. Schinnerl, W.C. Pomerantz, X. Wang, P. Wipf, and S.H. Gellman, *Origins of the high 14-helix propensity of cyclohexyl-rigidified residues in β -peptides.* Organic Letters, 2007. **9**(9): p. 1801-1804.
 45. Appella, D.H., L.A. Christianson, I.L. Karle, D.R. Powell, and S.H. Gellman, *β -Peptide foldamers: Robust helix formation in a new family of β -amino acid oligomers.* Journal of the American Chemical Society, 1996. **118**(51): p. 13071-13072.
 46. Del Borgo, M.P., A.I. Mechler, D. Traore, C. Forsyth, J.A. Wilce, M.C.J. Wilce, M.I. Aguilar, and P. Perlmutter, *Supramolecular self-assembly of N-acetyl-capped β -peptides leads to nano- to macroscale fiber formation.* Angewandte Chemie - International Edition, 2013. **52**(32): p. 8266-8270.
 47. Kulkarni, K., S. Motamed, N. Habila, P. Perlmutter, J.S. Forsythe, M.-I. Aguilar, and M.P. Del Borgo, *Orthogonal strategy for the synthesis of dual-functionalised [small beta]³-peptide based hydrogels.* Chemical Communications, 2016. **52**(34): p. 5844-5847.
 48. Matson, J.B., C.J. Newcomb, R. Bitton, and S.I. Stupp, *Nanostructure-templated control of drug release from peptide amphiphile nanofiber gels.* Soft Matter, 2012. **8**(13): p. 3586-3595.
 49. Rubert Pérez, C., N. Stephanopoulos, S. Sur, S. Lee, C. Newcomb, and S. Stupp, *The Powerful Functions of Peptide-Based Bioactive Matrices for Regenerative Medicine.* Annals of Biomedical Engineering, 2015. **43**(3): p. 501-514.
 50. Cui, H., T. Muraoka, A.G. Cheetham, and S.I. Stupp, *Self-Assembly of Giant Peptide Nanobelts.* Nano Letters, 2009. **9**(3): p. 945-951.
 51. Habibi, N., N. Kamaly, A. Memic, and H. Shafiee, *Self-assembled peptide-based nanostructures: Smart nanomaterials toward targeted drug delivery.* Nano Today, 2016. **11**(1): p. 41-60 .
 52. Brea, R.J., C. Reiriz, and J.R. Granja, *Towards functional bionanomaterials based on self-assembling cyclic peptide nanotubes.* Chemical Society Reviews, 2010. **39**(5): p. 1448-1456.
 53. Woolfson, D.N. and M.G. Ryadnov, *Peptide-based fibrous biomaterials: some things old, new and borrowed.* Current Opinion in Chemical Biology, 2006. **10**(6): p. 559-567.

54. Mason, J.M. and K.M. Arndt, *Coiled Coil Domains: Stability, Specificity, and Biological Implications*. ChemBioChem, 2004. **5**(2): p. 170-176.
55. Lazar, K.L., H. Miller-Auer, G.S. Getz, J.P.R.O. Orgel, and S.C. Meredith, *Helix-turn-helix peptides that form α -helical fibrils: Turn sequences drive fibril structure*. Biochemistry, 2005. **44**(38): p. 12681-12689.
56. Dong, H., S.E. Paramonov, and J.D. Hartgerink, *Self-Assembly of α -Helical Coiled Coil Nanofibers*. Journal of the American Chemical Society, 2008. **130**(41): p. 13691-13695.
57. Potekhin, S.A., T.N. Melnik, V. Popov, N.F. Lanina, A.A. Vazina, P. Rigler, A.S. Verdini, G. Corradin, and A.V. Kajava, *De novo design of fibrils made of short α -helical coiled coil peptides*. Chemistry and Biology, 2001. **8**(11): p. 1025-1032.
58. Woolfson, D.N., *Building fibrous biomaterials from α -helical and collagen-like coiled-coil peptides*. Peptide Science, 2010. **94**(1): p. 118-127.
59. Mondal, S. and E. Gazit, *The Self-Assembly of Helical Peptide Building Blocks*. ChemNanoMat, 2016. **2**(5): p. 323-332.
60. Wu, Y. and J.H. Collier, *α -Helical coiled-coil peptide materials for biomedical applications*. Wiley Interdisciplinary Reviews: Nanomedicine and Nanobiotechnology, 2016: p. 1-17.
61. Woolfson, D.N. and T. Alber, *Predicting oligomerization states of coiled coils*. Protein Science : A Publication of the Protein Society, 1995. **4**(8): p. 1596-1607.
62. Harbury, P.B., T. Zhang, P.S. Kim, and T. Alber, *A switch between two-, three-, and four-stranded coiled coils in GCN4 leucine zipper mutants*. Science, 1993. **262**(5138): p. 1401.
63. Woolfson, D.N., G.J. Bartlett, A.J. Burton, J.W. Heal, A. Niitsu, A.R. Thomson, and C.W. Wood, *De novo protein design: how do we expand into the universe of possible protein structures?* Current Opinion in Structural Biology, 2015. **33**: p. 16-26.
64. Banwell, E.F., E.S. Abelardo, D.J. Adams, M.A. Birchall, A. Corrigan, A.M. Donald, M. Kirkland, L.C. Serpell, M.F. Butler, and D.N. Woolfson, *Rational design and application of responsive [α]-helical peptide hydrogels*. Nat Mater, 2009. **8**(7): p. 596-600.
65. Pandya, M.J., G.M. Spooner, M. Sunde, J.R. Thorpe, A. Rodger, and D.N. Woolfson, *Sticky-End Assembly of a Designed Peptide Fiber Provides Insight into Protein Fibrillogenesis†*. Biochemistry, 2000. **39**(30): p. 8728-8734.

66. Ryadnov, M.G. and D.N. Woolfson, *Introducing Branches into a Self-Assembling Peptide Fiber*. *Angewandte Chemie International Edition*, 2003. **42**(26): p. 3021-3023.
67. Ryadnov, M.G. and D.N. Woolfson, *Engineering the morphology of a self-assembling protein fibre*. *Nature Materials*, 2003. **2**(5): p. 329-332.
68. Fletcher, J.M., R.L. Harniman, F.R.H. Barnes, A.L. Boyle, A. Collins, J. Mantell, T.H. Sharp, M. Antognozzi, P.J. Booth, N. Linden, M.J. Miles, R.B. Sessions, P. Verkade, and D.N. Woolfson, *Self-assembling cages from coiled-coil peptide modules*. *Science*, 2013. **340**(6132): p. 595-599.
69. Thomson, A.R., C.W. Wood, A.J. Burton, G.J. Bartlett, R.B. Sessions, R.L. Brady, and D.N. Woolfson, *Computational design of water-soluble α -helical barrels*. *Science*, 2014. **346**(6208): p. 485-488.
70. Burgess, N.C., T.H. Sharp, F. Thomas, C.W. Wood, A.R. Thomson, N.R. Zaccai, R.L. Brady, L.C. Serpell, and D.N. Woolfson, *Modular Design of Self-Assembling Peptide-Based Nanotubes*. *Journal of the American Chemical Society*, 2015. **137**(33): p. 10554-10562.
71. Thomas, F., N.C. Burgess, A.R. Thomson, and D.N. Woolfson, *Controlling the assembly of coiled-coil peptide nanotubes*. *Angewandte Chemie - International Edition*, 2016. **55**(3): p. 987-991.
72. Woolfson, D.N., G.J. Bartlett, M. Bruning, and A.R. Thomson, *New currency for old rope: from coiled-coil assemblies to α -helical barrels*. *Current Opinion in Structural Biology*, 2012. **22**(4): p. 432-441.
73. Mahmoud, Z.N., D.J. Grundy, K.J. Channon, and D.N. Woolfson, *The non-covalent decoration of self-assembling protein fibers*. *Biomaterials*, 2010. **31**(29): p. 7468-7474.
74. Smith, A.M., E.F. Banwell, W.R. Edwards, M.J. Pandya, and D.N. Woolfson, *Engineering Increased Stability into Self-Assembled Protein Fibers*. *Advanced Functional Materials*, 2006. **16**(8): p. 1022-1030.
75. Sharp, T.H., M. Bruning, J. Mantell, R.B. Sessions, A.R. Thomson, N.R. Zaccai, R.L. Brady, P. Verkade, and D.N. Woolfson, *Cryo-transmission electron microscopy structure of a gigadalton peptide fiber of de novo design*. *Proceedings of the National Academy of Sciences*, 2012. **109**(33): p. 13266-13271.
76. Xu, C., R. Liu, A.K. Mehta, R.C. Guerrero-Ferreira, E.R. Wright, S. Dunin-Horkawicz, K. Morris, L.C. Serpell, X. Zuo, J.S. Wall, and V.P. Conticello, *Rational design of helical*

- nanotubes from self-assembly of coiled-coil lock washers*. Journal of the American Chemical Society, 2013. **135**(41): p. 15565-15578.
77. Mondal, S., L. Adler-Abramovich, A. Lampel, Y. Bram, S. Lipstman, and E. Gazit, *Formation of functional super-helical assemblies by constrained single heptad repeat*. Nature Communications, 2015. **6**: p. 8615.
78. Betz, S.F. and W.F. DeGrado, *Controlling Topology and Native-like Behavior of de Novo-Designed Peptides: Design and Characterization of Antiparallel Four-Stranded Coiled Coils*. Biochemistry, 1996. **35**(21): p. 6955-6962.
79. Slovic, A.M., J.D. Lear, and W.F. DeGrado, *De novo design of a pentameric coiled-coil: decoding the motif for tetramer versus pentamer formation in water-soluble phospholamban**. The Journal of Peptide Research, 2005. **65**(3): p. 312-321.
80. Egelman, E.H., C. Xu, F. DiMaio, E. Magnotti, C. Modlin, X. Yu, E. Wright, D. Baker, and V.P. Conticello, *Structural Plasticity of Helical Nanotubes Based on Coiled-Coil Assemblies*. Structure, 2015. **23**(2): p. 280-289.
81. Gelse, K., E. Pöschl, and T. Aigner, *Collagens—structure, function, and biosynthesis*. Advanced Drug Delivery Reviews, 2003. **55**(12): p. 1531-1546.
82. He, L. and P. Theato, *Collagen and collagen mimetic peptide conjugates in polymer science*. European Polymer Journal, 2013. **49**(10): p. 2986-2997.
83. Sarkar, B., L.E.R. O'Leary, and J.D. Hartgerink, *Self-Assembly of Fiber-Forming Collagen Mimetic Peptides Controlled by Triple-Helical Nucleation*. Journal of the American Chemical Society, 2014. **136**(41): p. 14417-14424.
84. Fallas, J.A., J. Dong, Y.J. Tao, and J.D. Hartgerink, *Structural Insights into Charge Pair Interactions in Triple Helical Collagen-like Proteins*. Journal of Biological Chemistry, 2012. **287**(11): p. 8039-8047.
85. Fallas, J.A., L.E.R. O'Leary, and J.D. Hartgerink, *Synthetic collagen mimics: Self-assembly of homotrimers, heterotrimers and higher order structures*. Chemical Society Reviews, 2010. **39**(9): p. 3510-3527.
86. Li, Y. and S.M. Yu, *Targeting and mimicking collagens via triple helical peptide assembly*. Current Opinion in Chemical Biology, 2013. **17**(6): p. 968-975.
87. Przybyla, D.E. and J. Chmielewski, *Higher-order assembly of collagen peptides into nano- and microscale materials*. Biochemistry, 2010. **49**(21): p. 4411-4419.

88. Jalan, A.A. and J.D. Hartgerink, *Simultaneous Control of Composition and Register of an AAB-Type Collagen Heterotrimer*. *Biomacromolecules*, 2012. **14**(1): p. 179-185.
89. Fallas, J.A. and J.D. Hartgerink, *Computational design of self-assembling register-specific collagen heterotrimers*. *Nature Communications*, 2012. **3**: p. 1087.
90. Gauba, V. and J.D. Hartgerink, *Synthetic Collagen Heterotrimers: Structural Mimics of Wild-Type and Mutant Collagen Type I*. *Journal of the American Chemical Society*, 2008. **130**(23): p. 7509-7515.
91. Gauba, V. and J.D. Hartgerink, *Surprisingly High Stability of Collagen ABC Heterotrimer: Evaluation of Side Chain Charge Pairs*. *Journal of the American Chemical Society*, 2007. **129**(48): p. 15034-15041.
92. Gauba, V. and J.D. Hartgerink, *Self-Assembled Heterotrimeric Collagen Triple Helices Directed through Electrostatic Interactions*. *Journal of the American Chemical Society*, 2007. **129**(9): p. 2683-2690.
93. Jalan, A.A. and J.D. Hartgerink, *Pairwise interactions in collagen and the design of heterotrimeric helices*. *Current Opinion in Chemical Biology*, 2013. **17**(6): p. 960-967.
94. Luo, J. and Y.W. Tong, *Self-assembly of collagen-mimetic peptide amphiphiles into biofunctional nanofiber*. *ACS Nano*, 2011. **5**(10): p. 7739-7747.
95. Kojima, C., S. Tsumura, A. Harada, and K. Kono, *A Collagen-Mimic Dendrimer Capable of Controlled Release*. *Journal of the American Chemical Society*, 2009. **131**(17): p. 6052-6053.
96. Khew, S.T., Q.J. Yang, and Y.W. Tong, *Enzymatically crosslinked collagen-mimetic dendrimers that promote integrin-targeted cell adhesion*. *Biomaterials*, 2008. **29**(20): p. 3034-3045.
97. Shih, T.K. and W.T. Yen, *Template-assembled triple-helical peptide molecules: Mimicry of collagen by molecular architecture and integrin-specific cell adhesion*. *Biochemistry*, 2008. **47**(2): p. 585-596.
98. Wojtowicz, A.M., A. Shekaran, M.E. Oest, K.M. Dupont, K.L. Templeman, D.W. Hutmacher, R.E. Guldborg, and A.J. Garcia, *Coating of biomaterial scaffolds with the collagen-mimetic peptide GFOGER for bone defect repair*. *Biomaterials*, 2010. **31**(9): p. 2574-2582.

99. Yamazaki, C.M., Y. Kadoya, K. Hozumi, H. Okano-Kosugi, S. Asada, K. Kitagawa, M. Nomizu, and T. Koide, *A collagen-mimetic triple helical supramolecule that evokes integrin-dependent cell responses*. *Biomaterials*, 2010. **31**(7): p. 1925-1934.
100. Hennessy, K.M., B.E. Pollot, W.C. Clem, M.C. Phipps, A.A. Sawyer, B.K. Culpepper, and S.L. Bellis, *The effect of collagen I mimetic peptides on mesenchymal stem cell adhesion and differentiation, and on bone formation at hydroxyapatite surfaces*. *Biomaterials*, 2009. **30**(10): p. 1898-1909.
101. Krishna, O.D., A.K. Jha, X. Jia, and K.L. Kiick, *Integrin-mediated adhesion and proliferation of human MSCs elicited by a hydroxyproline-lacking, collagen-like peptide*. *Biomaterials*, 2011. **32**(27): p. 6412-6424.
102. Nanda, M. and K.N. Ganesh, *4(R / S)-guanidinyloxy collagen peptides: On-resin synthesis, complexation with plasmid DNA, and the role of peptides in enhancement of transfection*. *Journal of Organic Chemistry*, 2012. **77**(8): p. 4131-4135.
103. Cejas, M.A., W.A. Kinney, C. Chen, J.G. Vinter, H.R. Almond, K.M. Balss, C.A. Maryanoff, U. Schmidt, M. Breslav, A. Mahan, E. Lacy, and B.E. Maryanoff, *Thrombogenic collagen-mimetic peptides: Self-assembly of triple helix-based fibrils driven by hydrophobic interactions*. *Proceedings of the National Academy of Sciences of the United States of America*, 2008. **105**(25): p. 8513-8518.
104. Ulijn, R.V. and A.M. Smith, *Designing peptide based nanomaterials*. *Chemical Society Reviews*, 2008. **37**(4): p. 664-675.
105. Richardson, J.S. and D.C. Richardson, *Natural β -sheet proteins use negative design to avoid edge-to-edge aggregation*. *Proceedings of the National Academy of Sciences*, 2002. **99**(5): p. 2754-2759.
106. Dasgupta, A., J.H. Mondal, and D. Das, *Peptide hydrogels*. *RSC Advances*, 2013. **3**(24): p. 9117-9149.
107. Jiménez, J.L., E.J. Nettleton, M. Bouchard, C.V. Robinson, C.M. Dobson, and H.R. Saibil, *The protofilament structure of insulin amyloid fibrils*. *Proceedings of the National Academy of Sciences of the United States of America*, 2002. **99**(14): p. 9196-9201.
108. Mendes, A.C., E.T. Baran, R.L. Reis, and H.S. Azevedo, *Self-assembly in nature: Using the principles of nature to create complex nanobiomaterials*. *Wiley Interdisciplinary Reviews: Nanomedicine and Nanobiotechnology*, 2013. **5**(6): p. 582-612.

109. Cheng, P.-N., C. Liu, M. Zhao, D. Eisenberg, and J.S. Nowick, *Amyloid β -Sheet Mimics that Antagonize Amyloid Aggregation and Reduce Amyloid Toxicity*. *Nature chemistry*, 2012. **4**(11): p. 927-933.
110. Pham, J.D., R.K. Spencer, K.H. Chen, and J.S. Nowick, *A Fibril-Like Assembly of Oligomers of a Peptide Derived from β -Amyloid*. *Journal of the American Chemical Society*, 2014. **136**(36): p. 12682-12690.
111. Görbitz, C.H., *The structure of nanotubes formed by diphenylalanine, the core recognition motif of Alzheimer's β -amyloid polypeptide*. *Chemical Communications*, 2006(22): p. 2332-2334.
112. Balbach, J.J., Y. Ishii, O.N. Antzutkin, R.D. Leapman, N.W. Rizzo, F. Dyda, J. Reed, and R. Tycko, *Amyloid fibril formation by A β 16-22, a seven-residue fragment of the Alzheimer's β -amyloid peptide, and structural characterization by solid state NMR*. *Biochemistry*, 2000. **39**(45): p. 13748-13759.
113. Streets, A.M., Y. Sourigues, R.R. Kopito, R. Melki, and S.R. Quake, *Simultaneous Measurement of Amyloid Fibril Formation by Dynamic Light Scattering and Fluorescence Reveals Complex Aggregation Kinetics*. *PLoS ONE*, 2013. **8**(1): p. 1-10.
114. Ruggeri, F.S., J. Adamcik, J.S. Jeong, H.A. Lashuel, R. Mezzenga, and G. Dietler, *Influence of the β -Sheet Content on the Mechanical Properties of Aggregates during Amyloid Fibrillization*. *Angewandte Chemie International Edition*, 2015. **54**(8): p. 2462-2466.
115. Ruggeri, F.S., J. Habchi, A. Cerreta, and G. Dietler, *AFM-based single molecule techniques: Unraveling the amyloid Pathogenic Species*. *Current Pharmaceutical Design*, 2016. **22**(26): p. 3950-3970.
116. Lee, G., W. Lee, H. Lee, C.Y. Lee, K. Eom, and T. Kwon, *Self-assembled amyloid fibrils with controllable conformational heterogeneity*. *Scientific Reports*, 2015. **5**.
117. Gazit, E., *Mechanisms of amyloid fibril self-assembly and inhibition*. *FEBS Journal*, 2005. **272**(23): p. 5971-5978.
118. Gazit, E., *A possible role for π -stacking in the self-assembly of amyloid fibrils*. *FASEB Journal*, 2002. **16**(1): p. 77-83.
119. Smith, A., *Fibril Formation by Short Synthetic Peptides*, in *Protein Aggregation and Fibrillogenesis in Cerebral and Systemic Amyloid Disease*. Springer Netherlands: Dordrecht. 2012. p. 29-51.

120. Zhang, S., T. Holmes, C. Lockshin, and A. Rich, *Spontaneous assembly of a self-complementary oligopeptide to form a stable macroscopic membrane*. Proceedings of the National Academy of Sciences of the United States of America, 1993. **90**(8): p. 3334-3338.
121. Zhang, S., C. Lockshin, A. Herbert, E. Winter, and A. Rich, *Zuotin, a putative Z-DNA binding protein in Saccharomyces cerevisiae*. EMBO Journal, 1992. **11**(10): p. 3787-3796.
122. Zhao, X., J. Dai, and S. Zhang. *The fabrication of self-assembling peptides into nanofiber scaffolds through molecular self-assembly*. Material Research Society symposium proceedings, 2004. **823**.
123. Loo, Y., S. Zhang, and C.A.E. Hauser, *From short peptides to nanofibers to macromolecular assemblies in biomedicine*. Biotechnology Advances, 2012. **30**(3): p. 593-603.
124. Zhao, X. and S. Zhang, *Designer self-assembling peptide materials*. Macromolecular Bioscience, 2007. **7**(1): p. 13-22.
125. Gelain, F., A. Horii, and S. Zhang, *Designer self-assembling peptide scaffolds for 3-D tissue cell cultures and regenerative medicine*. Macromolecular Bioscience, 2007. **7**(5): p. 544-551.
126. Horii, A., X. Wang, F. Gelain, and S. Zhang, *Biological designer self-assembling peptide nanofiber scaffolds significantly enhance osteoblast proliferation, differentiation and 3-D migration*. PLoS ONE, 2007. **2**(2).
127. Ravichandran, R., M. Griffith, and J. Phopase, *Applications of self-assembling peptide scaffolds in regenerative medicine: The way to the clinic*. Journal of Materials Chemistry B, 2014. **2**(48): p. 8466-8478.
128. Kisiday, J., M. Jin, B. Kurz, H. Hung, C. Semino, S. Zhang, and A.J. Grodzinsky, *Self-assembling peptide hydrogel fosters chondrocyte extracellular matrix production and cell division: Implications for cartilage tissue repair*. Proceedings of the National Academy of Sciences, 2002. **99**(15): p. 9996-10001.
129. Chau, Y., Y. Luo, A.C.Y. Cheung, Y. Nagai, S. Zhang, J.B. Kobler, S.M. Zeitels, and R. Langer, *Incorporation of a matrix metalloproteinase-sensitive substrate into self-assembling peptides - A model for biofunctional scaffolds*. Biomaterials, 2008. **29**(11): p. 1713-1719.

130. Ni, N., Y. Hu, H. Ren, C. Luo, P. Li, J.-B. Wan, and H. Su, *Self-Assembling Peptide Nanofiber Scaffolds Enhance Dopaminergic Differentiation of Mouse Pluripotent Stem Cells in 3-Dimensional Culture*. PLoS ONE, 2013. **8**(12): p. e84504.
131. Guo, J., K.K.G. Leung, H. Su, Q. Yuan, L. Wang, T.H. Chu, W. Zhang, J.K.S. Pu, G.K.P. Ng, W.M. Wong, X. Dai, and W. Wu, *Self-assembling peptide nanofiber scaffold promotes the reconstruction of acutely injured brain*. Nanomedicine: Nanotechnology, Biology, and Medicine, 2009. **5**(3): p. 345-351.
132. Ellis-Behnke, R.G., Y.-X. Liang, S.-W. You, D.K.C. Tay, S. Zhang, K.-F. So, and G.E. Schneider, *Nano neuro knitting: Peptide nanofiber scaffold for brain repair and axon regeneration with functional return of vision*. Proceedings of the National Academy of Sciences of the United States of America, 2006. **103**(13): p. 5054-5059.
133. Puramatrix, 3-D matrix medical technology. Waltham, MA, 2012.
134. Aligholi, H., S.M. Rezayat, H. Azari, S. Ejtemaei Mehr, M. Akbari, S.M. Modarres Mousavi, F. Attari, F. Alipour, G. Hassanzadeh, and A. Gorji, *Preparing neural stem/progenitor cells in PuraMatrix hydrogel for transplantation after brain injury in rats: A comparative methodological study*. Brain Research, 2016. **1642**: p. 197-208.
135. Kondo, Y., T. Nagasaka, S. Kobayashi, N. Kobayashi, and T. Fujiwara, *Management of peritoneal effusion by sealing with a self-assembling nanofiber polypeptide following pelvic surgery*. Hepato-gastroenterology, 2014. **61**(130): p. 349-353.
136. Moradi, F., M. Bahktiari, M.T. Joghataei, M. Nobakht, M. Soleimani, G. Hasanzadeh, A. Fallah, S. Zarbakhsh, L.B. Hejazian, M. Shirmohammadi, and F. Maleki, *BD PuraMatrix peptide hydrogel as a culture system for human fetal Schwann cells in spinal cord regeneration*. Journal of Neuroscience Research, 2012. **90**(12): p. 2335-2348.
137. Reches, M. and E. Gazit, *Casting metal nanowires within discrete self-assembled peptide nanotubes*. Science, 2003. **300**(5619): p. 625-627.
138. Yan, X., P. Zhu, and J. Li, *Self-assembly and application of diphenylalanine-based nanostructures*. Chemical Society Reviews, 2010. **39**(6): p. 1877-1890.
139. Reches, M. and E. Gazit, *Designed aromatic homo-dipeptides: Formation of ordered nanostructures and potential nanotechnological applications*. Physical Biology, 2006. **3**(1).
140. Reches, M. and E. Gazit, *Formation of closed-cage nanostructures by self-assembly of aromatic dipeptides*. Nano Letters, 2004. **4**(4): p. 581-585.

141. Silva, R.F., D.R. Araújo, E.R. Silva, R.A. Ando, and W.A. Alves, *L -Diphenylalanine microtubes as a potential drug-delivery system: Characterization, release kinetics, and cytotoxicity*. Langmuir, 2013. **29**(32): p. 10205-10212.
142. Reches, M. and E. Gazit, *Self-assembly of peptide nanotubes and amyloid-like structures by charged-termini-capped diphenylalanine peptide analogues*. Israel Journal of Chemistry, 2005. **45**(3): p. 363-371.
143. Yan, X., Q. He, K. Wang, L. Duan, Y. Cui, and J. Li, *Transition of cationic dipeptide nanotubes into vesicles and oligonucleotide delivery*. Angewandte Chemie - International Edition, 2007. **46**(14): p. 2431-2434.
144. Yan, X., Y. Cui, Q. He, K. Wang, J. Li, W. Mu, B. Wang, and Z.C. Ou-yang, *Reversible transitions between peptide nanotubes and vesicle-like structures including theoretical modeling studies*. Chemistry - A European Journal, 2008. **14**(19): p. 5974-5980.
145. Yan, X., Y. Cui, Q. He, K. Wang, and J. Li, *Organogels based on self-assembly of diphenylalanine peptide and their application to immobilize quantum dots*. Chemistry of Materials, 2008. **20**(4): p. 1522-1526.
146. Ryu, J. and C.B. Park, *High-temperature self-assembly of peptides into vertically well-aligned nanowires by aniline vapor*. Advanced Materials, 2008. **20**(19): p. 3754-3758.
147. Li, R., A. Rodriguez, D.R. Nisbet, C.J. Barrow, and R.J. Williams, *Self-Assembled Peptide Nanostructures for the Fabrication of Cell Scaffolds*, in *Micro and Nanofabrication Using Self-Assembled Biological Nanostructures*. 2014. p. 33-61.
148. Burch, R.M., M. Weitzberg, N. Blok, R. Muhlhauser, D. Martin, S.G. Farmer, J.M. Bator, J.R. Connor, C. Ko, W. Kuhn, B.A. McMillan, M. Raynor, B.G. Shearer, C. Tiffany, and D.E. Wilkins, *Erratum: N-(Fluorenyl-9-methoxy-carbonyl) amino acids, a class of antiinflammatory agents with a different mechanism of action (Proc. Natl. Acad. Sci. USA (January 1991) 88 (355-359))*. Proceedings of the National Academy of Sciences of the United States of America, 1991. **88**(6): p. 2612.
149. Toledano, S., R.J. Williams, V. Jayawarna, and R.V. Ulijn, *Enzyme-triggered self-assembly of peptide hydrogels via reversed hydrolysis*. Journal of the American Chemical Society, 2006. **128**(4): p. 1070-1071.
150. Mahler, A., M. Reches, M. Rechter, S. Cohen, and E. Gazit, *Rigid, self-assembled hydrogel composed of a modified aromatic dipeptide*. Advanced Materials, 2006. **18**(11): p. 1365-1370.

151. Williams, R.J., T.E. Hall, V. Glattauer, J. White, P.J. Pasic, A.B. Sorensen, L. Waddington, K.M. McLean, P.D. Currie, and P.G. Hartley, *The in vivo performance of an enzyme-assisted self-assembled peptide/protein hydrogel*. *Biomaterials*, 2011. **32**(22): p. 5304-5310.
152. Vegners, R., I. Shestakova, I. Kalvinsh, R.M. Ezzell, and P.A. Janmey, *Use of a gel-forming dipeptide derivative as a carrier for antigen presentation*. *Journal of Peptide Science*, 1995. **1**(6): p. 371-378.
153. Tang, C., A.M. Smith, R.F. Collins, R.V. Ulijn, and A. Saiani, *Fmoc-Diphenylalanine Self-Assembly Mechanism Induces Apparent pK_a Shifts*. *Langmuir*, 2009. **25**(16): p. 9447-9453.
154. Fleming, S., S. Debnath, P.W.J.M. Frederix, N.T. Hunt, and R.V. Ulijn, *Insights into the coassembly of hydrogelators and surfactants based on aromatic peptide amphiphiles*. *Biomacromolecules*, 2014. **15**(4): p. 1171-1184.
155. Fleming, S. and R.V. Ulijn, *Design of nanostructures based on aromatic peptide amphiphiles*. *Chemical Society Reviews*, 2014. **43**(23): p. 8150-8177.
156. Jayawarna, V., M. Ali, T.A. Jowitt, A.F. Miller, A. Saiani, J.E. Gough, and R.V. Ulijn, *Nanostructured Hydrogels for Three-Dimensional Cell Culture Through Self-Assembly of Fluorenylmethoxycarbonyl-Dipeptides*. *Advanced Materials*, 2006. **18**(5): p. 611-614.
157. Yang, Z., H. Gu, D. Fu, P. Gao, J.K. Lam, and B. Xu, *Enzymatic formation of supramolecular hydrogels*. *Advanced Materials*, 2004. **16**(16).
158. Yang, Z., H. Gu, Y. Zhang, L. Wang, and B. Xu, *Small molecule hydrogels based on a class of antiinflammatory agents*. *Chemical Communications*, 2004(2): p. 208-209.
159. Williams, R.J., J. Gardiner, A.B. Sorensen, S. Marchesan, R.J. Mulder, K.M. McLean, and P.G. Hartley, *Monitoring the early stage self-assembly of enzyme-assisted peptide hydrogels*. *Australian Journal of Chemistry*, 2013. **66**(5): p. 572-578.
160. Williams, R.J., A.M. Smith, R. Collins, N. Hodson, A.K. Das, and R.V. Ulijn, *Enzyme-assisted self-assembly under thermodynamic control*. *Nature Nanotechnology*, 2009. **4**(1): p. 19-24.
161. Williams, R.J., R.J. Mart, and R.V. Ulijn, *Exploiting biocatalysis in peptide self-assembly*. *Biopolymers*, 2010. **94**(1): p. 107-117.

162. Tao, K., A. Levin, L. Adler-Abramovich, and E. Gazit, *Fmoc-modified amino acids and short peptides: Simple bio-inspired building blocks for the fabrication of functional materials*. Chemical Society Reviews, 2016. **45**(14): p. 3935-3953.
163. Zhang, Y., H. Gu, Z. Yang, and B. Xu, *Supramolecular Hydrogels Respond to Ligand–Receptor Interaction*. Journal of the American Chemical Society, 2003. **125**(45): p. 13680-13681.
164. Orbach, R., L. Adler-Abramovich, S. Zigerson, I. Mironi-Harpaz, D. Seliktar, and E. Gazit, *Self-assembled Fmoc-peptides as a platform for the formation of nanostructures and hydrogels*. Biomacromolecules, 2009. **10**(9): p. 2646-2651.
165. Orbach, R., I. Mironi-Harpaz, L. Adler-Abramovich, E. Mossou, E.P. Mitchell, V.T. Forsyth, E. Gazit, and D. Seliktar, *The rheological and structural properties of Fmoc-peptide-based hydrogels: The effect of aromatic molecular architecture on self-assembly and physical characteristics*. Langmuir, 2012. **28**(4): p. 2015-2022.
166. Li, R., C.C. Horgan, B. Long, A.L. Rodriguez, L. Mather, C.J. Barrow, D.R. Nisbet, and R.J. Williams, *Tuning the mechanical and morphological properties of self-assembled peptide hydrogels via control over the gelation mechanism through regulation of ionic strength and the rate of pH change*. RSC Advances, 2015. **5**(1): p. 301-307.
167. Zhou, M., A.M. Smith, A.K. Das, N.W. Hodson, R.F. Collins, R.V. Ulijn, and J.E. Gough, *Self-assembled peptide-based hydrogels as scaffolds for anchorage-dependent cells*. Biomaterials, 2009. **30**(13): p. 2523-2530.
168. Zhou, M., R.V. Ulijn, and J.E. Gough, *Extracellular matrix formation in self-assembled minimalistic bioactive hydrogels based on aromatic peptide amphiphiles*. Journal of Tissue Engineering, 2014. **5**: p. 2041731414531593.
169. Li, R., S. Pavuluri, K. Bruggeman, B.M. Long, A.J. Parnell, A. Martel, S.R. Parnell, F.M. Pfeffer, A.J.C. Dennison, K.R. Nicholas, C.J. Barrow, D.R. Nisbet, and R.J. Williams, *Coassembled nanostructured bioscaffold reduces the expression of proinflammatory cytokines to induce apoptosis in epithelial cancer cells*. Nanomedicine: Nanotechnology, Biology, and Medicine, 2016. **12**(5): p. 1397-1407.
170. Rodriguez, A.L., T.Y. Wang, K.F. Bruggeman, R. Li, R.J. Williams, C.L. Parish, and D.R. Nisbet, *Tailoring minimalist self-assembling peptides for localized viral vector gene delivery*. Nano Research, 2016. **9**(3): p. 674-684.

171. Horgan, C.C., A.L. Rodriguez, R. Li, K.F. Bruggeman, N. Stupka, J.K. Raynes, L. Day, J.W. White, R.J. Williams, and D.R. Nisbet, *Characterisation of minimalist co-assembled fluorenylmethyloxycarbonyl self-assembling peptide systems for presentation of multiple bioactive peptides*. Acta Biomaterialia, 2016. **38**: p. 11-22.
172. Tomasini, C. and N. Castellucci, *Peptides and peptidomimetics that behave as low molecular weight gelators*. Chemical Society Reviews, 2013. **42**(1): p. 156-172.
173. Pochan, D.J., J.P. Schneider, J. Kretsinger, B. Ozbas, K. Rajagopal, and L. Haines, *Thermally reversible hydrogels via intramolecular folding and consequent self-assembly of a de novo designed peptide*. Journal of the American Chemical Society, 2003. **125**(39): p. 11802-11803.
174. Ozbas, B., J. Kretsinger, K. Rajagopal, J.P. Schneider, and D.J. Pochan, *Salt-triggered peptide folding and consequent self-assembly into hydrogels with tunable modulus*. Macromolecules, 2004. **37**(19): p. 7331-7337.
175. Altunbas, A., N. Sharma, M.S. Lamm, C. Yan, R.P. Nagarkar, J.P. Schneider, and D.J. Pochan, *Peptide-silica hybrid networks: Biomimetic control of network mechanical behavior*. ACS Nano, 2010. **4**(1): p. 181-188.
176. Schneider, J.P., D.J. Pochan, B. Ozbas, K. Rajagopal, L. Pakstis, and J. Kretsinger, *Responsive hydrogels from the intramolecular folding and self-assembly of a designed peptide*. Journal of the American Chemical Society, 2002. **124**(50): p. 15030-15037.
177. Lamm, M.S., K. Rajagopal, J.P. Schneider, and D.J. Pochan, *Laminated morphology of nontwisting β -sheet fibrils constructed via peptide self-assembly*. Journal of the American Chemical Society, 2005. **127**(47): p. 16692-16700.
178. Rajagopal, K. and J.P. Schneider, *Self-assembling peptides and proteins for nanotechnological applications*. Current Opinion in Structural Biology, 2004. **14**(4): p. 480-486.
179. Haines-Butterick, L.A., D.A. Salick, D.J. Pochan, and J.P. Schneider, *In vitro assessment of the pro-inflammatory potential of β -hairpin peptide hydrogels*. Biomaterials, 2008. **29**(31): p. 4164-4169.
180. Kretsinger, J.K., L.A. Haines, B. Ozbas, D.J. Pochan, and J.P. Schneider, *Cytocompatibility of self-assembled β -hairpin peptide hydrogel surfaces*. Biomaterials, 2005. **26**(25): p. 5177-5186.

181. Haines, L.A., K. Rajagopal, B. Ozbas, D.A. Salick, D.J. Pochan, and J.P. Schneider, *Light-activated hydrogel formation via the triggered folding and self-assembly of a designed peptide*. Journal of the American Chemical Society, 2005. **127**(48): p. 17025-17029.
182. Micklitsch, C.M., P.J. Knerr, M.C. Branco, R. Nagarkar, D.J. Pochan, and J.P. Schneider, *Zinc-triggered hydrogelation of a self-assembling β -hairpin peptide*. Angewandte Chemie - International Edition, 2011. **50**(7): p. 1577-1579.
183. Rajagopal, K., M.S. Lamm, L.A. Haines-Butterick, D.J. Pochan, and J.P. Schneider, *Tuning the pH responsiveness of β -hairpin peptide folding, self-assembly, and hydrogel material formation*. Biomacromolecules, 2009. **10**(9): p. 2619-2625.
184. Altunbas, A., S.J. Lee, S.A. Rajasekaran, J.P. Schneider, and D.J. Pochan, *Encapsulation of Curcumin in Self-Assembling Peptide Hydrogels as Injectable Drug Delivery Vehicles*. Biomaterials, 2011. **32**(25): p. 5906-5914.
185. Haines-Butterick, L., K. Rajagopal, M. Branco, D. Salick, R. Rughani, M. Pilarz, M.S. Lamm, D.J. Pochan, and J.P. Schneider, *Controlling hydrogelation kinetics by peptide design for three-dimensional encapsulation and injectable delivery of cells*. Proceedings of the National Academy of Sciences, 2007. **104**(19): p. 7791-7796.
186. Lindsey, S., J.H. Piatt, P. Worthington, C. Sönmez, S. Satheye, J.P. Schneider, D.J. Pochan, and S.A. Langhans, *Beta hairpin peptide hydrogels as an injectable solid vehicle for neurotrophic growth factor delivery*. Biomacromolecules, 2015. **16**(9): p. 2672-2683.
187. Joo, S.H., *Cyclic Peptides as Therapeutic Agents and Biochemical Tools*. Biomolecules & Therapeutics, 2012. **20**(1): p. 19-26.
188. Ghadiri, M.R., J.R. Granja, and L.K. Buehler, *Artificial transmembrane ion channels from self-assembling peptide nanotubes*. Nature, 1994. **369**(6478): p. 301-304.
189. Ghadiri, M.R., J.R. Granja, R.A. Milligan, D.E. McRee, and N. Khazanovich, *Self-assembling organic nanotubes based on a cyclic peptide architecture*. Nature, 1993. **366**(6453): p. 324-327.
190. Valéry, C., F. Artzner, and M. Paternostre, *Peptide nanotubes: Molecular organisations, self-assembly mechanisms and applications*. Soft Matter, 2011. **7**(20): p. 9583-9594.

191. Brea, R.J., *Self-Assembling Cyclic Peptide-Based Nanomaterials*, in *Ideas in Chemistry and Molecular Sciences: Advances in Nanotechnology, Materials and Devices*. 2010. p. 1-22.
192. Gazit, E., *Self-assembled peptide nanostructures: The design of molecular building blocks and their technological utilization*. *Chemical Society Reviews*, 2007. **36**(8): p. 1263-1269.
193. Motesharej, K. and M.R. Ghadiri, *Diffusion-limited size-selective ion sensing based on SAM-supported peptide nanotubes*. *Journal of the American Chemical Society*, 1997. **119**(46): p. 11306-11312.
194. Fernandez-Lopez, S., H.-S. Kim, E.C. Choi, M. Delgado, J.R. Granja, A. Khasanov, K. Kraehenbuehl, G. Long, D.A. Weinberger, K.M. Wilcoxon, and M.R. Ghadiri, *Antibacterial agents based on the cyclic d,l-[alpha]-peptide architecture*. *Nature*, 2001. **412**(6845): p. 452-455.
195. Chapman, R., M. Danial, M.L. Koh, K.A. Jolliffe, and S. Perrier, *Design and properties of functional nanotubes from the self-assembly of cyclic peptide templates*. *Chemical Society Reviews*, 2012. **41**(18): p. 6023-6041.
196. Chapman, R., K.A. Jolliffe, and S. Perrier, *Multi-shell soft nanotubes from cyclic peptide templates*. *Advanced Materials*, 2013. **25**(8): p. 1170-1172.
197. Chapman, R., M.L. Koh, G.G. Warr, K.A. Jolliffe, and S. Perrier, *Structure elucidation and control of cyclic peptide-derived nanotube assemblies in solution*. *Chemical Science*, 2013. **4**(6): p. 2581-2589.
198. Chapman, R., K.A. Jolliffe, and S. Perrier, *Modular design for the controlled production of polymeric nanotubes from polymer/peptide conjugates*. *Polymer Chemistry*, 2011. **2**(9): p. 1956-1963.
199. Danial, M., C. My-Nhi Tran, P.G. Young, S. Perrier, and K.A. Jolliffe, *Janus cyclic peptide-polymer nanotubes*. *Nature Communications*, 2013. **4**: p. 2780.
200. Blunden, B.M., R. Chapman, M. Danial, H. Lu, K.A. Jolliffe, S. Perrier, and M.H. Stenzel, *Drug conjugation to cyclic peptide-polymer self-assembling nanotubes*. *Chemistry - A European Journal*, 2014. **20**(40): p. 12745-12749.
201. Webber, M.J., E.J. Berns, and S.I. Stupp, *Supramolecular Nanofibers of Peptide Amphiphiles for Medicine*. *Israel Journal of Chemistry*, 2013. **53**(8): p. 530-554.

202. Matson, J.B. and S.I. Stupp, *Self-assembling peptide scaffolds for regenerative medicine*. Chemical Communications, 2012. **48**(1): p. 26-33.
203. Cui, H., M.J. Webber, and S.I. Stupp, *Self-assembly of peptide amphiphiles: from molecules to nanostructures to biomaterials*. Biopolymers, 2010. **94**(1): p. 1-18.
204. Silva, G.A., C. Czeisler, K.L. Niece, E. Beniash, D.A. Harrington, J.A. Kessler, and S.I. Stupp, *Selective differentiation of neural progenitor cells by high-epitope density nanofibers*. Science, 2004. **303**(5662): p. 1352-5.
205. Webber, M.J., J.A. Kessler, and S.I. Stupp, *Emerging peptide nanomedicine to regenerate tissues and organs*. Journal of Internal Medicine, 2010. **267**(1): p. 71-88.
206. Stupp, S.I., R.H. Zha, L.C. Palmer, H. Cui, and R. Bitton, *Self-assembly of biomolecular soft matter*. Faraday Discussions, 2013. **166**: p. 9-30.
207. Jun, H.W., V. Yuwono, S.E. Paramonov, and J.D. Hartgerink, *Enzyme-Mediated Degradation of Peptide-Amphiphile Nanofiber Networks*. Advanced Materials, 2005. **17**(21): p. 2612-2617.
208. Niece, K.L., J.D. Hartgerink, J.J.J.M. Donners, and S.I. Stupp, *Self-Assembly Combining Two Bioactive Peptide-Amphiphile Molecules into Nanofibers by Electrostatic Attraction*. Journal of the American Chemical Society, 2003. **125**(24): p. 7146-7147.
209. Pashuck, E.T. and S.I. Stupp, *Direct Observation of Morphological Transformation from Twisted Ribbons into Helical Ribbons*. Journal of the American Chemical Society, 2010. **132**(26): p. 8819-8821.
210. Trent, A., R. Marullo, B. Lin, M. Black, and M. Tirrell, *Structural properties of soluble peptide amphiphile micelles*. Soft Matter, 2011. **7**(20): p. 9572-9582.
211. Miravet, J.F., B. Escuder, M.D. Segarra-Maset, M. Tena-Solsona, I.W. Hamley, A. Dehsorkhi, and V. Castelletto, *Self-assembly of a peptide amphiphile: transition from nanotape fibrils to micelles*. Soft Matter, 2013. **9**(13): p. 3558-3564.
212. Dehsorkhi, A., V. Castelletto, I.W. Hamley, J. Adamcik, and R. Mezzenga, *The effect of pH on the self-assembly of a collagen derived peptide amphiphile*. Soft Matter, 2013. **9**(26): p. 6033-6036.
213. Muraoka, T., C.Y. Koh, H. Cui, and S.I. Stupp, *Light-triggered bioactivity in three dimensions*. Angewandte Chemie - International Edition, 2009. **48**(32): p. 5946-5949.

214. Hamley, I.W., A. Dehsorkhi, V. Castelletto, S. Furzeland, D. Atkins, J. Seitsonen, and J. Ruokolainen, *Reversible helical unwinding transition of a self-assembling peptide amphiphile*. *Soft Matter*, 2013. **9**(39): p. 9290-9293.
215. Webber, M.J., C.J. Newcomb, R. Bitton, and S.I. Stupp, *Switching of Self-Assembly in a Peptide Nanostructure with a Specific Enzyme*. *Soft matter*, 2011. **7**(20): p. 9665-9672.
216. Paramonov, S.E., H.W. Jun, and J.D. Hartgerink, *Self-assembly of peptide-amphiphile nanofibers: The roles of hydrogen bonding and amphiphilic packing*. *Journal of the American Chemical Society*, 2006. **128**(22): p. 7291-7298.
217. Berndt, P., G.B. Fields, and M. Tirrell, *Synthetic lipidation of peptides and amino acids: Monolayer structure and properties*. *Journal of the American Chemical Society*, 1995. **117**(37): p. 9515-9522.
218. Stupp, S.I., *Self-Assembly and Biomaterials*. *Nano Letters*, 2010. **10**(12): p. 4783-4786.
219. Velichko, Y.S., S.I. Stupp, and M.O. de la Cruz, *Molecular Simulation Study of Peptide Amphiphile Self-Assembly*. *The Journal of Physical Chemistry B*, 2008. **112**(8): p. 2326-2334.
220. Webber, M.J., J. Tongers, C.J. Newcomb, K.-T. Marquardt, J. Bauersachs, D.W. Losordo, and S.I. Stupp, *Supramolecular nanostructures that mimic VEGF as a strategy for ischemic tissue repair*. *Proceedings of the National Academy of Sciences*, 2011. **108**(33):1338-13443.
221. Webber, M.J., J. Tongers, M.-A. Renault, J.G. Roncalli, D.W. Losordo, and S.I. Stupp, *Development of bioactive peptide amphiphiles for therapeutic cell delivery*. *Acta Biomaterialia*, 2010. **6**(1): p. 3-11.
222. Xu, X.-D., Y. Jin, Y. Liu, X.-Z. Zhang, and R.-X. Zhuo, *Self-assembly behavior of peptide amphiphiles (PAs) with different length of hydrophobic alkyl tails*. *Colloids and Surfaces B: Biointerfaces*, 2010. **81**(1): p. 329-335.
223. Zhang, H., M. Yu, A. Song, Y. Song, X. Xin, J. Shen, and S. Yuan, *Modulating hierarchical self-assembly behavior of a peptide amphiphile/nonionic surfactant mixed system*. *RSC Advances*, 2016. **6**(11): p. 9186-9193.
224. Löwik, D.W.P.M., J. Garcia-Hartjes, J.T. Meijer, and J.C.M. Van Hest, *Tuning secondary structure and self-assembly of amphiphilic peptides*. *Langmuir*, 2005. **21**(2): p. 524-526.

225. Hamley, I.W., A. Dehsorkhi, V. Castelletto, M.N.M. Walter, C.J. Connon, M. Reza, and J. Ruokolainen, *Self-Assembly and Collagen-Stimulating Activity of a Peptide Amphiphile Incorporating a Peptide Sequence from Lumican*. *Langmuir*, 2015. **31**(15): p. 4490-4495.
226. Hong, Y., R.L. Legge, S. Zhang, and P. Chen, *Effect of Amino Acid Sequence and pH on Nanofiber Formation of Self-Assembling Peptides EAK16-II and EAK16-IV*. *Biomacromolecules*, 2003. **4**(5): p. 1433-1442.
227. Xu, X., Y. Li, H. Li, R. Liu, M. Sheng, B. He, and Z. Gu, *Smart Nanovehicles Based on pH-Triggered Disassembly of Supramolecular Peptide-Amphiphiles for Efficient Intracellular Drug Delivery*. *Small*, 2014. **10**(6): p. 1133-1140.
228. Ghosh, A., E.T. Dobson, C.J. Buettner, M.J. Nicholl, and J.E. Goldberger, *Programming pH-Triggered Self-Assembly Transitions via Isomerization of Peptide Sequence*. *Langmuir*, 2014. **30**(51): p. 15383-15387.
229. Chen, Y., H.X. Gan, and Y.W. Tong, *pH-controlled hierarchical self-assembly of peptide amphiphile*. *Macromolecules*, 2015. **48**(8): p. 2647-2653.
230. Aggeli, A., M. Bell, L.M. Carrick, C.W.G. Fishwick, R. Harding, P.J. Mawer, S.E. Radford, A.E. Strong, and N. Boden, *pH as a trigger of peptide β -sheet self-assembly and reversible switching between nematic and isotropic phases*. *Journal of the American Chemical Society*, 2003. **125**(32): p. 9619-9628.
231. Cote, Y., I.W. Fu, E.T. Dobson, J.E. Goldberger, H.D. Nguyen, and J.K. Shen, *Mechanism of the pH-controlled self-assembly of nanofibers from peptide amphiphiles*. *Journal of Physical Chemistry C*, 2014. **118**(29): p. 16272-16278.
232. Ghosh, A., M. Haverick, K. Stump, X. Yang, M.F. Tweedle, and J.E. Goldberger, *Fine-tuning the pH trigger of self-assembly*. *Journal of the American Chemical Society*, 2012. **134**(8): p. 3647-3650.
233. Deng, M., D. Yu, Y. Hou, and Y. Wang, *Self-assembly of peptide-amphiphile C12-A β (11-17) into nanofibrils*. *Journal of Physical Chemistry B*, 2009. **113**(25): p. 8539-8544.
234. Gopalan, Romila D., Mark P. Del Borgo, Adam I. Mechler, P. Perlmutter, and M.-I. Aguilar, *Geometrically Precise Building Blocks: the Self-Assembly of β -Peptides*. *Chemistry & Biology*, 2015. **22**(11): p. 1417-1423.
235. Cheng, R.P., S.H. Gellman, and W.F. DeGrado, *β -peptides: From structure to function*. *Chemical Reviews*, 2001. **101**(10): p. 3219-3232.

236. Torres, E., E. Gorrea, K.K. Burusco, E. Da Silva, P. Nolis, F. Rúa, S. Bousset, I. Díez-Pérez, S. Dannenberg, S. Izquierdo, E. Giralt, C. Jaime, V. Branchadell, and R.M. Ortuño, *Folding and self-assembling with β -oligomers based on (1R,2S)-2-aminocyclobutane-1-carboxylic acid*. *Organic and Biomolecular Chemistry*, 2010. **8**(3): p. 564-575.
237. Del Borgo, M.P., K. Kulkarni, and M.I. Aguilar, *Unique Functional Materials Derived from β -Amino Acid Oligomers*. *Australian Journal of Chemistry*, 2017. **70**(2): p. 126-129.
238. Seebach, D., P.E. Ciceri, M. Overhand, B. Jaun, D. Rigo, L. Oberer, U. Hommel, R. Amstutz, and H. Widmer, *170. Probing the helical secondary structure of short-chain β -peptides*. *Helvetica Chimica Acta*, 1996. **79**(8): p. 2043-2066.
239. Podlech, J. and D. Seebach, *The Arndt-Eistert reaction in peptide chemistry: A facile access to homopeptides*. *Angewandte Chemie (International Edition in English)*, 1995. **34**(4): p. 471-472.
240. Seebach, D. and J.L. Matthews, *β -peptides: A surprise at every turn*. *Chemical Communications*, 1997(21): p. 2015-2022.
241. Aguilar, M.I., A.W. Purcell, R. Devi, R. Lew, J. Rossjohn, A.I. Smith, and P. Perlmutter, *β -Amino acid-containing hybrid peptides - New opportunities in peptidomimetics*. *Organic and Biomolecular Chemistry*, 2007. **5**(18): p. 2884-2890.
242. Appella, D.H., J.J. Barchi Jr, S.R. Durell, and S.H. Gellman, *Formation of short, stable helices in aqueous solution by β -amino acid hexamers [2]*. *Journal of the American Chemical Society*, 1999. **121**(10): p. 2309-2310.
243. Seebach, D., D.F. Hook, and A. Glättli, *Helices and other secondary structures of β - and γ -peptides*. *Biopolymers - Peptide Science Section*, 2006. **84**(1): p. 23-37.
244. Rathore, N., S.H. Gellman, and J.J. de Pablo, *Thermodynamic Stability of β -Peptide Helices and the Role of Cyclic Residues*. *Biophysical Journal*, 2006. **91**(9): p. 3425-3435.
245. Raguse, T.L., J.R. Lai, and S.H. Gellman, *Evidence that the β -peptide 14-helix is stabilized by β 3-residues with side-chain branching adjacent to the β -carbon atom*. *Helvetica Chimica Acta*, 2002. **85**(12): p. 4154-4164.
246. Langenhan, J.M., I.A. Guzei, and S.H. Gellman, *Parallel Sheet Secondary Structure in β -Peptides*. *Angewandte Chemie International Edition*, 2003. **42**(21): p. 2402-2405.

247. Pohl, G., T. Beke, I.G. Csizmadia, and A. Perczel, *Extended Apolar β -Peptide Foldamers: The Role of Axis Chirality on β -Peptide Sheet Stability*. *The Journal of Physical Chemistry B*, 2010. **114**(29): p. 9338-9348.
248. Daura, X., K. Gademann, H. Schäfer, B. Jaun, D. Seebach, and W.F. van Gunsteren, *The β -Peptide Hairpin in Solution: Conformational Study of a β -Hexapeptide in Methanol by NMR Spectroscopy and MD Simulation*. *Journal of the American Chemical Society*, 2001. **123**(10): p. 2393-2404.
249. Wu, Y.-D., W. Han, D.-P. Wang, Y. Gao, and Y.-L. Zhao, *Theoretical Analysis of Secondary Structures of β -Peptides*. *Accounts of Chemical Research*, 2008. **41**(10): p. 1418-1427.
250. Wang, P.S.P. and A. Schepartz, *β -Peptide bundles: Design. Build. Analyze. Biosynthesize*. *Chemical Communications*, 2016. **52**(47): p. 7420-7432.
251. Appella, D.H., L.A. Christianson, I.L. Karle, D.R. Powell, and S.H. Gellman, *Synthesis and Characterization of trans-2-Aminocyclohexanecarboxylic Acid Oligomers: An Unnatural Helical Secondary Structure and Implications for β -Peptide Tertiary Structure*. *Journal of the American Chemical Society*, 1999. **121**(26): p. 6206-6212.
252. Raguse, T.L., J.R. Lai, P.R. LePlae, and S.H. Gellman, *Toward β -peptide tertiary structure: Self-association of an amphiphilic 14-helix in aqueous solution*. *Organic Letters*, 2001. **3**(24): p. 3963-3966.
253. Raguse, T.L., E.A. Porter, B. Weisblum, and S.H. Gellman, *Structure–Activity Studies of 14-Helical Antimicrobial β -Peptides: Probing the Relationship between Conformational Stability and Antimicrobial Potency*. *Journal of the American Chemical Society*, 2002. **124**(43): p. 12774-12785.
254. Giuliano, M.W., W.S. Horne, and S.H. Gellman, *An α/β -peptide helix bundle with a pure β 3-amino acid core and a distinctive quaternary structure*. *Journal of the American Chemical Society*, 2009. **131**(29): p. 9860-9861.
255. Horne, W.S. and S.H. Gellman, *Foldamers with heterogeneous backbones*. *Accounts of Chemical Research*, 2008. **41**(10): p. 1399-1408.
256. Cheng, R.P. and W.F. DeGrado, *Long-range interactions stabilize the fold of a non-natural oligomer*. *Journal of the American Chemical Society*, 2002. **124**(39): p. 11564-11565.

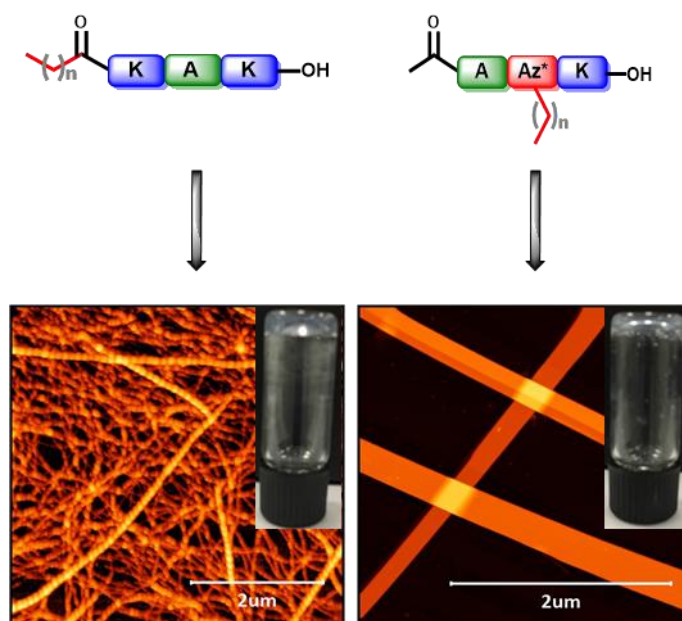
257. Craig, C.J., J.L. Goodman, and A. Schepartz, *Enhancing β -Peptide Bundle Stability by Design*. ChemBioChem, 2011. **12**(7): p. 1035-1038.
258. Daniels, D.S., E.J. Petersson, J.X. Qiu, and A. Schepartz, *High-resolution structure of a β -peptide bundle*. Journal of the American Chemical Society, 2007. **129**(6): p. 1532-1533.
259. Goodman, J.L., M.A. Molski, J. Qiu, and A. Schepartz, *Tetrameric β 3-peptide bundles*. ChemBioChem, 2008. **9**(10): p. 1576-1578.
260. Melicher, M.S., J. Chu, A.S. Walker, S.J. Miller, R.H.G. Baxter, and A. Schepartz, *A β -boronopeptide bundle of known structure as a vehicle for polyol recognition*. Organic Letters, 2013. **15**(19): p. 5048-5051.
261. Wang, P.S.P., J.B. Nguyen, and A. Schepartz, *Design and high-resolution structure of a β 3-peptide bundle catalyst*. Journal of the American Chemical Society, 2014. **136**(19): p. 6810-6813.
262. Stupp, S.I. and L.C. Palmer, *Supramolecular Chemistry and Self-Assembly in Organic Materials Design*. Chemistry of Materials, 2013. **26**: p. 507-518.
263. Pomerantz, W.C., V.M. Yuwono, R. Drake, J.D. Hartgerink, N.L. Abbott, and S.H. Gellman, *Lyotropic Liquid Crystals Formed from ACHC-Rich β -Peptides*. Journal of the American Chemical Society, 2011. **133**(34): p. 13604-13613.
264. Pomerantz, W.C., V.M. Yuwono, C.L. Pizzey, J.D. Hartgerink, N.L. Abbott, and S.H. Gellman, *Nanofibers and lyotropic liquid crystals from a class of self-assembling β -peptides*. Angewandte Chemie - International Edition, 2008. **47**(7): p. 1241-1244.
265. Kim, J., S. Kwon, S.H. Kim, C.K. Lee, J.H. Lee, S.J. Cho, H.S. Lee, and H. Ihee, *Microtubes with rectangular cross-section by self-assembly of a short β -peptide foldamer*. Journal of the American Chemical Society, 2012. **134**(51): p. 20573-20576.
266. Kwon, S., A. Jeon, S.H. Yoo, I.S. Chung, and H.S. Lee, *Unprecedented molecular architectures by the controlled self-assembly of a β -Peptide foldamer*. Angewandte Chemie - International Edition, 2010. **49**(44): p. 8232-8236.
267. Kwon, S., B.J. Kim, H.K. Lim, K. Kang, S.H. Yoo, J. Gong, E. Yoon, J. Lee, I.S. Choi, H. Kim, and H.S. Lee, *Magnetotactic molecular architectures from self-assembly of β -peptide foldamers*. Nature Communications, 2015. **6**. 8747.

268. Kwon, S., H.S. Shin, J. Gong, J.-H. Eom, A. Jeon, S.H. Yoo, I.S. Chung, S.J. Cho, and H.-S. Lee, *Self-Assembled Peptide Architecture with a Tooth Shape: Folding into Shape*. Journal of the American Chemical Society, 2011. **133**(44): p. 17618-17621.
269. Yoo, S.H. and H.-S. Lee, *Foldectures: 3D Molecular Architectures from Self-Assembly of Peptide Foldamers*. Accounts of Chemical Research, 2017. **50**(4): p. 832-841.
270. Matsuura, K., *Rational design of self-assembled proteins and peptides for nano- and micro-sized architectures*. RSC Advances, 2014. **4**(6): p. 2942-2953.
271. Seoudi, R.S., M.P. Del Borgo, K. Kulkarni, P. Perlmutter, M.-I. Aguilar, and A. Mechler, *Supramolecular self-assembly of 14-helical nanorods with tunable linear and dendritic hierarchical morphologies*. New Journal of Chemistry, 2016. **12**: 2243--2246.
272. Seoudi, R.S., A. Dowd, M. Del Borgo, K. Kulkarni, P. Perlmutter, M.I. Aguilar, and A. Mechler, *Amino acid sequence controls the self-assembled superstructure morphology of N-acetylated tri- β -peptides*. Pure and Applied Chemistry, 2015. **87**(9-10): p. 1021-1028.
273. Seoudi R.S., M.G. Hinds, D.J.D. Wilson, C.G. Adda, M.P. Del Borgo, M.I. Aguilar, P. Perlmutter, and A. Mechler, *Self-assembled nanomaterials based on beta (β^3) tetrapeptides*. Nanotechnology, 2016. **27**(13): p. 135606.
274. Luder, K., K. Kulkarni, H.W. Lee, R.E. Widdop, M.P. Del Borgo, and M.I. Aguilar, *Decorated self-assembling β 3-tripeptide foldamers form cell adhesive scaffolds*. Chemical Communications, 2016. **52**(24): p. 4549-4552.
275. Motamed, S., M.P. Del Borgo, K. Kulkarni, N. Habila, K. Zhou, P. Perlmutter, J.S. Forsythe, and M.I. Aguilar, *A self-assembling [small beta]-peptide hydrogel for neural tissue engineering*. Soft Matter, 2016. **12**(8): p. 2243-2246.

Chapter Two

Alkyl Chain Position Dictates the Self-Assembly Architecture of β^3 -Peptide Amphiphiles

The design, synthesis and self-assembled morphology of β^3 -peptide amphiphiles was investigated. AFM and TEM analysis revealed that the alkyl chain position significantly influenced the morphology and size of self-assembled nanostructures. The alkyl chain at R_0 or R_1 resulted in the formation of twisted ribbons, while those at R_2 or R_3 formed nanobelts. In addition, stable supramolecular hydrogels were formed under physiological conditions. The driving force for the self-assembly was the collective balance of hydrogen bonding, hydrophobic interactions and electrostatic attraction. These results demonstrated the significance of modifying building blocks in order to obtain controlled supramolecular self-assembled β^3 -peptide-derived architectures.



2.1 Introduction

Oligomers of β^3 -peptides are a versatile class of molecules that have demonstrated unique self-assembly properties [1-5]. *N*-acetylated β^3 -peptides in particular, are known to spontaneously form fibrous structures with a large range of irregular morphologies and sizes [6, 7]. For example, a β^3 -tripeptide with the sequence β^3 Leu- β^3 Ile- β^3 Ala (LIA), was recently reported to self-assemble into diverse morphologies and size in different solvents [7]. Similarly, β^3 -peptides with the same composition but different β^3 -amino acid sequence also underwent self-assembly demonstrating that this class of β^3 -peptides self-assembled irrespective of sequence [8, 9]. However, the irregular morphology and size of the resultant fibres limit the application of β^3 -peptides. Given that the control of self-assembly is an important prerequisite for future applications, there is a need to develop new strategies for control of material properties.

Several studies have demonstrated that incorporation of an alkyl chain within a self-assembling α -peptide is a method to control self-assembly to form cylindrical nanofibres with uniform diameter [10-14]. In order to achieve a similar level of control, it was hypothesised that introducing an alkyl chain into the β^3 -peptide monomer will control the self-assembly and produce nanostructures with defined architectures.

The first section of this chapter describes the design and synthesis of a series of β^3 -peptide amphiphiles using alkyl chains of different lengths that were incorporated into the β^3 -peptide sequence at different positions. The second section describes the self-assembly of the synthesised β^3 -peptide amphiphiles and characterisation of the morphologies using high-resolution AFM and TEM. In addition, the ability of these β^3 -peptide amphiphiles to form stable hydrogels were investigated. The results in this chapter provide a promising strategy for controlling the self-assembly of β^3 -peptides which also yielded β^3 -peptide-based hydrogels for functionalisation and potential application as biomaterials.

2.2 Design of β^3 -Peptide Amphiphiles

N-acetylated β^3 -tripeptides are known to form 14-helices with a near perfect pitch of three residues per turn and stabilised by six axially-oriented intermolecular hydrogen bonds [1, 2,

6]. Figure 2.1 shows a schematic of the β^3 -tripeptide self-assembly motif which creates an alignment of β^3 -amino acid side chains along each face of the helix. The position of the side chains on the exterior of the helical structure also offers a significant opportunity to precisely modify or attach functional moieties to the final product.

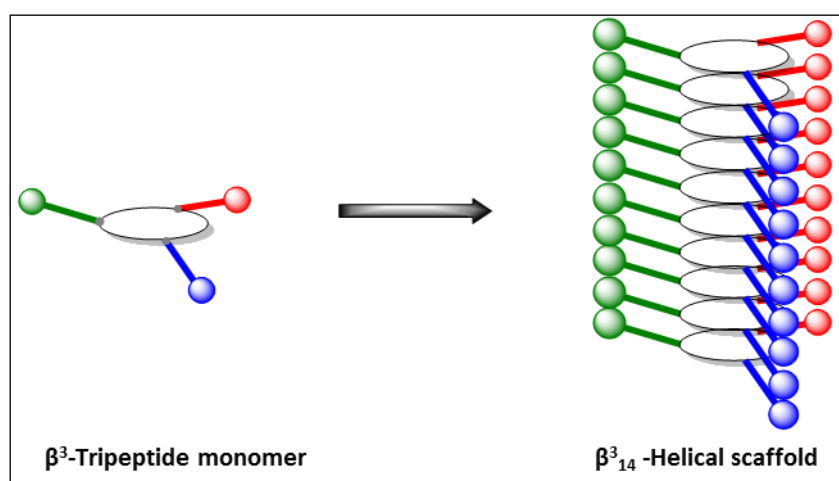


Figure 2.1: Alignment of side chains for self-assembled *N*-acetylated β^3 -tripeptides. The monomer consists of three β^3 -amino acid residues (represented in red, blue and green colours). The monomer forms helical scaffold with side chains presented directly atop one another outside the helix.

A β^3 -peptide amphiphile is defined in this study as a class of molecule that combines the structural features of a β^3 -peptide and a hydrophobic alkyl chain. Each β^3 -peptide amphiphile was designed with β^3 -homoalanine (β^3 A), β^3 -homolysine (β^3 K) for solubility and β^3 -homoazidoalanine (β^3 Az*) which is a novel amino acid that contains a methylazide sidechain which allows for orthogonal lipidation. *N*-terminal acetylation was required to provide the hydrogen bond pair for the self-assembly to occur [1]. To understand the role of alkyl chain position in dictating the self-assembly, each β^3 -peptide amphiphile was designed with a single alkyl chain coupled to the β^3 -peptide backbone at four different locations referred to as R_0 , R_1 , R_2 , and R_3 based on the residue to which the alkyl chain was coupled. Figure 2.2 shows the structure of β^3 -peptide amphiphiles synthesised with alkyl chain lengths of C_{12} , C_{14} and C_{16} at different positions.

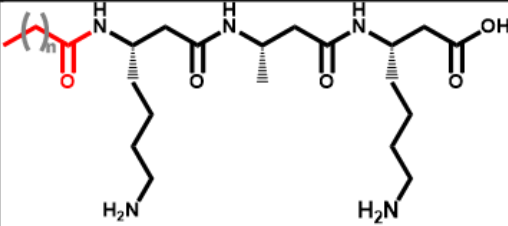
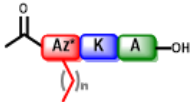
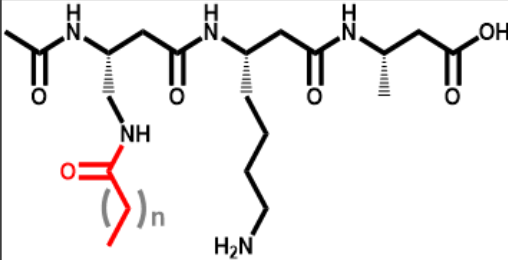
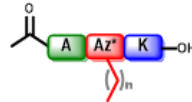
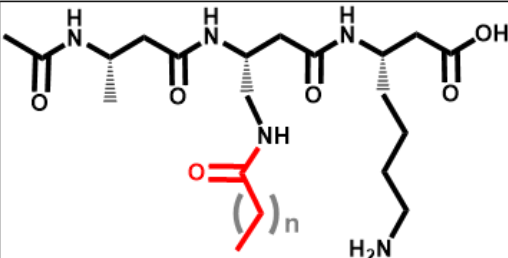
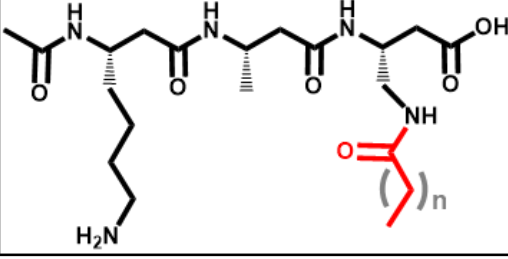
Alkyl chain position	Design	Chemical structure
R₀		
R₁		
R₂		
R₃		

Figure 2.2: Design of β^3 -peptide amphiphiles with alkyl chain (red colour) where $n = 9, 11$ or 13 at positions $R_0, R_1, R_2,$ and R_3 .

Furthermore, a peptide without an alkyl chain and another without an acyl cap were also synthesized to act as controls.

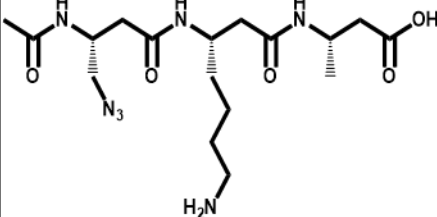
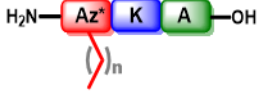
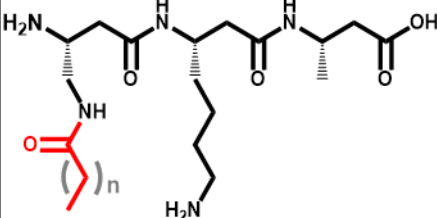
Alkyl chain position	Design	Chemical structure
NA		
		

Figure 2.3: Design for control peptides: without the alkyl chain and without the *N*-terminal capped acetyl group.

2.3 Materials and methods

2.3.1 Materials, Chemicals and Reagents

- Fmoc- β^3 -homo-alanine-OH, Fmoc- β^3 -homo-lysine(Boc)-OH, Wang resin, O-benzotriazole-N,N,N',N'-tetramethyl-uronium-hexafluoro-phosphate (HBTU) and Triisopropylsilane (TIS) were purchased from GL Biochem Ltd (Shanghai, China).
- N,N-Diisopropylethylamine (DIPEA) and N,N-Dimethylformamide (DMF) were purchased from Auspep (Melbourne, Australia).
- Trifluoroacetic acid (TFA) was purchased from Oakwood Chemical Co. (Estill, SC, USA).
- 4-Dimethylaminopyridine (DMAP), acetic anhydride, dodecanoic acid (lauric acid), tetradecanoic acid (Myristic acid) and hexadecanoic acid (Palmitic acid) were purchased from Aldrich Chemical Co. Inc. (St Louis, MO, USA).
- Dichloromethane (DCM), Tetrahydrofuran (THF), Piperidine, Diethyl ether (Ether) and HPLC grade Acetonitrile (ACN) were purchased from Merck KGaA (Darmstadt, Germany).
- Fmoc-L-Dbu(N₃)-OH (Fmoc- β^3 -homo-azidoalanine) was purchased from Iris Biotech GmbH (Marktredwitz, Germany).
- Triphenylphosphine (PPh₃) was purchased from BDH Chemicals (Pooles, England).
- Phosphate buffer saline (pH 7.4) was purchased from Gibco® life technologies™ (New York, USA).

2.3.2 Synthesis of β^3 -peptide amphiphiles

β^3 -peptide amphiphiles were synthesised using solid phase peptide synthesis (SPPS). The synthesis was carried out on a 0.1 mmol scale where the first β^3 -amino acid was attached to Wang resin using 3.1 eq β^3 -amino acid, 3 eq HBTU, 4.5 eq DIPEA and 0.1 eq DMAP, dissolved in DMF overnight with constant mixing. The resin was then washed 3 times with DMF before deprotection of the Fmoc group on the first β^3 -amino acid with 20% piperidine in DMF (2 x 20 min). The by-products were removed by washing 5 times with DMF after deprotection. The second β^3 -amino acid was then coupled to the free *N*-terminus of the first β^3 -amino acid using 3.1 eq β^3 AA, 3 eq HBTU and 4.5 eq DIPEA in DMF for 1 hour. The cycles were repeated until the β^3 -tripeptide sequences were completed.

Alkylation and acetylation were carried out following the final coupling of β^3 -amino acid in the sequence. The β^3 -tripeptides with the sequences; C₁₂-KAK-OH (**P1**), C₁₄-KAK-OH (**P2**) and C₁₆-KAK-OH (**P3**), were alkylated at the *N*-terminus and referred to as R₀. The Fmoc on the *N*-terminal residue was deprotected before coupling the alkyl chains with lauric acid (3.1 eq.), myristic acid (3.1 eq.) and palmitic acid (2 eq.) to **P1**, **P2** and **P3** respectively using 3 eq HBTU and 4.5 eq DIPEA for coupling C₁₂ and C₁₄ in DMF, while 2 eq HBTU and 6 eq DIPEA were used for coupling palmitic acids in DMF. *N*-terminal acetylation was carried out before alkylation was performed for β^3 -tripeptides with the sequences Ac-Az*(C₁₂)KA-OH (**P4**), Ac-Az*(C₁₄)KA-OH (**P5**), Ac-Az*(C₁₆)KA-OH (**P6**), Ac-AAz*(C₁₂)K-OH (**P7**), Ac-AAz*(C₁₄)K-OH (**P8**), Ac-AAz*(C₁₆)K-OH (**P9**), Ac-KAAz*(C₁₂)-OH (**P10**), Ac-KAAz*(C₁₄)-OH (**P11**) and Ac-KAAz*(C₁₆)-OH (**P12**). For *N*-terminal acetylation, the Fmoc-protecting group of the *N*-terminal β^3 -amino acid was cleaved off before the addition of 0.45 mL acetic anhydride and 0.05 mL DIPEA in 4.5 mL DMF (2×20 min). For the alkylation, reduction of the azide moiety to an amine was carried out using 3 eq PPh₃ dissolved in THF and H₂O (4:1). This was incubated overnight or in a microwave for 2 hrs set at 60°, 100 W and 75 Psi. The mixture was then washed with THF/H₂O (4:1), DCM and DMF before the alkylation was performed as described above. The β^3 -peptide amphiphiles with alkyl chains attached to the amine of Az* at residue 1, 2 and 3 are called, R₁, R₂ and R₃ (for example **P4**, **P7** and **P10**) respectively. Two control peptides with the sequences Ac-Az*KA-OH (**P13**) and NH₂-Az*(C₁₄)KA-OH (**P14**) were also synthesised as described above but without alkylation and *N*-terminal acetylation respectively.

β^3 -tripeptides were cleaved off the resin with a 10 mL cleavage cocktail made with 2.5% v/v water, 2.5% v/v TIS in 95% TFA for 3 hrs. Thereafter, TFA was evaporated under a stream of N₂ and the synthesised product was precipitated by the addition of 40 mL diethyl ether. The precipitate was filtered through a sintered glass funnel and reconstituted in H₂O/ACN (3:1) before it was lyophilised overnight in the FreeZone® -105°C 4.5 L benchtop freeze dry system (Labcono, VWR).

2.3.3 Purification of β^3 -peptide amphiphiles

All β^3 -peptide amphiphiles were purified using a preparative reversed phase high-performance liquid chromatography (RP-HPLC) using an Agilent HP1200 system equipped

with a preparative column (C₁₈, 300 Å, 5 µm, 10 mm x 250 mm). The peptides with the alkyl chain length of C₁₂, C₁₄ and C₁₆ were first dissolved in 40%, 50% and 60% v/v ACN in H₂O respectively and filtered through a 0.45 µm Acrodisc® syringe filter with Supor® membrane (Pall Corporation), before injecting 5mL of the filtrate onto the preparative column. All the peptides were eluted with gradients from 20-70% over 60 min (Table 2.1) except for **P13** which was purified 0-20% over 50 min (Table 2.2), using 0.1% TFA in H₂O (Solution A) and 0.1% TFA in ACN (Solution B) at a flow rate of 6 mL/min. To assess peptide purity, the collected fractions were then analysed by analytical HPLC (Agilent HP1100) and mass confirmed by mass spectrometry (Agilent 1100 MSD SL). Fractions with the confirmed purity and molecular mass were pooled together and lyophilised.

Table 2.1: RP-HPLC gradient used for purifying **P1 – P12** and **P14**.

Time (min)	Buffer B (%)
0	20
50	70
55	98
57	98
60	20

Table 2.2: RP-HPLC gradient for purification of **P13**.

Time (min)	Buffer B (%)
0	0
50	20
52	98
54	98
60	0

2.3.4 Atomic force microscopy

All samples were dissolved in water to a final concentration of 0.25 mg/mL and incubated for at least 1 hr. Thereafter, 2 μ L of samples were placed on a freshly cleaved 12 mm mica and air dried at room temperature. Structural analysis was performed using AFM in air with NanoScope[®] IV equipped with a MultiMode™ head (Veeco Instrument Inc. New York, USA) and a Bruker AFM multimode VIII (Bruker Corporation Massachusetts, USA) powered by Peak Force[®] Tapping mode with ScanAsyst. Images were obtained using a 'J-scanner' or 'E-scanner'. The probe used was a mikromasch cantilever (NSC-15 'B' silicon cantilevers) with a force constant of 40 N/m. Topographic, phase and amplitude images were captured simultaneously using a scan frequency of 1 Hz. The captured images were processed, and measurement of height values was carried using Gwyddion 2.45 software. For the height values, 100 different measurements of self-assembled morphology was carried out by extracting the profiles before exporting to Microsoft Excel in order to produce normalised height profile graphs. Finally, statistical analysis was done using one-way ANOVA and Tukey's multiple comparison test.

2.3.5 Transmission electron microscopy

Structural analysis was carried out by TEM using 2 μ L peptide sample solution deposited onto a carbon-coated copper grid. The excess solution was gently blotted with filter paper and left to dry for 30 min under ambient conditions. Microscopy was done on a Hitachi H-7500 TEM (80 keV) and a FEI Tecnai G2 Spirit TEM (Oregon, USA) operated at 100 keV and 120 Kev. The captured images were processed and analysed using ImageJ software.

2.3.6 Hydrogel formation

All β^3 -peptide amphiphile samples were dissolved to a final concentration of 10 mg/mL in phosphate-buffered saline (PBS) solution. The peptide solutions were allowed to stand for 1 hr for visual inspection of hydrogels. Thereafter, the inversion test was carried to observe the formation of the hydrogel. A complete and stable hydrogel results in a zero visible

deformation, while a sample undergoing incomplete gel transition shows deformation in the form of flow towards the lid [15].

2.4 Results

2.4.1 Synthesis and purification of β^3 -peptide amphiphiles

To explore the effect of alkyl chain length and position in controlling the self-assembly of β^3 -peptides, 14 β^3 -peptide amphiphiles (**P1-P14**) were designed and synthesised as shown in Figures 2.2 and 2.3. The final β^3 -peptide amphiphiles **P1-P12** possess both a hydrophilic residue β K and hydrophobic alkyl chain (C_n where $n = 12, 14$ and 16). Figure 2.4 shows the SPPS of R_0 for **P1**, **P2** and **P3**, while Figure 2.5 shows the SPPS for R_1 , R_2 and R_3 . The synthesis of R_0 was performed without β Az* because the alkyl chain was coupled directly to the *N*-terminal end. Therefore, β K was used in place of β Az* because of its hydrophilic nature. For the synthesis of R_1 , R_2 or R_3 , the β Az* was used as a means to couple the alkyl chain to the side chain. This was achieved by converting the azide (N_3^-) group in β Az* to an amine via the Staudinger reduction [16]. The amine provided the handle for conjugation of the alkyl chain to the β^3 -peptide backbone.

In addition, the two control peptides **P13** and **P14** were synthesised without an alkyl side chain and *N*-terminal acylation respectively. The purpose of **P13** and **P14** was to provide more insight into the influence of the alkyl chain and *N*-terminal acetylation on the self-assembly of β^3 -peptides amphiphiles.

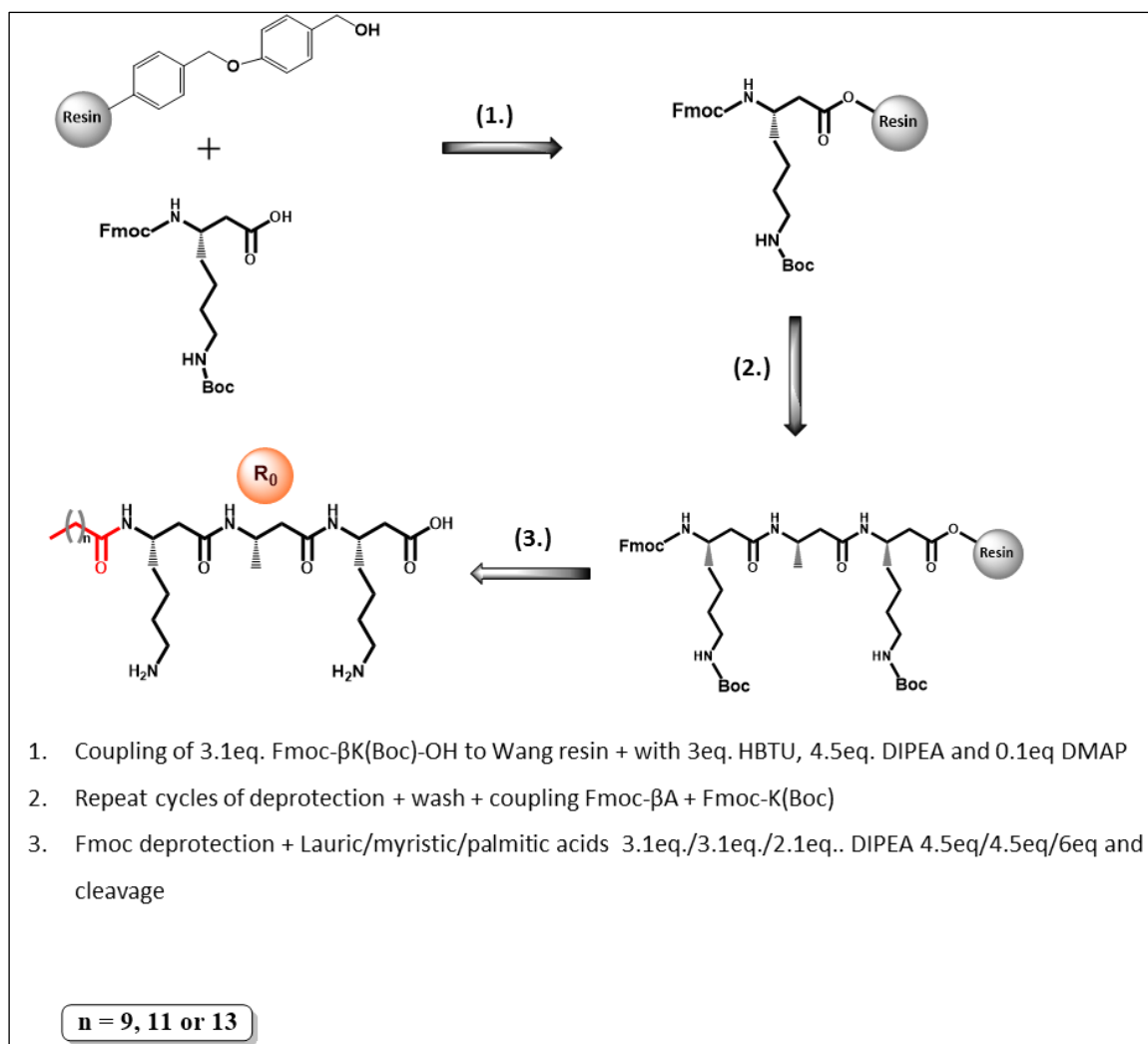


Figure 2.4: SPPS reaction sequence for **P1**, **P2** and **P3** in which alkyl chains were incorporated at the *N*-terminus.

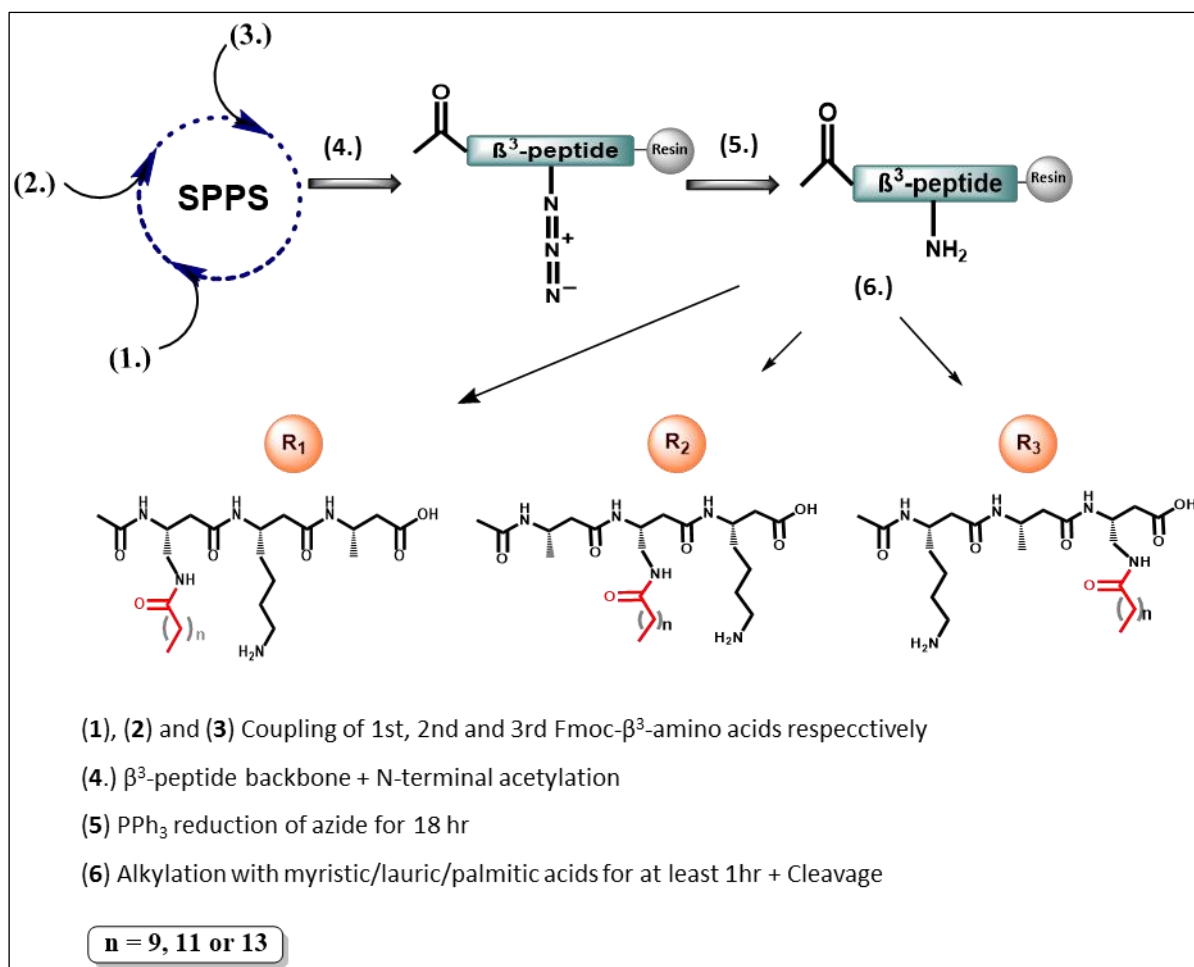


Figure 2.5: SPPS reaction sequence for R_1 , R_2 and R_3 β^3 -peptide amphiphiles. The β^3 -peptide backbone shows the side chain azide (N_3^-) of βAz^* before reduction to the amine via Staudinger reaction. This scheme was used for the synthesis of **P4** - **P12**. **P13** and **P14** were also synthesised using the same scheme but without the alkyl chain and N-terminal acetylation respectively.

The purified β^3 -peptide sequences, calculated mass and obtained mass are shown in Table 2.3. The mass obtained for the synthesised peptides corresponded to the calculated mass. Following synthesis and purification, the peptide fractions were analyzed by RP-HPLC for purity. The purity of each synthesised β^3 -peptide amphiphile was confirmed by the presence of only one main peak detected at 214 nm. The RP-HPLC chromatograms obtained for **P1** - **P14** analyses are shown in Figure 2.6.

Table 2.3: Synthesised and purified β^3 -peptide amphiphiles.

Alkyl chain position	Code	Alkyl chain length	Peptide Sequence	Calculated mass	Obtained mass
R ₀	P1	C ₁₂	C ₁₂ -KAK-OH	569.5	570.3
	P2	C ₁₄	C ₁₄ -KAK-OH	598.3	597.9
	P3	C ₁₆	C ₁₆ -KAK-OH	625.51	624.4
R ₁	P4	C ₁₂	Ac-Az*(C ₁₂)KA-OH	569.4	568.3
	P5	C ₁₄	Ac-Az*(C ₁₄)KA-OH	596.3	596.5
	P6	C ₁₆	Ac-Az*(C ₁₆)KA-OH	625.5	624.4
R ₂	P7	C ₁₂	Ac-AAz*(C ₁₂)K-OH	569.4	568.3
	P8	C ₁₄	Ac-AAz*(C ₁₄)K-OH	596.4	596.5
	P9	C ₁₆	Ac-AAz*(C ₁₆)K-OH	625.5	624.4
R ₃	P10	C ₁₂	Ac-KAAz*(C ₁₂)-OH	569.4	568.3
	P11	C ₁₄	Ac-KAAz*(C ₁₄)-OH	596.4	596.5
	P12	C ₁₆	Ac-KAAz*(C ₁₆)-OH	625.5	624.4
Controls	P13	-	Ac-Az*KA-OH	413.3	414.0
	P14	C ₁₄	NH ₂ -Az*(C ₁₄)KA-OH	555.4	556.3

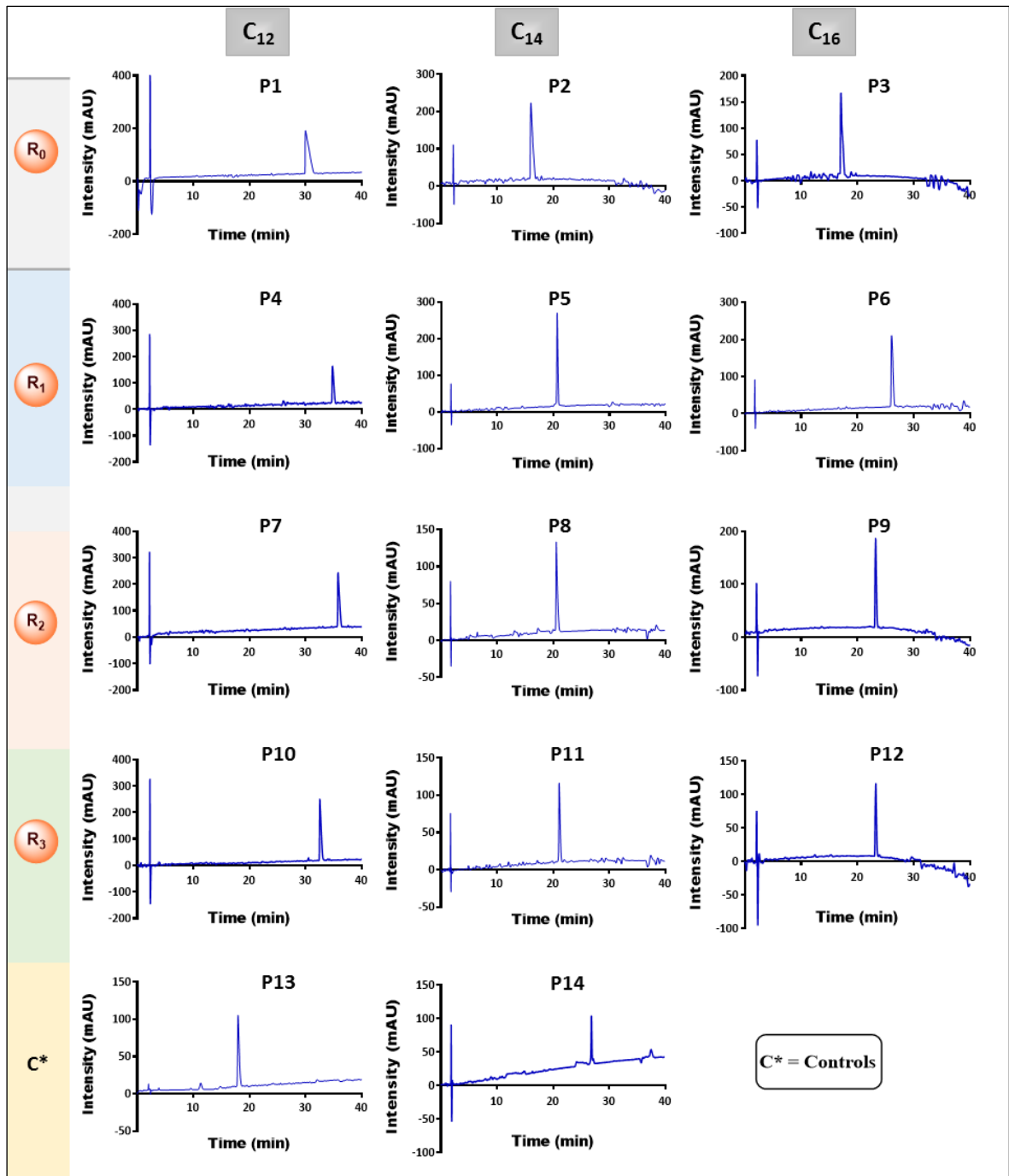


Figure 2.6: Chromatograms of analytical RP-HPLC for purified peptides **P1 – P14**.

2.4.2 Self-assembly of R₀ β³-peptide amphiphiles

AFM and TEM were used to characterise the self-assembled nanostructures of R₀ β³-peptide amphiphiles. The effect of alkyl chain length and position on the self-assembly of β³-peptide amphiphiles was investigated by dissolution of the samples in mq-H₂O. As shown in Figure 2.7, the AFM images revealed that **P1**, **P2** and **P3** formed nanofibres. Figure 2.7(A), (B) and (D) show an intertwined nanofibrous mesh. The nanofibres are long with a surface periodicity (indicated with white arrows). As an alternative, TEM images also revealed a similar morphology to that observed by AFM except for **P1** which could not be imaged by TEM. **P1** may require staining of the TEM grids which will increase the contrast of the image [17]. TEM images for **P2** and **P3** (Figure 2.7(C) and (E)) revealed evidence of twisted ribbons, consistent with the periodicity observed by AFM for both **P2** and **P3**. In addition, the variation in the length of alkyl chains did not show any effect (except for **P1**) on the self-assembled morphology for R₀ β³-peptide amphiphiles.

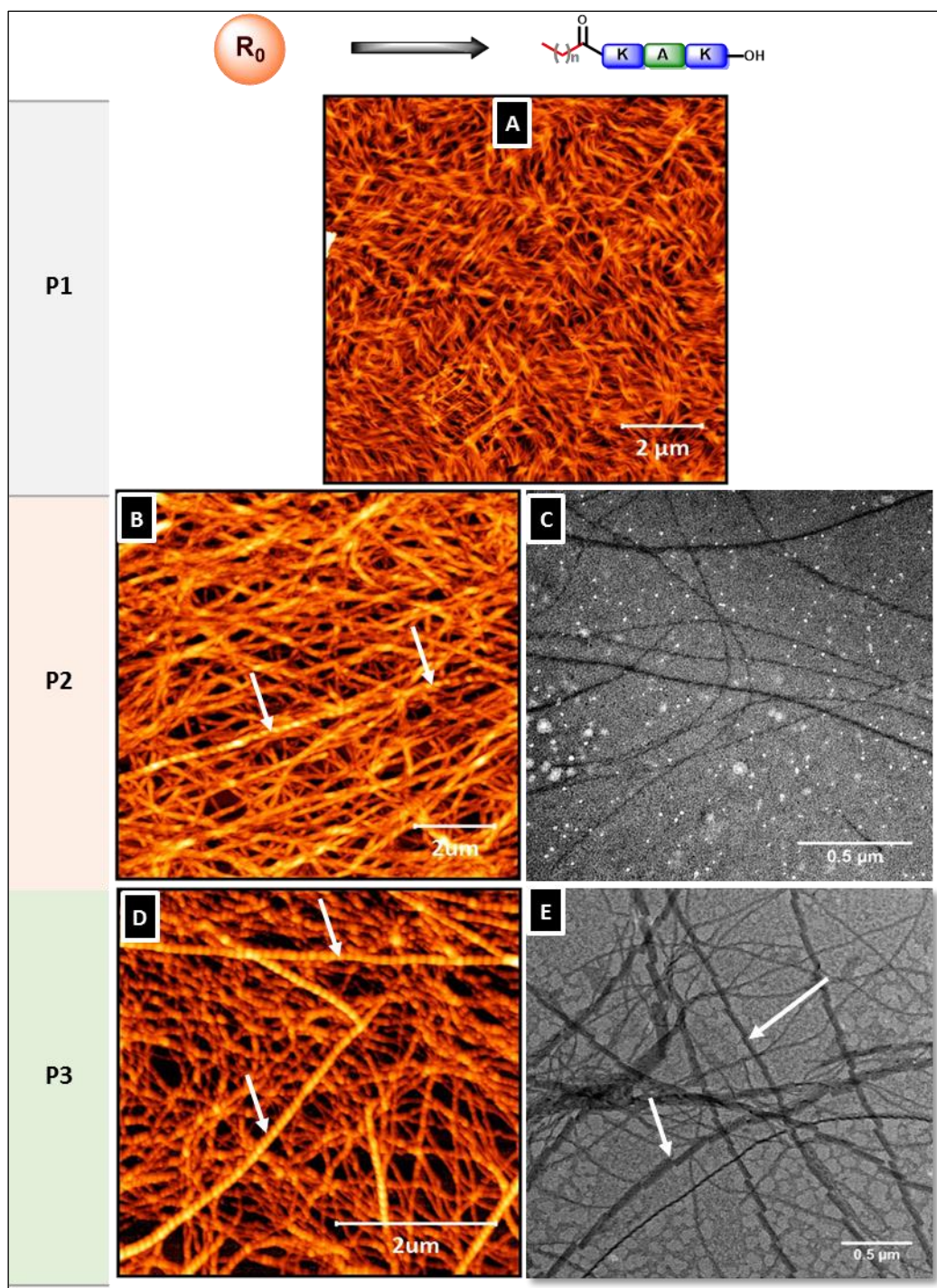


Figure 2.7: Self-assembled architectures of R_0 β^3 -peptide amphiphiles. (A) AFM image of **P1** nanofibres, (B) AFM and (C) TEM images of **P2** nanofibres, (D) AFM and (E) TEM images of **P3** nanofibres. The white arrows in (B), (D) and (E) indicate surface periodicity by AFM and twisted ribbons by TEM.

Figure 2.8 shows sections of **P2** and **P3** nanofibres which exhibited rope-like nanostructures with a surface periodicity. The surface profiles of these nanofibres were extracted and the topologies of the nanofibres revealed a periodicity of 1.6 ± 0.5 nm in height.

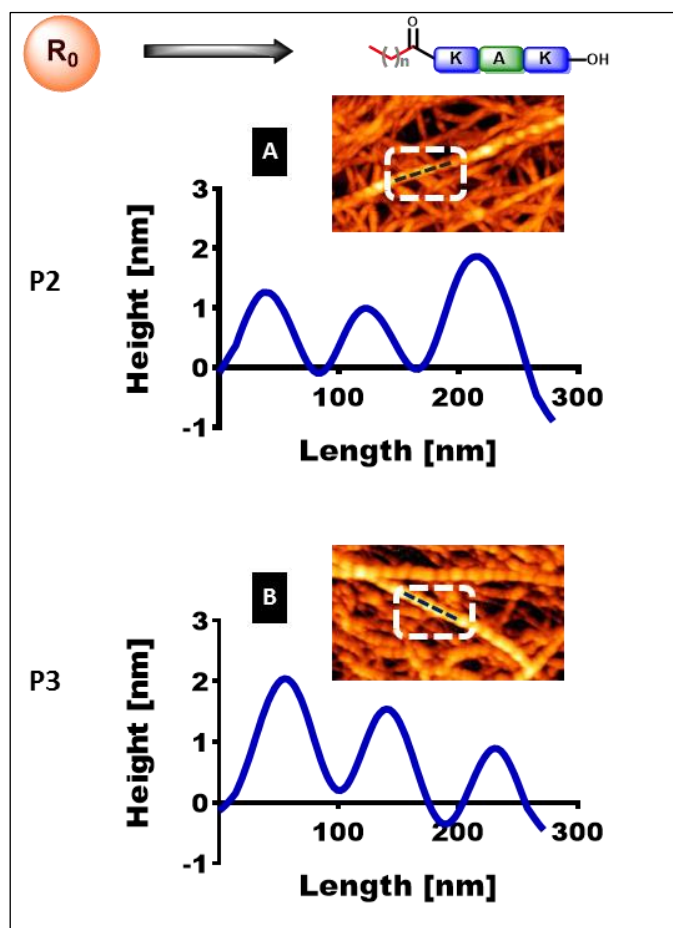
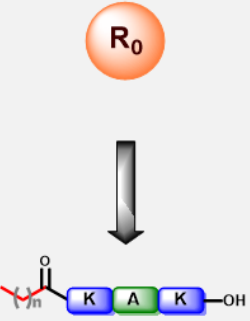
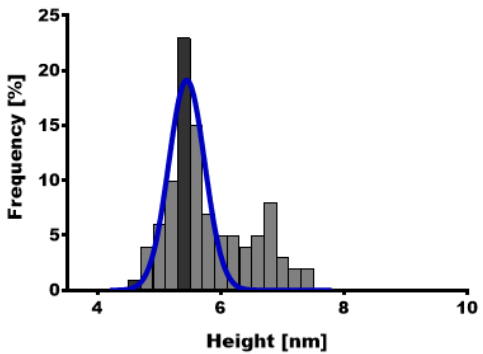
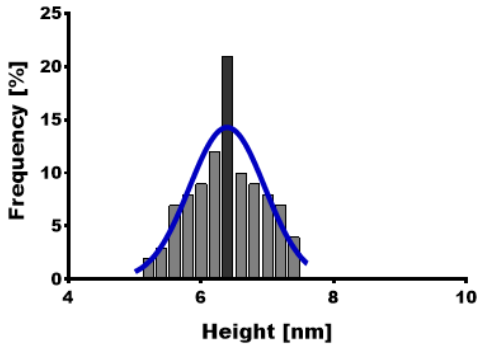
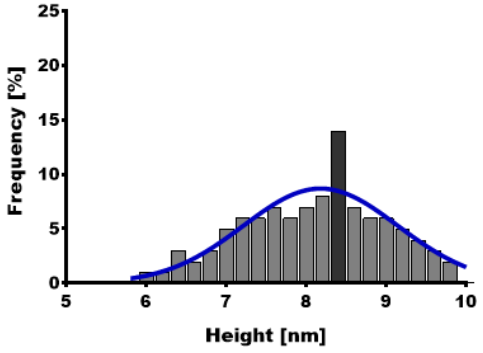


Figure 2.8: Extracted profiles of surface periodicity in self-assembled R_0 β^3 -peptide amphiphiles. (A) **P2** periodicity (B) **P3** periodicity. Inserted AFM images show the highlighted twisted ribbon sections of the extracted profiles.

To ascertain the dimensions of these twisted ribbons by AFM, a total of 100 height measurements were taken and used to determine the mean, mode, standard deviation (SD) and standard error of mean (SEM*) from the frequency distribution plots (Table 2.4). The average height value for each peptide from this distribution was taken to be the mean value from the Gaussian analysis curve. The average height values of **P1**, **P2** and **P3** are 5.4 ± 0.3 nm, 6.4 ± 0.6 nm and 8.2 ± 1.0 nm respectively. It was also observed that the height distribution of **P1** was bimodal. The heights increased as the alkyl chain length increases. The

height values of **P1** was found to be significantly lower than that of **P2** and **P3** ($p < 0.05$), and **P2** was significantly lower than **P3** ($p < 0.05$).

Table 2.4: Summary table of heights distribution for R_0 β^3 -peptides amphiphiles.

Alkyl chain position	Code	Height Distribution	Heights (nm)
	P1 C₁₂		Mean = 5.4 Mode = 5.4 SD = 0.3 SEM = 0.1
	P2 C₁₄		Mean = 6.4 Mode = 6.4 SD = 0.6 SEM = 0.1
	P3 C₁₆		Mean = 8.2 Mode = 8.4 SD = 1.0 SEM = 0.1

2.4.3 Self-assembly of R₁ β³-peptide amphiphiles

The R₁ β³-peptide amphiphiles **P4**, **P5** and **P6** also self-assembled into a nanofibrous architecture. Figure 2.9 shows the self-assembled nanostructure of **P4**, **P5** and **P6** which revealed an intertwined nanofibre mesh by both AFM and TEM. Despite the different positions of the alkyl chains in R₀ β³-peptide and R₁ β³-peptides, the morphological features are very similar. For example, AFM images revealed nanofibres with evidence of surface periodicity (Figure 2.9(A), (C) and (E)). It was also found that the different length of alkyl chains did not show any effect on the final self-assembled structure.

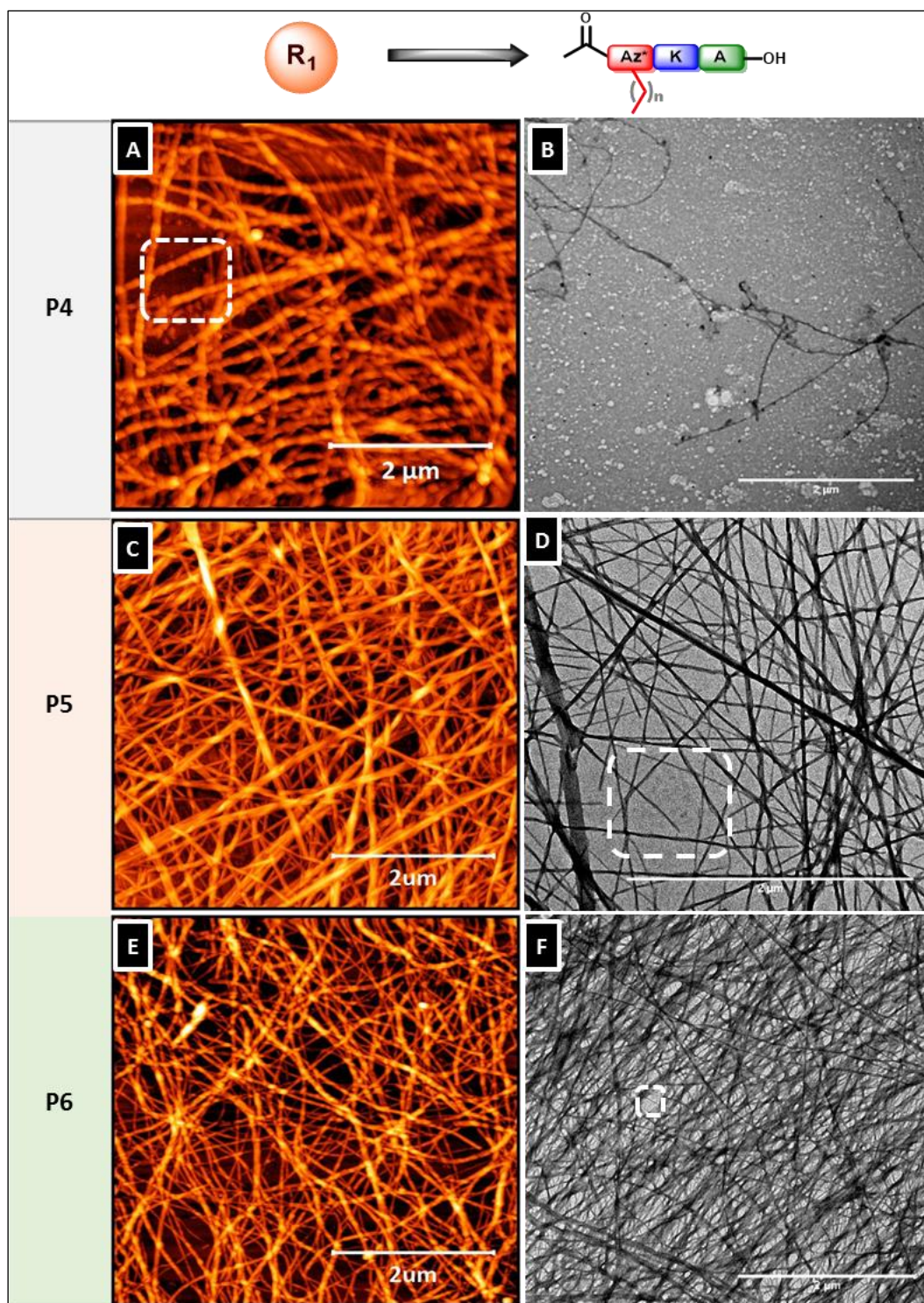


Figure 2.9: Self-assembled morphology of R_1 β^3 -peptide amphiphiles. (A) AFM and (B) TEM images of **P4** nanofibres, (C) AFM and (D) TEM of **P5** nanofibres, (E) AFM and (F) TEM images of **P6** nanofibres. The highlighted dotted boxes in (A), (D) and (E) are shown in high magnification in Figure 2.10.

The nanofibres presented by **P4**, **P5** and **P6** (Figures 2.9(A), (D) and (F)) were further analysed in which the extracted surface profile of **P4** revealed a periodicity of 0.9 ± 0.2 nm (Figures

2.10(A) and (B)). The TEM images of **P5** and **P6** (Figures 2.9(D) and (F)) were also analysed by high magnification ($\times 67000$). Figure 2.10(C) and (D) show several points (indicated by white arrows) where the twisted ribbon patterns occurred for **P5** and **P6**.

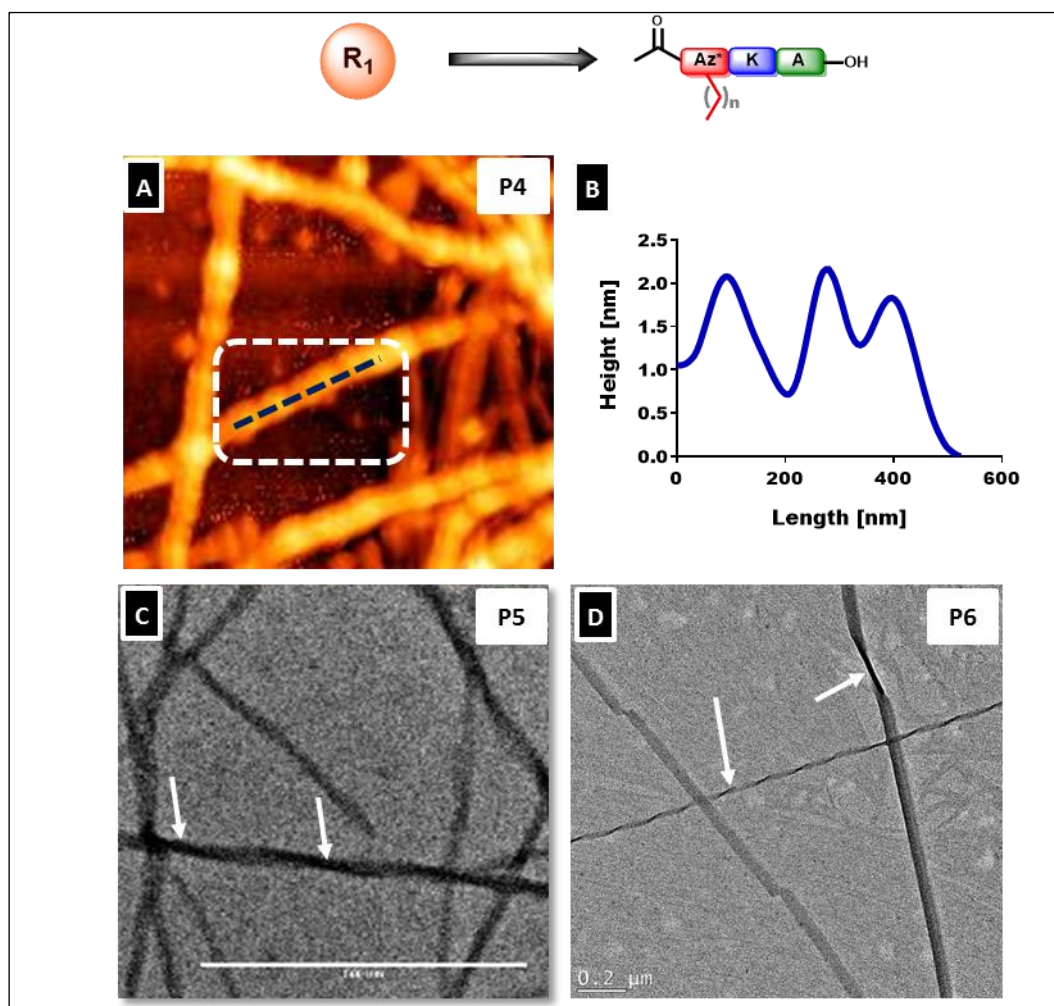
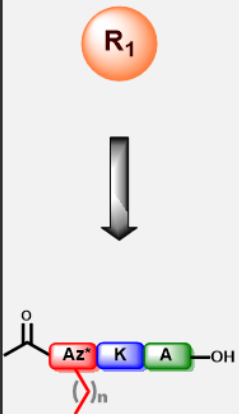
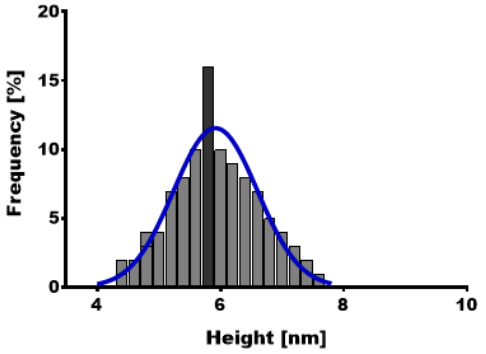
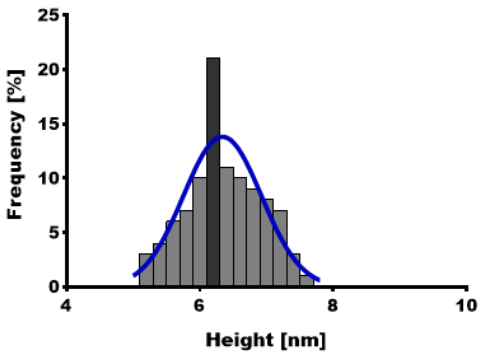
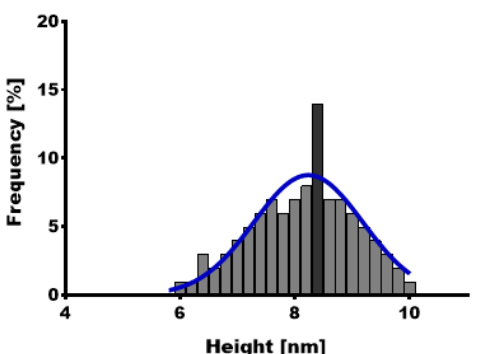


Figure 2.10: Surface profiles of R_1 β^3 -peptide amphiphiles by high-resolution AFM and TEM. (A) High magnification of AFM image for **P4** showing surface periodicity, (B) analysis of the extracted length profile along the surface of the nanofibre in A, (C) TEM high magnification ($\times 67,000$) image of **P5** and (D) high magnification ($\times 67,000$) of **P6**. White arrows used for (C) and (D) show the location of the twisted patterns.

The frequency distribution of the height values was obtained by AFM analysis (as previously described for R_0 β^3 -peptide amphiphiles). The average height of **P4**, **P5** and **P6** were found to be 5.8 ± 0.7 nm, 6.2 ± 0.6 nm and 8.4 ± 0.9 nm respectively (Table 2.5). As the hydrophobic alkyl chain length increases, the size was observed to also increase. For example a difference

in height values between **P4** and **P6** of ≈ 2 nm was observed. Regardless of the length of alkyl chain or position, the average height values for R_1 and R_0 β^3 -peptide amphiphiles were observed to be similar. The height values of R_1 peptides revealed that **P4** and **P5** are significantly lower than **P6** ($p < 0.05$) however, there was no significant difference in the height values between **P4** and **P5** ($p > 0.05$).

Table 2.5: Summary table of height distribution for R_1 β^3 -peptides amphiphiles.

Alkyl chain position	Code	Height Distribution	Height (nm)
	P4 		Mean = 5.9 Mode = 5.8 SD = 0.7 SEM = 0.1
	P5 		Mean = 6.3 Mode = 6.2 SD = 0.6 SEM = 0.1
	P6 		Mean = 8.2 Mode = 8.4 SD = 1.0 SEM = 0.1

2.4.4 Self-assembly of R₂ β³-peptide amphiphiles

The self-assembled morphology of R₂ β³-peptide amphiphiles were a stark contrast from those observed for R₀ and R₁ peptide amphiphiles. The AFM images of R₂ β³-peptide amphiphiles in Figure 2.11 revealed a distinct nanobelt morphology for **P7**, **P8** and **P9**. The nanobelts appeared flat, long and straight, and in comparison to the twisted ribbons displayed by R₀ and R₁, the nanobelts of R₂ β³-peptide amphiphiles did not exhibit any twisted patterns. The TEM images obtained under the same conditions further confirmed the rigid nanobelt morphology (Figure 2.11(B), (D) and (F)). Given that **P7**, **P8** and **P9** all formed nanobelts, this indicates that variation in the length of alkyl chain did not affect the type of self-assembled morphology for R₂ β³-peptide amphiphiles. However, the change in self-assembled structures from the twisted ribbon to nanobelt was dictated by only switching the position of the alkyl chain from R₀/R₁ to R₂ on the β³-peptide backbone.

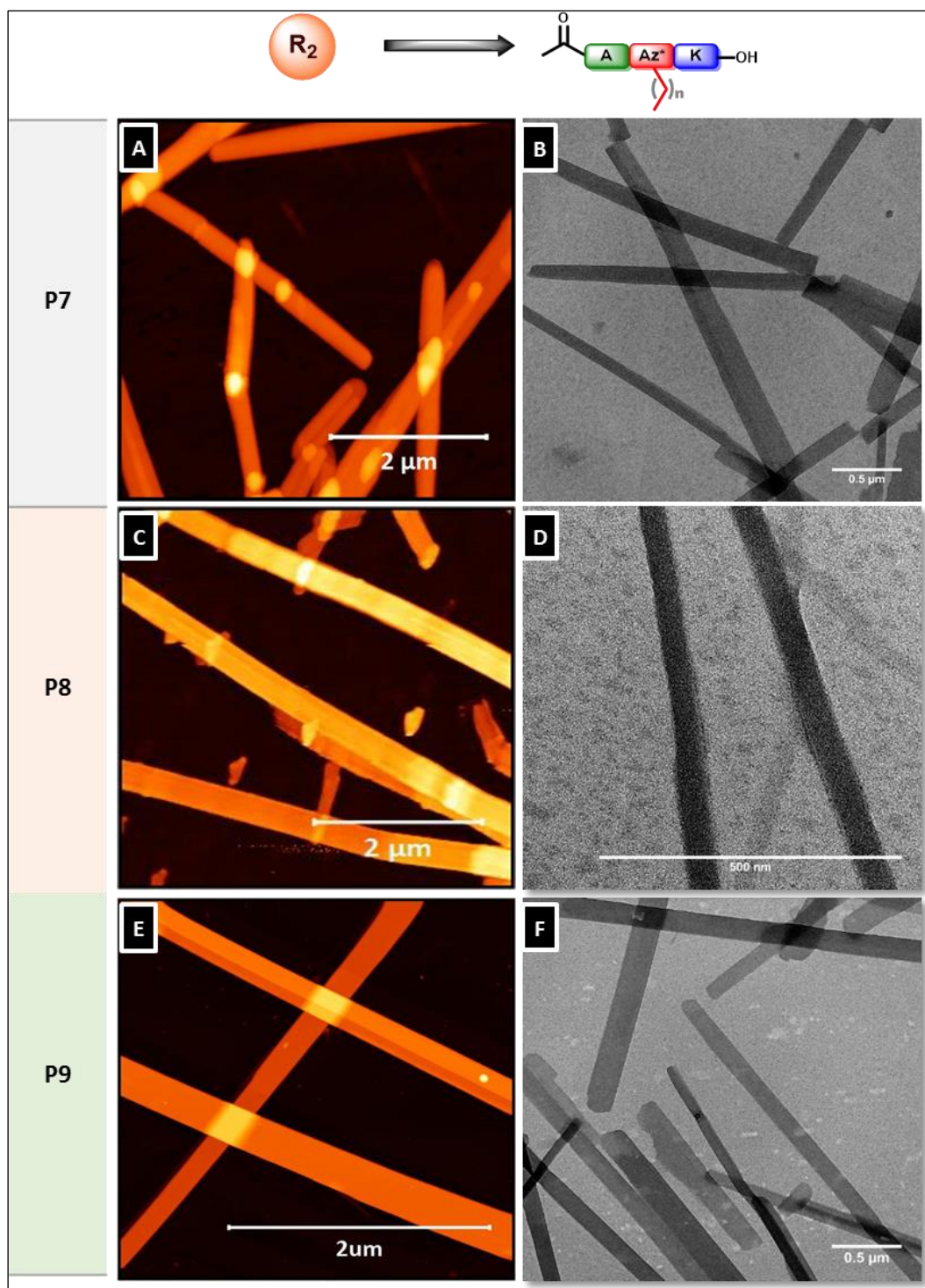


Figure 2.11: Self-assembled morphology of $R_2 \beta^3$ -peptide amphiphiles. (A) AFM and (B) TEM images of **P7** nanobelts, (C) AFM and (D) TEM images of **P8** nanobelts, (E) AFM and (F) TEM images of **P9** nanobelts.

In order to further understand the surface features of the nanobelts, the images in Figure 2.11 were converted to a 3D format which shows well-defined rigid nanobelts (Figures

2.12(A), (C) and (E)). The surface topological profiles were extracted and graphically presented as shown in Figures 2.12(B), (D) and (F). The profiles revealed that the nanobelts have flat plateaus with wide architecture of more than 200 nm. Wider nanostructures formed as a result of smaller nanobelts that merged together by lateral association. For example, a rod-like surface profile was observed for **P7** (Figures 2.12(A) and (B)) which merged to form a wider nanobelt surface. The decrease in height value on the surface for profile 1 of **P7**, (Figure 2.12(B)) indicates the point where two nanobelts merged. Similarly, profiles 1 and 2 for **P8** (Figure 2.12(D)) also shows merging points for three and two nanobelts respectively. For **P9**, profile 2 (Figure 2.12(F)) shows two nanobelts with different height values that merged together to give a single nanobelt.

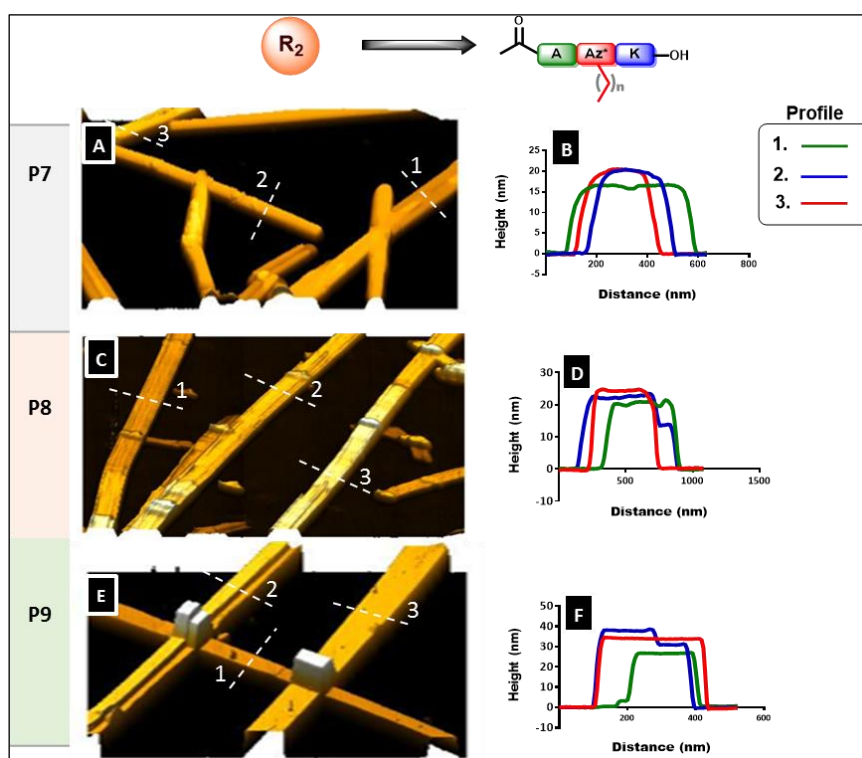
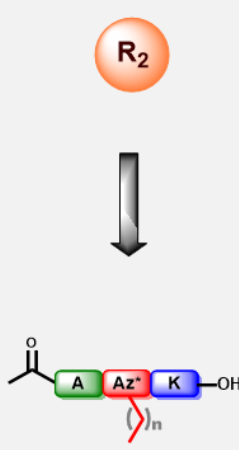
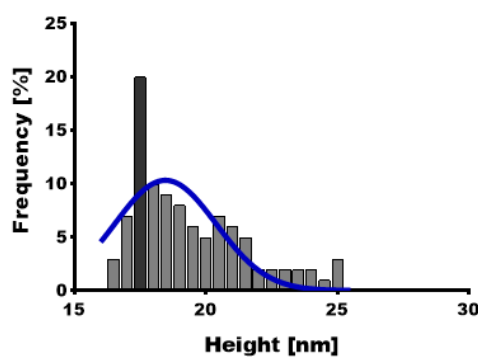
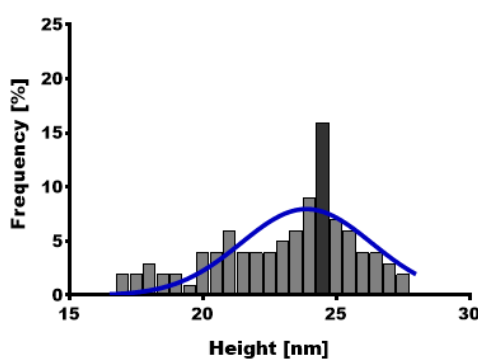
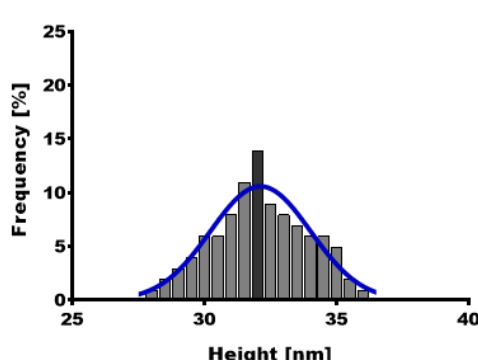


Figure 2.12: Surface topology of self-assembled nanobelts of R_2 β^3 -peptide amphiphiles by AFM. (A) 3D image of **P7**, (B) graphical presentation using extracted profiles from sections of (A), (C) 3D image of **P8**, (D) graphical presentation using extracted profiles of C, (E) 3D image of **P9**, (F) graphical presentation using extracted profiles of (E).

The average height values for **P7**, **P8** and **P9** nanobelts were obtained by AFM from the frequency distribution plot (as previously described for R_0 peptide amphiphiles). Table 2.6

shows the heights to be 18.5 ± 1.9 nm, 23.9 ± 2.5 nm and 32.1 ± 1.9 nm for **P7**, **P8** and **P9** respectively. The height values of **P7** are significantly lower than those of **P8** and **P9** ($p < 0.05$) while the height values of **P8** are significantly lower than that of **P9** ($p < 0.05$). In addition, the height values of R_2 peptides are significantly higher than R_0 and R_1 peptides ($p < 0.05$). This suggests that the length of the alkyl chain significantly influenced the size of the nanobelts for R_2 β^3 -peptide amphiphiles.

Table 2.6: Summary table of height distribution for R₂ β³-peptides amphiphiles.

Alkyl chain position	Code	Height Distribution	Height (nm)
	<p>P7</p> <p>C₁₂</p>		<p>Mean = 18.5</p> <p>Mode = 17.5</p> <p>SD = 1.9</p> <p>SEM = 0.4</p>
	<p>P8</p> <p>C₁₄</p>		<p>Mean = 23.9</p> <p>Mode = 24.5</p> <p>SD = 2.5</p> <p>SEM = 0.4</p>
	<p>P9</p> <p>C₁₆</p>		<p>Mean = 32.1</p> <p>Mode = 32.0</p> <p>SD = 1.9</p> <p>SEM = 0.1</p>

2.4.5 Self-assembly of R₃ β³-peptide amphiphiles

The self-assembled morphology of R₃ β³-peptide amphiphiles is shown in Figure 2.13. The AFM and TEM images of **P10**, **P11** and **P12** revealed nanobelts which overlap with each other at various points in different directions (Figures 2.13(A), (C), (E) and (F)). The nanobelts formed by R₃ β³-peptide amphiphiles are structurally similar to that of R₂ β³-peptide amphiphiles. This result indicates that the variation in alkyl chain length does not have an effect on the type of self-assembled nanostructure for the R₃ series and that the position of the alkyl chain exerts a similar effect on morphology as R₂.

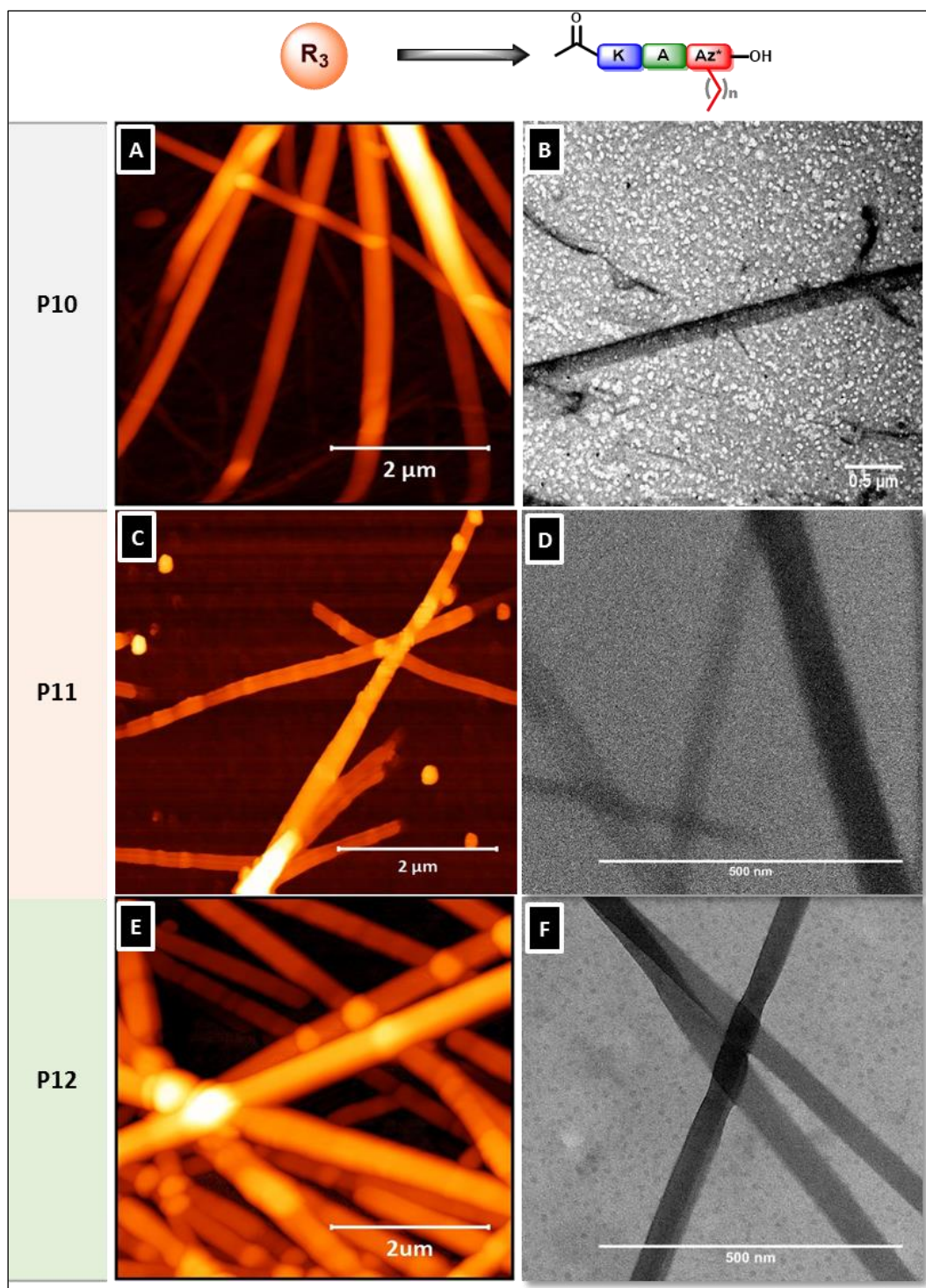


Figure 2.13: Self-assembled morphology of R_3 β^3 -peptide amphiphiles. (A) AFM and (B) TEM images of **P10** nanobelts, (C) AFM and (D) TEM images of **P11** nanobelts, (E) AFM and (F) TEM images of **P12** nanobelts.

The images in Figure 2.13 were also analysed for surface topology as described for R_2 β^3 -peptide amphiphiles. Figure 2.14 shows the 3D images and graphical presentation of the

extracted profiles for **P10**, **P11** and **P12** (Figures 2.14(B), (D) and (F)), which revealed rod-like surface similar to **P7** and flat plateaus similar to that of **P8** and **P9**.

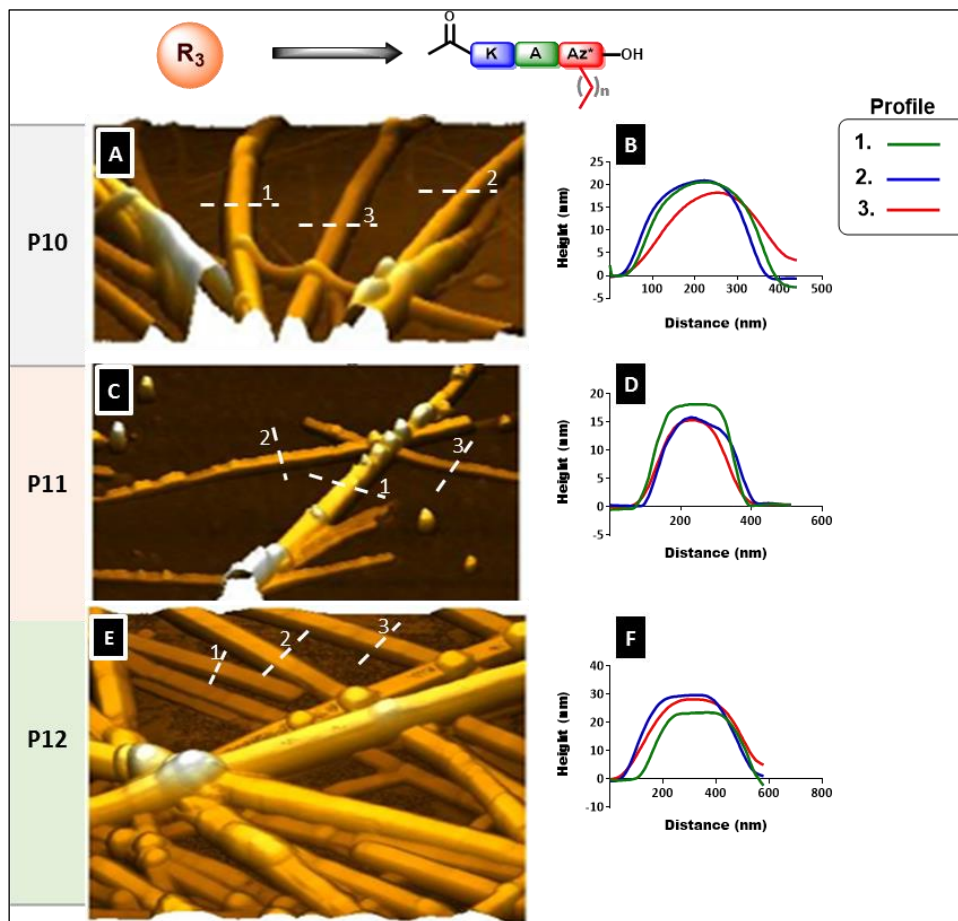
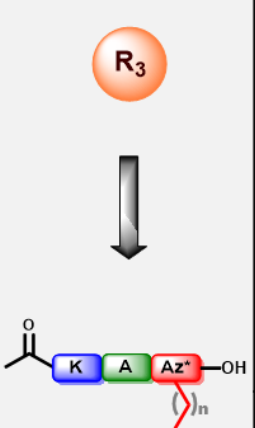
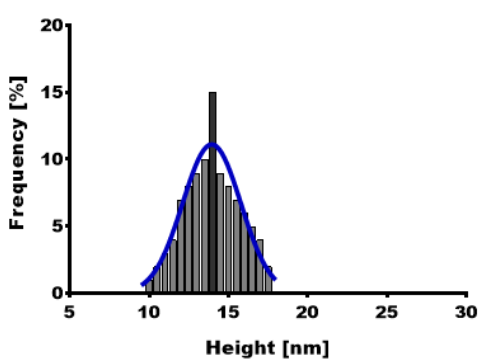
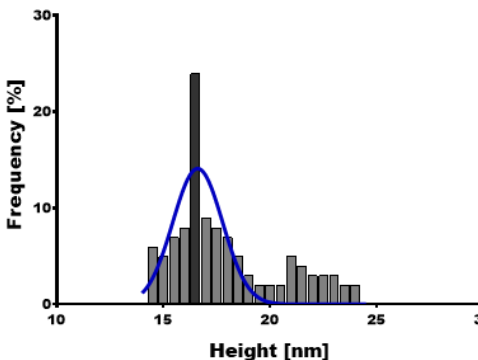
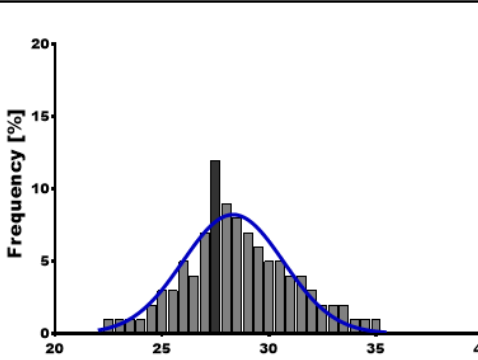


Figure 2.14: Surface topology of self-assembled nanobelts of $R_3 \beta^3$ -peptide amphiphiles by AFM. (A) 3D image of **P10**, (B) graphical presentation using extracted profiles from sections of (A), (C) 3D image of **P11**, (D) graphical presentation using extracted profiles of (C), (E) 3D image of **P12**, (F) graphical presentation using extracted profiles of (E).

The height values for **P10**, **P11** and **P12** nanobelts are shown in Table 2.7 obtained as previously described. The average height values were found to be 13.9 ± 1.8 nm, 16.6 ± 1.2 nm, and 28.3 ± 2.4 nm for **P10**, **P11** and **P12** respectively. The height values of **P10** are significantly lower than those of **P11** and **P12** ($p < 0.05$) while **P11** is significantly lower than that of **P12** ($P < 0.05$). This suggest that increase in length of alkyl chain influenced the size distribution of nanobelts in $R_3 \beta^3$ -peptide amphiphiles.

Table 2.7: Summary table for height distribution of R₃ β³-peptides amphiphiles.

Alkyl chain position	Code	Height Distribution	Height (nm)
	<p>P10</p> <p>C₁₂</p>		<p>Mean =13.9</p> <p>Mode = 13.9</p> <p>SD = 1.8</p> <p>SEM = 0.1</p>
	<p>P11</p> <p>C₁₄</p>		<p>Mean =16.6</p> <p>Mode = 16.5</p> <p>SD = 1.2</p> <p>SEM = 0.2</p>
	<p>P12</p> <p>C₁₆</p>		<p>Mean =28.3</p> <p>Mode = 28.3</p> <p>SD = 2.4</p> <p>SEM = 0.2</p>

2.4.6 Self-assembly of unacylated β³-peptides

The AFM analysis of the control peptide **P13** (without an alkyl chain) revealed dendritic fibres with irregular shapes (Figure 2.15(A)). The self-assembled structures spread across the surface in a disordered pattern exhibiting different morphologies to **P1-P12** which were functionalised with alkyl chains. The height values of the nanostructures in **P13** are shown in

Figure 2.15(C). This revealed variable sizes with the extracted height profiles for sections 1, 2 and 3 (Figure 2.15(A)) indicating values of ≈ 40 nm, ≈ 115 nm and ≈ 220 nm respectively (Figure 2.15(C)). This also suggests a lack of control in **P13** self-assembly.

On the other hand, the control peptide **P14** (without N-terminal acetyl group) revealed aggregate-like nanostructures with no signs of nanofibre formation (Figure 2.15(B)).

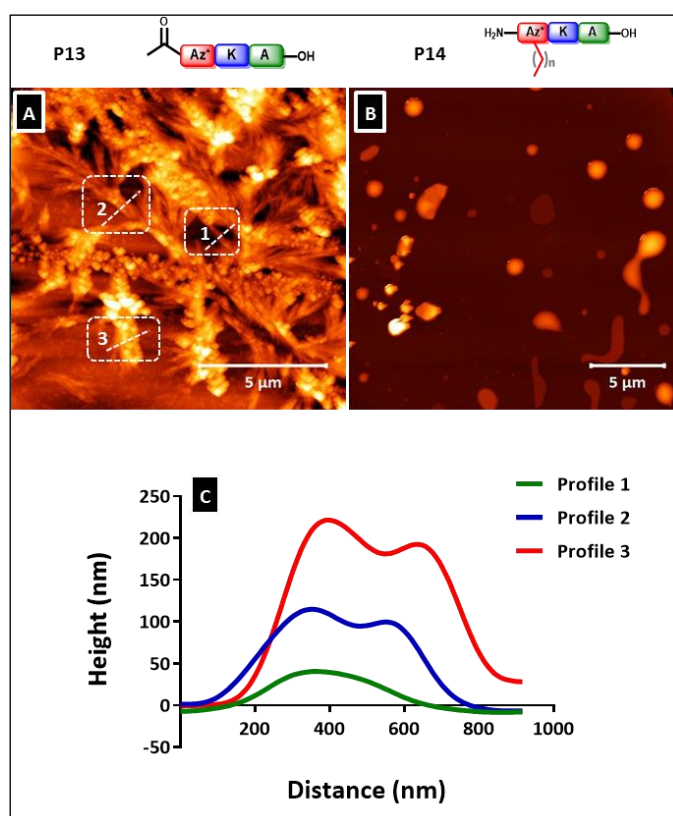


Figure 2.15: Self-assembled morphologies for unacylated β^3 -peptide (A) Dendritic fibres with other morphologies for **P13**, (B) no fibre formation for **P14** and (C) height values of extracted profiles of (A).

In comparison with **P1-P13**, the absence of an *N*-terminal acetyl-capped end in **P14** was the only difference and thus confirming its significant role in previous studies [6-9].

2.4.7 Hydrogel formation

The inverted-vial method is still the simplest way to initially confirm the formation of a supramolecular hydrogel [18]. According to the visual inspection performed, supramolecular

hydrogels were formed without any external aid at 10 mg/mL concentration for **P2-P11** in PBS (pH 7.4) as shown in Figure 2.16, while only **P1** and **P12** did not form hydrogels at 10 mg/mL. The hydrogels retained their 3D structures and were able to support their own weight. The stable hydrogelated structure is comparable to previous studies [19-22] and was also maintained under physiological conditions for at least 2 weeks.

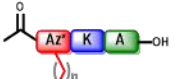
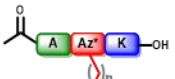
Alkyl chain position	C ₁₂	C ₁₄	C ₁₆
 	P1  NG	P2  G	P3  G
 	P4  G	P5  G	P6  G
 	P7  G	P8  G	P9  G
 	P10  G	P11  G	P12  NG

Figure 2.16: Visual evidence of hydrogels formed from β^3 -peptide amphiphiles. *G = gel, *NG= no gel.

2.5 Discussion

The overall goal of this chapter is to explore strategies for controlling the self-assembly of β^3 -peptides. To achieve this, a new series of β^3 -peptide amphiphiles **P1** – **P12** were synthesised. As shown in Figure 2.2, the control of fibre morphology was attempted by varying the alkyl chain position and alkyl chain length. It was found that the presence of either C₁₂, C₁₄ or C₁₆ alkyl chains lengths resulted in a controlled self-assembly compared to previous non-acylated peptides to come from our laboratory. In particular, the presence of fibres of fairly uniform diameter was the most striking observation as opposed to the dendritic and macroscopic fibres previously reported [6]. The effect of these alkyl chains on peptide self-assembly is consistent with previous studies in which alkyl chains of least 10 carbons were required to control the self-assembly of α -peptide amphiphiles [10, 12, 14, 23-30].

In most α -peptide amphiphiles the hydrophobic alkyl chain is introduced by coupling palmitic acid with the *N*-terminal amine of a short peptide on resin [11, 26, 27, 31-34]. Other reports have also revealed that the control of α -peptide amphiphile self-assembly was not only due to the incorporation of alkyl chains, but also due to the variation of peptide sequence length [35], or by incorporating a proline [36, 37] or a phenylalanine [38, 39] residue in the peptide sequence. This suggests the possibilities of also controlling the one-dimensional (1D) nanostructures through the rational choice of amino acid residues. In this study, twisted ribbons and nanobelts were formed by switching the alkyl chain position within the β^3 -peptide backbone. However, understanding the molecular design of the building blocks will be helpful in deciphering the self-assembly motif of β^3 -peptide amphiphiles. This approach of switching the building block order within the sequence was similarly used in previous reports for α -peptide amphiphiles [40].

The self-assembly of *N*-acetylated β^3 -peptide containing only β^3 -amino acids with a tripeptide as the shortest possible repeating unit is known to occur by head-to-tail orientation, driven by hydrogen bonding between the amine proton at position *i* and a carbonyl at position *i* + 2 to form 14 helical fibres [41, 6]. Hydrogen bonding is common in polypeptides which also stabilises α -helical [42] and β -sheet conformations [43], which are also found in the structural domain of α -peptide amphiphile self-assemblies [12]. The orientation of the hydrogen bond is also important for perfect geometry [44, 45].

The AFM and TEM images revealed that the incorporation of an alkyl chain into the β^3 -peptide monomer at different positions did not disrupt nanofibre self-assembly suggesting that the intermolecular hydrogen bonding between the β^3 -peptide amphiphile monomers was remarkably resilient. The unique property of the β^3 -peptide self-assembly motif was not compromised even when the side chains were functionalised [46, 5, 47]. Most significantly, compared to other peptide-based self-assembling materials, these results further illustrate that *N*-acetylated β^3 -tripeptides form fibrous scaffolds in solution irrespective of the β^3 -peptide sequence [6-9].

2.5.1 Self-assembled morphologies of β^3 -peptide amphiphiles

The self-assembly of R_0/R_1 and R_2/R_3 into twisted ribbons and nanobelts respectively utilises the head-to-tail hydrogen bonding motif that is associated with *N*-acetyl β^3 -tripeptides. The molecular structure and the arrangement of side chains on the exterior face of the helix for R_0 (C_n -KAK-OH) and R_1 (Ac-Az(C_n)KA-OH) are shown in Figure 2.17. The location of alkyl chains on the exterior of the helix gives further opportunity for higher order assembly via hydrophobic interactions. The presence of the *N*-terminal hydrogen acceptor in the acyl groups of both peptides provided the complete 6 axially oriented donor-acceptor interactions, which enabled nanofibre formation and elongation as the monomer aligned axially via hydrogen bonding.

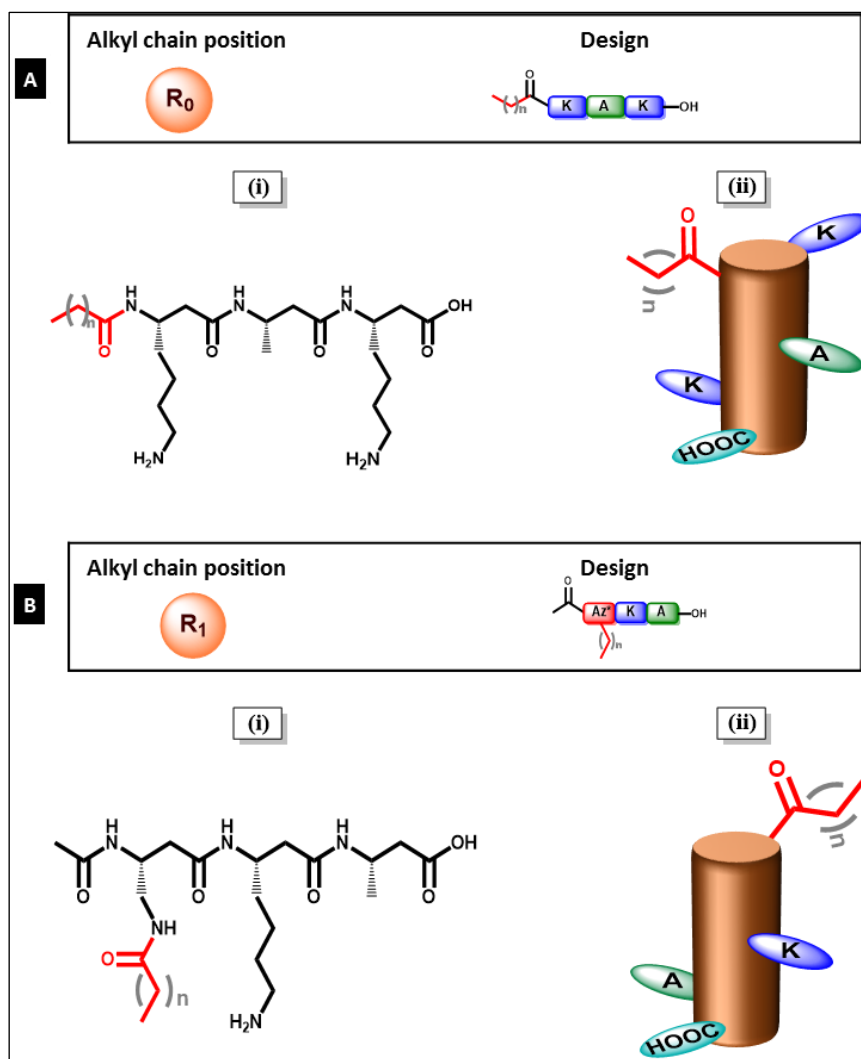


Figure 2.17: Chemical structures (i) and helical net diagram (ii) of (A) R_0 and (B) R_1 β^3 -peptide amphiphiles. The helical net diagram shows that positions of side chains and C-terminal carboxyl group outside the helix ($n=9, 11$ and 13).

The presence of the alkyl chains at the exterior of the helix for R_0 and R_1 peptides would have resulted in hydrophobic interactions between nanofibrils. The formation of twisted ribbons by these peptides was attributed to hierarchical assembly of the nanofibrils through lateral associations. Previous studies for self-assembled α -peptide amphiphiles have predominantly exploited lateral non-covalent interactions [23, 48-53]. The driving forces that governed self-assembly of α -peptide amphiphiles to cylindrical nanofibres arise from the combined effect of hydrophobic interactions of the alkyl chains, hydrogen bonding among the middle peptide segments, and electrostatic interactions between the charged amino acids [10, 11, 29, 54-56]. A number of studies have proposed that the hydrophobic alkyl chains of α -peptide amphiphiles are screened from the aqueous environment, which results in a rod-like shape

that eventually forms fibres with hydrophilic peptide component on the surface while the hydrophobic alkyl chains pack in the core of the structure [11, 14, 57]. In this study, β^3 -peptide amphiphiles may have self-assembled laterally by hydrophobic interaction to form an interior core similar to that of α -peptide amphiphile fibres. However, the internal packing of alkyl chains within the hydrophobic core requires the ideal orientation of peptide monomers [11, 58]. Nieuwland et al. reported two different packing possibilities for alkyl chains in α -peptide amphiphiles nanostructures, in which the alkyl chains form a bilayer with non-interdigitation or complete interdigitation [37]. In addition, Cui et al. also demonstrated using X-ray diffraction studies that alkyl chains in twisted ribbons are loosely packed within the hydrophobic core [40]. Therefore, the formation of twisted ribbons by β^3 -peptide amphiphiles may be attributed to the loose packing of alkyl chains in a non-interdigitated pattern. The space between the alkyl chains in the hydrophobic core allows flexibility within the nanostructure which accounts for the twisted patterns and intertwined network.

On the other hand, the chemical structure and helical net diagram of R_2 and R_3 β^3 -peptide amphiphiles are shown in Figure 2.18 in which the arrangement of the side chains, alkyl chain and C-terminal carboxyl group is at the exterior of the helix (Figure 2.18). Given that the morphology of the R_2 and R_3 β^3 -peptide amphiphiles are different from that of R_0 and R_1 peptide amphiphiles, the self-assembly is likely to have followed a different pathway of internal organisation. From previous reports, it has been revealed that nanobelts of α -peptide amphiphiles were formed as a result of the close-packed organisation of α -peptide segments and complete interdigitation of alkyl chains [40, 59, 60]. Therefore, given that R_2 and R_3 peptide amphiphiles formed similar nanobelts to α -peptide amphiphiles, the alkyl chains may have packed in an interdigitated pattern. This is also consistent with other proposed models for interdigitated alkyl chains with self-assembled nanobelts of α -peptide amphiphiles with sequences that consist of alternating hydrophobic and hydrophilic amino acids [32, 40, 59], and with a non-alternating monomer that exhibits multiple equilibria between non-covalent interactions [61-65].

Given that the geometrical compatibility and packing of building blocks are key factors that influence molecular self-assembly [33, 66-70], the contrasting morphologies observed for R_0/R_1 and R_2/R_3 peptides may be attributed to the different positions of alkyl chains which

eventually dictated the self-assembly of β^3 -peptide amphiphiles possibly due to the molecular packing order within the nanostructures.

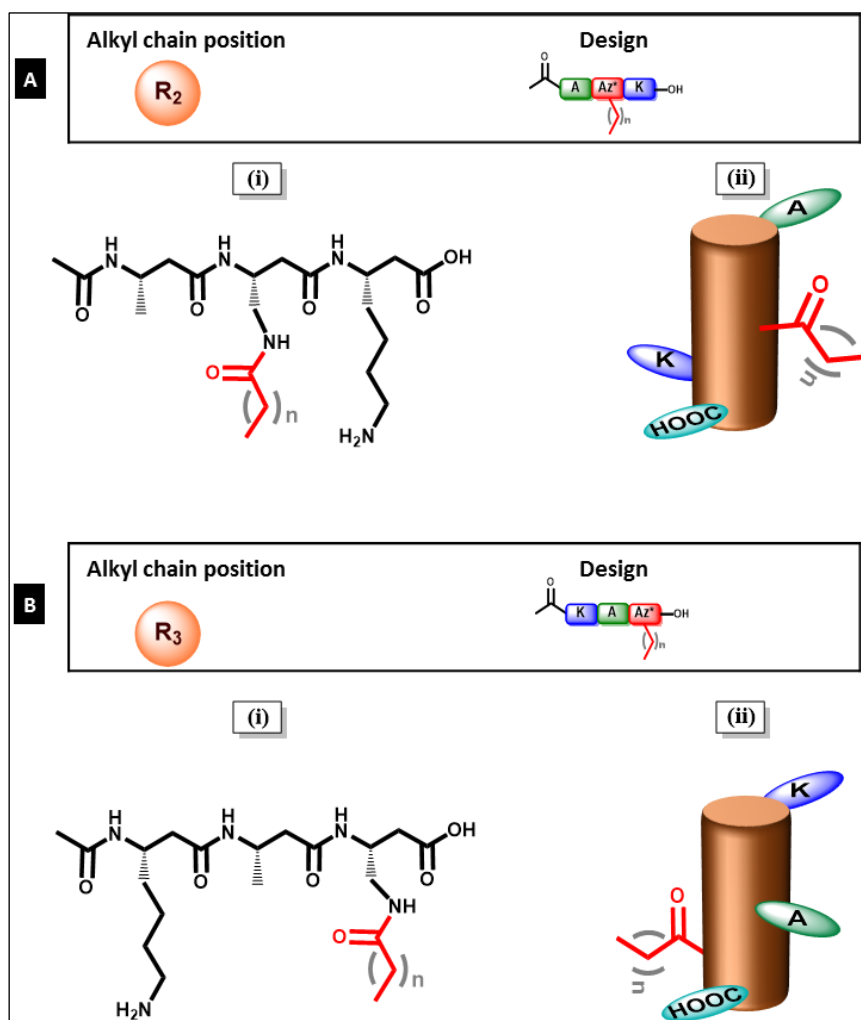


Figure 2.18: Chemical structures (i) and helical net diagram (ii) of (A) R₂ and (B) R₃ β^3 -peptide amphiphiles. The helical net diagram shows that positions of side chains and C-terminal carboxyl group outside the helix ($n=9, 11$ and 13).

In terms of size, self-assembled nanostructures of previously reported α -peptide amphiphiles revealed that cylindrical nanofibres and twisted ribbons are of a uniform diameter between 7-9 nm, and often many micrometers long [40, 71, 72, 30]. On the basis of the data obtained in this study for β^3 -peptide amphiphiles, the AFM height value of ≈ 8 nm for twisted ribbons (formed by **P3** and **P6**) is within the same range as that reported for α -peptide amphiphiles. In addition, the bimodal distribution observed for **P1**, also suggest that small fibres can merge into larger structures. Also, a previous report of α -peptide amphiphile nanobelts with the

sequence C₁₆-VEVE-OH, revealed long nanobelts that were formed after two days with heights between 10 – 20 nm [59]. In comparison with β^3 -peptide amphiphiles nanobelts, the height values of \approx 18 nm and \approx 23 nm for **P7** and **P8** respectively are similar to that of α -peptide amphiphiles.

Apart from the hydrophobic interaction that promotes lateral self-assembly, it has also been shown that electrostatic interaction contributes to the stability of cylindrical nanofibres of α -peptide amphiphiles [56, 71, 70, 73-76]. Electrostatic attraction has also been used to control the self-assembly behavior of α -peptide amphiphiles, using different numbers of charged α -amino acid residues in the peptide sequence [77]. In addition, electrostatic interaction between terminal charges of α -peptides has been shown to direct the twisting of nanofibres, which induce lateral stacking to form twisted ribbons and nanobelts [78]. In β^3 -peptide amphiphiles, electrostatic attraction is possible between the protonated β K residue and deprotonated C-terminal carboxylic group displayed on the surface of the nanofibrils. Therefore, from the AFM and TEM results obtained it is apparent that electrostatic attraction between charged groups on the nanofibril surface also contributes to the supramolecular self-assembly of these materials.

An additional goal of this study is to explore the ability of β^3 -peptide amphiphiles to form hydrogels. Peptide-based hydrogels are an attractive biomaterial for potential application in tissue engineering, drug delivery, and three-dimensional (3D) cell culture [18, 79]. In this study, the test for hydrogel formation was carried out for **P1-P12** which revealed supramolecular hydrogels for **P2 – P11** at 10 mg/mL concentration. This is comparable to previous studies that form hydrogels with nanofibrous scaffolds from peptide-based materials [19-21]. Peptides that form hydrogels are known to entrap water within the networks and are formed due to noncovalent interactions [18, 80-82]. The inability of **P1** and **P12** to form hydrogel may be due to the type of solvent system or concentration, however other conditions might be effective for hydrogelation of these peptides.

Our group has recently reported the hydrogelation properties of **P4** which exhibited a storage modulus of 1.2 kPa. Additionally, the hydrogel could completely recover following high strain, thereby demonstrating the injectable nature of this gel [46]. The hydrogels of β^3 -peptide amphiphiles in this study appear to be consistent with other hydrogels produced from α -peptide amphiphiles [21, 40, 51, 83-88]. However, previous reports have shown that the

formation of hydrogels using β -amino acid-containing peptides was based on external stimuli [82, 89], including changes in pH and temperature, thus, raising concerns over their utility for cell encapsulation in tissue engineering applications. The unique advantage of β^3 -peptide amphiphile hydrogels is that they do not require a pH or thermal trigger for gelation. Given that biomaterials suffer from degradation by proteolytic enzymes which limit their long-term application, β^3 -peptide amphiphile hydrogels would be preferable to provide long-term physical support with improved biostability [46]. In addition, most hydrogels described in the literature are formed from fibrous networks [19, 34, 40, 90-92] which are identical to those observed in R_0 and R_1 β^3 -peptide amphiphiles. Although the formation of hydrogels from nanobelts like those observed in R_2 and R_3 β^3 -peptide amphiphiles are rare, Zhang et al. recently reported the formation of hydrogels from α -peptide amphiphiles that form flat, stiff and straight nanobelts [50, 61]. This was achieved in a hierarchical manner by modulating the self-assembly behavior of α -peptide amphiphile with the sequence C_{16} -GHK-OH in the presence of a zwitterionic surfactant mixed systems.

2.5.2 Towards a model for the self-assembly of β^3 -peptide amphiphiles

The observations and analysis carried out for images obtained by AFM and TEM of **P1 – P12** are summarised below:

1. Self-assembled nanostructures of **P1-P12** exhibited a controlled dimension when compared to that of **P13**. As described previously, the variation in alkyl chain length was found to significantly influence the size of self-assembled morphology. In particular, the height values for β^3 -peptide amphiphiles are between 5-8 nm and 14-32 nm for twisted ribbons and nanobelts respectively (Figure 2.19). The similarity in height values for R_0/R_1 , and R_2/R_3 peptides, also suggest a similar mode of self-assembly.

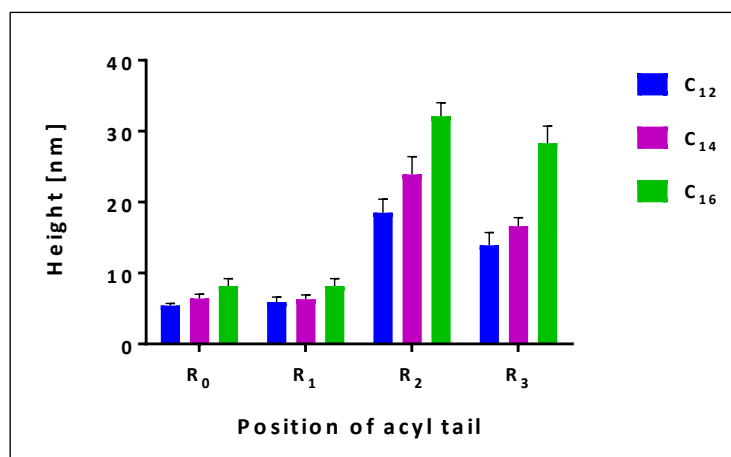


Figure 2.19: Summary of height values for β^3 -peptide amphiphiles nanofibres obtained by AFM.

2. The height values also suggest bundling of β^3 -peptide amphiphiles between nanorods. Since the diameter of a single β^3 -peptide nanorod is known to be 0.5 nm [6], it is possible that **P6** for example with a height value of ≈ 8 nm will contain more than one individual nanorods.
3. The self-assembled morphology for β^3 -peptide amphiphile revealed uniform morphology for each sample which clearly contrasts with that of **P13**.
4. The surface topology for **P1-P12** revealed periodicity by AFM and twisted patterns by TEM for both R₀ and R₁ peptides, while the nanobelts exhibited flat surfaces for both R₂ and R₃ peptides.

In order to propose a model for β^3 -peptide amphiphile self-assembly, additional information is required for the self-assembled nanostructures, in particular the internal molecular organisation of the self-assembled monomers. The next chapter will present investigations into the internal packing order of β^3 -peptide amphiphiles by AFM nanoindentation.

2.6 Conclusion

This study presents the design, synthesis and self-assembly of β^3 -peptide amphiphiles. The control of morphology was investigated by incorporating an alkyl chain into the β^3 -peptide sequence to produce new series of β^3 -peptide amphiphiles, which self-assembled to yield stable and well-defined nanostructures. The results demonstrated the significance of alkyl chain position in controlling the morphology of **P1** – **P12**, in which twisted ribbons and nanobelts were generated by switching the position from R_0/R_1 to R_2/R_3 respectively. This is in contrast to **P13** which had no alkyl chain in the sequence and thus, self-assembled to fibrous morphologies of several sizes and shapes. The variation in the length of alkyl chains (C_{12} , C_{14} and C_{16}) was also found to influence the height values of self-assembled nanostructures. The driving forces that governed the self-assembly of β^3 -peptide amphiphiles include intermolecular hydrogen bonding among the β^3 -peptide monomers, hydrophobic interactions of the alkyl chains, and electrostatic attraction between protonated β K and deprotonated C-terminal carboxylic acid. As an excellent starting point for exploring biomedical applications, the β^3 -peptide amphiphiles also formed supramolecular hydrogels, which provides a unique type of soft matter with abundant opportunities for the rational development of biomaterials. Therefore, since β^3 -peptide amphiphiles have distinct properties different from α -peptide amphiphiles which include inherent metabolic stability and sequence independent self-assembly, these peptides can be tailored to produce materials with varied morphologies and properties through chemical modification.

References

1. Del Borgo, M.P., K. Kulkarni, and M.I. Aguilar, *Unique Functional Materials Derived from β -Amino Acid Oligomers*. Australian Journal of Chemistry, 2017. **70**(2): p. 126-129.
2. Gopalan, Romila D., Mark P. Del Borgo, Adam I. Mechler, P. Perlmutter, and M.-I. Aguilar, *Geometrically Precise Building Blocks: the Self-Assembly of β -Peptides*. Chemistry & Biology, 2015. **22**(11): p. 1417-1423.
3. Satav, T., P. Korevaar, T.F.A. de Greef, J. Huskens, and P. Jonkheijm, *Modulating the Nucleated Self-Assembly of Tri- β -Peptides Using Cucurbit[n]urils*. Chemistry – A European Journal, 2016. **22**(36): p. 12675-12679.
4. Pizzey, C.L., W.C. Pomerantz, B.J. Sung, V.M. Yuwono, S.H. Gellman, J.D. Hartgerink, A. Yethiraj, and N.L. Abbott, *Characterization of nanofibers formed by self-assembly of β -peptide oligomers using small angle x-ray scattering*. Journal of Chemical Physics, 2008. **129**(9).
5. Luder, K., K. Kulkarni, H.W. Lee, R.E. Widdop, M.P. Del Borgo, and M.I. Aguilar, *Decorated self-assembling β 3-tripeptide foldamers form cell adhesive scaffolds*. Chemical Communications, 2016. **52**(24): p. 4549-4552.
6. Del Borgo, M.P., A.I. Mechler, D. Traore, C. Forsyth, J.A. Wilce, M.C.J. Wilce, M.I. Aguilar, and P. Perlmutter, *Supramolecular self-assembly of N-acetyl-capped β -peptides leads to nano- to macroscale fiber formation*. Angewandte Chemie - International Edition, 2013. **52**(32): p. 8266-8270.
7. Seoudi, R.S., M.P. Del Borgo, K. Kulkarni, P. Perlmutter, M.-I. Aguilar, and A. Mechler, *Supramolecular self-assembly of 14-helical nanorods with tunable linear and dendritic hierarchical morphologies*. New Journal of Chemistry, 2016. **12**: 2243-2246.
8. Seoudi, R.S., A. Dowd, M. Del Borgo, K. Kulkarni, P. Perlmutter, M.I. Aguilar, and A. Mechler, *Amino acid sequence controls the self-assembled superstructure morphology of N-acetylated tri- β -peptides*. Pure and Applied Chemistry, 2015. **87**(9-10): p. 1021-1028.
9. Seoudi R.S., M.G. Hinds, D.J.D. Wilson, C.G. Adda, M.P. Del Borgo, M.I. Aguilar, P. Perlmutter, and A. Mechler, *Self-assembled nanomaterials based on beta (β^3) tetrapeptides*. Nanotechnology, 2016. **27**(13): p. 135606.

10. Hartgerink, J.D., E. Beniash, and S.I. Stupp, *Peptide-amphiphile nanofibers: A versatile scaffold for the preparation of self-assembling materials*. Proceedings of the National Academy of Sciences of the United States of America, 2002. **99**(8): p. 5133-5138.
11. Cui, H., M.J. Webber, and S.I. Stupp, *Self-assembly of peptide amphiphiles: from molecules to nanostructures to biomaterials*. Biopolymers, 2010. **94**(1): p. 1-18.
12. Ortony, J.H., C.J. Newcomb, J.B. Matson, L.C. Palmer, P.E. Doan, B.M. Hoffman, and S.I. Stupp, *Internal dynamics of a supramolecular nanofibre*. Nat Mater, 2014. **13**(8): p. 812-816.
13. Dehsorkhi, A., V. Castelletto, and I.W. Hamley, *Self-assembling amphiphilic peptides*. Journal of Peptide Science, 2014. **20**(7):p. 453-67.
14. Lee, O.-S., S.I. Stupp, and G.C. Schatz, *Atomistic Molecular Dynamics Simulations of Peptide Amphiphile Self-Assembly into Cylindrical Nanofibers*. Journal of the American Chemical Society, 2011. **133**(10): p. 3677-3683.
15. Liebmann, T., S. Rydholm, V. Akpe, and H. Brismar, *Self-assembling Fmoc dipeptide hydrogel for in situ 3D cell culturing*. BMC Biotechnology, 2007. **7**:88.
16. Vallée, M.R.J., P. Majkut, I. Wilkening, C. Weise, G. Müller, and C.P.R. Hackenberger, *Staudinger-phosphonite reactions for the chemoselective transformation of azido-containing peptides and proteins*. Organic Letters, 2011. **13**(20): p. 5440-5443.
17. Thompson, R.F., M. Walker, C.A. Siebert, S.P. Muench, and N.A. Ranson, *An introduction to sample preparation and imaging by cryo-electron microscopy for structural biology*. Methods, 2016. **100**: p. 3-15.
18. Du, X., J. Zhou, J. Shi, and B. Xu, *Supramolecular Hydrogelators and Hydrogels: From Soft Matter to Molecular Biomaterials*. Chemical Reviews, 2015. **115**(24): p. 13165-13307.
19. Berns, E.J., S. Sur, L. Pan, J.E. Goldberger, S. Suresh, S. Zhang, J.A. Kessler, and S.I. Stupp, *Aligned neurite outgrowth and directed cell migration in self-assembled monodomain gels*. Biomaterials, 2014. **35**(1): p. 185-95.
20. Lindsey, S., J.H. Piatt, P. Worthington, C. Sönmez, S. Satheye, J.P. Schneider, D.J. Pochan, and S.A. Langhans, *Beta hairpin peptide hydrogels as an injectable solid vehicle for neurotrophic growth factor delivery*. Biomacromolecules, 2015. **16**(9): p. 2672-2683.

21. Black, K.A., B.F. Lin, E.A. Wonder, S.S. Desai, E.J. Chung, B.D. Ulery, R.S. Katari, and M.V. Tirrell, *Biocompatibility and Characterization of a Peptide Amphiphile Hydrogel for Applications in Peripheral Nerve Regeneration*. Tissue Engineering. Part A, 2015. **21**(7-8): p. 1333-1342.
22. Wan, Y., Z. Wang, J. Sun, and Z. Li, *Extremely Stable Supramolecular Hydrogels Assembled from Nonionic Peptide Amphiphiles*. Langmuir, 2016. **32**(30): p. 7512-7518.
23. Wang, J.Q., Y.J. Sun, J.R. Dai, Y.R. Zhao, M.W. Cao, D. Wang, and H. Xu, *Effects of alkyl chain length and peptide charge distribution on self-assembly and hydrogelation of lipopeptide amphiphiles*. Wuli Huaxue Xuebao/ Acta Physico - Chimica Sinica, 2015. **31**(7): p. 1365-1373.
24. Dube, N., J.W. Seo, H. Dong, J.Y. Shu, R. Lund, L.M. Mahakian, K.W. Ferrara, and T. Xu, *Effect of alkyl length of peptide-polymer amphiphile on cargo encapsulation stability and pharmacokinetics of 3-helix micelles*. Biomacromolecules, 2014. **15**(8): p. 2963-2970.
25. Gore, T., Y. Dori, Y. Talmon, M. Tirrell, and H. Bianco-Peled, *Self-assembly of model collagen peptide amphiphiles*. Langmuir, 2001. **17**(17): p. 5352-5360.
26. Miravet, J.F., B. Escuder, M.D. Segarra-Maset, M. Tena-Solsona, I.W. Hamley, A. Dehsorkhi, and V. Castelletto, *Self-assembly of a peptide amphiphile: transition from nanotape fibrils to micelles*. Soft Matter, 2013. **9**(13): p. 3558-3564.
27. Hamley, I.W., A. Dehsorkhi, V. Castelletto, M.N.M. Walter, C.J. Connon, M. Reza, and J. Ruokolainen, *Self-Assembly and Collagen-Stimulating Activity of a Peptide Amphiphile Incorporating a Peptide Sequence from Lumican*. Langmuir, 2015. **31**(15): p. 4490-4495.
28. Castelletto, V., R.M. Gouveia, C.J. Connon, and I.W. Hamley, *New RGD-peptide amphiphile mixtures containing a negatively charged diluent*. Faraday Discussions, 2013. **166**: p. 381-397.
29. Korevaar, P.A., C.J. Newcomb, E.W. Meijer, and S.I. Stupp, *Pathway selection in peptide amphiphile assembly*. Journal of the American Chemical Society, 2014. **136**(24): p. 8540-8543.
30. Palmer, L.C. and S.I. Stupp, *Molecular Self-Assembly into One-Dimensional Nanostructures*. Accounts of Chemical Research, 2008. **41**(12): p. 1674-1684.

31. Stupp, S.I. and L.C. Palmer, *Supramolecular Chemistry and Self-Assembly in Organic Materials Design*. Chemistry of Materials, 2013. **26**: p. 507-518.
32. Moyer, T.J., H. Cui, and S.I. Stupp, *Tuning nanostructure dimensions with supramolecular twisting*. Journal of Physical Chemistry B, 2013. **117**(16): p. 4604-4610.
33. Missirlis, D., A. Chworos, C.J. Fu, H.A. Khant, D.V. Krogstad, and M. Tirrell, *Effect of the peptide secondary structure on the peptide amphiphile supramolecular structure and interactions*. Langmuir, 2011. **27**(10): p. 6163-6170.
34. Stendahl, J.C., M.S. Rao, M.O. Guler, and S.I. Stupp, *Intermolecular forces in the self-assembly of peptide amphiphile nanofibers*. Advanced Functional Materials, 2006. **16**(4): p. 499-508.
35. Marullo, R., M. Kastantin, L.B. Drews, and M. Tirrell, *Peptide contour length determines equilibrium secondary structure in protein-analogous micelles*. Biopolymers, 2013. **99**(9): p. 573-581.
36. Löwik, D.W.P.M., I.O. Shklyarevskiy, L. Ruizendaal, P.C.M. Christianen, J.C. Maan, and J.C.M. Van Hest, *A highly ordered material from magnetically aligned peptide amphiphile nanofiber assemblies*. Advanced Materials, 2007. **19**(9): p. 1191-1195.
37. Nieuwland, M., L. Ruizendaal, A. Brinkmann, L. Kroon-Batenburg, J.C.M. Van Hest, and D.W.P.M. Löwik, *A structural study of the self-assembly of a palmitoyl peptide amphiphile*. Faraday Discussions, 2013. **166**: p. 361-379.
38. Hamley, I.W., A. Dehsorkhi, V. Castelletto, S. Fuzeland, D. Atkins, J. Seitsonen, and J. Ruokolainen, *Reversible helical unwinding transition of a self-assembling peptide amphiphile*. Soft Matter, 2013. **9**(39): p. 9290-9293.
39. Pashuck, E.T. and S.I. Stupp, *Direct Observation of Morphological Transformation from Twisted Ribbons into Helical Ribbons*. Journal of the American Chemical Society, 2010. **132**(26): p. 8819-8821.
40. Cui, H., A.G. Cheetham, E.T. Pashuck, and S.I. Stupp, *Amino acid sequence in constitutionally isomeric tetrapeptide amphiphiles dictates architecture of one-dimensional nanostructures*. Journal of the American Chemical Society, 2014. **136**(35): p. 12461-12468.
41. Cheng, R.P., S.H. Gellman, and W.F. DeGrado, *β -peptides: From structure to function*. Chemical Reviews, 2001. **101**(10): p. 3219-3232.

42. Pauling, L., R.B. Corey, and H.R. Branson, *The structure of proteins: Two hydrogen-bonded helical configurations of the polypeptide chain*. Proceedings of the National Academy of Sciences, 1951. **37**(4): p. 205-211.
43. Pauling, L. and R.B. Corey, *Configurations of Polypeptide Chains With Favored Orientations Around Single Bonds: Two New Pleated Sheets*. Proceedings of the National Academy of Sciences of the United States of America, 1951. **37**(11): p. 729-740.
44. Perrin, C.L. and J.B. Nielson, *"Strong" hydrogen bonds in chemistry and biology*, in *Annual Review of Physical Chemistry*. 1997. p. 511-544.
45. Kortemme, T., A.V. Morozov, and D. Baker, *An orientation-dependent hydrogen bonding potential improves prediction of specificity and structure for proteins and protein-protein complexes*. Journal of Molecular Biology, 2003. **326**(4): p. 1239-1259.
46. Motamed, S., M.P. Del Borgo, K. Kulkarni, N. Habila, K. Zhou, P. Perlmutter, J.S. Forsythe, and M.I. Aguilar, *A self-assembling [small beta]-peptide hydrogel for neural tissue engineering*. Soft Matter, 2016. **12**(8): p. 2243-2246.
47. Kulkarni, K., S. Motamed, N. Habila, P. Perlmutter, J.S. Forsythe, M.-I. Aguilar, and M.P. Del Borgo, *Orthogonal strategy for the synthesis of dual-functionalised [small beta]³-peptide based hydrogels*. Chemical Communications, 2016. **52**(34): p. 5844-5847.
48. Capito, R.M., H.S. Azevedo, Y.S. Velichko, A. Mata, and S.I. Stupp, *Self-assembly of large and small molecules into hierarchically ordered sacs and membranes*. Science, 2008. **319**(5871): p. 1812-1816.
49. Zhao, X., F. Pan, H. Xu, M. Yaseen, H. Shan, C.A.E. Hauser, S. Zhang, and J.R. Lu, *Molecular self-assembly and applications of designer peptide amphiphiles*. Chemical Society Reviews, 2010. **39**(9): p. 3480-3498.
50. Zhang, H., M. Yu, A. Song, Y. Song, X. Xin, J. Shen, and S. Yuan, *Modulating hierarchical self-assembly behavior of a peptide amphiphile/nonionic surfactant mixed system*. RSC Advances, 2016. **6**(11): p. 9186-9193.
51. Lin, B.F., K.A. Megley, N. Viswanathan, D.V. Krogstad, L.B. Drews, M.J. Kade, Y. Qian, and M.V. Tirrell, *PH-responsive branched peptide amphiphile hydrogel designed for applications in regenerative medicine with potential as injectable tissue scaffolds*. Journal of Materials Chemistry, 2012. **22**(37): p. 19447-19454.

52. Garifullin, R. and M.O. Guler, *Supramolecular chirality in self-assembled peptide amphiphile nanostructures*. Chemical Communications, 2015. **51**(62): p. 12470-12473.
53. Dehsorkhi, A., R.M. Gouveia, A.M. Smith, I.W. Hamley, V. Castelletto, C.J. Connon, M. Reza, and J. Ruokolainen, *Self-assembly of a dual functional bioactive peptide amphiphile incorporating both matrix metalloprotease substrate and cell adhesion motifs*. Soft Matter, 2015. **11**(16): p. 3115-3124.
54. Hamley, I.W., *Self-assembly of amphiphilic peptides*. Soft Matter, 2011. **7**(9): p. 4122-4138.
55. Da Silva, R.M.P., D. Van Der Zwaag, L. Albertazzi, S.S. Lee, E.W. Meijer, and S.I. Stupp, *Super-resolution microscopy reveals structural diversity in molecular exchange among peptide amphiphile nanofibres*. Nature Communications, 2016. **7**:11561.
56. Velichko, Y.S., S.I. Stupp, and M.O. de la Cruz, *Molecular Simulation Study of Peptide Amphiphile Self-Assembly*. The Journal of Physical Chemistry B, 2008. **112**(8): p. 2326-2334.
57. Trent, A., R. Marullo, B. Lin, M. Black, and M. Tirrell, *Structural properties of soluble peptide amphiphile micelles*. Soft Matter, 2011. **7**(20): p. 9572-9582.
58. Jiang, H., M.O. Guler, and S.I. Stupp, *The internal structure of self-assembled peptide amphiphiles nanofibers*. Soft Matter, 2007. **3**(4): p. 454-462.
59. Cui, H., T. Muraoka, A.G. Cheetham, and S.I. Stupp, *Self-assembly of giant peptide nanobelts*. Nano Letters, 2009. **9**(3): p. 945-951.
60. Versluis, F., H.R. Marsden, and A. Kros, *Power struggles in peptide-amphiphile nanostructures*. Chemical Society Reviews, 2010. **39**(9): p. 3434-3444.
61. Zhang, H., J. Sun, X. Xin, W. Xu, J. Shen, Z. Song, and S. Yuan, *Modulating self-assembly behavior of a salt-free peptide amphiphile (PA) and zwitterionic surfactant mixed system*. Journal of Colloid and Interface Science, 2016. **467**: p. 43-50.
62. Palladino, P., V. Castelletto, A. Dehsorkhi, D. Stetsenko, and I.W. Hamley, *Conformation and self-association of peptide amphiphiles based on the KTTKS collagen sequence*. Langmuir, 2012. **28**(33): p. 12209-12215.
63. Castelletto, V., I.W. Hamley, J. Adamcik, R. Mezzenga, and J. Gummel, *Modulating self-assembly of a nanotape-forming peptide amphiphile with an oppositely charged surfactant*. Soft Matter, 2012. **8**(1): p. 217-226.

64. Castelletto, V., I.W. Hamley, J. Perez, L. Abezgauz, and D. Danino, *Fibrillar superstructure from extended nanotapes formed by a collagen-stimulating peptide*. Chemical Communications, 2010. **46**(48): p. 9185-9187.
65. Dehsorkhi, A., V. Castelletto, I.W. Hamley, J. Adamcik, and R. Mezzenga, *The effect of pH on the self-assembly of a collagen derived peptide amphiphile*. Soft Matter, 2013. **9**(26): p. 6033-6036.
66. Tsonchev, S., G.C. Schatz, and M.A. Ratner, *Hydrophobically-driven self-assembly: A geometric packing analysis*. Nano Letters, 2003. **3**(5): p. 623-626.
67. Chen, Y., F. Qiu, Y. Lu, Y.K. Shi, and X. Zhao, *Geometrical shape of hydrophobic section determines the self-assembling structure of peptide detergents and bolaamphiphilic peptides*. Current Nanoscience, 2009. **5**(1): p. 69-74.
68. Martinek, T.A. and F. Fülöp, *Side-chain control of β -peptide secondary structures: Design principles*. European Journal of Biochemistry, 2003. **270**(18): p. 3657-3666.
69. Wang, P.S.P., C.J. Craig, and A. Schepartz, *Relationship between side-chain branching and stoichiometry in β 3-peptide bundles*. Tetrahedron, 2012. **68**(23): p. 4342-4345.
70. Fu, I.W. and H.D. Nguyen, *Sequence-dependent structural stability of self-assembled cylindrical nanofibers by peptide amphiphiles*. Biomacromolecules, 2015. **16**(7): p. 2209-2219.
71. Niece, K.L., J.D. Hartgerink, J.J.J.M. Donners, and S.I. Stupp, *Self-Assembly Combining Two Bioactive Peptide-Amphiphile Molecules into Nanofibers by Electrostatic Attraction*. Journal of the American Chemical Society, 2003. **125**(24): p. 7146-7147.
72. Hartgerink, J.D., E. Beniash, and S.I. Stupp, *Self-assembly and mineralization of peptide-amphiphile nanofibers*. Science, 2001. **294**(5547): p. 1684-8.
73. Fu, I.W., C.B. Markegard, B.K. Chu, and H.D. Nguyen, *The role of electrostatics and temperature on morphological transitions of hydrogel nanostructures self-assembled by peptide amphiphiles via molecular dynamics simulations*. Advanced Healthcare Materials, 2013. **2**(10): p. 1388-1400.
74. Lee, O.S., V. Cho, and G.C. Schatz, *Modeling the self-assembly of peptide amphiphiles into fibers using coarse-grained molecular dynamics*. Nano Letters, 2012. **12**(9): p. 4907-4913.

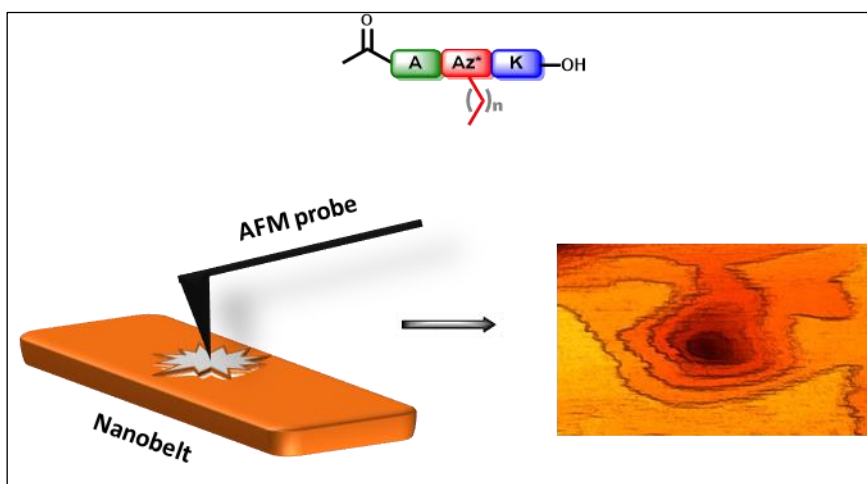
75. Lai, C.T., N.L. Rosi, and G.C. Schatz, *All-Atom Molecular Dynamics Simulations of Peptide Amphiphile Assemblies That Spontaneously Form Twisted and Helical Ribbon Structures*. *Journal of Physical Chemistry Letters*, 2017. **8**(10): p. 2170-2174.
76. Tsonchev, S., G.C. Schatz, and M.A. Ratner, *Electrostatically-directed self-assembly of cylindrical peptide amphiphile nanostructures*. *Journal of Physical Chemistry B*, 2004. **108**(26): p. 8817-8822.
77. Goldberger, J.E., E.J. Berns, R. Bitton, C.J. Newcomb, and S.I. Stupp, *Electrostatic control of bioactivity*. *Angewandte Chemie - International Edition*, 2011. **50**(28): p. 6292-6295.
78. Hu, Y., R. Lin, P. Zhang, J. Fern, A.G. Cheetham, K. Patel, R. Schulman, C. Kan, and H. Cui, *Electrostatic-driven lamination and untwisting of β -sheet assemblies*. *ACS Nano*, 2016. **10**(1): p. 880-888.
79. Huang, H., A.I. Herrera, Z. Luo, O. Prakash, and X.S. Sun, *Structural transformation and physical properties of a hydrogel-forming peptide studied by NMR, transmission electron microscopy, and dynamic rheometer*. *Biophysical Journal*, 2012. **103**(5): p. 979-988.
80. Thota, C.K., N. Yadav, and V.S. Chauhan, "A novel highly stable and injectable hydrogel based on a conformationally restricted ultrashort peptide". 2016. **6**: p. 31167.
81. Seow, W.Y. and C.A.E. Hauser, *Short to ultrashort peptide hydrogels for biomedical uses*. *Materials Today*, 2014. p. 381-388.
82. Nanda, J. and A. Banerjee, *β -Amino acid containing proteolitically stable dipeptide based hydrogels: Encapsulation and sustained release of some important biomolecules at physiological pH and temperature*. *Soft Matter*, 2012. **8**(12): p. 3380-3386.
83. Weingarten, A.S., R.V. Kazantsev, L.C. Palmer, M. McClendon, A.R. Koltonow, P.S. SamuelAmanda, D.J. Kiebalá, M.R. Wasielewski, and S.I. Stupp, *Self-assembling hydrogel scaffolds for photocatalytic hydrogen production*. *Nat Chem*, 2014. **6**(11): p. 964-970.
84. Zhang, S., M.A. Greenfield, A. Mata, L.C. Palmer, R. Bitton, J.R. Mantei, C. Aparicio, M.O. De La Cruz, and S.I. Stupp, *A self-assembly pathway to aligned monodomain gels*. *Nature Materials*, 2010. **9**(7): p. 594-601.

85. Beniash, E., J.D. Hartgerink, H. Storrie, J.C. Stendahl, and S.I. Stupp, *Self-assembling peptide amphiphile nanofiber matrices for cell entrapment*. Acta Biomaterialia, 2005. **1**(4): p. 387-397.
86. Matson, J.B., C.J. Newcomb, R. Bitton, and S.I. Stupp, *Nanostructure-templated control of drug release from peptide amphiphile nanofiber gels*. Soft Matter, 2012. **8**(13): p. 3586-3595.
87. Matson, J.B. and S.I. Stupp, *Self-assembling peptide scaffolds for regenerative medicine*. Chemical Communications, 2012. **48**(1): p. 26-33.
88. Matson, J.B., R.H. Zha, and S.I. Stupp, *Peptide self-assembly for crafting functional biological materials*. Current Opinion in Solid State and Materials Science, 2011. **15**(6): p. 225-235.
89. Yang, Z., G. Liang, and B. Xu, *Supramolecular hydrogels based on β -amino acid derivatives*. Chemical Communications, 2006(7): p. 738-740.
90. McClendon, M.T. and S.I. Stupp, *Tubular hydrogels of circumferentially aligned nanofibers to encapsulate and orient vascular cells*. Biomaterials, 2012. **33**(23): p. 5713-5722.
91. Greenfield, M.A., J.R. Hoffman, M. Olvera de la Cruz, and S.I. Stupp, *Tunable Mechanics of Peptide Nanofiber Gels*. Langmuir, 2009. **26**(5): p. 3641-3647.
92. Lee, K.Y. and D.J. Mooney, *Hydrogels for tissue engineering*. Chemical Reviews, 2001. **101**(7): p. 1869-1879.

Chapter Three

AFM Nanoindentation to Probe the Internal Molecular Organisation of Self-Assembled β^3 -Peptide Amphiphiles

The internal molecular organisation of self-assembled R_2 β^3 -peptide amphiphiles was investigated via nanoindentation by AFM. The indentation was carried out in an aqueous environment to punch holes in self-assembled nanobelts. The topographic images of the holes created revealed a sheet-like organisation of the internal architecture. Experimental dimensions were obtained and used to further develop the proposed self-assembly model for the nanobelts. Nanoindentation by AFM provides the means to unravel the internal molecular organisation of β^3 -peptide-based materials.



3.1 Introduction

In the preceding chapter, AFM and TEM images for R₂ β^3 -peptides **P7**, **P8** and **P9** revealed well-defined nanobelts after self-assembly in water. The internal molecular organisation of these β^3 -peptide amphiphiles is still unknown. In order to propose a model for β^3 -peptide amphiphile self-assembly, the aim of this chapter is to determine the internal organisation using AFM nanoindentation.

Techniques that are commonly utilised for studying self-assembled nanostructures of peptide-based materials include SAX, XRD and small-angle neutron scattering (SANS) [1-7]. However, the need to align the fibrillar assemblies to a preferred direction for the orientation of fibre diffractions and the final correlation of observed diffraction patterns with proposed models remains a challenge.

Presently, AFM nanoindentation is mostly used for the determination of mechanical properties in nanostructures [8-19]. Recently Del Mercato *et al.* demonstrated the fracture of amyloid-like fibrils via nanoindentation while investigating Young's modulus using AFM in air [20]. However, the images obtained from the fractured fibrils did not show internal features after indentation. Thus, in order to visualise the interior of **P7**, **P8** and **P9** nanobelts, it was envisaged that an AFM nanoindentation performed in a hydrated system may provide a softer material for easier and controlled penetration of the AFM tip into the nanostructure. At the same time, the morphological and nanomechanical properties (Young's modulus) of the nanostructures can be immediately characterised.

The first part of this chapter describes the protocol used to achieve the nanoindentation followed by the correlation of the data into a proposed self-assembly model.

3.2 Materials and methods

3.2.1 Materials

- OLTESPA-R3 0.01-0.02 ohm-cm silicon probe was purchased from Bruker Corporation, (Billerica, Massachusetts, United States).
- **P7**, **P8** and **P9** (synthesised in chapter two)
- All other materials and methods are as described previously in Chapter 2.

3.2.2 AFM Nanoindentation

Nanoindentation was investigated using an OLTESPA-R3 0.01-0.02 ohm-cm silicon probe with a spring constant of 2 N/m, resonance frequency of 70 kHz and cantilever tip radius of 7 nm. The protocol for tapping mode AFM was previously described in Section 2.3.4. The only modification was the use of 35 μ L of distilled water in a fluid cell. The principle of nanoindentation is based on bringing the AFM tip close to the sample and punching a hole using a specific trigger threshold. The AFM tip was used to measure the sample topology while submerged in solution and enclosed in a fluid cell. The nanoindentation was performed when the AFM tip precisely approached and punched into the sample until the predefined force was reached before the tip was retracted. This was achieved by first manoeuvring the AFM tip with successive “Offset” and “Zoom” in order to identify the position to indent on the sample. During this complete cycle the position of the tip, as well as the force exerted on the cantilever were accurately monitored, resulting in a force-distance curve. The force curve or ramp was achieved with a trigger threshold of 100 nm, 200 nm and 250 nm for **P7**, **P8** and **P9** nanobelts respectively. Nanoindentation was performed at various positions on the fibres by bringing into contact the sample and the AFM tip in a vertical movement facilitated by a predefined ramp size [21]. The topographic, phase and amplitude images were captured simultaneously and processed using Gwyddion 2.45 software after nanoindentation.

3.2.3 Quantitative nanomechanical mapping of P7, P8 and P9 nanobelts

The peak force quantitative nanomechanical mapping (PF-QNM) was performed in a fluid cell using the OLTESPA-R3 probe on a MultiMode 8 Bruker’s AFM under ambient conditions. To

ascertain deflection sensitivity, the AFM tip was first calibrated using a clean sapphire surface. Thereafter, surface topology and Young's modulus mapping were performed for **P7**, **P8** and **P9** at a scan rate of 1 Hz. All the images were captured simultaneously with typical scan sizes of $\leq 10 \mu\text{m}$. Images were captured and analysed using the software Nanoscope analyser and Gwyddion 2.45 software.

3.3 Results

3.3.1 AFM nanoindentation of R_2 β^3 -peptide amphiphile nanobelts

Given that the AFM tip radius is 7 nm, only **P7**, **P8** and **P9** nanobelts were investigated because the height values were >18 nm and this can accommodate the indentation force triggers without crashing the AFM tip. Nanoindentation was not carried out for twisted ribbons of R_0 and R_1 β^3 -peptides because the height values are ≤ 8 nm. Nanoindentation of all R_2 β^3 -peptide amphiphile (**P7**, **P8** and **P9**) nanobelts was carried out either along the edge or in the middle of a single nanobelt as shown in Figure 3.1. The two different positions were used in order to ascertain whether the internal features of the nanobelts were similar at various locations along the fibre.

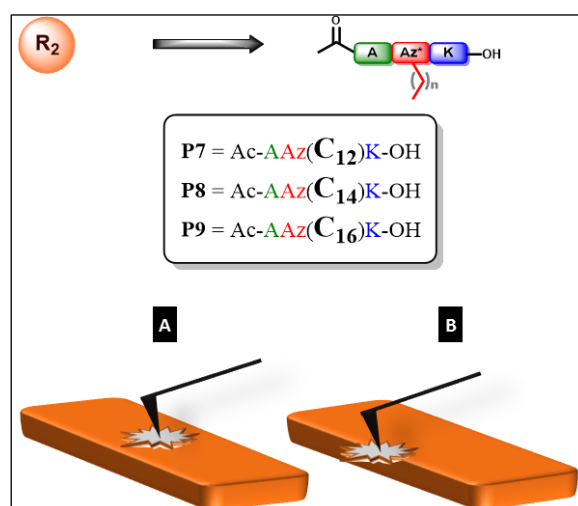


Figure 3.1: Positions of AFM cantilever tip on nanobelts during nanoindentation. (A) Central position and (B) exterior position.

3.3.2 Nanoindentation of **P7** nanobelts

Figure 3.2 shows the AFM images of the holes created after the indentations carried at the central position of the peptide **P7** for three different nanobelts with a trigger threshold of 100 nm. All the holes created by the AFM tip appeared to be irregular in shape and size. The images captured did not reveal good internal features at this position.

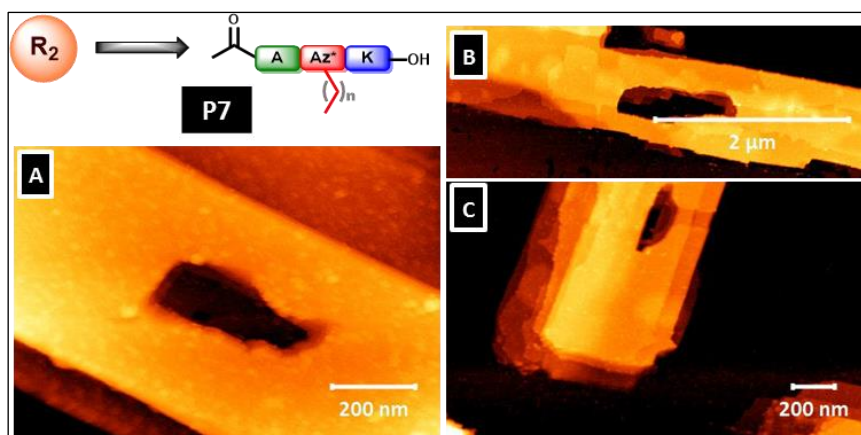


Figure 3.2: Nanoindentation of **P7** at the central position for three different nanobelts (A), (B) and (C).

The alternative indentation at the edge of **P7** nanobelt was performed by adjusting the position of the cantilever using the offset and zoom control parameters. The indentation was carried out using a trigger threshold of 100nm. Figure 3.3 shows that **P7** nanobelt was notched at the edge and the image revealed internal features that depict a stepwise pattern. The notched section was also magnified (Figure 3.3(B)), and this convincingly indicated that the layers are stacked (3D image Figure 3.3(B)).

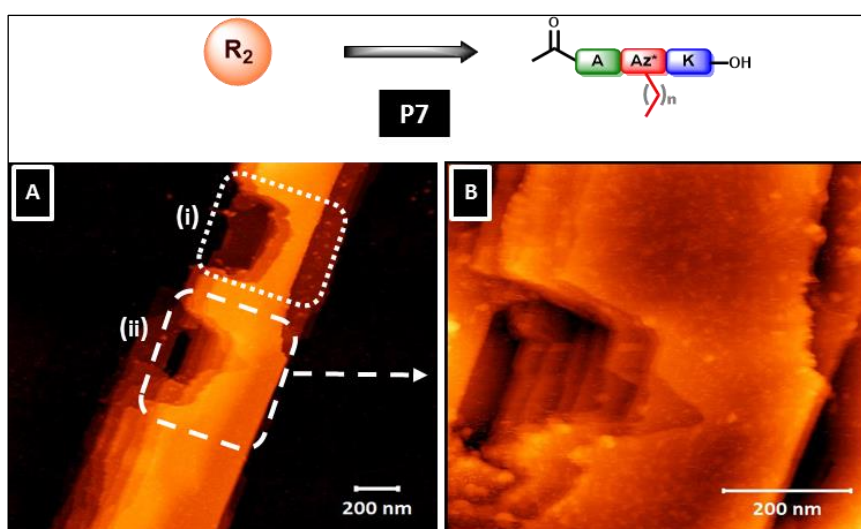


Figure 3.3: AFM nanoindentation of **P7** at the edge of the nanobelt. (A) Nanoindentations of nanobelt at two lateral positions (i) and (ii). (B) Magnified image of highlighted section (ii) in (A).

The images were further analysed by extracting the profiles of the nano-holes which was subsequently fitted with a Gaussian function. Figure 3.4(A) shows the extracted profile of the surface for one section of **P7** that was indented. The graph also corresponds to the stepwise pattern observed from the images. The height profiles were used to generate the frequency distribution plot in order to determine the dimension of the layers from 100 different height measurements. Figure 3.4(B) shows the height distribution which was used to determine the mean, mode, standard deviation (SD) and standard error of mean (SEM). The average height value was found to be 2.6 ± 0.3 nm. This value corresponds to AFM height value of 2.65 nm that was previously observed for small step-like architectures in self-assembled α -peptide amphiphile nanobelts [7].

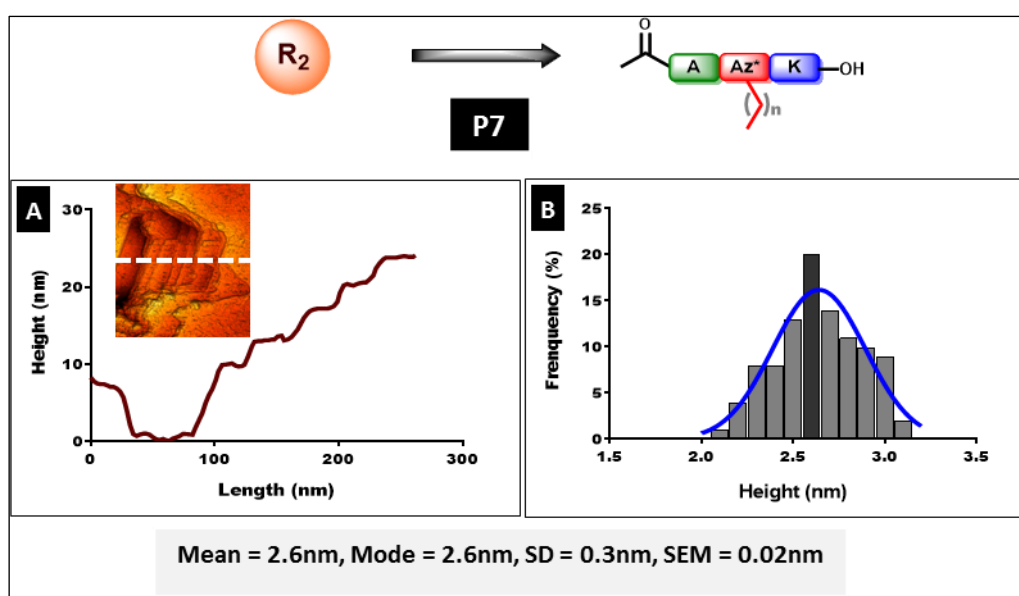


Figure 3.4: Height profiles of the internal features in **P7** nanobelt after AFM nanoindentation. (A) Example of a graphical presentation of an extracted profile from the inserted 3D image and (B) frequency distribution of 100 height measurements.

3.3.3 Nanoindentation of **P8** nanobelts

The nanoindentation of **P8** was also carried out at two different locations. Figures 3.5(A) and (C) show the indentations at the central position in which holes were created with a trigger threshold of 200 nm which is higher than the trigger threshold of 100 nm used for **P7**. A section of the nanobelt near the hole in Figure 3.5(A) was removed after the indentation. The

surface topology of this section was extracted to obtain two graphical profiles (Figure 3.5(B)). Profile 1 shows the height values to be ≈ 25 nm for the nanobelt, while profile 2 shows a stepwise decrease in height from ≈ 25 nm, ≈ 21 nm and ≈ 19 nm suggesting that a single layer is ≈ 3 nm. The 3D image (Figure 3.5(C)) provided a better view of the layers from the highlighted blue section of Figure 3.5(A). Similarly, Figure 3.5(D) shows nanoindentations on a different nanobelt in which holes were created at the central position. In contrast to **P7**, some layers were observed underneath the hole (highlighted in blue Figure 3.5(E)) and magnified to show the 3D orientation (Figure 3.5(F)).

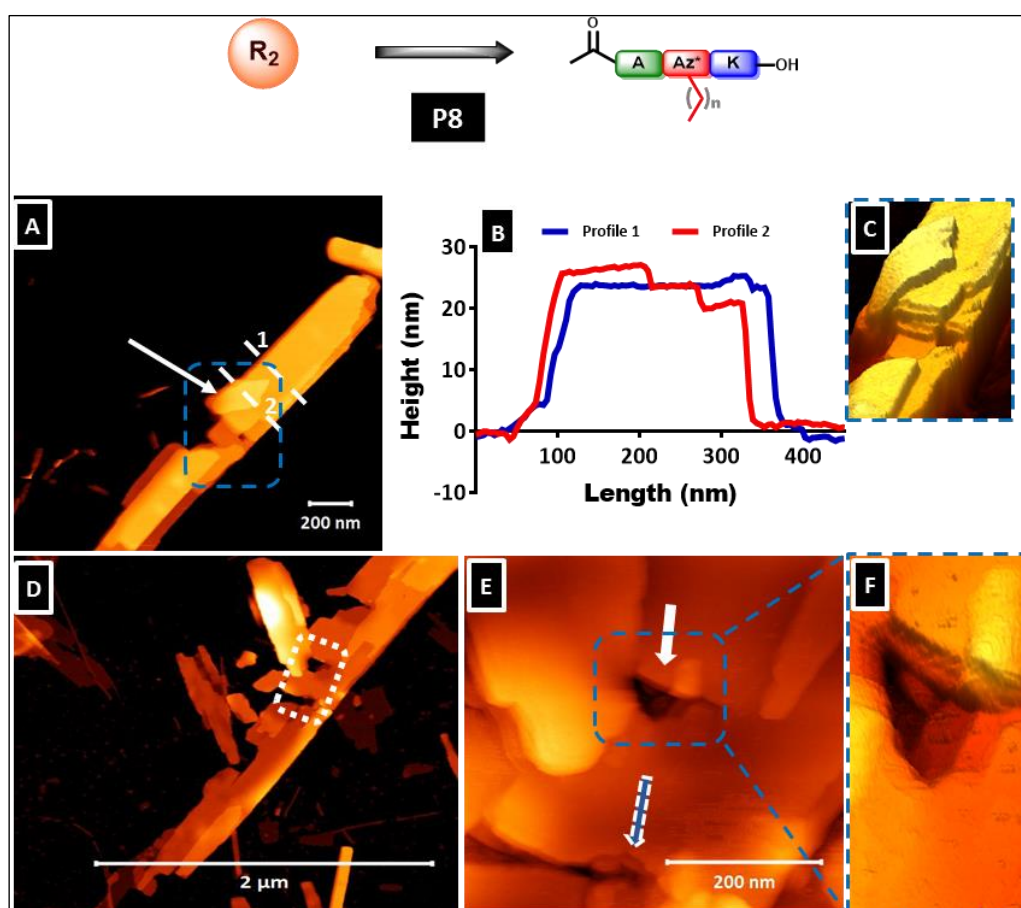


Figure 3.5: AFM nanoindentation of **P8** at the central position. (A) Hole created by indentation, the white arrow shows a layer of a fractured part of the nanobelt that was removed near the hole when the trigger threshold was applied, (B) height profile of the two sections 1 and 2 in (A), (C) 3D image of the highlighted blue section in (A), (D) nanoindentations of another nanobelt showing holes highlighted in white, and (E) magnified image of highlighted white section in (D), and (F) 3D image of the highlighted blue section in (E).

The second indentation for **P8** was carried out at the lateral position (Figure 3.6). A trigger threshold of 200 nm was applied which resulted in small cracks at the edge of the nanobelt (white arrows in Figure 3.6(A)). The **P8** nanobelts were very stiff and thus difficult to notch at the edge even after four consecutive indentations. However, the nanobelt exhibited grooves of multiple layers as shown in the 3D image in Figure 3.6(B).

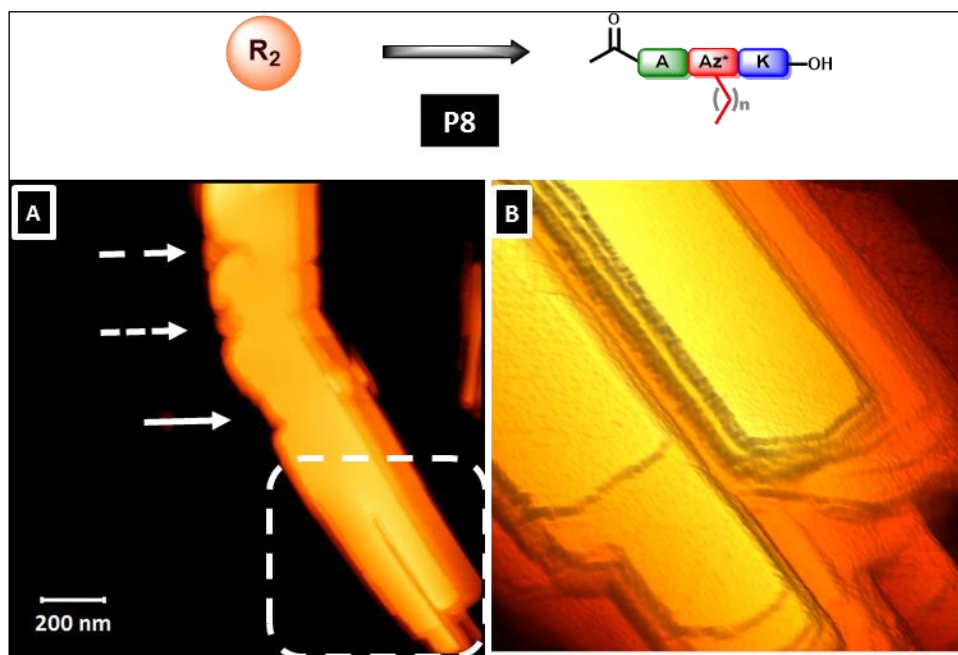


Figure 3.6: AFM nanoindentation at the lateral position of **P8**. (A) Three different indentations indicated by white arrows and (B) 3D image of a highlighted section of (A) showing grooves of several layers.

From the holes and openings created, the features were analysed by extracting the height profiles of the surface topology (Figure 3.7(A)) as described previously. For example, the hole in Figure 3.5(D) was graphically presented which shows three layers that are arranged in a step-wise pattern. Frequency distribution of the height values for the layers was analysed to obtain the normal distribution curve in Figure 3.7(B). The average height value for each layer of **P8** was found to be 2.8 ± 0.2 nm which is ≈ 0.2 nm more than the layers in **P7**.

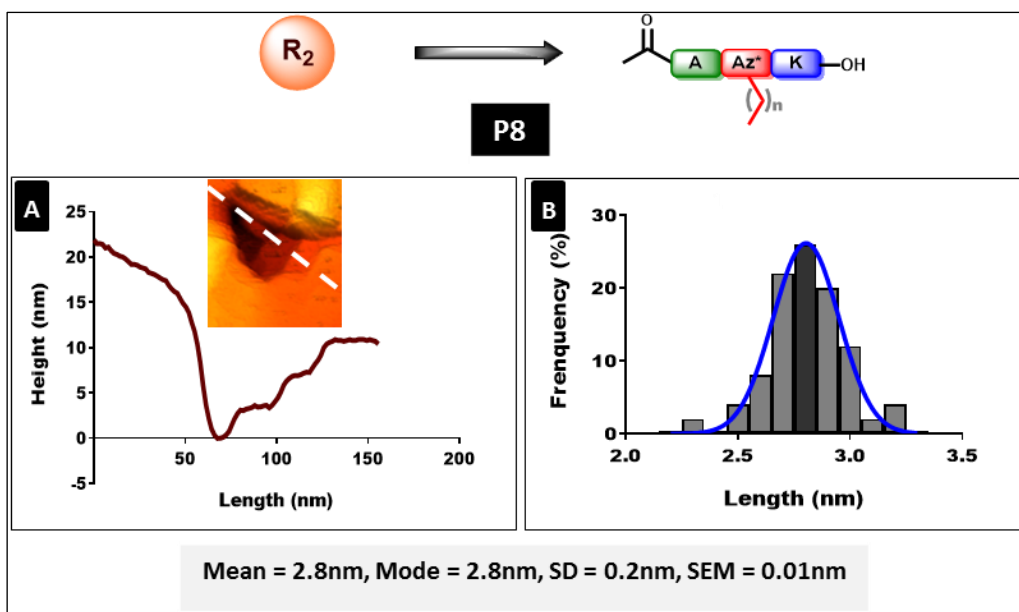


Figure 3.7: Measurements of layers in **P8** after AFM nanoindentation. (A) Example of a graphical presentation of an extracted profile of inserted 3D image showing the arrangement of layers and (B) frequency distribution of the height values obtained from both central and lateral indentations.

3.3.4 Nanoindentation of **P9** nanobelts

The nanoindentation of **P9** was carried out with a trigger threshold of 250 nm which is higher than the value used for **P7** and **P8**. A trigger threshold below 250 nm did not produce any indentation of **P9** indicating these fibres to be the stiffest of this series. Figures 3.8(A) and (C) show two different holes created at the central positions after nanoindentation. The magnified images (Figure 3.8(B) and (D)) together with the 3D images of the indented sections of **P9** revealed distinct layers on the surface which appeared stacked atop of each other. This further reinforced the previous observation of multiple layers that were observed in **P7** and **P8**.

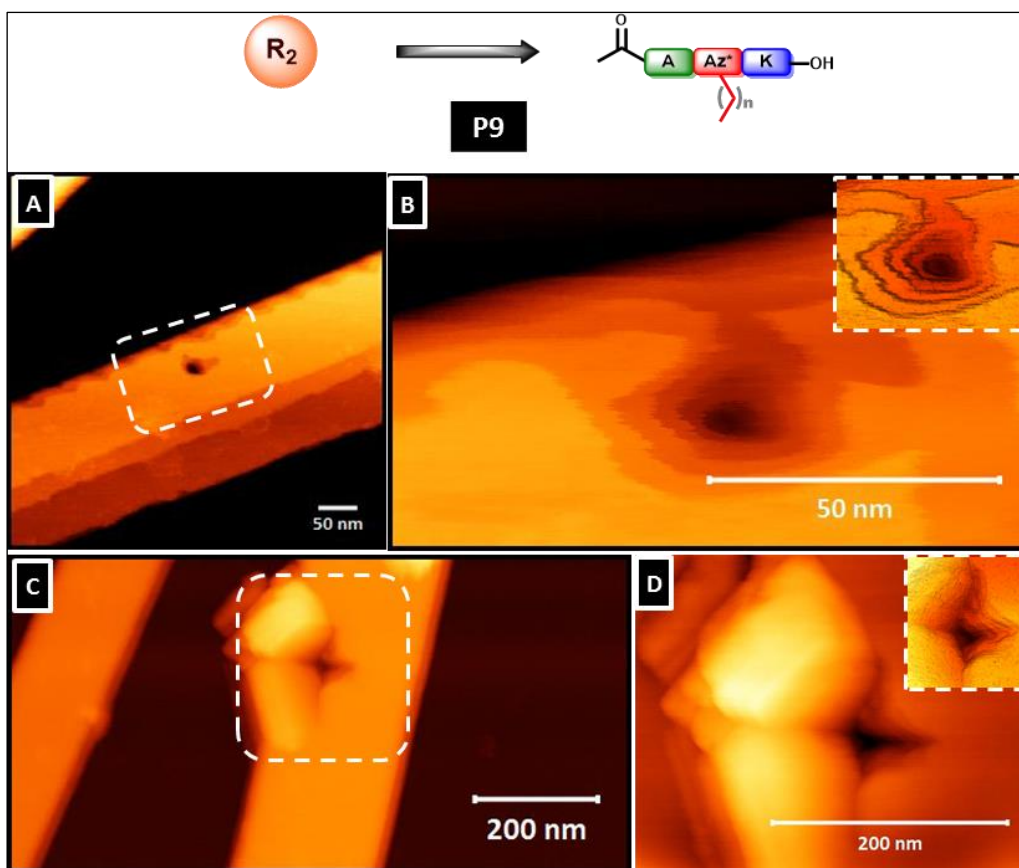


Figure 3.8: AFM nanoindentation of **P9** at the central position. (A) The hole created after indentation, (B) magnification of highlighted section in (A) showing staircase-like morphology of the interior, (C) hole created in another nanobelt after indentation and (D) magnification of highlighted section in (C) showing the interior stacking of layers. Inserts are 3D images of (B) and (D).

Nanoindentation of **P9** was also carried out at the edge with a trigger threshold of 250 nm. Figures 3.9(A) and (B) show that the nanobelts were notched at the edge to reveal the internal structural arrangement. The result indicated a similar internal organisation comparable to previously observed images of **P7** and **P8**, thus suggesting that the self-assembly mechanism of R_2 β^3 -peptide amphiphiles might be similar.

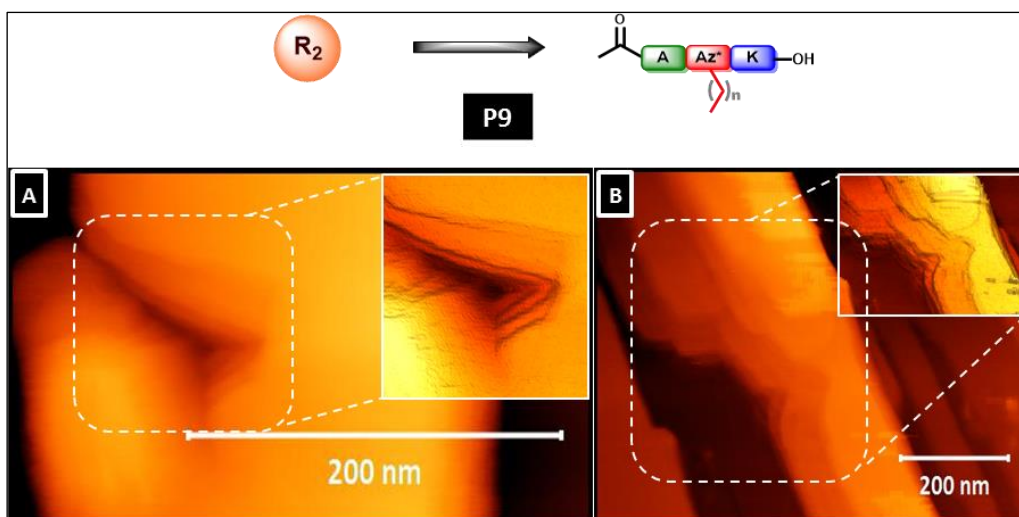


Figure 3.9: AFM nanoindentation of **P9** at the edge position showing indentations that exposed the underlying layers. Inserts are 3D images of (A) and (B).

The structural analysis of the indented sections of **P9** was carried out as previously described. The extracted profile for the surface topology of one of the holes (Figure 3.10(A)), revealed the internal architecture of multiple layers stacked on each other. The normal distribution curve (Figure 3.10(B)) shows the average height value for each layer to be 3.0 ± 0.2 nm.

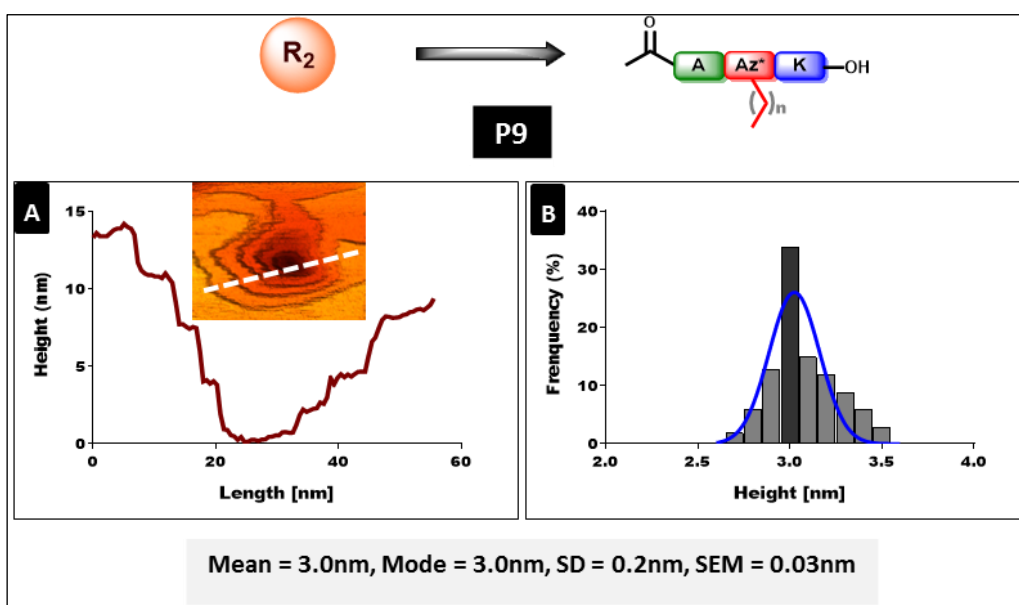


Figure 3.10: Measurement of the internal organisation of self-assembled **P9**. (A) Example of a graphical presentation of an extracted profile of inserted 3D image showing the arrangement of layers and (B) frequency distribution of height values from 100 measurements.

In comparison, Figure 3.11 shows the summary of all the sizes for the layers from **P7**, **P8** and **P9**. The size of **P7** layer (2.8 ± 0.2 nm) is significantly lower ($p < 0.0001$) than **P8** (2.6 ± 0.2 nm) and **P9** (3.0 ± 0.2) while the size of **P8** layer is significantly lower than that of **P9** ($p < 0.0001$). It also suggests that as the length of alkyl chain increases (**P7** = C₁₂, **P8** = C₁₄ and **P9** = C₁₆), the size of the layers also increases. These values were used to propose the self-assembly model for β^3 -peptide amphiphiles.

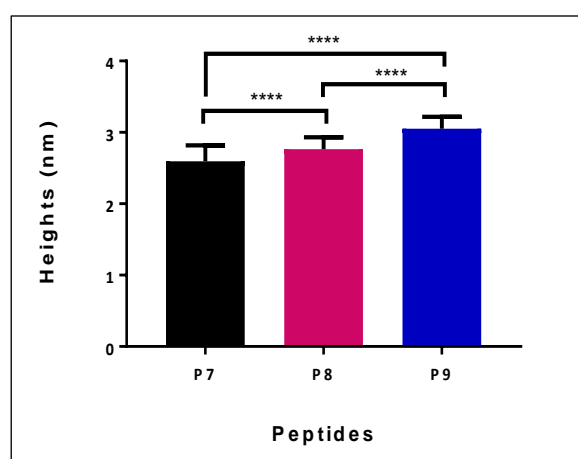


Figure 3.11: Summary of height values for the layers from **P7**, **P8** and **P9** after nanoindentation. One-way ANOVA Tukey's multiple comparisons test was used for the analysis where p values < 0.0001 (****) is significant.

3.3.5 PeakForce nanomechanical properties

To ascertain the stiffness of **P7**, **P8** and **P9** nanobelts, the individual force curves from each tap that occurs during the nanoindentation imaging process was analysed using PF-QNM. The morphology and Young's modulus of the nanobelts were measured simultaneously when the AFM tip penetrated into the nanobelts. Figure 4.12 shows the modulus for **P7**, **P8** and **P9** to be ≈ 7.4 MPa, ≈ 12.4 MPa and ≈ 16.5 MPa respectively. The stiffness for **P7** is significantly lower than that of **P8** ($p \leq 0.01$) and **P9** ($p \leq 0.0001$) while **P8** is significantly lower in stiffness than **P9** ($p \leq 0.01$). The data also suggest that modulus increases with increase in alkyl chain length.

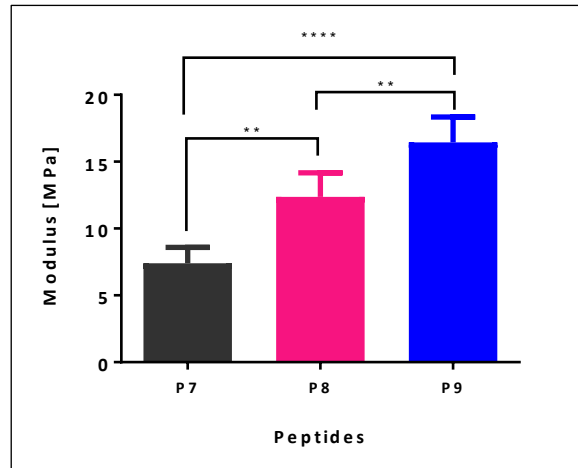


Figure 3.12: Young's modulus for **P7**, **P8** and **P9** obtained by PF-QNM in a liquid environment. One-way ANOVA Tukey's multiple comparisons test was used for the analysis where p values are < 0.01 (**) and < 0.0001 (****).

3.4 Discussion

3.4.1 Structural and mechanical properties of P7, P8 and P9 nanobelts

Nanoindentation by AFM was used to investigate the internal molecular packing of self-assembled nanobelts of **P7**, **P8** and **P9** in a hydrated environment. Several holes were created by punching the nanostructures with the AFM tip which exposed the internal architecture of the self-assembled nanobelts. This involved manipulation of the AFM tip in the fluid by vertical and horizontal adjustments including control of the trigger thresholds. Although this technique is commonly used for quantitative measurements of mechanical properties in nanostructures [14, 20, 18, 22, 23, 16], the method developed in this chapter allows the probing of β^3 -peptide-based material in a liquid environment.

The only example of AFM nanoindentation found in literature that is related to this study is the work reported by Del Mercati et al., which was carried out in order to determine the mechanical properties of single amyloid-like fibril from a poly-pentapeptide and their applicability in nanobiotechnology [20]. They demonstrated the use of AFM nanoindentation in air to fracture a fibril with nanometric control by the AFM tip to obtain a longitudinal cross-sectional gap of ≈ 135 nm. Figures 3.13(A) and (B) show the single fibril that was fractured via AFM nanoindentation. While the single fibril was broken into two parts after the indentation, there was no evidence of internal molecular features.

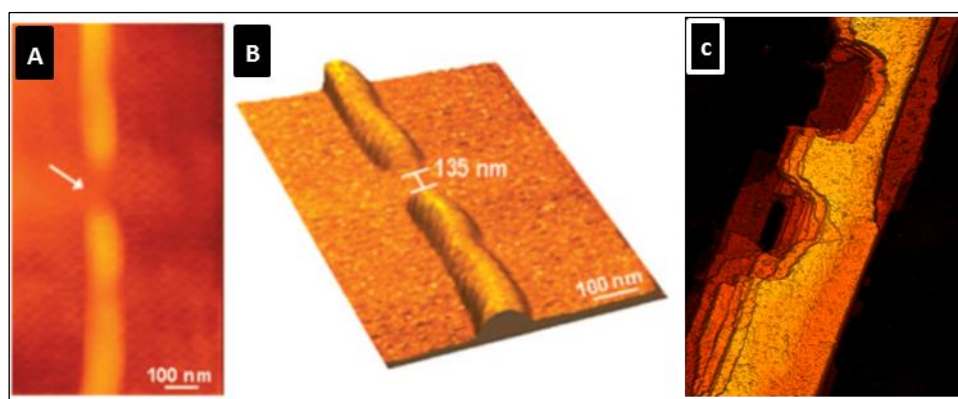


Figure 3.13: AFM nanoindentation of a single amyloid-like fibril. (A) Fibre fracture indicated by the arrow, (B) 3D image after fracture with a final gap of 135 nm was obtained (A and B from reference [20] used with permission from the American Chemical Society) and (C) 3D image of **P7** after nanoindentation.

In contrast to the report of Del Mercato et al., this present study describes AFM nanoindentation of β^3 -peptide amphiphiles in a hydrated environment to obtain a variety of nanoscale holes which revealed the internal features of the nanostructure. In comparison, Figure 3.13(C) shows an example of two holes that were punched through the edge of **P7** which clearly show the topology of the internal features. The internal features of the nanobelts after indentation revealed evidence of layers with the average height values of 2.6 ± 0.3 nm, 2.8 ± 0.2 nm and 3.0 ± 0.2 nm for **P7**, **P8** and **P9** respectively. Cui et al. have reported similar nanostructure with layers (but not by nanoindentation) which exhibited bilayers for an α -peptide amphiphile (C₁₆-VEVE) which was ≈ 2 nm in height [6]. These features are also similar to the multi-layered steps observed on the surface of nanobelts that are atop of each other [7]. The results obtained in this study are consistent with the multiple layers observed previously for α -peptide amphiphile nanobelts utilising SAXS, which formed bilayer organisation in the interior of the nanostructure [7, 24, 25].

The hydrated environment used for nanoindentation in this study played an important role in enhancing the penetration of the AFM tip into the nanobelts. Previously, indentations were carried out in air using a range of trigger thresholds between 350 – 400 nm which was not sufficient to punch a hole through the nanobelts. In some cases, it completely fractured the nanostructures with no useful internal information. However, holes were created when the nanoindentation was carried out in fluid with a trigger threshold of 100 nm, 200 nm and 250 nm for **P7**, **P8** and **P9** respectively. The hydrated samples proved to be softer and more malleable than the dry samples. The ability to study samples in a liquid environment provides a significant advantage for maintaining physiological conditions for future applications [26-33].

PF-QNM was also used to determine the stiffness of **P7**, **P8** and **P9** nanobelts. The analysis of the mechanical properties indicated a significant decrease in stiffness from **P9** > **P8** > **P7** which is linked to the inherent molecular design of individual molecules [34, 35]. In a previous study, the variations in α -peptide sequences were reported to affect the mechanical properties of nanofibres from α -peptide amphiphiles [36]. The peptides were initially designed by increasing the number of valine residues which raised the mechanical stiffness, whereas alanine tends to reduce the stiffness. The high stiffness correlated with the increase in hydrophobicity and noncovalent interactions. Therefore, the changes observed for Young's

modulus in this study suggest that there are different levels of thickness and rigidity in the nanobelts which could be due to the increase in alkyl chain length from C₁₂, C₁₄ and C₁₆. This also accounts for the differences in the trigger threshold that was used for indentation of **P7**, **P8** and **P9** nanobelts. The variation in stiffness is based on the internal organisation of individual molecules which is also commonly observed in α -peptide amphiphiles [37, 36, 38]. The Young's modulus of ≈ 7.4 MPa, ≈ 12.4 MPa and ≈ 16.5 MPa obtained for **P7**, **P8** and **P9** respectively, suggest that these peptides can contribute to the development of new generation of biomaterials for example, as the stiffness is within the range of the mechanical properties of tissues such as cartilage tissue or skin tissue which is characterised by stiffness ranging between 5 – 100 MPa [39-42]. Furthermore, as far as we can ascertain, there is no report in literature that describes such superior stiffness for β^3 -peptide materials. However, in the case of α -peptides, Young's modulus ranging from 3.5 – 7.0 MPa was obtained for amyloid-like fibrils, [20], whereas Guo et al. obtained 5 - 50 MPa for insulin amyloid-like fibrils [14]. The relative simplicity of the technique used in this study can facilitate rapid collection of quantitative information related to the packing density and heterogeneity of self-assembled β^3 -peptide-based materials.

3.4.2 Self-assembly model for **P7**, **P8** and **P9** nanobelts

The results obtained in this study have highlighted important directions for the self-assembly model of R₂ β^3 -peptide amphiphile nanobelts, which is based on the following observations;

- The visualised AFM images after nanoindentation revealed multiple layers that are stacked atop of each other.
- A regular spacing of height values for the layers was observed for **P7**, **P8** and **P9**.

In order to estimate theoretical dimensions of the self-assembled materials, β^3 -peptides adopt 14-helices in which the diameter of the backbone core of a 14-helical turn for a single self-assembled β^3 -tripeptide nanorod is known to be ≈ 0.5 nm [43-46]. The angle and average length of a carbon – carbon bond in a fully saturated alkyl chain are 109.5° and 0.15 nm respectively [47-50]. The estimated length of the alkyl chain for example **P7** (with C₁₂) will therefore be 6nm and together with nanorod diameter of 0.5 nm, the total size of **P7** will be

1.4 nm in size $((0.15 \text{ nm} \times 6) + 0.5 \text{ nm})$. In a similar manner, **P8** and **P9** will be 1.55 nm and 1.7 nm respectively (Figure 3.14).

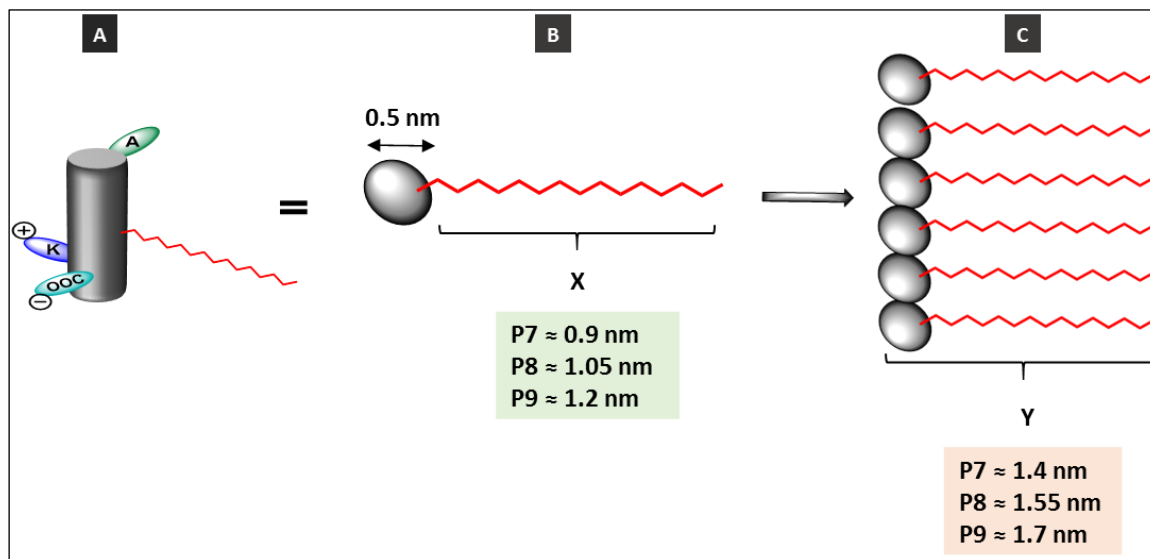


Figure 3.14: Proposed self-assembly model for **P7**, **P8** and **P9** nanobelts (A) Helical net diagram of β^3 -tripeptide with all side chains located outside the helix, (B) a representation of the top view of a single monomer, "X" is the size of alkyl chain length, (C) self-assembled nanofibril with alkyl chains aligned at one side of the nanofibril, "Y" is the size of a single nanofibril.

It was described previously in Chapter 2 that the nanofibrils of self-assembled β^3 -peptide amphiphiles undergo lateral association via hydrophobic interaction and electrostatic attraction to form higher ordered structures (Figure 3.15). The experimental values obtained in this chapter were found to be consistent with the calculated values of a bilayer based on the assumptions underpinning the calculated values (Table 3.1).

Table 3.1: Summary of experimental height values and calculated sizes for **P7**, **P8** and **P9** bilayers.

Peptide	Calculated values (nm)	Experimental values (nm)
P7	2.8	2.6
P8	3.1	2.8
P9	3.4	3.0

The packing of the alkyl chain is critical for the type of morphology that will be produced. In Chapter 2 it was proposed that the packing of alkyl chains in twisted ribbons (R_0 and R_1) are non-interdigitated while they may be interdigitated in the nanobelts (R_2 and R_3). However, from the images obtained using AFM nanoindentation for the R_2 series of β^3 -peptide amphiphiles, it is still not clear how the alkyl chains pack within the nanostructures of β^3 -peptide amphiphiles. Although several reports have already demonstrated via SAXS, SANS and XRD that the alkyl chains of α -peptide amphiphiles which form nanobelts pack mainly by complete interdigitation which results in a straight rigid structure lacking twist or curvature [1, 51, 6]. Taking this into consideration, the alkyl chains may also tilt to an angle [52] which may also influence the packing and final self-assembled structure. The proposed packing possibilities for alkyl chains in the β^3 -peptide amphiphiles may be with or without tilting as shown in Figure 3.15 in non-interdigitated and interdigitated packing (Figure 3.15).

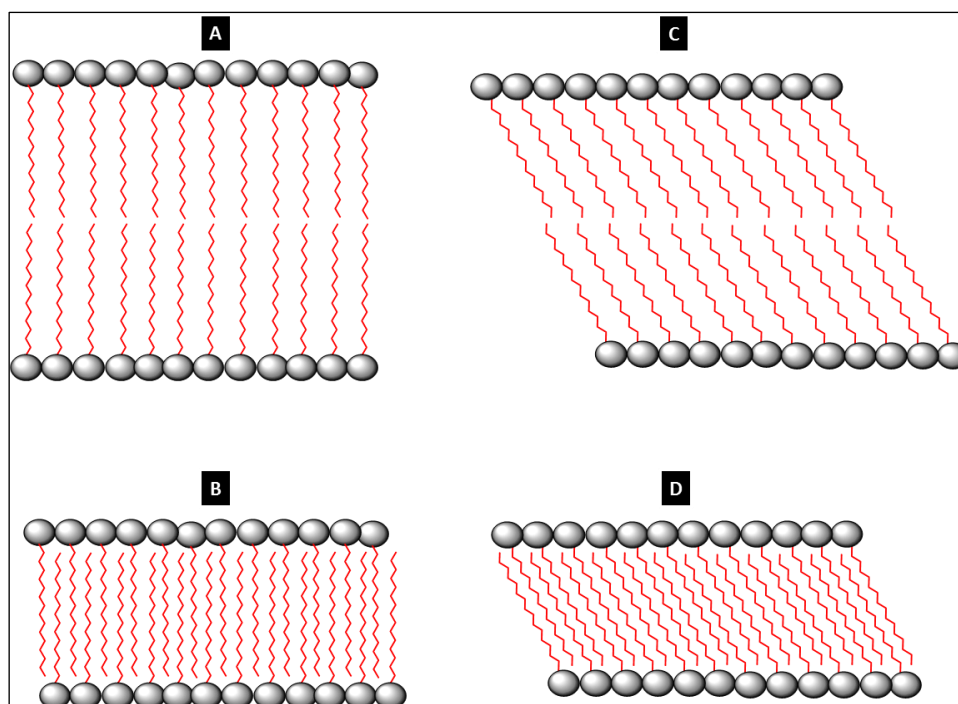


Figure 3.15: Possible self-assembly mechanisms for alkyl chain packing of β^3 -peptides amphiphiles. (A) Non-interdigitated, (B) interdigitated, (C) non-interdigitated tilt and (D) interdigitated tilt.

The values obtained experimentally suggest that there may be two nanofibrils associating laterally via hydrophobic interaction to form a bilayer “Z” (Figure 3.16(A)) with a calculated dimension of 2.8 nm, 3.1 nm and 3.4 nm for **P7**, **P8** and **P9** respectively. Given that the heights “H” (Figure 3.16(C)) of R_2 nanobelts with C_{12} , C_{14} and C_{16} alkyl chains are ≈ 18 nm, ≈ 25 nm and ≈ 32 nm respectively, this indicates that the bilayers are stacked together on top of each other to form a supramolecular structure (Figure 3.16(B)).

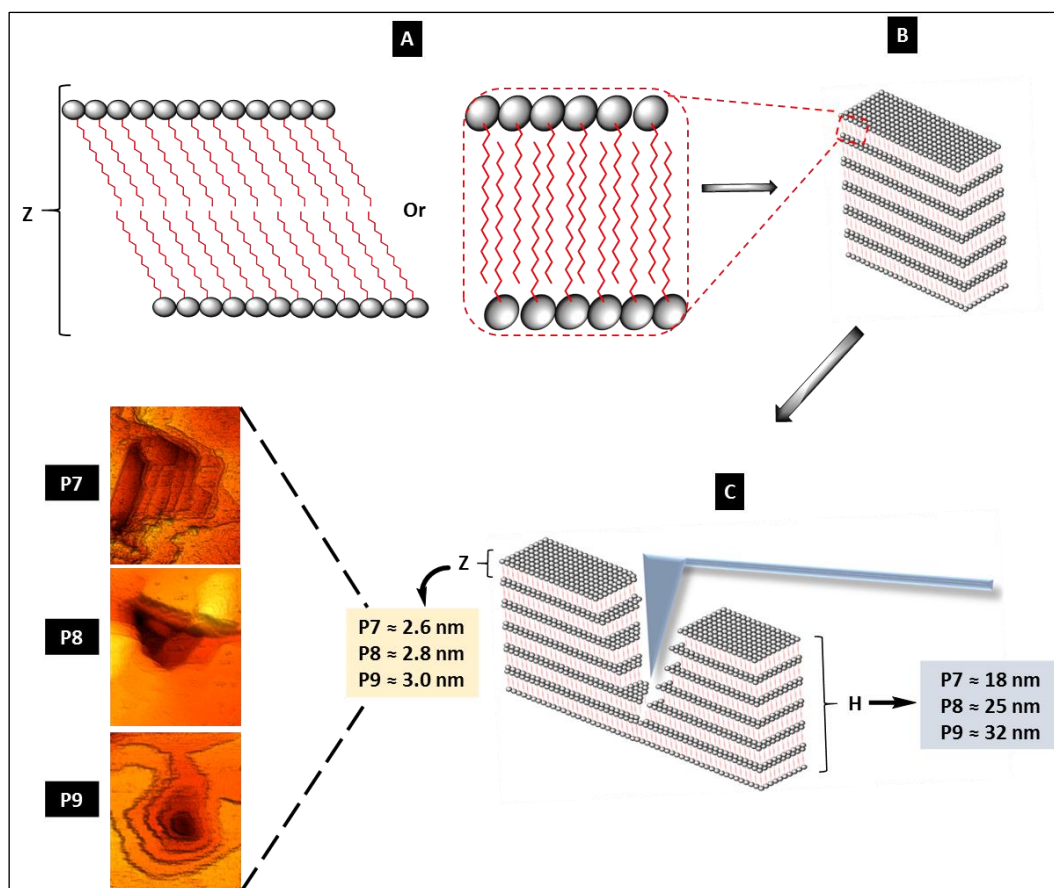


Figure 3.16: Self-assembly model for **P7**, **P8** and **P9** nanobelts. (A) Complete interdigitation of alkyl chain to form single bilayer “Z”, (B) bilayers stacked together to form flat nanobelt, (C) a schematic diagram for nanoindentation with an AFM tip which exposed the internal structure of nanobelts. The height values “H” were previously obtained in Chapter 2. Inserted 3D images show evidence of stacked layers.

Bilayer stacking along the z-direction was reported to be a major factor that is responsible for the thickness, size and stiffness of nanobelts in α -peptide amphiphiles [6, 36]. The self-assembly model of α -peptide amphiphile nanobelts with interdigitated packing of alkyl chains among the α -peptide segments was previously characterised using SANS and a bilayer spacing of 4.3 nm was obtained [6]. This value was also consistent with the AFM measurements, thus suggesting that a height value of 12 nm corresponds to the stacking of 3 α -peptide amphiphile bilayers. Similarly, Castelletto *et al.* provided a model using XRD and SAXS data to show that nanostructure of a self-assembling α -peptide amphiphile (C_{16} -KTTKS) formed nanobelts with a bilayer configuration in the internal structure [24, 7]. The bilayers revealed regular spacing of 5.2 nm and stabilised by hydrogen bonding. They specifically observed small steps with height values of 2.65 nm which corresponded to exactly half of one layer. The formation of a

bilayer in this study is also in agreement with other reports for nanobelts formation, which identified the common motifs of association via hydrophobic interaction of alkyl chains and the sequence order of α -amino acids [51, 25]. Therefore, the AFM images and dimensions obtained in this study of R_2 β^3 -peptide amphiphiles suggest that a bilayer structure which stacks along the z-direction is a strong possibility. If this is the case, the internal dimensions indicate that there are approximately 7, 9 and 11 bilayers that stack together to form the nanobelts of **P7**, **P8** and **P9** respectively.

As a follow-up from the information gathered in Chapter 2 and with the present insight into how nanobelts self-assemble, a possible model for the self-assembly of R_0 and R_1 β^3 -peptide amphiphiles that form twisted ribbons is shown in Figure 3.17. The alkyl chains of each nanofibril promote hydrophobic interactions to form a non-interdigitated bilayer-like architecture (Figure 3.17(B)) which eventually forms the interior hydrophobic core of the nanostructure. Although some degree of interdigitation is possible, non-interdigitated alkyl chain packing (with and without tilting) is shown here for R_0 and R_1 due to the fact that non-interdigitated packing is known to promote flexibility and twisting of nanofibres [51]. Electrostatic attraction between positively charged β K residues and the negatively charged C-terminal carboxyl group can also promote the lateral assembly by bundling of the nanofibrils. The combined influence of both electrostatic attraction and hydrophobic interaction of the non-interdigitated alkyl chains result in twisted ribbons. Further analysis is required to confirm the validity of this model. This model also demonstrates the collective balance of electrostatic interaction, hydrophobic interaction and hydrogen bonding which are pivotal for the formation of self-assembled nanostructures of β^3 -peptide amphiphiles [53-61].

In terms of the potential of using other techniques to probe the molecular and supramolecular organisation of β^3 -peptide amphiphiles, SAXS for example can provide quantitative nanoscale density differences in the self-assembled twisted ribbons and nanobelts. SAXS measurements was previously reported by Pizzey et al., to characterise fibre-like nanostructures that are formed by sequence-directed assembly of oligomeric β^3 -peptides [62]. The result from this study implies that SAXS can also be used to potentially deliver the size distribution and characteristic distances that will help to quantitatively resolve the structural organisation of self-assembled β^3 -peptide amphiphiles. This could be achieved via the elastic scattering patterns of X-ray when it travels through the self-assembled

nanostructures at small angles of $0.1 - 10^\circ$. It should be noted however, that we lack any definitive models of β^3 -peptide assembly, which are governed by a different set of parameters than α -peptides and are yet to be described. This means that the utilisation of SAXS and SANS is only possible once a complete model using fibre diffraction has been completed.

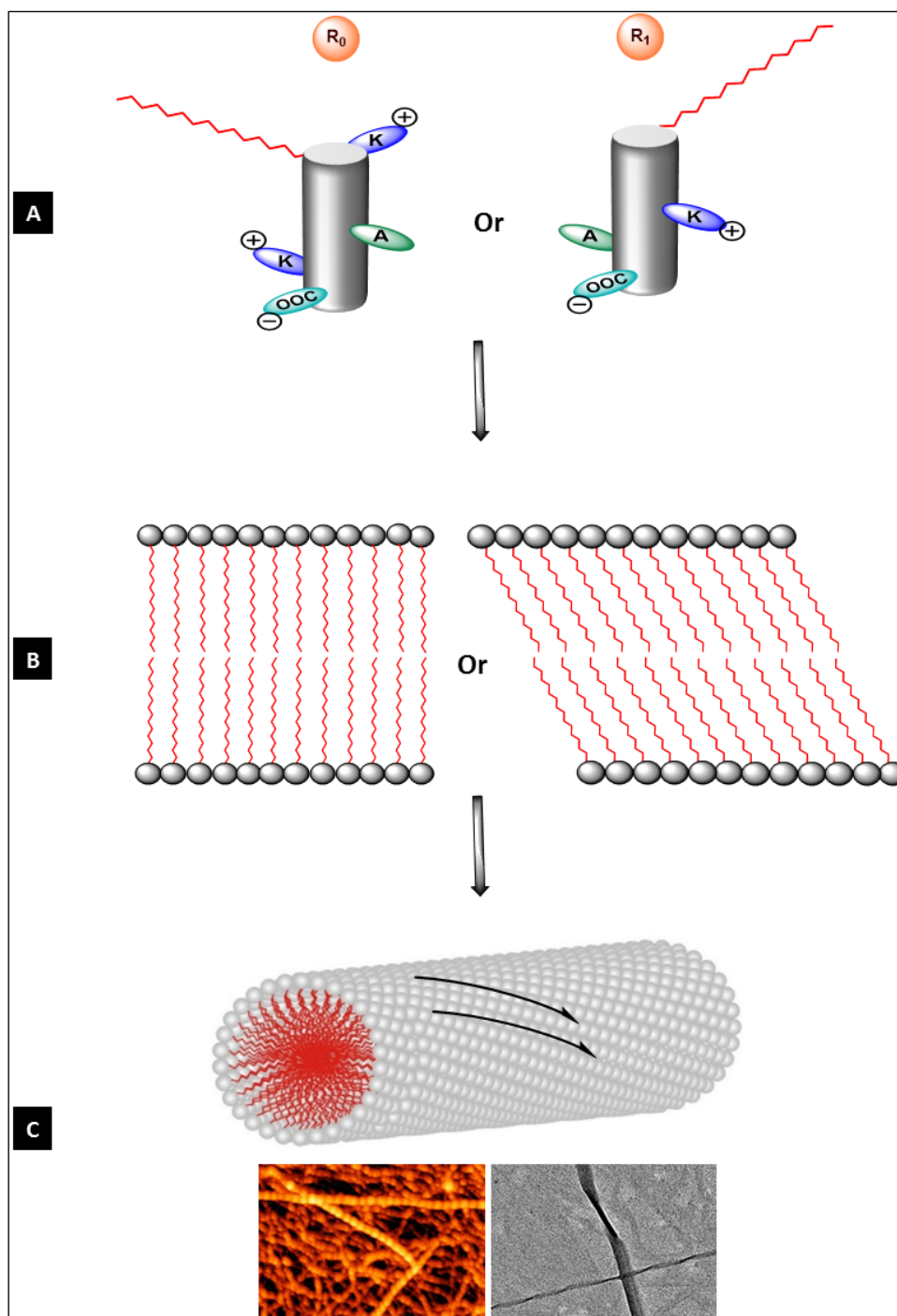


Figure 3.16: Proposed self-assembly model for twisted ribbons of β^3 -peptide amphiphiles. (A) Helical net diagram for R_0 and R_1 β^3 -peptide monomer showing positively charged βK and negatively charged C-terminus, (B) hydrophobic interaction of alkyl chains forming non-interdigitated packing with and without tilting of alkyl chains, (C) formation of twisted ribbon shown showing nanofibre mesh with periodicity and twisted patterns by AFM and TEM images from Chapter 2.

3.5 Conclusion

The results presented in this chapter described the use of AFM nanoindentation to investigate the internal molecular packing of self-assembled nanobelts for **P7**, **P8** and **P9** in a liquid environment. The indentation at the central and at the edge positions with the AFM tip created holes which revealed the internal features of the nanobelts which are multiple bilayers that can be seen easily from the AFM images. The bilayers stacked together exhibiting a regular spacing of 2.6 ± 0.3 nm, 2.8 ± 0.2 nm and 3.0 ± 0.2 nm for **P7**, **P8** and **P9** nanobelts respectively. The dimensions of the bilayer obtained experimentally are consistent with the calculated values which were subsequently used in determining the self-assembly model. AFM nanoindentation was demonstrated to be a versatile imaging technique that offers an additional high-resolution alternative for studying the internal packing order of self-assembled peptide-based materials along with the mechanical properties. The stiffness of **P7**, **P8** and **P9** nanobelts was found to be ≈ 7.4 MPa, ≈ 12.4 MPa and ≈ 16.5 Mpa respectively. By using PF-QNM, Young's modulus was measured and shown that nanobelts from the same R_2 β^3 -peptide series that differ only in the length of alkyl chain, exhibit significantly different values of stiffness. AFM nanoindentation can also be used in combination with other methods, for example, SAXS, XRD, and Cryo-EM in resolving the self-assembly pattern of nanostructures. Furthermore, the ability to perform AFM nanoindentation in a fluid environment vastly increases the potential applications of AFM technology under physiological conditions and real-time observations of samples.

References

1. Nieuwland, M., L. Ruizendaal, A. Brinkmann, L. Kroon-Batenburg, J.C.M. Van Hest, and D.W.P.M. Löwik, *A structural study of the self-assembly of a palmitoyl peptide amphiphile*. Faraday Discussions, 2013. **166**: p. 361-379.
2. Morris, K.L. and L.C. Serpell, *X-ray fibre diffraction studies of amyloid fibrils*, in *Methods in Molecular Biology*. 2012. p. 121-135.
3. Hamley, I.W., A. Dehsorkhi, V. Castelletto, M.N.M. Walter, C.J. Connon, M. Reza, and J. Ruokolainen, *Self-Assembly and Collagen-Stimulating Activity of a Peptide Amphiphile Incorporating a Peptide Sequence from Lumican*. Langmuir, 2015. **31**(15): p. 4490-4495.
4. Kornmueller, K., I. Letofsky-Papst, K. Gradauer, C. Mikl, F. Cacho-Nerin, M. Leypold, W. Keller, G. Leitinger, H. Amenitsch, and R. Prassl, *Tracking morphologies at the nanoscale: self-assembly of an amphiphilic designer peptide into a double helix superstructure*. Nano Research, 2015. **8**(6): p. 1822-1833.
5. Palladino, P., V. Castelletto, A. Dehsorkhi, D. Stetsenko, and I.W. Hamley, *Conformation and self-association of peptide amphiphiles based on the KTTKS collagen sequence*. Langmuir, 2012. **28**(33): p. 12209-12215.
6. Cui, H., T. Muraoka, A.G. Cheetham, and S.I. Stupp, *Self-assembly of giant peptide nanobelts*. Nano Letters, 2009. **9**(3): p. 945-951.
7. Castelletto, V., I.W. Hamley, J. Adamcik, R. Mezzenga, and J. Gummel, *Modulating self-assembly of a nanotape-forming peptide amphiphile with an oppositely charged surfactant*. Soft Matter, 2012. **8**(1): p. 217-226.
8. Shao, J., Y. Wang, X. Chen, X. Hu, and C. Du, *Nanomechanical properties of poly(l-lactide) nanofibers after deformation*. Colloids and Surfaces B: Biointerfaces, 2014. **120**: p. 97-101.
9. Tan, E.P.S. and C.T. Lim, *Nanoindentation study of nanofibers*. Applied Physics Letters, 2005. **87**(12): p. 1-3.
10. Tan, E.P.S. and C.T. Lim, *Mechanical characterization of nanofibers – A review*. Composites Science and Technology, 2006. **66**(9): p. 1102-1111.

11. Kol, N., L. Adler-Abramovich, D. Barlam, R.Z. Shneck, E. Gazit, and I. Rouso, *Self-assembled peptide nanotubes are uniquely rigid bioinspired supramolecular structures*. Nano Letters, 2005. **5**(7): p. 1343-1346.
12. Kurland, N.E., Z. Drira, and V.K. Yadavalli, *Measurement of nanomechanical properties of biomolecules using atomic force microscopy*. Micron, 2012. **43**(2-3): p. 116-128.
13. Marchetti, M., G.J.L. Wuite, and W.H. Roos, *Atomic force microscopy observation and characterization of single virions and virus-like particles by nano-indentation*. Current Opinion in Virology, 2016. **18**: p. 82-88.
14. Guo, S. and B.B. Akhremitchev, *Packing density and structural heterogeneity of insulin amyloid fibrils measured by AFM nanoindentation*. Biomacromolecules, 2006. **7**(5): p. 1630-1636.
15. Neugirg, B.R., S.R. Koebley, H.C. Schniepp, and A. Fery, *AFM-based mechanical characterization of single nanofibres*. Nanoscale, 2016. **8**(16): p. 8414-8426.
16. Sweers, K.K.M., M.L. Bennink, and V. Subramaniam, *Nanomechanical properties of single amyloid fibrils*. Journal of Physics: Condensed Matter, 2012. **24**(24): p. 243101.
17. Helen, W., P. De Leonardis, R.V. Ulijn, J. Gough, and N. Tirelli, *Mechanosensitive peptide gelation: Mode of agitation controls mechanical properties and nano-scale morphology*. Soft Matter, 2011. **7**(5): p. 1732-1740.
18. Wenger, M.P.E., L. Bozec, M.A. Horton, and P. Mesquida, *Mechanical Properties of Collagen Fibrils*. Biophysical Journal, 2007. **93**(4): p. 1255-1263.
19. Notbohm, J., B. Poon, and G. Ravichandran, *Analysis of nanoindentation of soft materials with an atomic force microscope*. Journal of Materials Research, 2011. **27**(1): p. 229-237.
20. del Mercato, L.L., G. Maruccio, P.P. Pompa, B. Bochicchio, A.M. Tamburro, R. Cingolani, and R. Rinaldi, *Amyloid-like Fibrils in Elastin-Related Polypeptides: Structural Characterization and Elastic Properties*. Biomacromolecules, 2008. **9**(3): p. 796-803.
21. Adamcik, J. and R. Mezzenga, *Study of amyloid fibrils via atomic force microscopy*. Current Opinion in Colloid & Interface Science, 2012. **17**(6): p. 369-376.
22. Wenger, M.P.E., M.A. Horton, and P. Mesquida, *Nanoscale scraping and dissection of collagen fibrils*. Nanotechnology, 2008. **19**(38).
23. Sweers, K., K. van der Werf, M. Bennink, and V. Subramaniam, *Nanomechanical properties of α -synuclein amyloid fibrils: a comparative study by nanoindentation*,

- harmonic force microscopy, and Peakforce QNM*. Nanoscale Research Letters, 2011. **6**(1): p. 270-270.
24. Castelletto, V., I.W. Hamley, J. Perez, L. Abezgauz, and D. Danino, *Fibrillar superstructure from extended nanotapes formed by a collagen-stimulating peptide*. Chemical Communications, 2010. **46**(48): p. 9185-9187.
 25. Moyer, T.J., H. Cui, and S.I. Stupp, *Tuning nanostructure dimensions with supramolecular twisting*. Journal of Physical Chemistry B, 2013. **117**(16): p. 4604-4610.
 26. Baró, A.M. and R.G. Reifenger, *Atomic Force Microscopy in Liquid: Biological Applications*. Atomic Force Microscopy in Liquid: Biological Applications. 2012.
 27. Last, J.A., P. Russell, P.F. Nealey, and C.J. Murphy, *The Applications of Atomic Force Microscopy to Vision Science*. Investigative Ophthalmology & Visual Science, 2010. **51**(12): p. 6083-6094.
 28. Müller, D.J. and Y.F. Dufrêne, *Atomic force microscopy: A nanoscopic window on the cell surface*. Trends in Cell Biology, 2011. **21**(8): p. 461-469.
 29. Santos, N.C. and M.A.R.B. Castanho, *An overview of the biophysical applications of atomic force microscopy*. Biophysical Chemistry, 2004. **107**(2): p. 133-149.
 30. Francis, L.W., P.D. Lewis, C.J. Wright, and R.S. Conlan, *Atomic force microscopy comes of age*. Biology of the cell / under the auspices of the European Cell Biology Organization, 2010. **102**(2): p. 133-143.
 31. Gadegaard, N., *Atomic force microscopy in biology: technology and techniques*. Biotechnic & Histochemistry, 2006. **81**(2-3): p. 87-97.
 32. Korayem, M.H., N. Ebrahimi, and M.S. Sotoudegan, *Frequency response of atomic force microscopy microcantilevers oscillating in a viscous liquid: A comparison of various methods*. Scientia Iranica, 2011. **18**(5): p. 1116-1125.
 33. Frewin, C.L., *Atomic Force Microscopy Investigations into Biology – From Cell to Protein*. Intech open science, 2012: p. 1-370.
 34. Webber, M.J., E.J. Berns, and S.I. Stupp, *Supramolecular Nanofibers of Peptide Amphiphiles for Medicine*. Israel Journal of Chemistry, 2013. **53**(8): p. 530-554.
 35. Vajtai, R., *Springer Handbook of Nanomaterials*. 2013: Springer Berlin Heidelberg.
 36. Pashuck, E.T., H. Cui, and S.I. Stupp, *Tuning Supramolecular Rigidity of Peptide Fibers through Molecular Structure*. Journal of the American Chemical Society, 2010. **132**(17): p. 6041-6046.

37. Zhan, F.K., S.M. Hsu, H. Cheng, and H.C. Lin, *Remarkable influence of alkyl chain lengths on supramolecular hydrogelation of naphthalene diimide-capped dipeptides*. RSC Advances, 2015. **5**(60): p. 48961-48964.
38. Jun, H.W., S.E. Paramonov, H. Dong, N. Forraz, C. McGuckin, and J.D. Hartgerink, *Tuning the mechanical and bioresponsive properties of peptide-amphiphile nanofiber networks*. Journal of Biomaterials Science, Polymer Edition, 2008. **19**(5): p. 665-676.
39. Shimizu T., B.-K.C., Y.-W. Chung, A. Greiner, N. Higashi, H.-J.Kim, N. Kimizuka, T. Koga · B.-I, Lee · M, Lee · J. H.Wendorff, *Self-Assembled Nanomaterials*. Advances in Polymer Science, 2008: p. 1-186.
40. Ní Annaidh, A., K. Bruyère, M. Destrade, M.D. Gilchrist, and M. Otténio, *Characterization of the anisotropic mechanical properties of excised human skin*. Journal of the Mechanical Behavior of Biomedical Materials, 2012. **5**(1): p. 139-148.
41. Pal, S., *Mechanical Properties of Biological Materials*, in *Design of Artificial Human Joints & Organs*. 2014, Springer US: Boston, MA. p. 23-40.
42. Griffin, M.F., B.C. Leung, Y. Premakumar, M. Szarko, and P.E. Butler, *Comparison of the mechanical properties of different skin sites for auricular and nasal reconstruction*. Journal of Otolaryngology - Head & Neck Surgery, 2017. **46**(1): p. 33.
43. Del Borgo, M.P., A.I. Mechler, D. Traore, C. Forsyth, J.A. Wilce, M.C.J. Wilce, M.I. Aguilar, and P. Perlmutter, *Supramolecular self-assembly of N-acetyl-capped β -peptides leads to nano- to macroscale fiber formation*. Angewandte Chemie - International Edition, 2013. **52**(32): p. 8266-8270.
44. Kulkarni, K., S. Motamed, N. Habila, P. Perlmutter, J.S. Forsythe, M.-I. Aguilar, and M.P. Del Borgo, *Orthogonal strategy for the synthesis of dual-functionalised [small beta]3-peptide based hydrogels*. Chemical Communications, 2016. **52**(34): p. 5844-5847.
45. Motamed, S., M.P. Del Borgo, K. Kulkarni, N. Habila, K. Zhou, P. Perlmutter, J.S. Forsythe, and M.I. Aguilar, *A self-assembling [small beta]-peptide hydrogel for neural tissue engineering*. Soft Matter, 2016. **12**(8): p. 2243-2246.
46. Cheng, R.P., S.H. Gellman, and W.F. DeGrado, *β -peptides: From structure to function*. Chemical Reviews, 2001. **101**(10): p. 3219-3232.
47. Lide Jr, D.R., *A survey of carbon-carbon bond lengths*. Tetrahedron, 1962. **17**(3-4): p. 125-134.

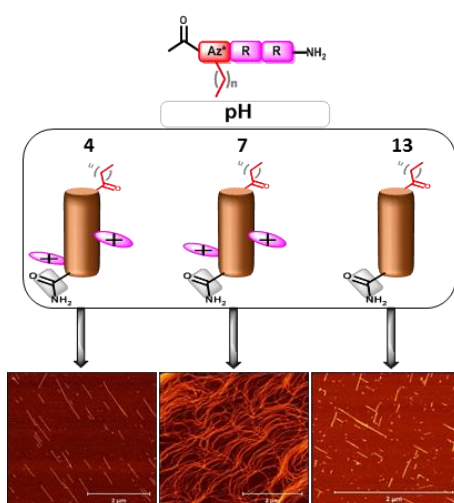
48. Dodziuk, H., *Strained Hydrocarbons: Beyond the Van-t Hoff and Le Bel Hypothesis*. Wiley-VCH Verlag GmbH & Co. KGaA, Weinheim (Germany): 2009; p. 1-471.
49. Detty, M.R. and M.B. O'Regan, *The Chemistry of Heterocyclic Compounds, Tellurium-Containing Heterocycles*. Wiley, New Jersey (USA): 2009: 53; p 1-511.
50. Roberts, D.J. and M.C. Caserio, *Basic Principles of Organic Chemistry, second edition* Benjamin, Inc. , Menlo Park, California (USA): 1977: p. 30-39.
51. Cui, H., A.G. Cheetham, E.T. Pashuck, and S.I. Stupp, *Amino acid sequence in constitutionally isomeric tetrapeptide amphiphiles dictates architecture of one-dimensional nanostructures*. Journal of the American Chemical Society, 2014. **136**(35): p. 12461-12468.
52. Laner, M., B.A.C. Horta, and P.H. Hünenberger, *Long-timescale motions in glycerol-monopalmitate lipid bilayers investigated using molecular dynamics simulation*. Journal of Molecular Graphics and Modelling, 2015. **55**: p. 48-64.
53. Cui, H., M.J. Webber, and S.I. Stupp, *Self-assembly of peptide amphiphiles: from molecules to nanostructures to biomaterials*. Biopolymers, 2010. **94**(1): p. 1-18.
54. Dehsorkhi, A., V. Castelletto, and I.W. Hamley, *Self-assembling amphiphilic peptides*. Journal of Peptide Science, 2014.7: p. 453-67.
55. Palmer, L.C. and S.I. Stupp, *Molecular Self-Assembly into One-Dimensional Nanostructures*. Accounts of chemical research, 2008. **41**(12): p. 1674-1684.
56. Stendahl, J.C., M.S. Rao, M.O. Guler, and S.I. Stupp, *Intermolecular forces in the self-assembly of peptide amphiphile nanofibers*. Advanced Functional Materials, 2006. **16**(4): p. 499-508.
57. Hamley, I.W., *Self-assembly of amphiphilic peptides*. Soft Matter, 2011. **7**(9): p. 4122-4138.
58. Stupp, S.I., R.H. Zha, L.C. Palmer, H. Cui, and R. Bitton, *Self-assembly of biomolecular soft matter*. Faraday Discussions, 2013. **166**: p. 9-30.
59. Gao, C., H. Li, Y. Li, S. Kewalramani, L.C. Palmer, V.P. Dravid, S.I. Stupp, M. Olvera de la Cruz, and M.J. Bedzyk, *Electrostatic Control of Polymorphism in Charged Amphiphile Assemblies*. The Journal of Physical Chemistry B, 2017. **121**(7): p. 1623-1628.
60. Tantakitti, F., J. Boekhoven, X. Wang, R.V. Kazantsev, T. Yu, J. Li, E. Zhuang, R. Zandi, J.H. Ortony, C.J. Newcomb, L.C. Palmer, G.S. Shekhawat, M.O. De La Cruz, G.C. Schatz,

- and S.I. Stupp, *Energy landscapes and functions of supramolecular systems*. Nature Materials, 2016. **15**(4): p. 469-476.
61. Yu, Z., A. Erbas, F. Tantakitti, L.C. Palmer, J.A. Jackman, M. Olvera de la Cruz, N.-J. Cho, and S.I. Stupp, *Co-assembly of Peptide Amphiphiles and Lipids into Supramolecular Nanostructures Driven by Anion- π Interactions*. Journal of the American Chemical Society, 2017. **139**(23): p. 7823-7830.
62. Pizzey, C.L., W.C. Pomerantz, B.J. Sung, V.M. Yuwono, S.H. Gellman, J.D. Hartgerink, A. Yethiraj, and N.L. Abbott, Characterization of nanofibers formed by self-assembly of B-peptide oligomers using small angle x-ray scattering. Journal of Chemical Physics, 2008. 129(9).

Chapter Four

pH-Controlled Self-Assembly of β^3 -Peptide Amphiphiles

The role of hydrogen bonding and electrostatic interactions in the axial and lateral self-assembly of β^3 -peptide amphiphiles was investigated by designing modified N-acetylated β^3 -peptide sequences incorporating β^3 -arginine (β^3 R) and a C-terminal amide. The surface charge of the β^3 R residue was altered by incubation of the β^3 -peptide in phosphate buffer pH 4, 7 and aqueous sodium hydroxide pH 13. Both the acidic and basic pH values disrupted head-to-tail and lateral self-assemblies resulting in truncated discrete nanofibres which contrasted with twisted ribbons and nanobelts of β^3 -peptide amphiphiles with C-terminal acids. In addition, at neutral pH, the modified β^3 -peptides formed a nanofibrous mesh which were quite distinct from the structures presented in Chapter 2. The height data values revealed a striking decrease in size at all pHs tested. These results clearly underscore a new perspective towards the rational design of novel materials that can switch morphology in response to changes in pH.



4.1 Introduction

The self-assembly of well-defined supramolecular nanostructures that change morphology and size in response to a specific condition depends on the control over non-covalent interactions [1-8]. This can be achieved by the rational design of sequences and tuning of environmental factors such as pH. The aim of this Chapter is to investigate the role of hydrogen bonding and electrostatic interactions during axial and lateral self-assemblies of β^3 -peptide amphiphiles via changes in pH.

In Chapter 2, the self-assembly of β^3 -peptide amphiphiles designated as R_0/R_1 and R_2/R_3 produced twisted ribbons and nanobelts respectively. The self-assembled morphologies were stabilised by the collective balance of non-covalent forces. In particular, hydrogen bonding and electrostatic interactions were identified as important driving forces for axial and lateral assembly. As a follow-up to that proposed model, this Chapter describes the modification of β^3 -peptide amphiphile sequences by incorporating β^3 -arginine (βR) and a C-terminal amide into an N-acetylated β^3 -tripeptide template. Axial and lateral self-assembly were manipulated at acidic, neutral and basic pH values. The first section of this Chapter describes the design and synthesis of β^3 -peptide amphiphile analogues with modified sequences for the proposed pH study. The second section describes the effect of pH on the self-assembly of β^3 -peptide amphiphiles. The pH-dependent self-assembly demonstrated the significance of pH environment and β^3 -peptide side chain interactions in supramolecular self-assembly, which can be further exploited for future applications in biomedicine.

4.2 Design of β^3 -peptide amphiphiles with a C-terminal amide

The modified β^3 -peptide amphiphiles **P15**, **P16**, **P17** and **P18** were designed based on the C_{16} -templates **P3**, **P6**, **P9** and **P12** (previously synthesised and reported in Chapter 2) which contained a C_{16} alkyl chain at the N-terminus (R_0), or at the side chain of residues 1 (R_1), 2 (R_2) and 3 (R_3) respectively. The C_{16} alkyl chain was chosen in preference to C_{12} and C_{14} because the morphologies produced in Chapter 2 by C_{16} β^3 -peptides are more well-defined and displayed the greatest differentiation between the twisted ribbon and nanobelt structures. In addition, the alkyl chain was positioned at R_0 , R_1 , R_2 and R_3 in order to understand the

influence of pH on the self-assembled morphology for each alkyl chain position. Since one of the goals of this Chapter is to investigate the role of electrostatic interactions in the lateral self-assembly of β^3 -peptide amphiphiles, β R was used in place of β K because it has a higher pKa value which ensures it remains protonated over a wider pH range [9-11].

Figure 4.1 shows the β^3 -peptide amphiphiles modified by incorporating β R (pKa (side chain) = 12.5) in place of β K (pKa (side chain) = 10.5) and β A. To mask the negative charge of the C-terminal carboxylic group at pH values above 2.0, the C-terminus was modified to yield a C-terminal carboxamide (CO-NH₂). The electrostatic properties of the building blocks change upon protonation or deprotonation of side chains, thus triggering or inhibiting specific non-covalent interactions which eventually dictates self-assembly and the structural features of the resulting supramolecular materials [12].

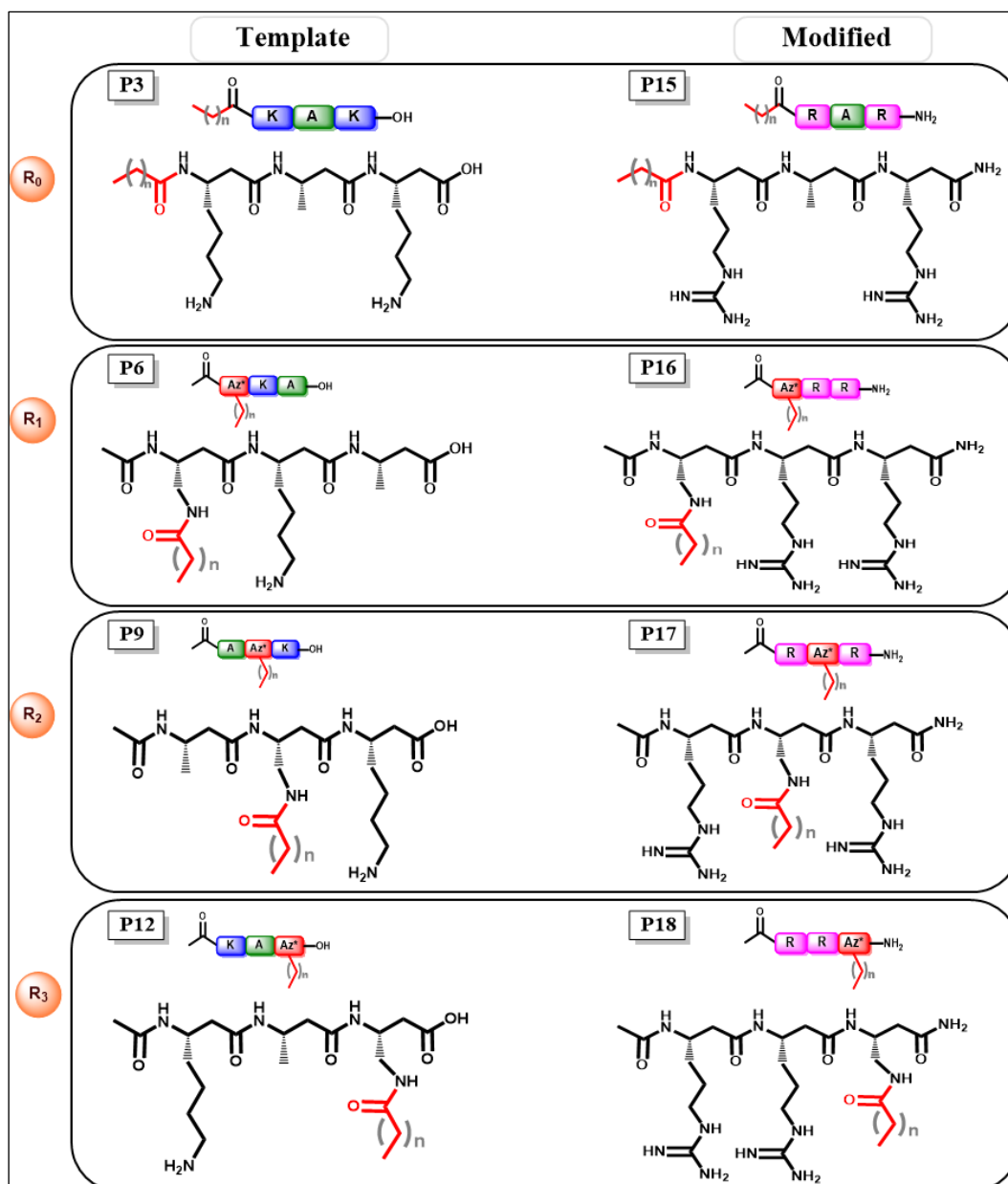


Figure 4.1: Chemical structures of modified β^3 -peptide amphiphiles. The C_{16} -templates (from Chapter 2) are **P3** (R₀), **P6** (R₁), **P9** (R₂) and **P12** (R₃) in which β R and a C-terminal amide were incorporated into the N-acetylated β^3 -tripeptide sequence to obtain the modified β^3 -peptides **P15** (R₀), **P16** (R₁), **P17** (R₂), and **P18** (R₃) with the C_{16} alkyl chain incorporated onto β^3 -azidohomoalanine (Az*). n denotes 13 carbons

Figure 4.2 shows two additional peptides **P19** and **P20** which were designed using **P16** and **P6** as C_{16} -templates respectively. These β^3 -peptides were designed to understand the influence of the C-terminal amide during self-assembly. Thus, **P19** has the same sequence as **P16** but

retains the free C-terminal carboxyl group, while **P20** has the same sequence as **P6** but contains a C-terminal amide.

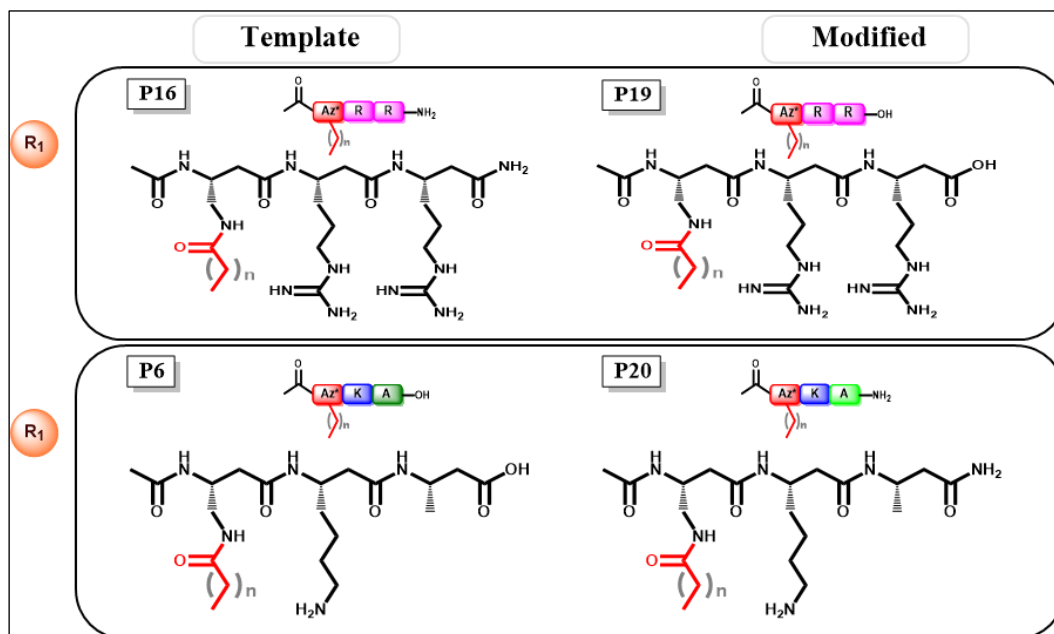


Figure 4.2: Chemical structures of additional β^3 -peptide amphiphiles used to further investigate the effect of the free acid and the amide at the C-terminus. The modified β^3 -peptides **P19** and **P20** are based on the C₁₆-templates **P16** and **P6** respectively. The C₁₆ alkyl chains were located at the R₁ position. Az* = β^3 -azidohomoalanine and n = 13.

4.3 Materials and Methods

4.3.1 Materials, Chemicals and Reagents

- Monosodium dihydrogen orthophosphate, disodium hydrogen phosphate and sodium hydroxide (NaOH) pellets were purchased from Sigma-Aldrich Ltd (St. Louis, Missouri USA)
- β^3 -Homo-arginine (Pbf)-OH and Rink amide AM resin were purchased from GL Biochem Ltd (Shanghai, China).
- ScanAsyst-fluid-Plus probes with silicon tip, a nitride lever bearing spring constant of 0.7 N/m and resonance frequency of 150 kHz were purchased from Bruker Corporation (Billerica, Massachusetts, United States).
- All other materials, chemicals and reagents used are as previously described in Chapters 2 and 3.

4.3.2 Synthesis of β^3 -peptide amphiphiles with C-terminal amides

The synthesis of modified β^3 -peptide amphiphiles commenced by attaching the first β^3 -amino acid to the Rink amide AM resin. This was performed immediately after deprotection of the resin with 20% piperidine in DMF (2×20 min) to remove the Fmoc protecting group. The coupling reaction was allowed to stand for 1 hour before the resin was washed 5 times with DMF to remove by-products and excess reagents. To attach the second β^3 -amino acid, the Fmoc protecting group of the first β^3 -amino acid was removed by deprotection (as described above). The synthesis cycle was repeated until the β^3 -peptide sequence was complete. The only exception was the double coupling of 3.1 molar excess Fmoc- β^3 -homo-arginine (pbf)-OH in the presence of HBTU (3 eq.) and DIPEA (4.5 eq.). The purification was carried out as previously described in Section 2.3.3. All peptides were purified using the same protocols as previously described (Section 2.3.3).

4.3.3 Atomic Force Microscopy in Fluid

All peptides were dissolved in phosphate buffer pH 4, 7 and aqueous NaOH pH 13 to a final concentration of 0.25 mg/mL and incubated for 24 hrs. Thereafter, 2 μ L of incubated samples were placed on a freshly cleaved 15 mm mica surface. Structural analysis was carried out using AFM in fluid whereby the topographic, phase and amplitude images were captured as previously described in Chapters 2 and 3. In addition, the height values of the nanofibres were determined for each β^3 -peptide amphiphile as previously described in Chapter 2.

4.4 Results and Discussion

To explore the effect of pH on axial and lateral self-assembly of β^3 -peptide amphiphiles, six *N*-acetylated β^3 -peptides were synthesised as shown in Table 4.1. Analysis of the synthesised β^3 -peptide amphiphiles by HPLC and mass spectrometry indicated that the correct β^3 -peptides were obtained and purity was confirmed by the presence of a single peak in analytical RP-HPLC chromatograms (Figure 4.3).

Table 4.1: Modified β^3 -peptide amphiphiles

Alkyl chain Position	Code	Modified Peptide Sequence	Calculated MW	Obtained MW
R_0	P15	C_{16} -RAR-NH ₂	681	681
R_1	P16	Ac- Az*(C ₁₆)RR-NH ₂	738	738
R_2	P17	Ac-R Az*(C ₁₆)R-NH ₂	738	738
R_3	P18	Ac-RR Az*(C ₁₆)-NH ₂	738	738
R_1	P19	Ac- Az*(C ₁₆)RR-OH	739	740
R_1	P20	Ac- Az*(C ₁₆)KA-NH ₂	625	625

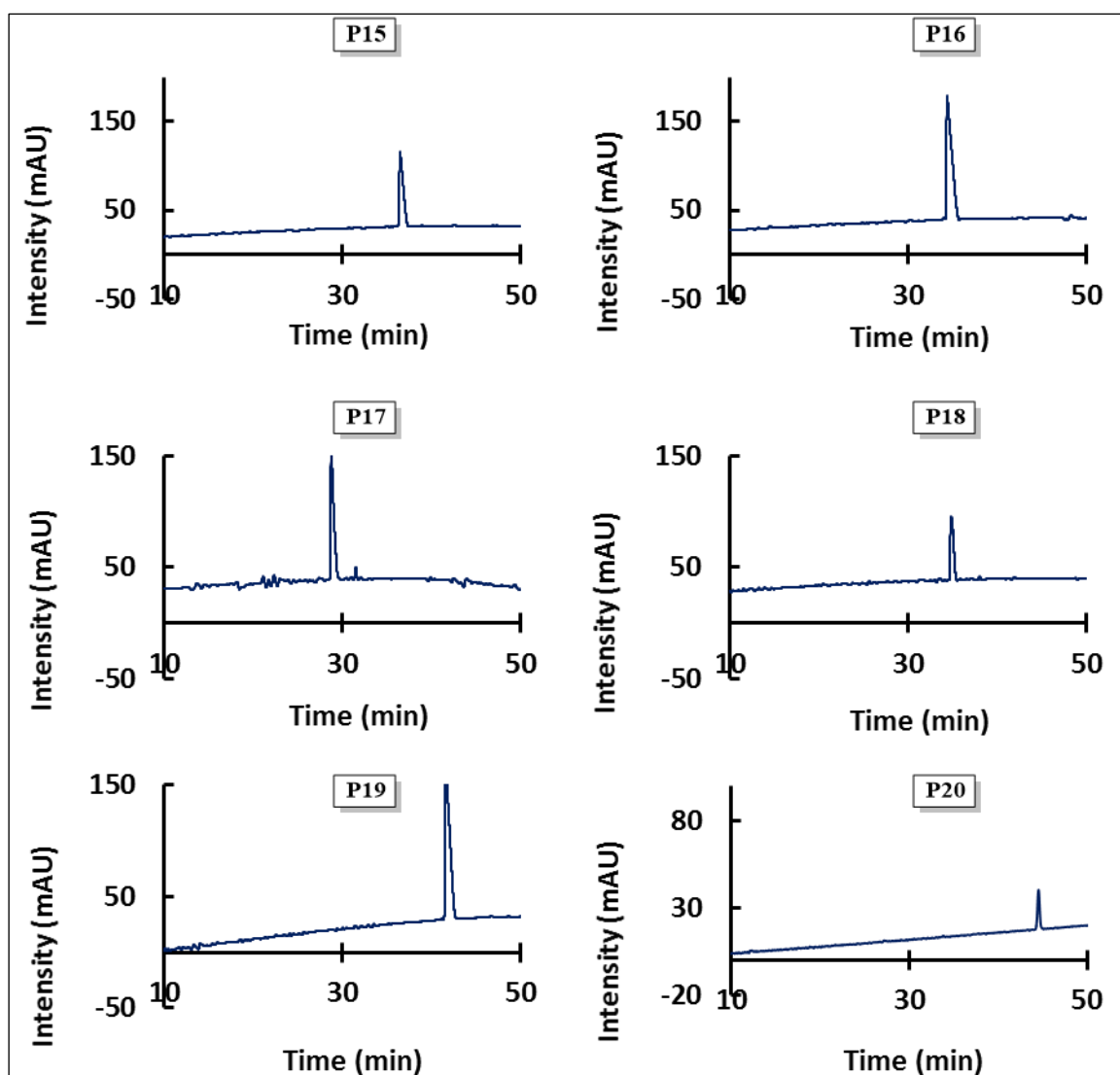


Figure 4.3: Analytical RP-HPLC chromatograms of purified β^3 -peptides amphiphiles namely; R_0 (**P15** = C_{16} -RAR-NH₂), R_1 (**P16** = Ac-Az*(C₁₆)RR-NH₂), R_2 (**P17** = Ac-RAz*(C₁₆)R-NH₂), R_3 (**P18** = Ac-RRAz*(C₁₆)-NH₂), R_1 (**P19** = Ac-Az*(C₁₆)RR-OH) and R_1 (**P20** = Ac-Az*(C₁₆)KA-NH₂).

4.4.1 Self-assembly of β^3 -peptide amphiphiles with a C-terminal amide

The supramolecular self-assembly of β^3 -peptide amphiphiles was reported in Chapters 2 and 3 to be driven by the overall balance of non-covalent forces for axial and lateral self-assemblies. These non-covalent interactions resulted in the formation of twisted ribbons and nanobelts from R_0/R_1 and R_2/R_3 β^3 -peptide amphiphiles respectively. Figure 4.4 shows the schematic illustration of the 3 non-covalent interactions that govern supramolecular self-assembly of β^3 -peptide amphiphiles. Axial head-to-tail self-assembly of *N*-acetyl β^3 -tripeptides is known to be responsible for fibre lengthening and facilitated by intermolecular hydrogen bonding (HB) of β^3 -peptide monomers [13-18]. Lateral self-assembly of β^3 -peptides is mediated largely by the β^3 -peptide side chains which result in fibre bundling and can be facilitated by both electrostatic attraction (EI) and hydrophobic interaction (HI) [17, 19].

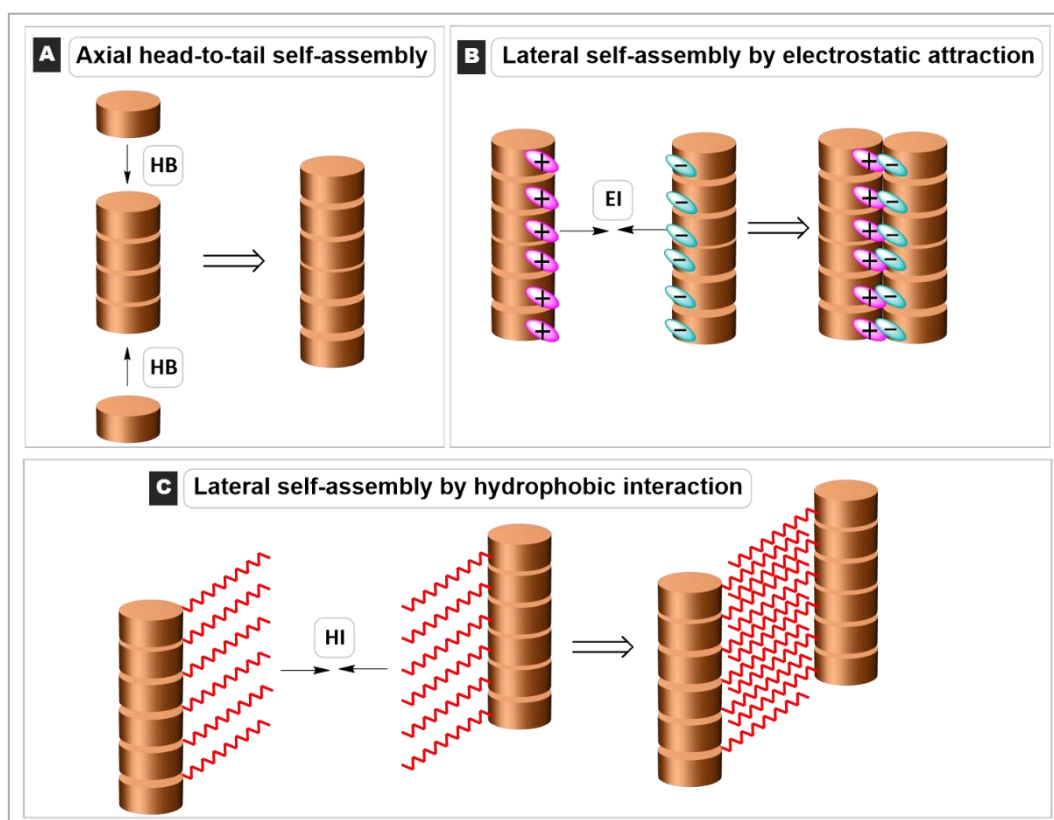


Figure 4.4: Schematic representation of the supramolecular self-assembly of β^3 -peptide amphiphiles. (A) Axial head-to-tail self-assembly via hydrogen bonding (HB), (B) lateral self-assembly by electrostatic attraction (EI) and (C) lateral self-assembly by hydrophobic interaction (HI) of alkyl chains.

In order to design specific nanostructures, rational control of non-covalent interactions is crucial [20]. An important parameter in directing supramolecular self-assembly is the overall charge of the peptide building block, which is also dependent on the pH of the environment [5, 21-23]. We hypothesised that incubating the modified β^3 -peptide amphiphiles in solutions of different pH values will disrupt the non-covalent interactions. The focus of this study therefore is to understand the control of self-assembled structures and properties of β^3 -peptide amphiphiles simply by switching the pH of the solution. The control of supramolecular self-assembly using pH to alter the surface charges of individual α -amino acid residues according to the α -amino acid pKa values has been demonstrated in several studies [12, 20, 21, 24-28]. The β R side chain of the modified β^3 -peptide amphiphiles was thus exploited to generate different protonation states when dissolved in phosphate buffer pH 4, 7 and aqueous NaOH pH 13 (Figure 4.5). At pH 4 and 7 the two β R residues are protonated while at pH 13 the β R side chains are deprotonated on the surface of the nanofibril. However, since the pKa value for β R is 12.5, the proportion of protonated β R at pH 7 is less than that at pH 4. The corresponding charged states of the template β^3 -peptides **P3**, **P6**, **P9** and **P12** that retain the C-terminal carboxyl group are shown schematically in Figure 4.6.

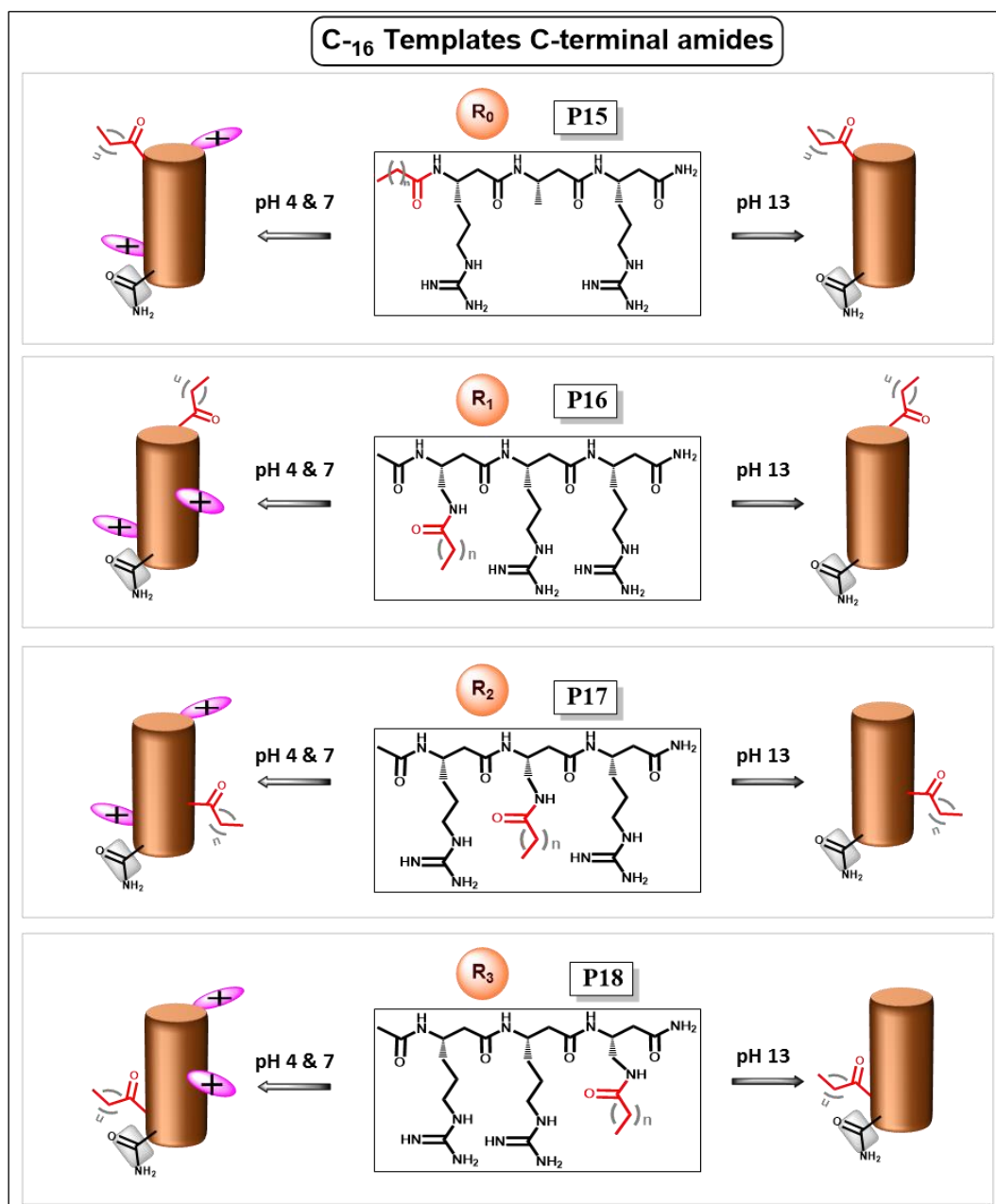


Figure 4.5: Schematic representation of protonated and deprotonated states of the βR residue in **P15**, **P16**, **P17** and **P18** at pH 4, 7 and 13, where $n = 13$.

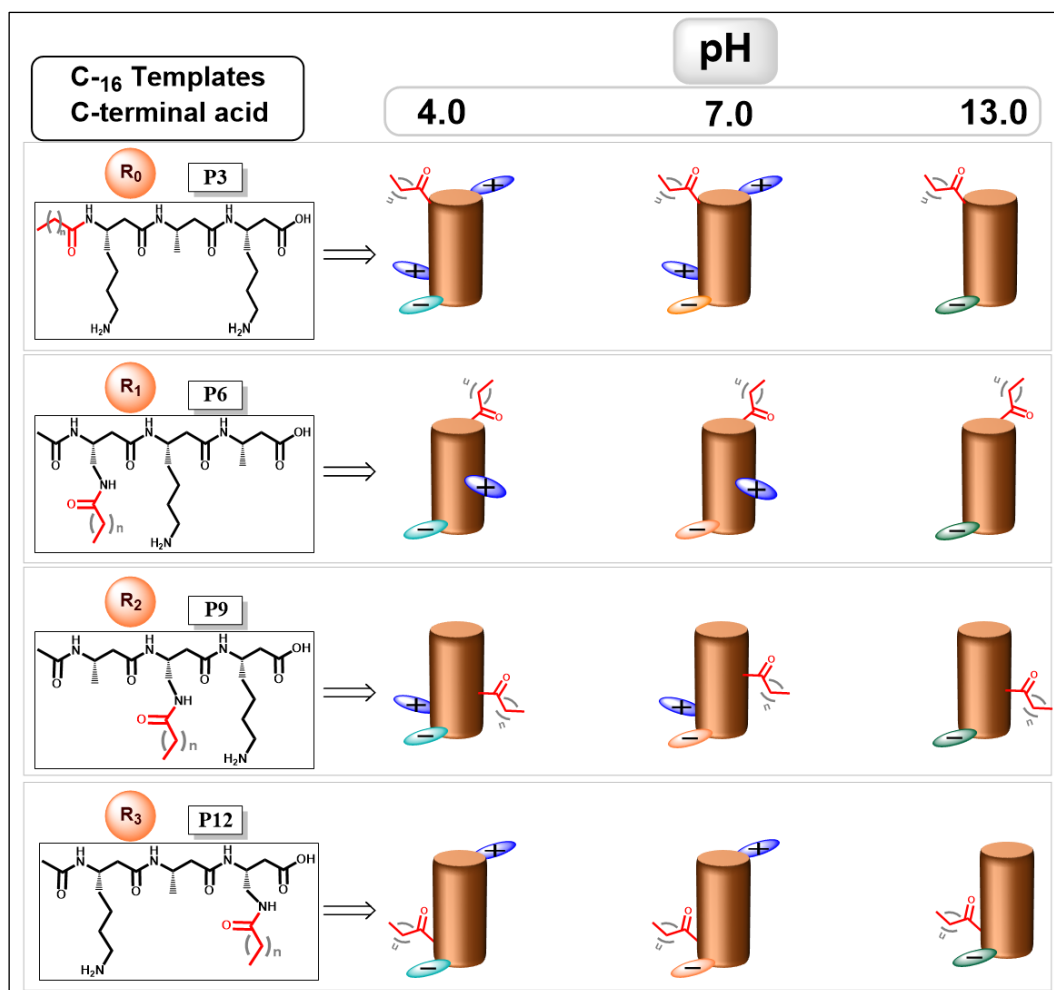


Figure 4.6: Schematic representation of protonated and deprotonated properties of template β^3 -peptides **P3**, **P6**, **P9** and **P12** with C-terminal carboxylic acids at pH 4, 7 and 13 ($n = 13$). The C-terminal COO^- is coloured differently at each pH to denote the different degree of protonation which impacts on the overall charge.

4.4.2 Self-assembly of R_0 β^3 -peptides (**P15** and **P3**)

The results obtained for **P15** (R_0 with C-terminal amide) revealed straight discrete nanofibres at pH 4 and 13 (Figure 4.7(A) and (E)), while at pH 7 a mesh-like network of long nanofibres was observed (Figure 4.7 (C)).

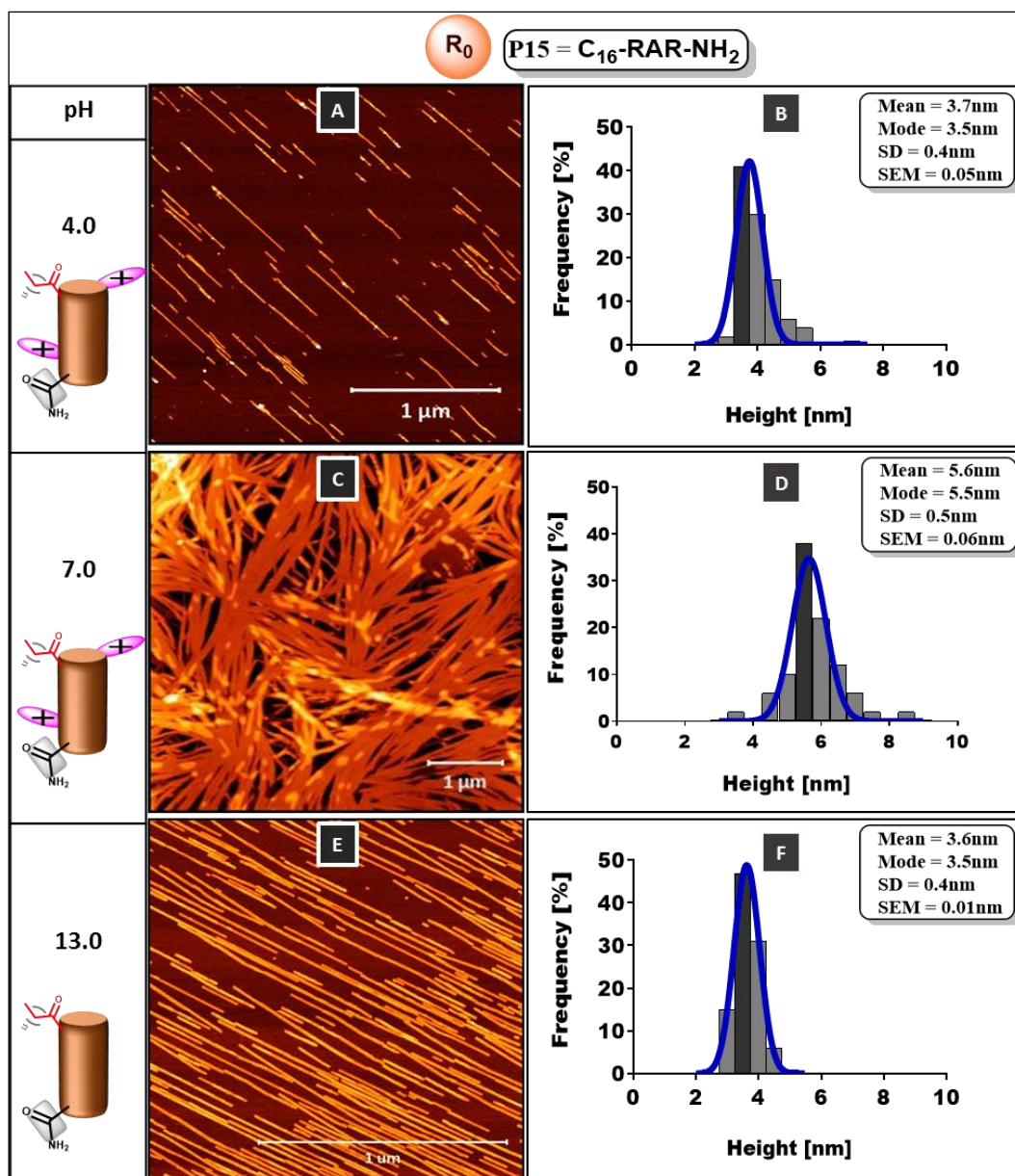


Figure 4.7: Self-assembly of **P15**. (A) nanofibres at pH 4, (B) height distribution for (A), (C) nanofibres at pH 7 (D) height distribution for (C), (E) nanofibres at pH 13 and (F) height distribution for (E).

In comparison with the elongated nanofibres at pH 7, the nanofibres at pH 4 and 13 were predominantly shorter in length and aligned in one direction. The height values for **P15** at pH 4, 7 and 13 were 3.7 ± 0.4 nm, 5.6 ± 0.5 nm and 3.6 ± 0.4 nm respectively (Figure 4.7(B), (D) and (F)) and were significantly lower at pH 4 ($p < 0.05$) than at pH 7. The short and discrete nanofibres at pH 4 and 13 for **P15** suggest that the acidic and basic pH influenced the axial

and lateral self-assembly. Significantly, the morphology of **P15** at pH 7 was considerably different to those of the R_0 β^3 -peptides presented in Chapter 2.

The effect of acidic and basic pH on the self-assembly of **P3** (the corresponding C_{16} -template with C_{16} alkyl chain at R_0 position) was also investigated as shown in Figure 4.8.

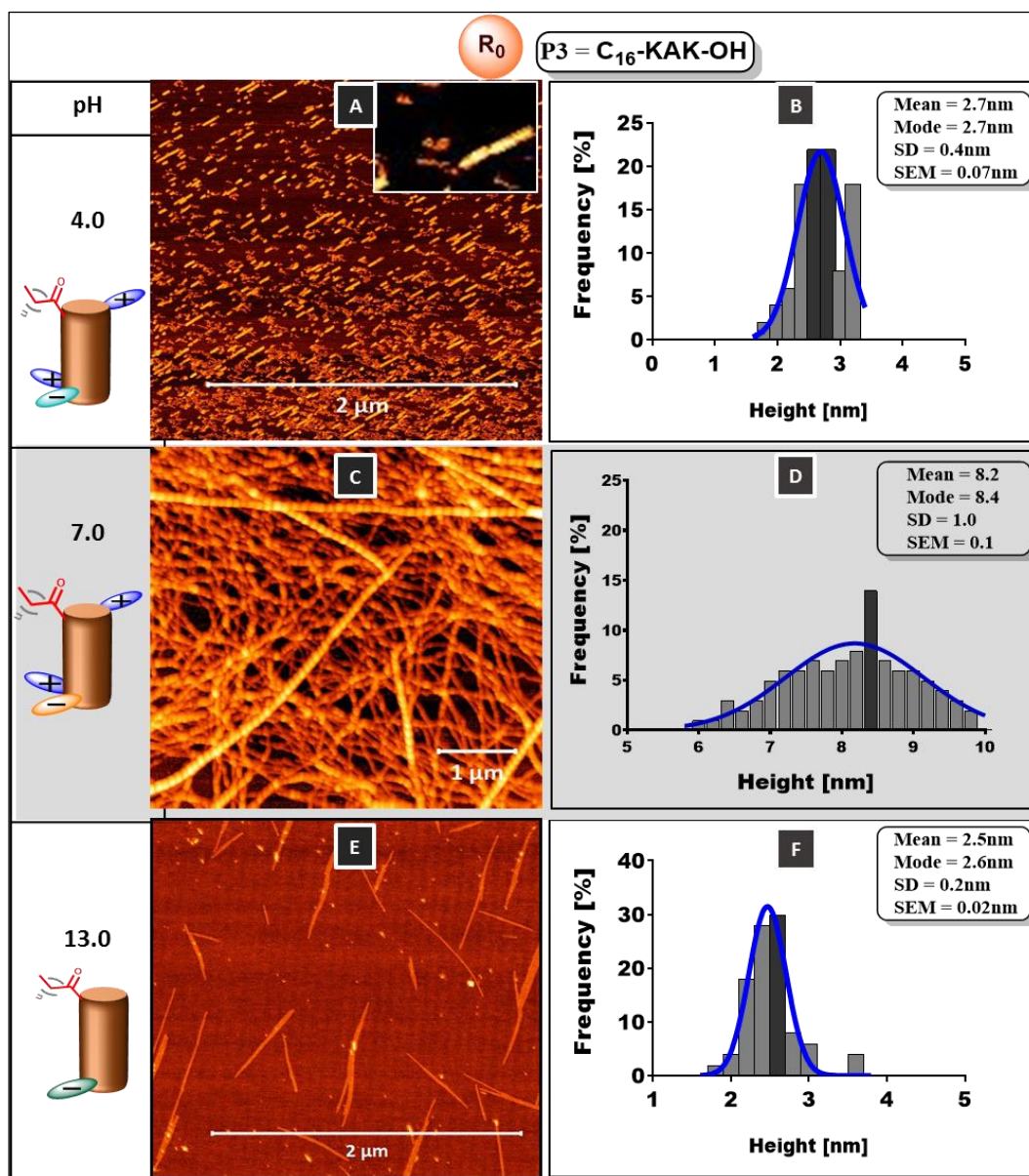


Figure 4.8: Self-assembly of **P3** at different pH environments. (A) Very short twisted ribbons at pH 4 (insert is high magnification of a twisted ribbon), (B) height distribution for (A), (C) nanofibre mesh in milliQ water, (D) height distribution for (C), (E) short nanofibres at pH 13, and (F) height distribution for (E). Note that the shaded data for pH 7 was obtained in Chapter 2.

As demonstrated in Chapter 2, **P3** formed a mesh of twisted ribbons in water as shown in Figure 4.8 (from Fig 2.7 (D) in Chapter 2). However, at pH 4 truncated rod-like twisted ribbons were observed (inset image in Figure 4.8 (A) shows a twist at high magnification) which also aligned in one direction and is very similar to the nanofibres observed above for the corresponding amidated analogue **P15**. The nanofibres formed by **P3** at pH 13 were also short in length but longer than the nanofibres at pH 4. The height values for **P3** at pH 4 and 13 were 2.7 ± 0.4 nm and 2.5 ± 0.2 nm respectively and were not significantly different ($p > 0.05$). However, the height values of **P3** were approximately 1 nm less than the values obtained for **P15** at pH 4 and 13. The stunted and discrete nanofibres observed for **P3** demonstrates that regardless of sequence or charge, β^3 -tripeptides that are acylated at the *N*-terminus are likely to show a switch in morphology at acidic and basic conditions.

Given that head-to-tail self-assembly of *N*-acetyl β^3 -tripeptides is facilitated by intermolecular hydrogen bonding which promotes fibre elongation, [13, 15, 29], the short nanofibres observed at pH 4 and 13 indicated that the hydrogen bond formation of the amidated **P15** monomer was suppressed, thus affecting the head-to-tail self-assembly and fibre elongation. This observation was also supported by the truncated rod-like fibrils that were formed by the corresponding template peptide **P3** with the free acid at pH 4 and 13.

In terms of the lateral self-assembly, given that there are two positively charged β R residues on the surface of the nanofibrils at pH 4, the discrete nanofibres may be due to electrostatic repulsion of the nanofibrils. Several reports using α -peptide amphiphiles with charged residues have demonstrated the control of lateral assembly by the inclusion of charged residues on the outer faces of fibres to reduce fibre bundling [24, 30-32]. Similarly, α -peptide amphiphiles have also been shown to change morphology when the pH is varied by deprotonation of the carboxylic acid moieties resulting in inter-strand repulsion between the interwoven fibres [33]. Stupp and colleagues have also shown that by increasing the electrostatic repulsion, the self-assembled fibre becomes a high energy structure that results in the formation of truncated small fibres of similar size [34], which is also seen in Fig 4.8A. In addition, Chen et al. also demonstrated a different model using complementary sequences made up of alternating charged α -amino acids which identified electrostatic repulsion as the major constraint for lateral assembly of nanofibres [20]. Therefore, the discrete nanofibres

observed at acidic pH for **P15** and **P3** could be due to electrostatic repulsion between the positively charged β R and β K residues respectively of individual nanofibrils.

In contrast to the observations at acidic and basic pH values, the long nanofibrous mesh at pH 7 for **P15** (with C-terminal amide) suggests that axial and lateral self-assemblies were not disrupted at neutral pH (compared to pH 4). The nanofibrous mesh of **P15** (Figure 4.7(C)) contains long and interwoven fibres with a few differences to that of **P3** (free acid) structure in milliQ water (Figure 4.8(C)). However, the fibres formed by **P15** showed no clear periodicity, were able to cluster into large bundles of ≈ 10.4 nm and exhibited a flat ribbon morphology. In comparison, **P3** fibres formed cylindrical fibres with a well-defined periodicity. The long nanofibrous mesh obtained for **P15** suggests that hydrogen bonding and electrostatic interactions associated with axial and lateral self-assembly respectively were enhanced at pH 7 for **P15** compared to **P3**.

The discrete nanofibres observed at pH 13 for **P15** (Figure 4.7(E)) suggest that lateral self-assembly was also restricted at this pH. Thus, the absence of charged groups on the surface of **P15** nanofibrils eliminated electrostatic forces and lateral self-assembly. In the case of **P3**, disruption of lateral self-assembly at pH 13 (Figure 4.8 (E)) may be due to electrostatic repulsion of negatively charged C-terminal carboxylate on the surface of the nanofibrils.

4.4.3 Self-assembly of R₁ peptides (**P16** and **P6**)

The self-assembly of **P16** (R₁ with C-terminal amide) also revealed short discrete nanofibres at pH 4 and 13 while a nanofibrous mesh formed at pH 7 (Figure 4.9). The heights for **P16** at pH 4, 7, and 13 were 3.2 ± 0.1 nm, 2.1 ± 0.6 nm and 4.5 ± 0.2 nm respectively (Figure 4.9 (B), (D) and (F)). The height values for **P16** at pH 4 were significantly lower than at pH 13, while at pH 7 the height value was significantly lower than heights at pH 4 and 13 ($p < 0.05$). These results for **P16** again suggest that head-to-tail and lateral self-assembly were suppressed at acidic and basic pH in a similar fashion to **P15**. Interestingly, these observations can also be correlated with the suppressed self-assembly of **P6** (free acid with alkyl chain at the R₁ position) at acidic and basic pH (Figure 4.10). While **P6** consistently formed a long fibrous mesh of twisted ribbons in aqueous solution (as shown in Chapter 2), the morphology of **P6** changed dramatically to truncated rod-like nanofibres at pH 4 and 13 (Figure 4.10 (A) and (E)).

The high magnification image at pH 4 (inset in Figure 4.10(A)) revealed short twisted ribbons (similar to **P3** at the same pH), while at pH 13, **P6** formed discrete straight nanofibres similar to **P16** at the same pH (Figure 4.9 (E)). The height values increased significantly ($p < 0.05$) from 4.5 ± 0.4 nm to 5.6 ± 0.4 nm for pH 4 and 13 respectively (Figures 4.10 (B) and (F)).

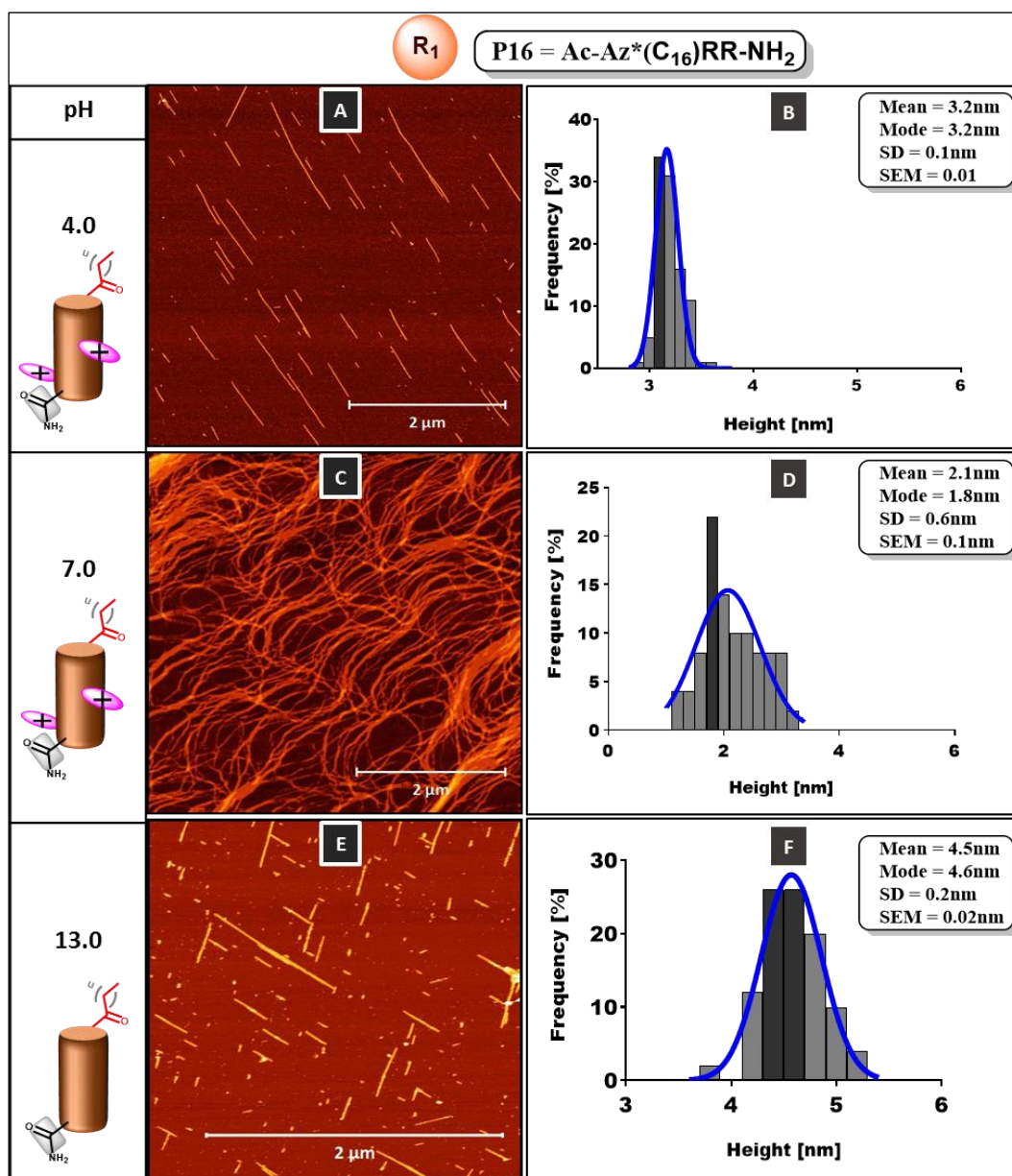


Figure 4.9: Self-assembly of **P16**. (A) Short nanofibres at pH 4, (B) height distribution for (A), (C) nanofibre mesh at pH 7 (D) height distribution for (C), (E) short nanofibres at pH 13 and (F) height distribution for (E).

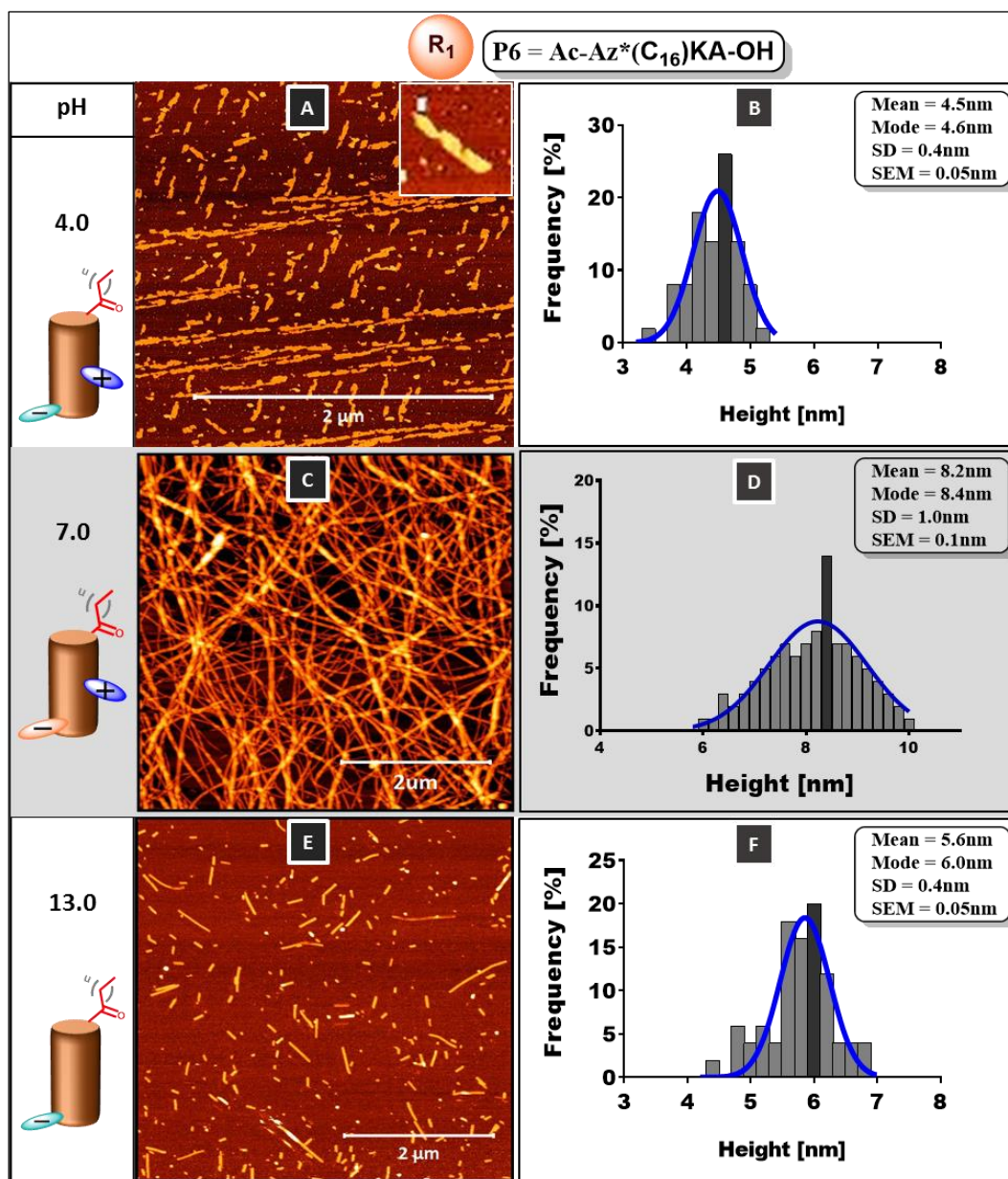


Figure 4.10: Self-assembly of **P6** at different pH environments. (A) Short twisted ribbons at pH 4 (insert is high magnification of a twisted ribbon), (B) height distribution for (A), (C) nanofibre mesh in milliQ water, (D) height distribution for (C), (E) short nanofibres at pH 13, and (F) height distribution for (E). Note that the shaded data for pH 7 was obtained in Chapter 2.

The long interwoven nanofibrous mesh of **P16** (R₁ with C-terminal amide) at pH 7 (Figure 4.9(C)) was also similar to that of **P6** (R₁ with C-terminal free acid) as shown in Figure 4.10(C)), again suggesting that head-to-tail self-assembly was not suppressed. However, the decreased size of the fibres formed by **P16** indicate a possible inhibition of lateral assembly.

4.4.4 Self-assembly of R₂ peptides (P17 and P9)

The self-assembly of **P17** (R₂ with C-terminal amide) at pH 4 and 13 resulted in short flexible nanofibres (Figure 4.11 (A) and (E)), while at pH 7, an intertwined nanofibre mesh was observed (Figure 4.11 (C)). The heights for **P17** at pH 4, 7, and 13 were 4.0 ± 0.6 nm, 7.0 ± 0.3 nm and 8.0 ± 0.7 nm respectively (Figure 4.11 (B), (D) and (F)). The height values at pH 4 were significantly lower ($p < 0.05$) than the values at pH 7 and 13, while there was no significant difference between the height values at pH 7 and 13 ($p > 0.05$). In addition, the height distribution at pH 7 was bimodal at ≈ 7.0 nm and ≈ 13.0 nm (Figure 4.11 (D)).

The self-assembled structures of **P17** contrast significantly with the rigid nanobelts that were previously observed for R₂ β^3 -peptides (**P9**) in Chapter 2. The short flexible nanofibres observed at acidic pH in this Chapter suggest that head-to-tail self-assembly was suppressed by the disruption of hydrogen bonding between the monomers. The **P17** nanofibres appeared thin and sparsely distributed and is most likely due to electrostatic repulsion between the two positively charged β R side chains on the surface of the nanofibrils which prevented lateral self-assembly. Slightly longer but relatively thin nanofibrils were observed at pH 13 (relative to pH 4), again suggesting suppression of lateral self-assembly at pH 13. However, it should be noted that the fibres produced by **P17** are larger than other peptide amides indicating that the ability of the C-terminal amide to H-bond may also contribute to lateral assembly.

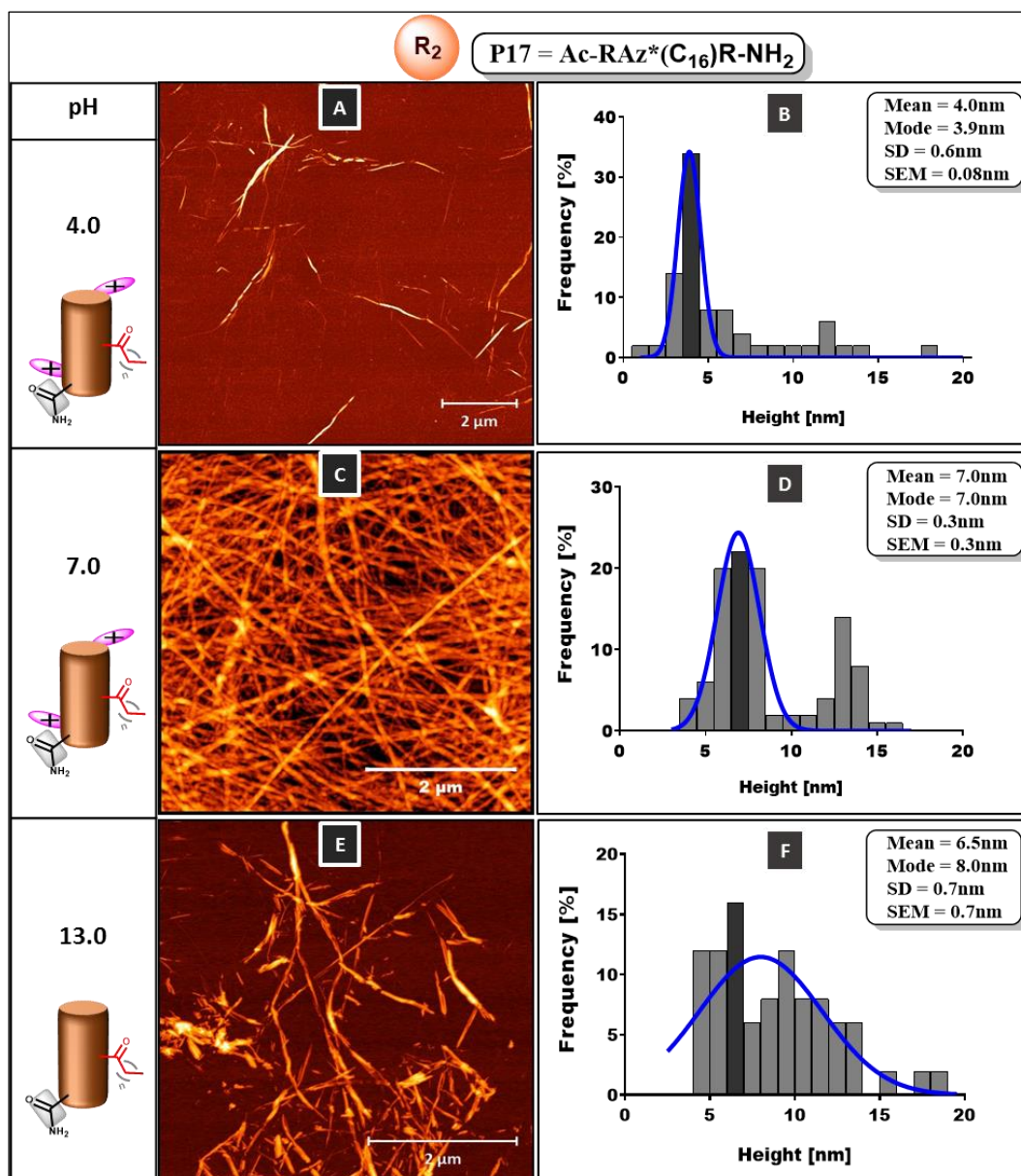


Figure 4.11: Self-assembly of **P17**. (A) Short nanofibres at pH 4, (B) height distribution for (A), (C) nanofibre mesh at pH 7 (D) height distribution for (C), (E) mixture of short and long nanofibres at pH 13 and (F) height distribution for (E).

The self-assembly of the corresponding free acid template β^3 -peptide **P9** (the C₁₆-template β^3 -peptide with the alkyl chain at the R₂ position) at pH 4 and 13 yielded long nanofibre bundles (Figure 4.12). The nanofibres appeared to be in the process of nanobelt formation with partial lateral self-assembly. The height values for **P9** at pH 4 and 13 were 3.2 ± 0.2 nm (Figure 4.12 (B)) and 6.1 ± 1.6 nm (Figure 4.12 (F)) respectively. This observation contrasts

significantly with the well-defined nanobelts that were previously observed in Chapter 2 for **P9** in water with a height of ≈ 32 nm.

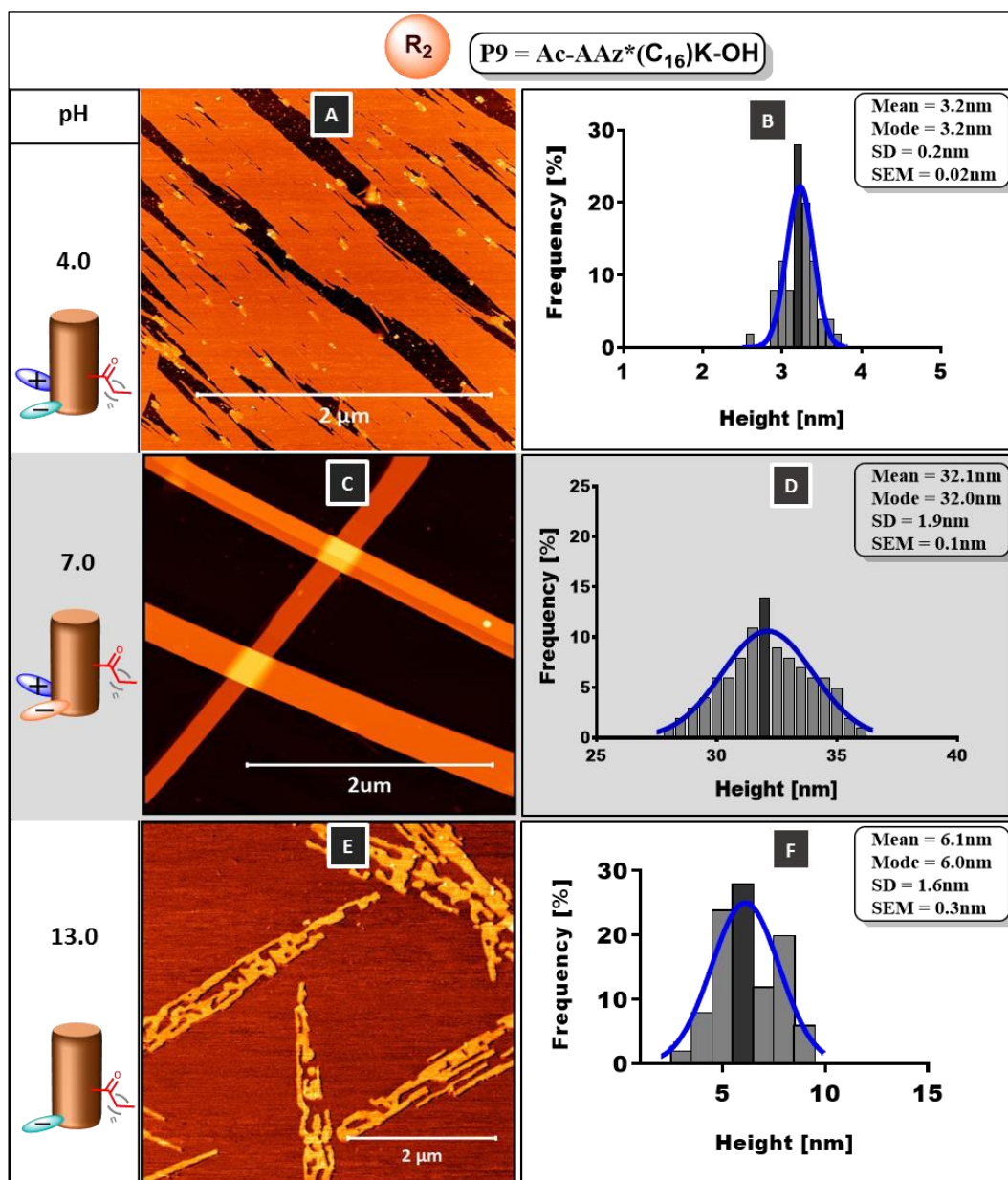


Figure 4.12: Self-assembly of **P9** at different pH environments. (A) Long nanofibrils bundling at pH 4, (B) height distribution for (A), (C) nanobelts in milliQ water, (D) height distribution for (C), (E) nanofibre bundles at pH 13, and (F) height distribution for (E). Note that the shaded data for pH 7 was obtained in Chapter 2.

Figure 4.12 shows the most striking outcome for pH-mediated self-assembly of R_2 β^3 -peptides in which a nanofibrous mesh was formed by **P17** (Figure 4.11(C) in place of nanobelts of **P9**

(Figure 4.12(C)) at neutral pH. Since the extent of protonation of β R is less at pH 7 than pH 4 for **P17**, electrostatic repulsion of nanofibrils at pH 7 was lower thus resulting in a nanofibre mesh. The β R residues inhibited the bilayer formation shown in Chapter 3 by electrostatic repulsion, which would indicate that the lower energy form for this self-assembled structure to be twisted ribbons similar to those of R_0/R_1 peptides (Chapter 2). This is the first example of switching the morphology of β^3 -peptide nanobelts to nanoribbons. A similar type of pH-controlled assembly was reported for the α -peptide amphiphile C_{16} -VEVE in which the nanobelts formed by this peptide was disrupted by deprotonation of glutamic acid residues, which led to the separation of multilayered nanobelt structures by inter-strand electrostatic repulsion [35].

4.4.5 Self-assembly of R_3 peptides (**P18** and **P12**)

The self-assembled morphologies of **P18** (R_3 with C-terminal amide) revealed predominantly short discrete nanofibres at pH 4 and 13, while a nanofibre mesh was observed at pH 7.0 (Figure 4.13). These self-assembled morphologies are similar to that observed for **P15** (R_0) and **P16** (R_1). The height values for **P18** were 3.5 ± 0.3 nm, 3.7 ± 0.7 nm and 2.9 ± 0.2 nm at pH 4, 7 and 13 respectively (Figure 4.13 (B), (D) and (F)) and were not significantly different ($p > 0.05$) at each pH value. A bimodal height distribution was also obtained at pH 13, with heights of 2.8 nm and 4.8 nm respectively.

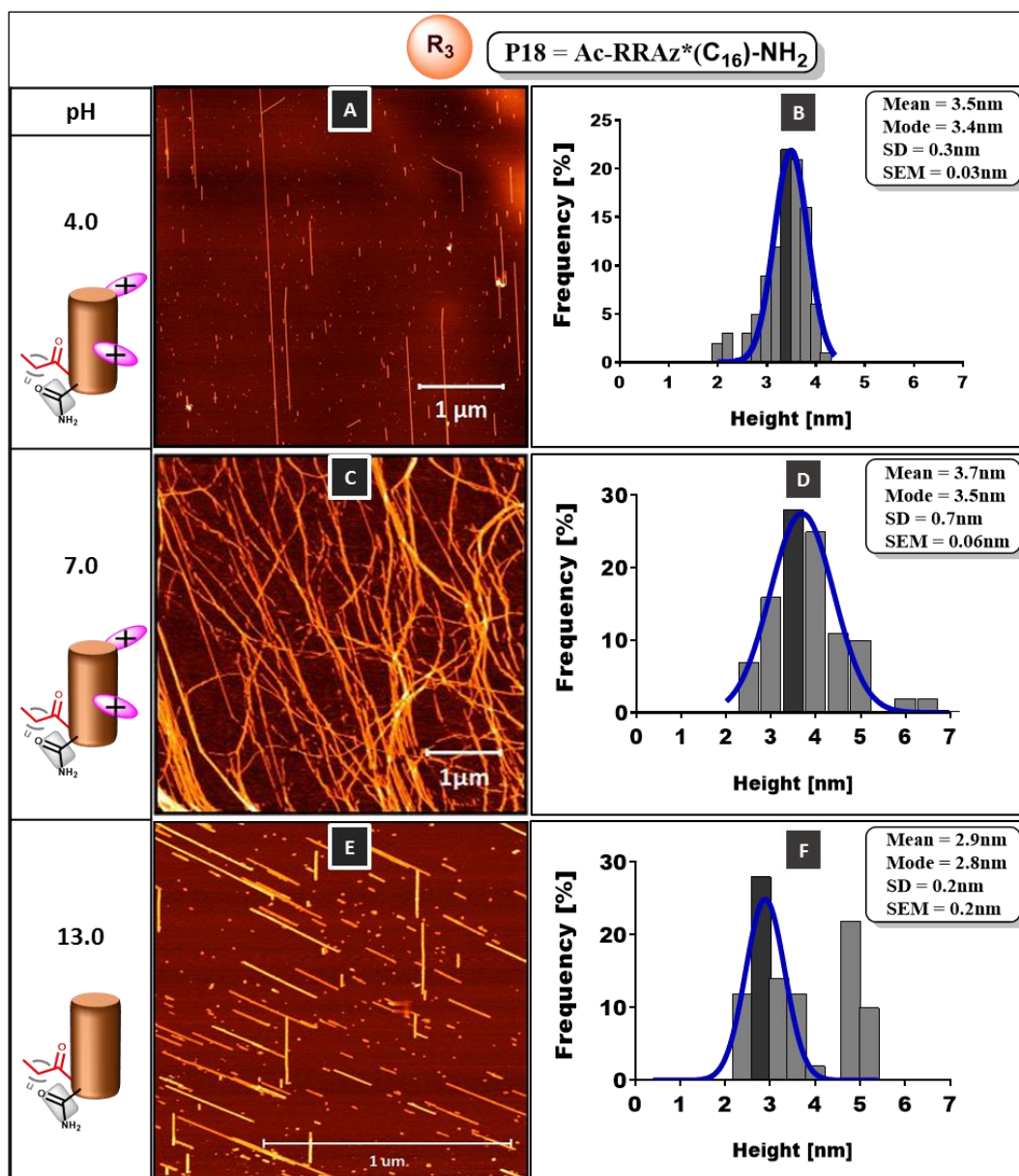


Figure 4.13: Self-assembly of **P18**. (A) Short nanofibres at pH 4, (B) height distribution for A (C) nanofibre mesh at pH 7 (D) height distribution for (C), (E) short nanofibres at pH 13 and (F) height distribution for (E).

The formation of truncated discrete nanofibres at pH 4 and 13 also suggest that axial head-to-tail and lateral self-assemblies were suppressed as previously described for **P15**, **P16** and **P17**. In comparison, the switch in morphologies of R₃ β³-peptides at neutral pH is shown in Figures 4.13(C) and 4.14(C) in which **P18** formed a nanofibre mesh in contrast to the template β³-peptide (**P12**, R₃ with free C-terminal acid) which formed nanobelts. The switch in morphology seen in these R₃ β³-peptides is reminiscent of those observed in the

corresponding R₂ β³-peptide amide (**P17**) suggesting a similar mechanism behind the morphology switch.

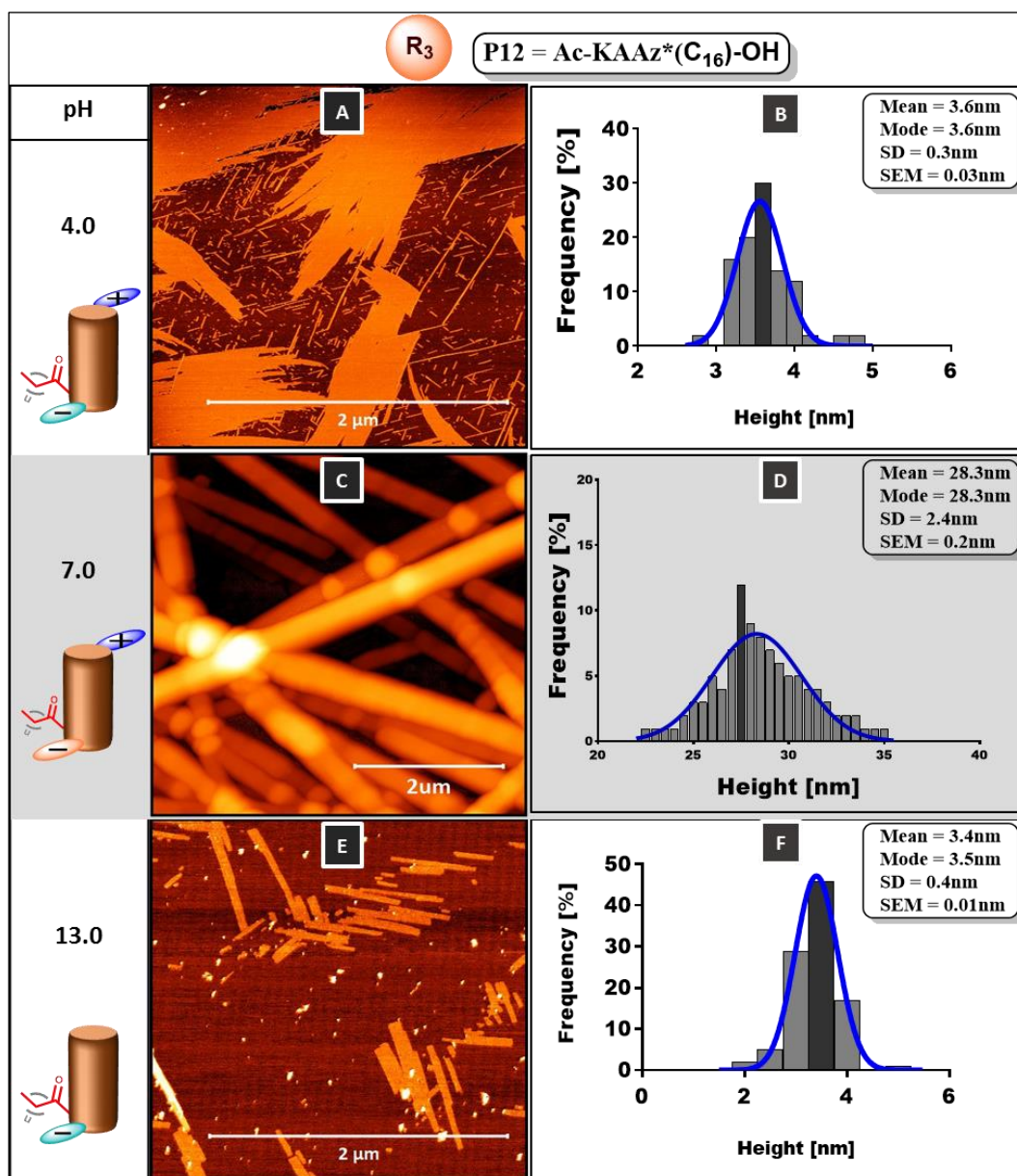


Figure 4.14: Self-assembly of **P12** at different pH environments. (A) Nanofibrils bundling at pH 4, (B) height distribution for (A), (C) nanobelts in milliQ water, (D) height distribution for (C), (E) short nanofibre bundles at pH 13, and (F) height distribution for (E). Note that the shaded data for pH 7 was obtained in Chapter 2.

The self-assembled structures obtained for the R₃ β³-peptide with free acid template **P12** at pH 4 and 13 revealed gradual formation of nanobelts that bundled laterally into flat structures

(Figure 4.14 (A)). The height of the nanobelts at neutral pH (≈ 28 nm) indicate a stacked bilayer structure similar to that seen in **P9** (data was obtained from Chapters 2 and 3). Conversely, the flat nanobelts observed at pH 4 and 13 are approximately 3.5nm, which would correspond to a single bilayer, suggesting that electrostatic repulsion is inhibiting growth of the fibre in the z-axis. However, H-bonding may be responsible for lateral interactions creating the flat nanobelts.

4.4.6 Self-assembly of β K-amide peptide and β R peptide with a free acid (**P19** and **P20**)

The self-assembly of **P15** (R_0), **P16** (R_1), **P17** (R_2) and **P18** (R_3) revealed remarkable morphological changes through the variation of pH. To further assess the role of electrostatic repulsion, a β^3 -peptide which contained two β R residues but also a C-terminal acid was we designed. We envisaged that this β^3 -peptide (**P19**), which was an acid analogue of **P16**, would display similar structures to those observed by the R_1 β^3 -peptides presented in Chapter 2. A β^3 -peptide analogue of **P6** that contained β K with a C-terminal amide was also designed and synthesised. These two additional β^3 -peptides are designated **P19** (R_1) and **P20** (R_1) with the sequences Ac-Az(C_{16})RR-OH and Ac-Az(C_{16})KA-NH₂ respectively.

Figure 4.15 shows the self-assembled morphology of **P19** in which truncated rod-like nanofibres were formed at pH 4 and 13 (Figure 4.15 (A)) which are similar to those observed for **P16** (R_1). Interestingly, the heights of the fibres formed at pH 4 (4.5 ± 0.4 nm) were higher than those observed for **P16** indicating some lateral assembly likely due to the partial deprotonation of the C-terminus and corresponding electrostatic attraction. In contrast, the heights of the fibres of **P19** at pH 13 (3.8 ± 0.3 nm) were significantly smaller than the fibres of **P16**, likely due to the electrostatic repulsion of the sole negative charge of the C-terminus. **P19** also self-assembled into a nanofibrous mesh at pH 7 in a similar fashion to **P6** (R_1). The formation of a nanofibre mesh with a fibre height of 5.5 ± 0.8 nm is evidence of lateral assembly (compared to 2.1 ± 0.6 nm for **P16**).

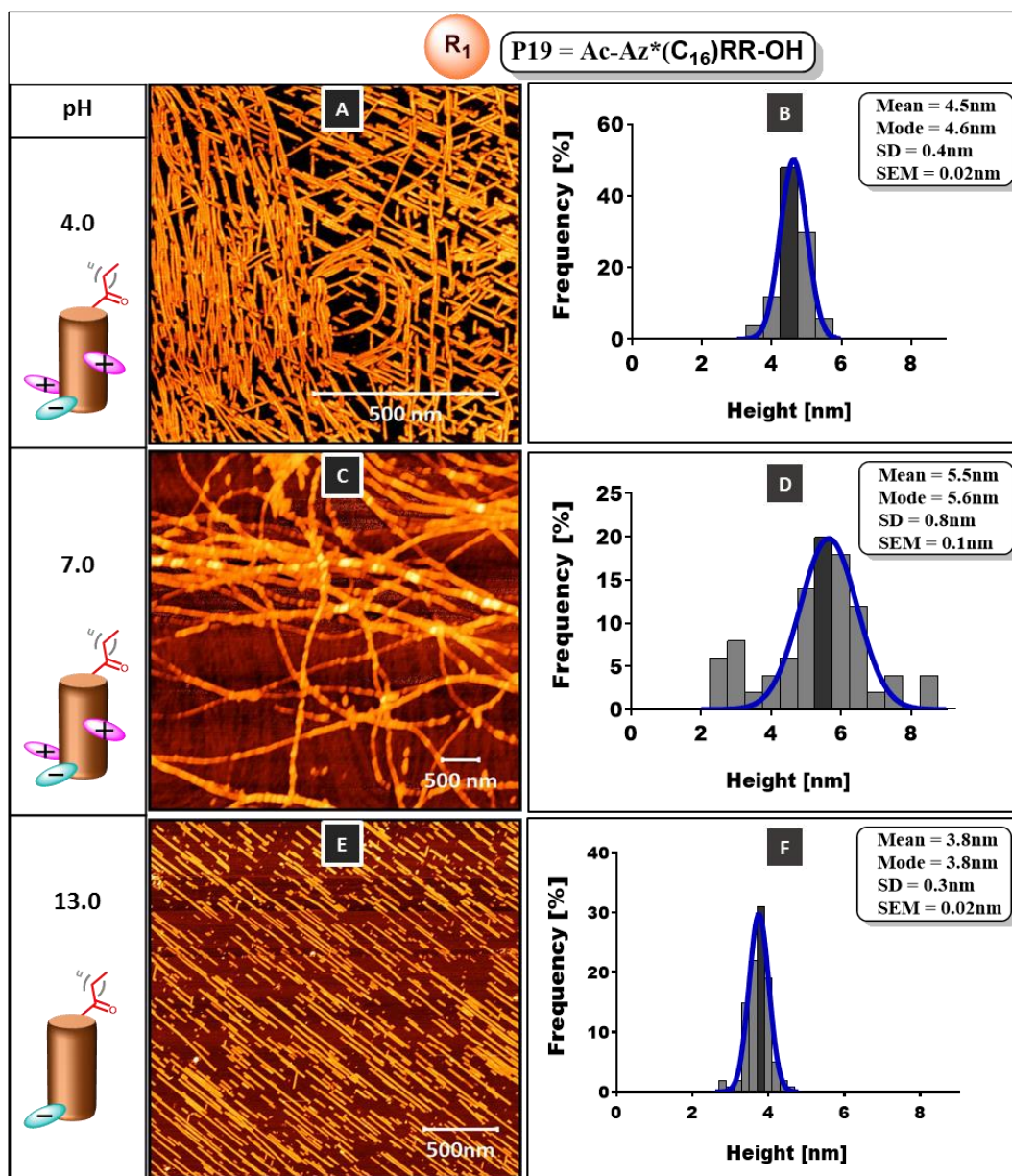


Figure 4.15: Self-assembly of **P19** in different pH environment. (A) Short nanorods at pH 4, (B) height distribution for (A), (C) nanofibres mesh at pH 7 (D) height distribution for (C), (E) truncated discrete nanofibres at pH 13 and (F) height distribution for (E).

A completely different self-assembled morphology was produced by **P20**. At pH 4 spherical particles were observed with height values of 6.2 ± 1.3 nm (Figure 4.16 (A) and (B)). Remarkably, the self-assembly of **P20** into spherical particles is the first example of *N*-acetyl β^3 -tripeptides adopting this architecture and is either a consequence of inhibition of the hydrogen bonding motif or the induction of a different mode of self-assembly.

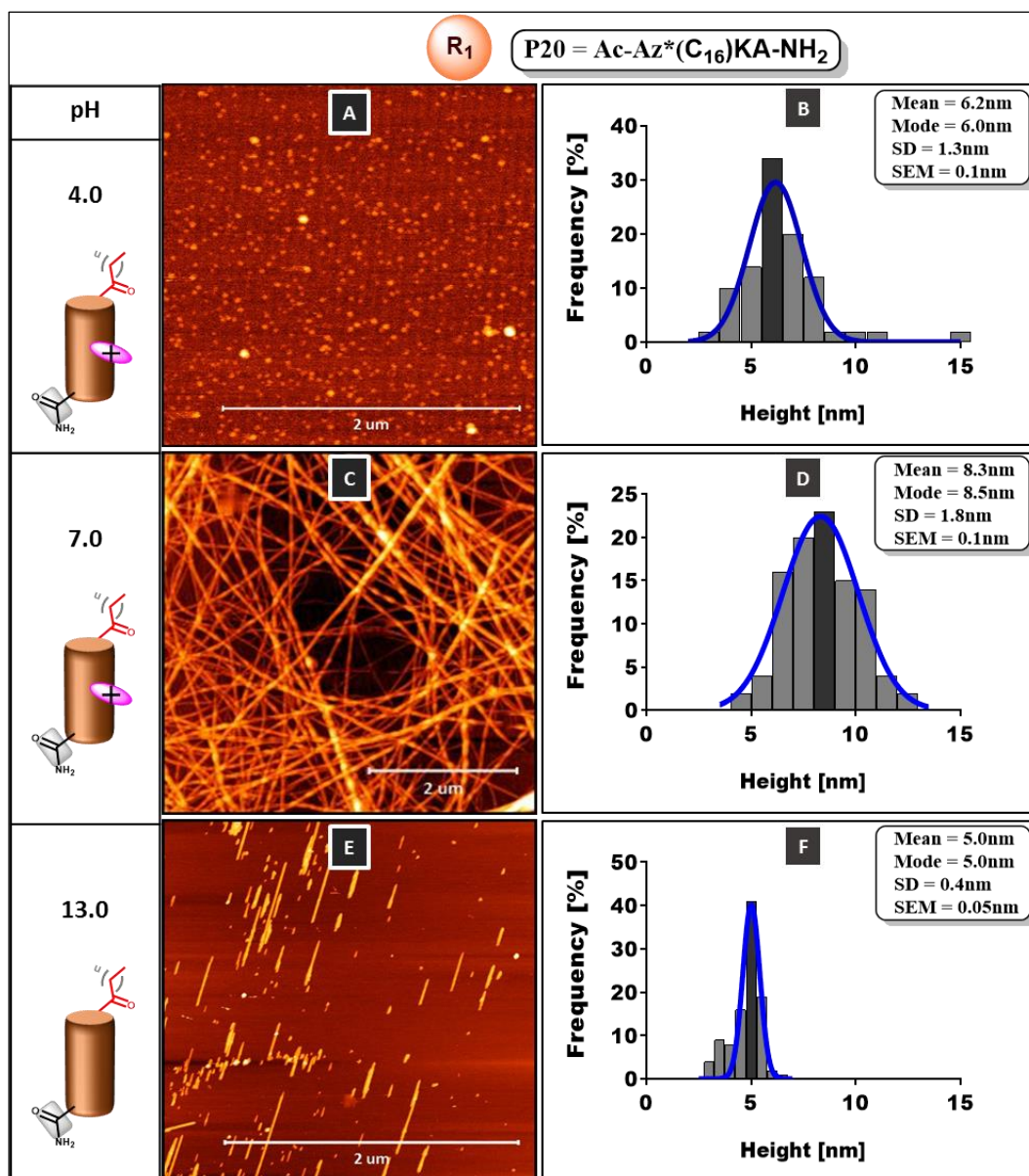


Figure 4.16: Self-assembly of **P20** in different pH environments. (A) Spherical particles at pH 4, (B) height distribution for (A), (C) nanofibre mesh at pH 7, (D) height distribution for (C), (E) truncated discrete nanofibres at pH 13 and (F) height distribution for (E).

It is possible that the formation of spherical particles was favoured by hydrophobic interaction of the alkyl chains which may have dominated over other interactions by forming an interior core. This may be similar to spherical assembly of α -peptide amphiphiles in which the hydrophobic interaction of alkyl chains pack into the interior core region [36-42]. In contrast, at pH 7, **P20** revealed a nanofibre mesh with some evidence of surface periodicity. This may be related to changes in the proportion of deprotonated β K residue as the pH increased from

4 to 7 towards the pKa value. On the other hand, at pH 13, **P20** formed discrete nanofibres that were similar to **P6** at this pH. The height values for the **P20** nanofibres at pH 7 and 13 were 8.3 ± 1.8 nm and 5.0 ± 0.4 nm respectively (Figure 4.16 (D) and (F)) and were significantly different ($p < 0.05$).

4.4.7 General Discussion

It is clear from the results presented in this Chapter that head-to-tail and lateral self-assembly were suppressed at pH 4 and 13 with the formation of truncated rod-like nanofibres, while significant self-assembly occurred at pH 7. Fibre dimensions have been used as an index for estimating the number of nanofibrils for α -peptide amphiphiles that assembled to produce bundles [20, 35, 43-48]. As shown in Figure 4.17, there was very little difference between the height values for all the β R-amide peptides **P15**, **P16**, **P17** and **P18** and they were all much smaller than the C₁₆-template β^3 -peptides presented in Chapter 2. In addition, the height values obtained for the modified β R-amide peptides at pH 4 and 13 were between 2.0 – 4.5 nm which suggest the possibility of a bilayer architecture in which nanofibrils comprised of 2 rows of monomers may associate via hydrophobic interactions.

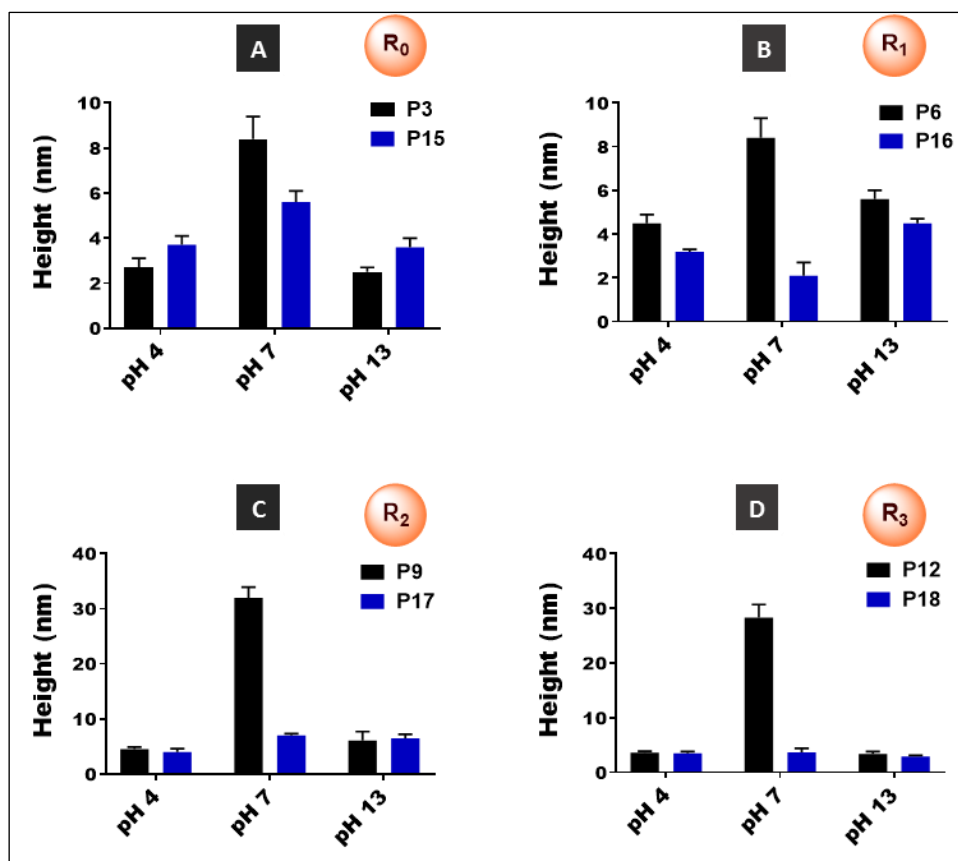


Figure 4.17: Summary of height values for the template (**P3**, **P6**, **P9** and **P12**) and modified β^3 -peptides (**P15**, **P16**, **P17** and **P18**). Height values for C_{16} -template peptides at pH 7 were obtained previously in Chapter 2. Height value at pH 7 for the template are generally higher than those of template peptides.

Overall, this study has demonstrated the control of axial head-to-tail and lateral self-assemblies of β^3 -peptide amphiphiles via pH. Figure 4.18 shows a schematic diagram of the major outcomes in this study for β^3 -peptide amphiphiles with C-terminal amides in which acidic and basic pH environment produced truncated rod-like nanofibres by suppressing intermolecular hydrogen bonding and electrostatic attraction. At neutral pH a nanofibrous mesh was produced regardless of the alkyl chain location suggesting that the C-terminal acid is critical to the formation of nanobelts.

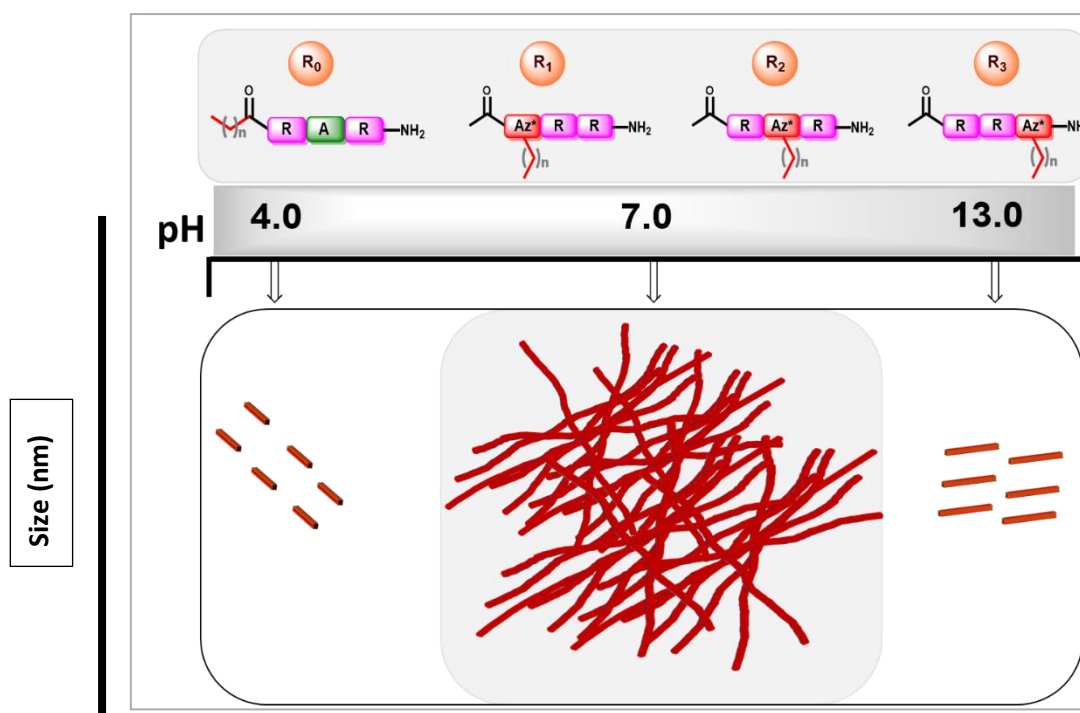


Figure 4.18: Schematic diagram for the pH control self-assembly of β^3 -peptide amphiphiles with C-terminal amides. Truncated discrete nanofibres were observed at acidic and basic pH while a nanofibrous mesh was produced at neutral pH.

Figure 4.19 shows the summary of the self-assembly for free acid β^3 -peptides amphiphiles (**P3**, **P6**, **P9** and **P12**). Truncated discrete rod-like nanofibres were produced at pH 4 and pH 13 by **P3** (R_0) and **P6** (R_1), while long nanofibres that appear as partly formed nanobelts were produced by **P9** (R_2) and **P12** (R_3). In comparison, as presented in Chapter 2, at neutral pH a nanofibre mesh was produced by **P3** (R_0) and **P6** (R_1) while large nanobelts formed by **P9** (R_2) and **P12** (R_3).

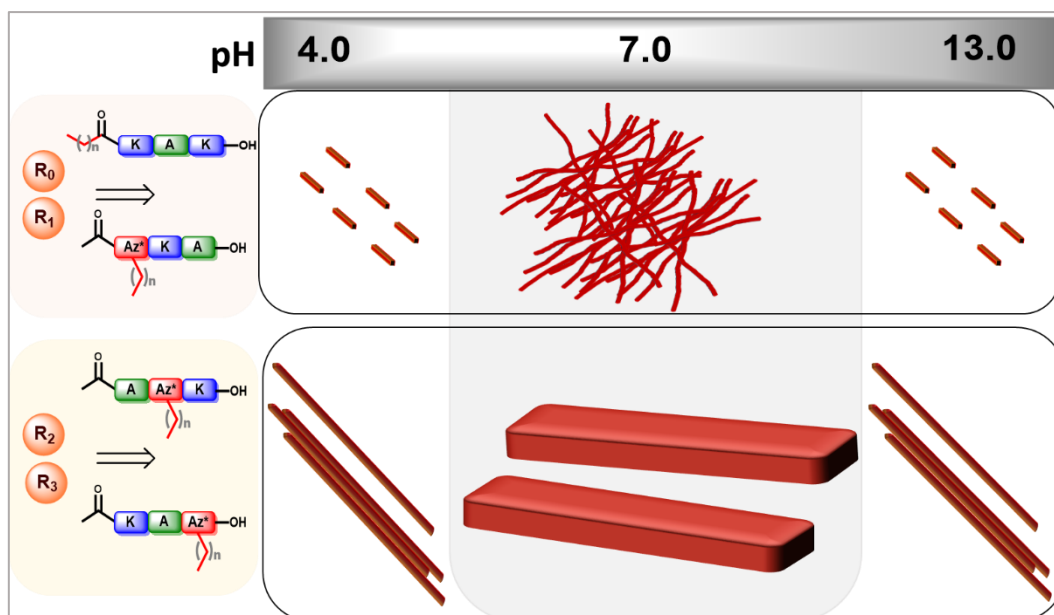


Figure 4.19: Schematic diagram for the pH control of β^3 -peptide amphiphiles with C-terminal free acids. For **P3** (R_0) and **P6** (R_1) truncated discrete nanofibres were observed at acidic and basic pH while a nanofibre mesh formed at pH 7. For **P9** (R_2) and **P12** (R_3) long fibres were produced at pH 4 and 13 while nanobelts formed at neutral pH.

Another unique outcome of this study is the alignment of nanofibres observed for some β^3 -peptide amphiphiles (for example **P15**, **P16** and **P17**) at pH 4 and pH 13 without an external trigger (Figure 4.18). Previous reports with α -peptide amphiphiles demonstrated the alignment of nanofibres only through the use of external influences such as dip-pen nanolithography [49], ultrasonication [50] or a magnetic field [51]. Weronki et al. also demonstrated the neutralisation of positively charged residues of α -peptide amphiphiles using basic pH which resulted in the alignment of nanofibres in a controlled parallel pattern on the surface of the mica (Figure 4.20 (B)) [52]. Fibre alignment at pH 13 for α -peptide fibres was attributed to a reduction in electrostatic interactions between the α -peptide amphiphile monomers [51]. The use of soft lithographic techniques to align and pattern nanofibres over large areas was also demonstrated under the influence of ultrasonic agitation and confinement of the topographic features with an elastomeric stamp [53]. The nanofibres yielded uniform height values on the substrate after the stamp was removed (Figure 4.20 (C)). In comparison, apart from the intrinsic metabolic stability of β^3 -peptides amphiphiles, the alignment of the nanofibres at acidic and basic pH may also represent a novel strategy for designing materials for specific application, for example biosensors.

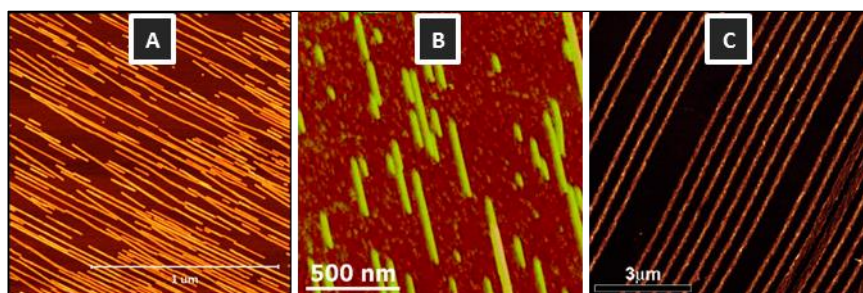


Figure 4.20: Self-assembled peptide nanofibre alignments. (A) Alignment of **P13** nanofibre at pH 13, (B) pH spontaneous alignment of α -peptide amphiphile (adapted from reference [52] with permission from American Chemical Society Copyright © 2010), and (C) lithographic technique alignment for α -peptide amphiphile (adapted from reference [53] with permission from American Chemical Society Copyright © 2007).

4.6 Conclusion

This Chapter described the design and self-assembly of pH-responsive *N*-acetyl β^3 -tripeptide amphiphiles containing β R residues and a C-terminal amide. The modified β^3 -peptide amphiphiles **P15** (R_0), **P16** (R_1), **P17** (R_2) and **P18** (R_3) were synthesised based on the β^3 -peptide templates **P3** (R_0), **P6** (R_1), **P9** (R_2) and **P12** (R_3) respectively to probe the role of hydrogen bonding and electrostatic interactions in the axial and lateral self-assembly via changes in pH above or below the pKa value of β R. It was found that axial head-to-tail self-assembly which is facilitated by intermolecular hydrogen bonding between β^3 -peptide monomers was suppressed at pH 4 and 13 to produce truncated rod-like nanofibres. In addition, a morphology switch between the nanobelt of R_2 and R_3 peptides (previously demonstrated in Chapters 2 and 3) to nanoribbons was achieved. Another notable outcome was the formation of aligned nanofibre patterns without an external stimulus. The well-defined discrete pattern was attributed to the disruption of lateral self-assembly between nanofibrils as a result of electrostatic repulsion at pH 4. In contrast, at pH 13 all the β R residues in **P15** (R_0), **P16** (R_1), **P17** (R_2) and **P18** (R_3) were deprotonated presenting neutral β^3 -peptide amphiphiles, therefore lateral self-assembly was most likely eliminated due to the absence of attractive electrostatic forces.

The suppression of axial and lateral self-assemblies of **P15** (R_0), **P16** (R_1), **P17** (R_2) and **P18** (R_3) was further investigated with corresponding β^3 -peptides amphiphiles with C-terminal acids **P3** (R_0), **P6** (R_1), **P9** (R_2) and **P12** (R_3) which produced similar results in the same pH environment. All the modified β^3 -peptides also self-assembled into a nanofibrous mesh at neutral pH which is similar to the results obtained in Chapter 2 for **P3** (R_0), **P6** (R_1), **P9** (R_2) and **P12** (R_3) in an aqueous environment. These results clearly confirm that the twisted ribbons and nanobelts observed for R_0/R_1 and R_2/R_3 β^3 -peptides respectively are mediated by hydrogen bonding, electrostatic attraction and hydrophobic interaction during self-assembly but that the relative contribution of each interaction can be manipulated to result in different morphologies. Furthermore, the results in this Chapter underscore that through rational design of β^3 -peptide amphiphile sequences, it is possible to develop dynamic materials that can switch morphology and size in response to changes in pH and also create new spherical nanoparticles. Future structural evaluation of the packing order will be helpful to elucidate the internal structure and obtain more insight of the design process.

References

1. Toksoz, S., R. Mammadov, A.B. Tekinay, and M.O. Guler, *Electrostatic effects on nanofiber formation of self-assembling peptide amphiphiles*. Journal of Colloid and Interface Science, 2011. **356**(1): p. 131-137.
2. Fu, I.W., C.B. Markegard, and H.D. Nguyen, *Solvent effects on kinetic mechanisms of self-assembly by peptide amphiphiles via molecular dynamics simulations*. Langmuir, 2015. **31**(1): p. 315-324.
3. Ozbas, B., J. Kretsinger, K. Rajagopal, J.P. Schneider, and D.J. Pochan, *Salt-triggered peptide folding and consequent self-assembly into hydrogels with tunable modulus*. Macromolecules, 2004. **37**(19): p. 7331-7337.
4. Niece, K.L., J.D. Hartgerink, J.J.J.M. Donners, and S.I. Stupp, *Self-Assembly Combining Two Bioactive Peptide-Amphiphile Molecules into Nanofibers by Electrostatic Attraction*. Journal of the American Chemical Society, 2003. **125**(24): p. 7146-7147.
5. Aggeli, A., M. Bell, L.M. Carrick, C.W.G. Fishwick, R. Harding, P.J. Mawer, S.E. Radford, A.E. Strong, and N. Boden, *pH as a trigger of peptide β -sheet self-assembly and reversible switching between nematic and isotropic phases*. Journal of the American Chemical Society, 2003. **125**(32): p. 9619-9628.
6. Cote, Y., I.W. Fu, E.T. Dobson, J.E. Goldberger, H.D. Nguyen, and J.K. Shen, *Mechanism of the pH-controlled self-assembly of nanofibers from peptide amphiphiles*. Journal of Physical Chemistry C, 2014. **118**(29): p. 16272-16278.
7. Ghosh, A., E.T. Dobson, C.J. Buettner, M.J. Nicholl, and J.E. Goldberger, *Programming pH-Triggered Self-Assembly Transitions via Isomerization of Peptide Sequence*. Langmuir, 2014. **30**(51): p. 15383-15387.
8. Qin, S.-Y., S.-S. Xu, R.-X. Zhuo, and X.-Z. Zhang, *Morphology Transformation via pH-Triggered Self-Assembly of Peptides*. Langmuir, 2012. **28**(4): p. 2083-2090.
9. Kubik, S., *Amino acid containing anion receptors*. Chemical Society Reviews, 2009. **38**(2): p. 585-605.
10. Armstrong, C.T., P.E. Mason, J.L.R. Anderson, and C.E. Dempsey, *Arginine side chain interactions and the role of arginine as a gating charge carrier in voltage sensitive ion channels*. Scientific Reports, 2016. **6**: p. 21759.

11. J. J. Rodrigues Jr., S.C.Z., D. T. Balogh, L. Misoguti, C. R. Mendonça, *Electronic charge delocalization in L-arginine probed with Z-scan measurement*. Annals of Optics-XXV ENFMC, 2002. **25**.
12. Frisch, H. and P. Besenius, *pH-switchable self-assembled materials*. Macromolecular Rapid Communications, 2015. **36**(4): p. 346-363.
13. Del Borgo, M.P., A.I. Mechler, D. Traore, C. Forsyth, J.A. Wilce, M.C.J. Wilce, M.I. Aguilar, and P. Perlmutter, *Supramolecular self-assembly of N-acetyl-capped β -peptides leads to nano- to macroscale fiber formation*. Angewandte Chemie - International Edition, 2013. **52**(32): p. 8266-8270.
14. Seoudi R.S., M.G. Hinds, D.J.D. Wilson, C.G. Adda, M.P. Del Borgo, M.I. Aguilar, P. Perlmutter, and A. Mechler, *Self-assembled nanomaterials based on beta (β^3) tetrapeptides*. Nanotechnology, 2016. **27**(13): p. 135606.
15. Seoudi, R.S., M.P. Del Borgo, K. Kulkarni, P. Perlmutter, M.-I. Aguilar, and A. Mechler, *Supramolecular self-assembly of 14-helical nanorods with tunable linear and dendritic hierarchical morphologies*. New Journal of Chemistry, 2015. 39: p. 3280-3287.
16. Seoudi, R.S., A. Dowd, M. Del Borgo, K. Kulkarni, P. Perlmutter, M.I. Aguilar, and A. Mechler, *Amino acid sequence controls the self-assembled superstructure morphology of N-acetylated tri- β^3 -peptides*. Pure and Applied Chemistry, 2015. **87**(9-10): p. 1021-1028.
17. Kulkarni, K., S. Motamed, N. Habila, P. Perlmutter, J.S. Forsythe, M.-I. Aguilar, and M.P. Del Borgo, *Orthogonal strategy for the synthesis of dual-functionalised [small beta]³-peptide based hydrogels*. Chemical Communications, 2016. **52**(34): p. 5844-5847.
18. Motamed, S., M.P. Del Borgo, K. Kulkarni, N. Habila, K. Zhou, P. Perlmutter, J.S. Forsythe, and M.I. Aguilar, *A self-assembling [small beta]-peptide hydrogel for neural tissue engineering*. Soft Matter, 2016. **12**(8): p. 2243-2246.
19. Del Borgo, M.P., K. Kulkarni, and M.I. Aguilar, *Unique Functional Materials Derived from β -Amino Acid Oligomers*. Australian Journal of Chemistry, 2017. **70**(2): p. 126-129.
20. Chen, Y., H.X. Gan, and Y.W. Tong, *pH-controlled hierarchical self-assembly of peptide amphiphile*. Macromolecules, 2015. **48**(8): p. 2647-2653.
21. Elgersma, R.C., L.M.J. Kroon-Batenburg, G. Posthuma, J.D. Meeldijk, D.T.S. Rijkers, and R.M.J. Liskamp, *pH-controlled aggregation polymorphism of amyloidogenic A β (16-*

- 22): *Insights for obtaining peptide tapes and peptide nanotubes, as function of the N-terminal capping moiety*. European Journal of Medicinal Chemistry, 2014. **88**(0): p. 55-65.
22. Zou, D.W., Z.X. Tie, M. Qin, C.M. Lu, and W. Wang, *Effect of phosphate on the self-assembly of peptide EMK16-II*. Chinese Physics Letters, 2009. **26**(8).
23. Zou, D., Z. Tie, C. Lu, M. Qin, X. Lu, M. Wang, W. Wang, and P. Chen, *Effects of hydrophobicity and anions on self-assembly of the peptide EMK16-II*. Biopolymers, 2010. **93**(4): p. 318-329.
24. Moyer, T.J., J.A. Finbloom, F. Chen, D.J. Toft, V.L. Cryns, and S.I. Stupp, *pH and amphiphilic structure direct supramolecular behavior in biofunctional assemblies*. Journal of the American Chemical Society, 2014. **136**(42): p. 14746-14752.
25. Hong, Y., R.L. Legge, S. Zhang, and P. Chen, *Effect of Amino Acid Sequence and pH on Nanofiber Formation of Self-Assembling Peptides EAK16-II and EAK16-IV*. Biomacromolecules, 2003. **4**(5): p. 1433-1442.
26. Yang, H., S.Y. Fung, M. Pritzker, and P. Chen, *Surface-assisted assembly of an ionic-complementary peptide: Controllable growth of nanofibers*. Journal of the American Chemical Society, 2007. **129**(40): p. 12200-12210.
27. Xu, X., Y. Li, H. Li, R. Liu, M. Sheng, B. He, and Z. Gu, *Smart Nanovehicles Based on pH-Triggered Disassembly of Supramolecular Peptide-Amphiphiles for Efficient Intracellular Drug Delivery*. Small, 2014. **10**(6): p. 1133-1140.
28. Jana, P., M. Ehlers, E. Zellermann, K. Samanta, and C. Schmuck, *pH-Controlled Formation of a Stable β -Sheet and Amyloid-like Fibers from an Amphiphilic Peptide: The Importance of a Tailor-Made Binding Motif for Secondary Structure Formation*. Angewandte Chemie - International Edition, 2016. **55**(49): p. 15287-15291.
29. Luder, K., K. Kulkarni, H.W. Lee, R.E. Widdop, M.P. Del Borgo, and M.I. Aguilar, *Decorated self-assembling β 3-tripeptide foldamers form cell adhesive scaffolds*. Chemical Communications, 2016. **52**(24): p. 4549-4552.
30. Goldberger, J.E., E.J. Berns, R. Bitton, C.J. Newcomb, and S.I. Stupp, *Electrostatic control of bioactivity*. Angewandte Chemie - International Edition, 2011. **50**(28): p. 6292-6295.
31. Papapostolou, D., A.M. Smith, E.D.T. Atkins, S.J. Oliver, M.G. Ryadnov, L.C. Serpell, and D.N. Woolfson, *Engineering nanoscale order into a designed protein fiber*. Proceedings

- of the National Academy of Sciences of the United States of America, 2007. **104**(26): p. 10853-10858.
32. Papapostolou, D., E.H.C. Bromley, C. Bano, and D.N. Woolfson, *Electrostatic control of thickness and stiffness in a designed protein fiber*. Journal of the American Chemical Society, 2008. **130**(15): p. 5124-5130.
 33. Jin, Y., X.-D. Xu, C.-S. Chen, S.-X. Cheng, X.-Z. Zhang, and R.-X. Zhuo, *Bioactive Amphiphilic Peptide Derivatives with pH Triggered Morphology and Structure*. Macromolecular Rapid Communications, 2008. **29**(21): p. 1726-1731.
 34. Tantakitti, F., J. Boekhoven, X. Wang, R.V. Kazantsev, T. Yu, J. Li, E. Zhuang, R. Zandi, J.H. Ortony, C.J. Newcomb, L.C. Palmer, G.S. Shekhawat, M.O. De La Cruz, G.C. Schatz, and S.I. Stupp, *Energy landscapes and functions of supramolecular systems*. Nature Materials, 2016. **15**(4): p. 469-476.
 35. Cui, H., T. Muraoka, A.G. Cheetham, and S.I. Stupp, *Self-assembly of giant peptide nanobelts*. Nano Letters, 2009. **9**(3): p. 945-951.
 36. Stupp, S.I., *Self-Assembly and Biomaterials*. Nano Letters, 2010. **10**(12): p. 4783-4786.
 37. Stupp, S.I., R.H. Zha, L.C. Palmer, H. Cui, and R. Bitton, *Self-assembly of biomolecular soft matter*. Faraday Discussions, 2013. **166**: p. 9-30.
 38. Velichko, Y.S., S.I. Stupp, and M.O. de la Cruz, *Molecular Simulation Study of Peptide Amphiphile Self-Assembly*. The Journal of Physical Chemistry B, 2008. **112**(8): p. 2326-2334.
 39. Jiang, H., M.O. Guler, and S.I. Stupp, *The internal structure of self-assembled peptide amphiphiles nanofibers*. Soft Matter, 2007. **3**(4): p. 454-462.
 40. Shimada, T., S. Lee, F.S. Bates, A. Hotta, and M. Tirrell, *Wormlike micelle formation in peptide-lipid conjugates driven by secondary structure transformation of the headgroups*. Journal of Physical Chemistry B, 2009. **113**(42): p. 13711-13714.
 41. Miravet, J.F., B. Escuder, M.D. Segarra-Maset, M. Tena-Solsona, I.W. Hamley, A. Dehsorkhi, and V. Castelletto, *Self-assembly of a peptide amphiphile: transition from nanotape fibrils to micelles*. Soft Matter, 2013. **9**(13): p. 3558-3564.
 42. Palladino, P., V. Castelletto, A. Dehsorkhi, D. Stetsenko, and I.W. Hamley, *Conformation and self-association of peptide amphiphiles based on the KTTKS collagen sequence*. Langmuir, 2012. **28**(33): p. 12209-12215.

43. Dagdas, Y.S., A. Tombuloglu, A.B. Tekinay, A. Dana, and M.O. Guler, *Interfiber interactions alter the stiffness of gels formed by supramolecular self-assembled nanofibers*. *Soft Matter*, 2011. **7**(7): p. 3524-3532.
44. Guo, H., J. Zhang, T. Xu, Z. Zhang, J. Yao, and Z. Shao, *The robust hydrogel hierarchically assembled from a pH sensitive peptide amphiphile based on silk fibroin*. *Biomacromolecules*, 2013. **14**(8): p. 2733-2738.
45. Sayar, M. and S.I. Stupp, *Assembly of one-dimensional supramolecular objects: From monomers to networks*. *Physical Review E - Statistical, Nonlinear, and Soft Matter Physics*, 2005. **72**(1): 011803.
46. Dehsorkhi, A., V. Castelletto, I.W. Hamley, J. Adamcik, and R. Mezzenga, *The effect of pH on the self-assembly of a collagen derived peptide amphiphile*. *Soft Matter*, 2013. **9**(26): p. 6033-6036.
47. Liao, H.S., J. Lin, Y. Liu, P. Huang, A. Jin, and X. Chen, *Self-assembly mechanisms of nanofibers from peptide amphiphiles in solution and on substrate surfaces*. *Nanoscale*, 2016. **8**(31): p. 14814-14820.
48. Tanaka, M., S. Abiko, T. Himejiwa, and T. Kinoshita, *Two-dimensional self-assembly of amphiphilic peptides; adsorption-induced secondary structural transition on hydrophilic substrate*. *Journal of Colloid and Interface Science*, 2015. **442**: p. 82-88.
49. Jiang, H. and S.I. Stupp, *Dip-pen patterning and surface assembly of peptide amphiphiles*. *Langmuir*, 2005. **21**(12): p. 5242-5246.
50. Hung, A.M. and S.I. Stupp, *Understanding factors affecting alignment of self-assembling nanofibers patterned by sonication-assisted solution embossing*. *Langmuir*, 2009. **25**(12): p. 7084-7089.
51. Reches, M. and E. Gazit, *Controlled patterning of aligned self-assembled peptide nanotubes*. *Nature Nanotechnology*, 2006. **1**(3): p. 195-200.
52. Weroński, K.J., P. Cea, I. Diez-Peréz, M.A. Busquets, J. Prat, and V. Girona, *Time-lapse atomic force microscopy observations of the morphology, growth rate, and spontaneous alignment of nanofibers containing a peptide-amphiphile from the hepatitis G virus (NS3 Protein)*. *Journal of Physical Chemistry B*, 2010. **114**(1): p. 620-625.

53. Hung, A.M. and S.I. Stupp, *Simultaneous Self-Assembly, Orientation, and Patterning of Peptide–Amphiphile Nanofibers by Soft Lithography*. *Nano Letters*, 2007. **7**(5): p. 1165-1171.

Chapter Five

Conclusions and Future Directions

5.1 Conclusions

N-acetyl- β^3 -tripeptides containing acyclic amino acids adopt a 14-helical conformation irrespective of the monomer sequence, allowing the self-assembly motif within these β^3 -peptides to be completely confined to the β^3 -peptide backbone. This unique self-assembly motif creates the opportunity for β^3 -amino acid sidechains to be involved in lateral self-assembly without perturbation to self-assembly. This led to the uncontrolled assembly of a variety of hierarchical structures that included a large range of sizes (from a few nanometres to centimetres) within the same sample [1-4]. In this dissertation, the control of structures formed by self-assembly of *N*-acetyl β^3 -tripeptides was achieved by the incorporation of fatty acids within the β^3 -peptide sequence. We hypothesised that lipidation of β^3 -amino acid side chains presented on one face of the 14-helix would offer an opportunity to better control self-assembly and limit the ability of these β^3 -peptides to form macrostructures [1, 5-8], without affecting their ability to self-assemble and form fibres in solution. Therefore, *N*-acetyl β^3 -tripeptides were lipidated to obtain the first *N*-acetyl- β^3 -peptide amphiphiles.

Chapter 2 describes the design, synthesis and self-assembly of 12 β^3 -peptide amphiphiles (**P1** – **P12**) in which the alkyl chains were placed at R_0 , R_1 , R_2 and R_3 positions on the β^3 -tripeptide sequence. The position of the alkyl chain dictated the type of self-assembled morphology produced as evident from the summary presented in Figure 5.1. Morphological characterisation by TEM and AFM showed that *N*-acetyl- β^3 -peptide amphiphiles with the alkyl chain at R_0 (**P1**, **P2** and **P3**) and R_1 (**P4**, **P5** and **P6**) self-assembled into twisted ribbons (Figure 5.1 (A), (B), (C), (D), (E) and (F)) while those with the alkyl chain at R_2 (**P7**, **P8** and **P9**) and R_3 (**P10**, **P11** and **P12**) formed nanobelts (Figure 5.1 (G), (H), (I), (J), (K) and (L)). This is a striking difference given that the composition of the β^3 -peptides are either identical or very similar and demonstrates the fine balance in the forces that govern the self-assembly of these β^3 -peptides. In particular, the location of acylation seems to be primarily responsible for the mode of hierarchical self-assembly and the internal packing order of the alkyl chains. Interestingly, the length of the alkyl chain produced subtle differences in the dimensions of the fibres but did not alter fibre morphology. Modifications to the general tripeptide structure with unsaturated fatty acids may provide further insight into fibre packing and is a logical next step forward. Additionally, the introduction of polyaromatic systems (for example, steroids) may provide some degree of control over self-assembly. Finally, introduction of carbohydrate

or PEG-based linkages may also exert control over self-assembly without decreasing the water solubility of the peptide. However, these would be unlikely to gelate.

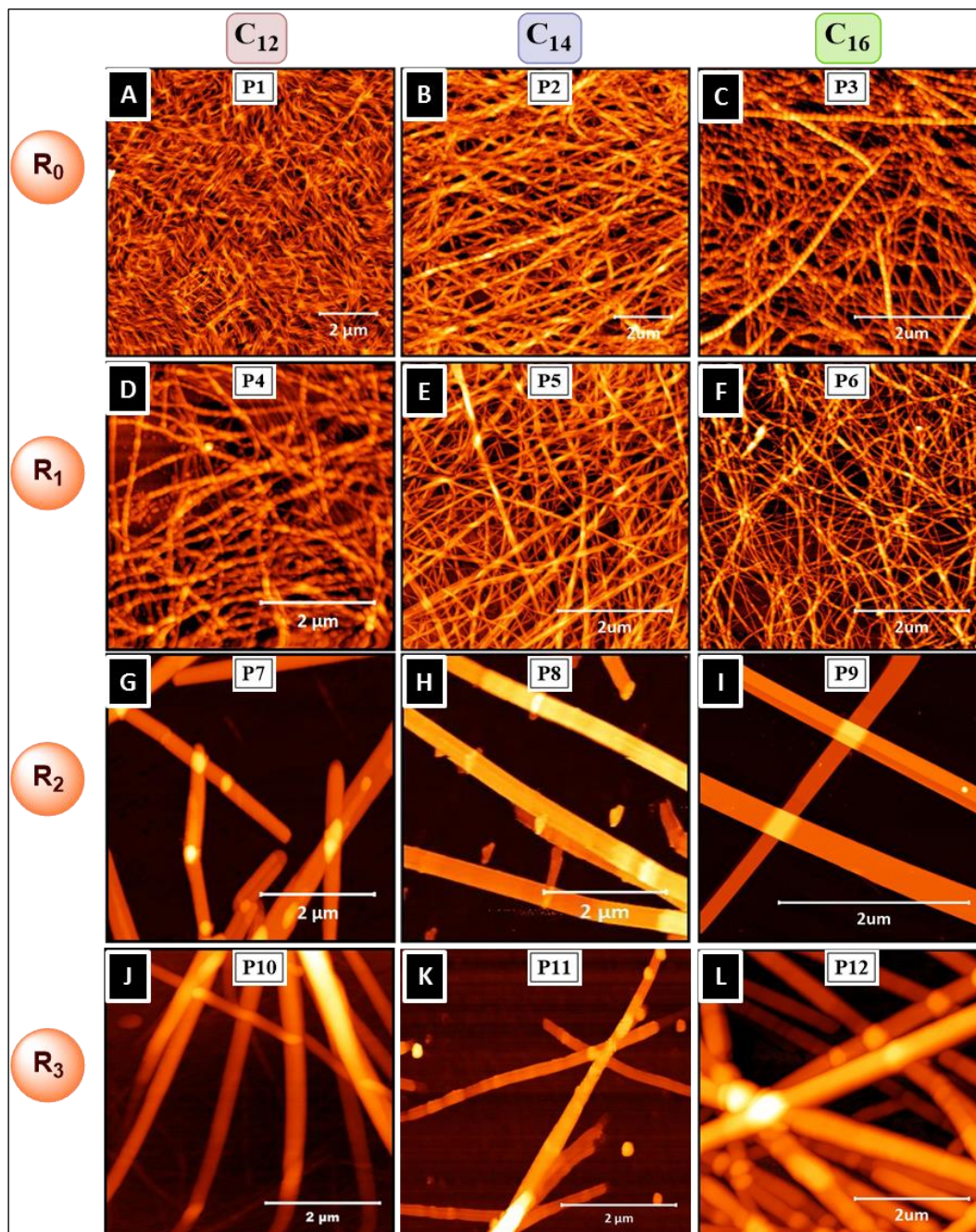


Figure 5.1: Summary of the self-assembled morphologies of β^3 -peptide amphiphiles with a free C-terminal acid.

To determine the suitability of these β^3 -peptide amphiphiles as biomaterials, stable supramolecular hydrogels were formed at 10mg/mL in PBS (pH 7.4) with **P2 – P11**. These

rapidly self-assembled in an aqueous environment and provide great potential for the development of finely tuned cellular microenvironments suitable for tissue engineering by chemical modification at the monomer level. Overall, the results in Chapter 2 demonstrated the role of the alkyl chain position in the control of self-assembled supramolecular architectures of *N*-acetyl- β^3 -peptides amphiphiles.

In Chapter 3, the internal molecular packing of the self-assembled *N*-acetyl- β^3 -peptide amphiphile nanobelts obtained in Chapter 2 was investigated using nanoindentation by AFM. The focus was to create holes in the nanostructure surface with the AFM tip to enable visualisation and characterisation of the internal packing structure. The indentation was carried out at different locations along the fibres (central and lateral) which exposed the multi-layered internal features of the nanobelts with a regular spacing of ≈ 2.6 nm, ≈ 2.8 nm and ≈ 3.0 nm for **P7**, **P8** and **P9** respectively. The results indicated that the stepwise internal features were bilayers which stack during self-assembly. These high-resolution images are the first evidence of the internal structure of the *N*-acetyl- β^3 -peptide amphiphile materials and lay the foundation for future structural analysis of these fibres. In addition, nanomechanical measurements of the fibres were made using AFM, which indicated that the length of the attached fatty acid contributed to the stiffness of the resulting fibres. The results of this Chapter also demonstrated that AFM nanoindentation can be used as a powerful tool to complement other techniques such as SAXS and fibre diffraction to investigate the internal organisation of self-assembled nanostructures.

In Chapter 4, the effect of pH on axial and lateral self-assembly of β^3 -peptide amphiphiles was investigated. This was achieved by designing 4 modified β^3 -peptide sequences (**P15 – P18**) which comprised β R and a C-terminal amide in each *N*-acetyl β^3 -tripeptide using the R_0/R_1 and R_2/R_3 β^3 -peptide amphiphile templates in Chapter 2 which self-assembled into twisted ribbons and nanobelts respectively. The protonation of the β R residues was achieved by self-assembly in phosphate buffer at pH 4 and 7, while deprotonation was achieved at pH 13. The AFM images of this set of β^3 -peptides at pH 4, 7 and 13 are reproduced in Figure 5.2 and a number of significant morphology changes were observed. Firstly, the nanobelt structures observed in Chapter 2 for the R_2 and R_3 β^3 -peptides were not evident at pH 7 for the β R-containing amidated β^3 -peptides, but were replaced by a fibrous mesh. Secondly, self-assembly of all the modified β^3 -peptide amphiphiles was significantly compromised at pH 4

and 13, clearly demonstrating that fibre morphology can be manipulated by changes in ionisation. In particular, the presence of short fibres indicates that the head-to-tail self-assembly was inhibited by high and low pH reflecting effects on the H-bonding or indeed effects on the ability of the *N*-acetyl β^3 -tripeptide to adopt the requisite 14-helix. In addition, the changes in ionisation impacted on the fibre widths as a result of suppressed lateral interactions.

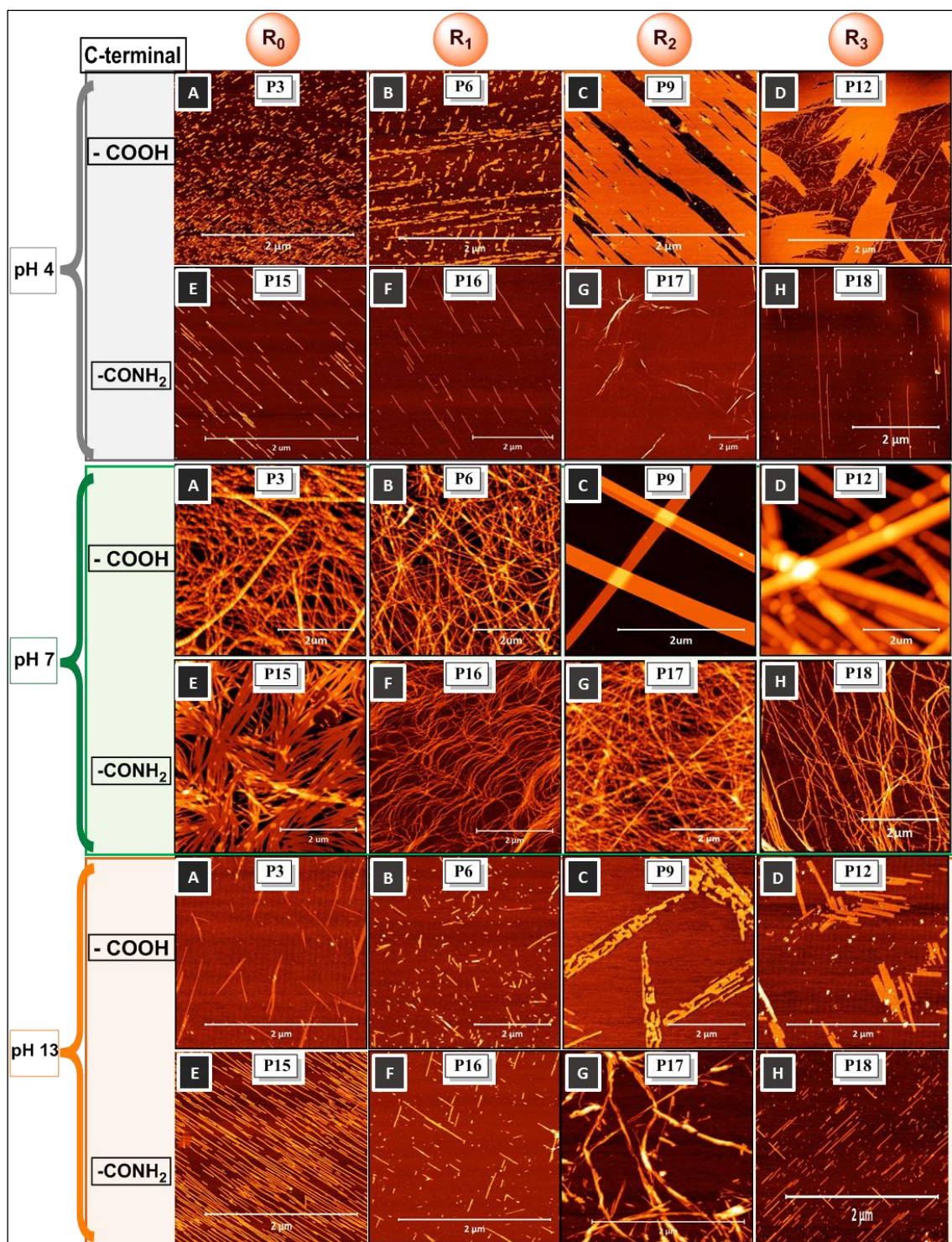


Figure 5.2: Summary of the pH-controlled self-assembled morphologies of β^3 -peptide amphiphiles.

Overall, the results of this chapter provide a rationale for the design of novel β^3 -peptide-based materials that can be manipulated through changes in pH.

5.2 Future Directions in β^3 -Peptide Amphiphile Design

The results presented in this Thesis provide a new platform for the supramolecular self-assembly of β^3 -peptide amphiphiles. Firstly, all peptides (unless they were not *N*-terminally acylated), self-assembled in either water or pH 7 buffer irrespective of sequence, further demonstrating that side chain modification does not impact on fibre formation and paving the way for the design of novel β^3 -amino acids to control either fibre morphology and/or function. This feature has important ramifications in the development of new biocompatible materials with long-term stability. However, before discussing the long-term applications, a number of structural features need immediate characterisation. Firstly, the results of nanoindentation by AFM can be built on through, for example, fibre diffraction of these samples and coupled with molecular dynamics to develop molecular models of these materials. This information is important to allow more rational design of the next generation of materials. Other high-resolution techniques such as cryoEM should also be explored to provide another avenue for structural determination.

Functionalisation of β^3 -peptide amphiphile monomers provides enormous scope for the design of new biomaterials with specifically engineered biorecognition properties by incorporating a variety of functional groups tailored for specific applications. When coupled with tailored structural properties, the possibilities are endless. Our group has recently functionalised **P5** (C_{14} , R_1 β^3 -peptide) by attaching the bioactive cell adhesion epitope RGD on the second residue of the *N*-acetyl β^3 -tripeptide sequence via an alloc-protected aminoethylamide [8]. The functionalised β^3 -peptide amphiphile self-assembled into a nanofibrous mesh architecture without perturbing the self-assembly motif (and still presenting functionality) as previously observed with **P5** without an RGD epitope. In a similar manner, future studies may include the attachment of other bioactive compounds to the side-chain of the second residue such as IKVAV (for neurite extension) and YIGSR (for neuron adhesion). Functionalisation of R_2 and R_3 β^3 -peptide amphiphile nanobelts can also be carried out by incorporating bioactive epitopes on the free residues. The co-assembly of functionalised β^3 -peptide amphiphiles will provide a new approach to biomaterial design, by mixing β^3 -peptides with different bioactive molecules at an optimised ratio in solution to produce a scaffold with multiple biological signals. A scaffold with multiple biological epitopes from β^3 -peptide amphiphiles could provide additional functionality to the self-assembled

nanostructure, allowing for bioactive epitopes to be multiplexed in a synergistic way to regulate cell activity. Co-assembly of multiple β^3 -peptide amphiphiles into a single nanostructure may thus offer additional functionality and mechanical properties of the self-assembled architecture.

To exploit the ability of these materials to form hydrogels and act as viable biomaterials that resemble the mechanical properties of the target tissue, the mechanical properties of these β^3 -peptides amphiphiles in terms of porosity and mechanical stability is necessary. The bulk properties of hydrogels not only depend on the intrinsic properties of the fibres but also on the network topology [10]. Given that the alkyl chain position exerts a significant effect of morphology, the position and the length of the alkyl chain can be incorporated into future hydrogel design to control matrix stiffness and hence regulate cell morphology and differentiation [16].

The formation of large nanobelts with a high aspect ratio provides an interesting avenue in the design of materials for energy applications. The incorporation of organic molecules like thiophenes and perylenes may form novel field-effect transistors and semiconducting materials. The ability to control the morphology switch between a fibrous mesh and nanobelts also provides an additional design feature which could be exploited in a wide range of applications. Thus, further manipulation of lateral interactions via changes in electrostatic and hydrophobic forces may provide additional control over the formation of twisted ribbons and nanobelts. This could be explored by probing the self-assembly of β^3 -peptide amphiphiles that comprise of β^3 -glutamic acid (βE) or β^3 -aspartic acid (βD) in place of βR and βK in the *N*-acetyl β^3 -tripeptide sequence.

It was observed in Chapter 4 that the R_1 β^3 -peptide with C-terminal amide, **P20** (Ac-Az*(C₁₆)KA-NH₂) formed spherical particles at pH 4. This is another significant outcome and may provide an avenue for the development of β^3 -peptide-based nanoparticles for a range of applications such as drug delivery similar to the spherical particles of α -peptide amphiphiles which are known to produce a geometric particle core that allows high drug loading per surface area [17]. These nanoparticles could also be easily modified to introduce cell targeting epitopes on the surface of the particle.

Overall, the control of the self-assembled morphology of β^3 -peptide amphiphiles was dictated by the molecular design of the building blocks in which the position of alkyl chain (R_0 , R_1 , R_2 and R_3) on the *N*-acetyl β^3 -tripeptide sequence together with molecular forces that define the lateral interactions, plays a crucial role in defining the final nanostructure. Therefore, this dissertation has significantly expanded the scope of β^3 -peptide self-assembly by establishing strategies for the design of a new generation of β^3 -peptide-based materials with geometric precision and potential for tailored functions.

References

1. Del Borgo, M.P., A.I. Mechler, D. Traore, C. Forsyth, J.A. Wilce, M.C.J. Wilce, M.I. Aguilar, and P. Perlmutter, *Supramolecular self-assembly of N-acetyl-capped β -peptides leads to nano- to macroscale fiber formation*. *Angewandte Chemie - International Edition*, 2013. **52**(32): p. 8266-8270.
2. Seoudi R.S., M.G. Hinds, D.J.D. Wilson, C.G. Adda, M.P. Del Borgo, M.I. Aguilar, P. Perlmutter, and A. Mechler, *Self-assembled nanomaterials based on beta (β^3) tetrapeptides*. *Nanotechnology*, 2016. **27**(13): p. 135606.
3. Seoudi, R.S., M.P. Del Borgo, K. Kulkarni, P. Perlmutter, M.-I. Aguilar, and A. Mechler, *Supramolecular self-assembly of 14-helical nanorods with tunable linear and dendritic hierarchical morphologies*. *New Journal of Chemistry*, 2015. 39: p. 3280-3287.
4. Seoudi, R.S., A. Dowd, M. Del Borgo, K. Kulkarni, P. Perlmutter, M.I. Aguilar, and A. Mechler, *Amino acid sequence controls the self-assembled superstructure morphology of N-acetylated tri- β^3 -peptides*. *Pure and Applied Chemistry*, 2015. **87**(9-10): p. 1021-1028.
5. Cheng, R.P., S.H. Gellman, and W.F. DeGrado, *β -peptides: From structure to function*. *Chemical Reviews*, 2001. **101**(10): p. 3219-3232.
6. Gellman, S.H., *Foldamers: A Manifesto*. *Accounts of Chemical Research*, 1998. **31**(4): p. 173-180.
7. Luder, K., K. Kulkarni, H.W. Lee, R.E. Widdop, M.P. Del Borgo, and M.I. Aguilar, *Decorated self-assembling β^3 -tripeptide foldamers form cell adhesive scaffolds*. *Chemical Communications*, 2016. **52**(24): p. 4549-4552.
8. Kulkarni, K., S. Motamed, N. Habila, P. Perlmutter, J.S. Forsythe, M.-I. Aguilar, and M.P. Del Borgo, *Orthogonal strategy for the synthesis of dual-functionalised [small beta] β^3 -peptide based hydrogels*. *Chemical Communications*, 2016. **52**(34): p. 5844-5847.
9. O'Brien, F.J., *Biomaterials & scaffolds for tissue engineering*. *Materials Today*, 2011. **14**(3): p. 88-95.
10. Gao, J., C. Tang, M.A. Elsayy, A.M. Smith, A.F. Miller, and A. Saiani, *Controlling Self-Assembling Peptide Hydrogel Properties through Network Topology*. *Biomacromolecules*, 2017. **18**(3): p. 826-834.

11. Boothroyd, S., A. Saiani, and A.F. Miller, *Controlling network topology and mechanical properties of co-assembling peptide hydrogels*. *Biopolymers*, 2014. **101**(6): p. 669-680.
12. Sinthuvanich, C., K.J. Nagy-Smith, S.T.R. Walsh, and J.P. Schneider, *Triggered Formation of Anionic Hydrogels from Self-Assembling Acidic Peptide Amphiphiles*. *Macromolecules*, 2017. **50**(15): p. 5643-5651.
13. Wan, Y., Z. Wang, J. Sun, and Z. Li, *Extremely Stable Supramolecular Hydrogels Assembled from Nonionic Peptide Amphiphiles*. *Langmuir*, 2016. **32**(30): p. 7512-7518.
14. Williams, R.J., T.E. Hall, V. Glattauer, J. White, P.J. Pasic, A.B. Sorensen, L. Waddington, K.M. McLean, P.D. Currie, and P.G. Hartley, *The in vivo performance of an enzyme-assisted self-assembled peptide/protein hydrogel*. *Biomaterials*, 2011. **32**(22): p. 5304-5310.
15. Black, K.A., B.F. Lin, E.A. Wonder, S.S. Desai, E.J. Chung, B.D. Ulery, R.S. Katari, and M.V. Tirrell, *Biocompatibility and Characterization of a Peptide Amphiphile Hydrogel for Applications in Peripheral Nerve Regeneration*. *Tissue Engineering. Part A*, 2015. **21**(7-8): p. 1333-1342.
16. Zhou, M., A.M. Smith, A.K. Das, N.W. Hodson, R.F. Collins, R.V. Ulijn, and J.E. Gough, *Self-assembled peptide-based hydrogels as scaffolds for anchorage-dependent cells*. *Biomaterials*, 2009. **30**(13): p. 2523-2530.
17. Boekhoven, J., R.H. Zha, F. Tantakitti, E. Zhuang, R. Zandi, C.J. Newcomb, and S.I. Stupp, *Alginate-peptide amphiphile core-shell microparticles as a targeted drug delivery system*. *RSC advances*, 2015. **5**(12): p. 8753-8756.
18. Cui, H., A.G. Cheetham, E.T. Pashuck, and S.I. Stupp, *Amino acid sequence in constitutionally isomeric tetrapeptide amphiphiles dictates architecture of one-dimensional nanostructures*. *Journal of the American Chemical Society*, 2014. **136**(35): p. 12461-12468.
19. Nieuwland, M., L. Ruizendaal, A. Brinkmann, L. Kroon-Batenburg, J.C.M. Van Hest, and D.W.P.M. Löwik, *A structural study of the self-assembly of a palmitoyl peptide amphiphile*. *Faraday Discussions*, 2013. **166**: p. 361-379.
20. Palladino, P., V. Castelletto, A. Dehsorkhi, D. Stetsenko, and I.W. Hamley, *Conformation and self-association of peptide amphiphiles based on the KTTKS collagen sequence*. *Langmuir*, 2012. **28**(33): p. 12209-12215.

21. Morris, K. and L. Serpell, *From natural to designer self-assembling biopolymers, the structural characterisation of fibrous proteins & peptides using fibre diffraction*. Chemical Society Reviews, 2010. **39**(9): p. 3445-3453.
22. Morris, K.L. and L.C. Serpell, *X-ray fibre diffraction studies of amyloid fibrils*, in *Methods in Molecular Biology*. 2012. p. 121-135.
23. Tsuruta, H. and T.C. Irving, *Experimental Approaches for Solution X-Ray Scattering and Fiber Diffraction*. Current opinion in structural biology, 2008. **18**(5): p. 601-608.
24. Hyland, L.L., M.B. Taraban, and Y.B. Yu, *Using Small-Angle Scattering Techniques to Understand Mechanical Properties of Biopolymer-Based Biomaterials*. Soft matter, 2013. **9**(43): p. 10218-10228.
25. Skou, S., R.E. Gillilan, and N. Ando, *Synchrotron-based small-angle X-ray scattering (SAXS) of proteins in solution*. Nature protocols, 2014. **9**(7): p. 1727-1739.
26. Goldberger, J.E., E.J. Berns, R. Bitton, C.J. Newcomb, and S.I. Stupp, *Electrostatic control of bioactivity*. Angewandte Chemie - International Edition, 2011. **50**(28): p. 6292-6295.
27. Dehsorkhi, A., R.M. Gouveia, A.M. Smith, I.W. Hamley, V. Castelletto, C.J. Connon, M. Reza, and J. Ruokolainen, *Self-assembly of a dual functional bioactive peptide amphiphile incorporating both matrix metalloprotease substrate and cell adhesion motifs*. Soft Matter, 2015. **11**(16): p. 3115-3124.
28. Hamley, I.W., A. Dehsorkhi, V. Castelletto, S. Furzeland, D. Atkins, J. Seitsonen, and J. Ruokolainen, *Reversible helical unwinding transition of a self-assembling peptide amphiphile*. Soft Matter, 2013. **9**(39): p. 9290-9293.
29. Newcomb, C.J., T.J. Moyer, S.S. Lee, and S.I. Stupp, *Advances in cryogenic transmission electron microscopy for the characterization of dynamic self-assembling nanostructures*. Current opinion in colloid & interface science, 2012. **17**(6): p. 350-359.
30. Sharp, T.H., M. Bruning, J. Mantell, R.B. Sessions, A.R. Thomson, N.R. Zaccai, R.L. Brady, P. Verkade, and D.N. Woolfson, *Cryo-transmission electron microscopy structure of a gigadalton peptide fiber of de novo design*. Proceedings of the National Academy of Sciences, 2012. **109**(33): p. 13266-13271.
31. Cui, H., T.K. Hodgdon, E.W. Kaler, L. Abezgauz, D. Danino, M. Lubovsky, Y. Talmon, and D.J. Pochan, *Elucidating the assembled structure of amphiphiles in solution via cryogenic transmission electron microscopy*. Soft Matter, 2007. **3**(8): p. 945-955.

32. Thompson, R.F., M. Walker, C.A. Siebert, S.P. Muench, and N.A. Ranson, *An introduction to sample preparation and imaging by cryo-electron microscopy for structural biology*. *Methods*, 2016. **100**: p. 3-15.

Appendix

Publications

The following publications resulted from research performed during the author's candidature.

1. Motamed, S., Del Borgo, M.P., Kulkarni, K., **Habila, N.**, Zhou, K., Perlmutter, P., Forsythe J.S., and Aguilar M.I. **A self-assembling β -peptide hydrogel for neural tissue engineering**, *Soft Matter*, 2016. 12: 2243-2246.
2. Kulkarni, K., Motamed, S., **Habila, N.**, Perlmutter, P., Forsythe J.S., and Aguilar M.I. and Del Borgo M.P. (2016). **Orthogonal strategy for the synthesis of dual-functionalised β^3 -peptide based hydrogels**. *Chem. Commun.*, 2016. 52: 5844—5847.